
Doctoral Dissertations

Student Theses and Dissertations

Summer 2014

Rapid repair of severely damaged RC columns under combined loading of flexure, shear, and torsion with externally bonded CFRP

Ruili He

Follow this and additional works at: https://scholarsmine.mst.edu/doctoral_dissertations



Part of the [Civil Engineering Commons](#)

Department: Civil, Architectural and Environmental Engineering

Recommended Citation

He, Ruili, "Rapid repair of severely damaged RC columns under combined loading of flexure, shear, and torsion with externally bonded CFRP" (2014). *Doctoral Dissertations*. 2323.

https://scholarsmine.mst.edu/doctoral_dissertations/2323

This thesis is brought to you by Scholars' Mine, a service of the Missouri S&T Library and Learning Resources. This work is protected by U. S. Copyright Law. Unauthorized use including reproduction for redistribution requires the permission of the copyright holder. For more information, please contact scholarsmine@mst.edu.

RAPID REPAIR OF SEVERELY DAMAGED RC COLUMNS UNDER
COMBINED LOADING OF FLEXURE, SHEAR, AND TORSION
WITH EXTERNALLY BONDED CFRP

by

RUILI HE

A DISSERTATION

Presented to the Faculty of the Graduate School of the
MISSOURI UNIVERSITY OF SCIENCE AND TECHNOLOGY

In Partial Fulfillment of the Requirements for the Degree

DOCTOR OF PHILOSOPHY

in

CIVIL ENGINEERING

2014

Approved by:

Lesley H. Sneed, Advisor

Abdeldjelil Belarbi

Genda Chen

John J. Myers

K. Chandrashekhara

PUBLICATION DISSERTATION OPTION

This dissertation has been prepared in the style such that the second section is composed of publications and submissions for publication in professional journals. The corresponding journal specifications were used to format each of the papers presented in this dissertation.

Paper I entitled “Seismic Repair of Reinforced Concrete Bridge Columns: A Review of Research Findings”, presented from page 6 to 39 in this dissertation, has been submitted to the Journal of Bridge Engineering (American Society of Civil Engineers (ASCE)). Paper II entitled “Rapid Repair of Severely Damaged RC Columns with Different Damage Conditions – An Experimental Study”, presented from page 40 to 81 in this dissertation, has been published in the International Journal of Concrete Structures and Materials (Springer) 2013, Volume 7, pp. 35-50. Paper III entitled “Rapid Repair of a Severely Damaged RC Column Having Fractured Bars Using Externally Bonded CFRP”, which has been published in Composite Structures (Elsevier Publishing) 2013, Volume 101, pp. 225-242, is presented from pages 82 to 134 in this dissertation. Paper IV entitled “Torsional Repair of Severely Damaged Column Using Carbon Fiber-Reinforced Polymer”, presented from page 135 to 170, was published in the ACI Structural Journal (American Concrete Institute (ACI)) 2013, Volume 111. Paper V, Pages 171-209 present the manuscript entitled “Post-Repair Seismic Performance of Damaged RC Bridge Columns with Fractured Bars – A Numerical Assessment”, which has been submitted to Earthquake Engineering & Structural Dynamics (John Wiley & Sons).

ABSTRACT

This research aimed to develop a technique to rapidly repair reinforced concrete (RC) bridge columns for emergency service restoration after severe earthquake damage has occurred. Experimental and analytical studies were conducted to study the performance and effectiveness of the proposed repair method. The experimental study included a series of 1/2-scale RC square bridge columns originally tested to failure under constant axial and increasing cyclic lateral loadings resulting in combined flexure, shear, and torsion with different torsional-to-flexural moment ratios. Using externally bonded carbon fiber reinforced polymer (CFRP) sheets, each column was repaired over a 3-day period and then retested under the same combined loading as the corresponding original column. Ruptured and/or buckled longitudinal reinforcing bars were not treated during the repair. A strength-based methodology was used to design the CFRP strengthening system to compensate for the strength loss due to the damage observed after the original test. Results indicated that the severely damaged columns were successfully repaired using the developed technique, with the exception of one column with fractured longitudinal reinforcing bars near the joint, which was only partially restored. The response of a prototype bridge structure was analyzed under earthquake loadings using OpenSees software considering different numbers and locations of repaired columns in the model. A technique was developed to model the response of the repaired column that accounted for the different damage and repair conditions along the column. The bridge models with one or more of the repaired columns were found to be capable of resisting the base shear and drift demand by the 40 ground motion records selected according to the target design spectrum, which confirmed the effectiveness of the repair.

ACKNOWLEDGMENTS

My sincere gratitude goes first to my advisor, Dr. Lesley Sneed. Without her continuous support, encouragement, and guidance throughout this study, this dissertation would never be accomplished. Dr. Lesley Sneed has been a mentor, colleague, as well as a friend to me. Thanks for her relentless belief in me and being always there when I need help. I would also like to thank all my committee members, Drs. Abeldjelil Belarbi, Genda Chen, John Myers, and K. Chandrashekhara for their valuable suggestions and guidance. I sincerely appreciate that they have devoted their valuable time to help improve my work. Special thanks go to Dr. Abeldjelil Belarbi for providing the test specimens and to Dr. Genda Chen for offering valuable comments on the analytical study.

This project was funded in part by the University of Missouri Research Board and the Center for Transportation Infrastructure and Safety (CTIS). Repair materials were donated by BASF Company. Their financial support and generous donations to this study are highly appreciated.

I also owe thanks to the staff in the Structures High Bay Lab at Missouri S&T, especially Jason Cox, John Bullock, Brian Swift, Gary Abbott, and Steve Gabel. My group members, Stephen Grelle, Corey Grace, Qian Li, Adam Morgan and Yang Yang also helped me a lot throughout the repair and testing processes. My special thanks go to Dr. Qian Li, who made much effort in preparing all the specimens in the previous study.

I am deeply indebted to my parents, and the families of my sisters and brothers. They have supported me both financially and spiritually during my academic endeavors. My special thanks go to my colleague and husband, Yang Yang, for his companionship and help in my PhD program.

TABLE OF CONTENTS

	Page
PUBLICATION DISSERTATION OPTION.....	iii
ABSTRACT.....	iv
ACKNOWLEDGMENTS	v
LIST OF ILLUSTRATIONS.....	x
LIST OF TABLES.....	xiii
SECTION	
1. INTRODUCTION	1
1.1. BACKGROUND	1
1.2. OBJECTIVES AND SCOPE OF WORK.....	3
1.3. SIGNIFICANCE.....	4
1.4. DISSERTATION OUTLINE.....	4
PAPER	
I. SEISMIC REPAIR OF REINFORCED CONCRETE BRIDGE COLUMNS: A REVIEW OF RESEARCH FINDINGS	6
Abstract	6
Introduction	7
Research Significance	9
Background - Earthquake Damage to RC Bridge Columns.....	9
Repair of RC Bridge Columns	11
Repair of RC Bridge Columns without Fractured Longitudinal Bars.....	11
Reinforced concrete (RC) jackets	12
Steel jackets	12
Fiber-reinforced polymer (FRP) jackets	13
Shape memory alloys (SMA)	18
Repair of RC Bridge Columns with Fractured Longitudinal Bars.....	19
Summary	23
Numerical Analysis of Repaired RC Bridge Columns.....	25
Modeling of Repaired RC Columns.....	25
Other Considerations.....	27
Summary	29
Concluding Remarks	29
Acknowledgements	30

References	31
List of Tables.....	36
List of Figures	36
II. RAPID REPAIR OF SEVERELY DAMAGED RC COLUMNS WITH DIFFERENT DAMAGE CONDITIONS: AN EXPERIMENTAL STUDY	40
Abstract	40
1. Introduction.....	41
2. Original Columns.....	42
3. Column Damage Conditions.....	43
4. Rapid Repair of Damaged Columns	44
4.1 Repair Materials	44
4.2 Repair Procedure	45
4.3 Test Setup and Loading Protocol	46
5. CFRP Layouts.....	47
6. Test Results.....	49
6.1 Summary of Failure Modes.....	49
6.2 General Behavior of Repaired Columns	50
6.3 Evaluation of the Repair Technique.....	51
6.3.1 Strength Index.....	52
6.3.2 Stiffness Index	52
6.3.3 Ductility Index	54
7. Conclusions.....	55
Acknowledgements	56
References	56
III. RAPID REPAIR OF A SEVERELY DAMAGED RC COLUMN HAVING FRACTURED BARS USING EXTERNALLY BONDED CFRP	82
ABSTRACT	82
1. Introduction.....	83
2. Background.....	84
2.1. Design of original columns	84
2.2. Damage evaluation of original columns.....	85
3. Column repair materials.....	86
4. Repair design	87
4.1. CFRP design.....	87
4.1.1. Column 1-R.....	87
4.1.2. Columns 2-R and 3-R	90
4.2. Anchorage	91
4.2.1. Column 1-R.....	91
4.2.2. Columns 2-R and 3-R	91

5. Repair procedure.....	92
6. Test procedure.....	92
7. Discussion of test results.....	94
7.1. Overall behavior and observed damage	94
7.2. Load-deformation response.....	95
7.3. Load-surface strain response.....	97
7.4. Comparison of the repaired and original columns	98
8. Conclusions.....	100
Acknowledgements	102
References	102
IV. TORSIONAL REPAIR OF SEVERELY DAMAGED COLUMN USING CARBON FIBER-REINFORCED POLYMER.....	135
ABSTRACT	135
INTRODUCTION.....	136
RESEARCH SIGNIFICANCE	137
EXPERIMENTAL PROGRAM.....	138
Description of original column	138
Loading protocol of original column	138
Damage evaluation of original column	139
Repair scheme	139
Loading protocol of repaired column.....	140
TORSIONAL REPAIR DESIGN USING EXTERNALLY BONDED CFRP.....	141
Predicting torsional strength of RC members with externally bonded FRP.....	141
Design of CFRP system for repaired column.....	143
EXPERIMENTAL RESULTS	144
Observed behavior and failure mode of repaired column	144
Torsional moment versus twist response	145
Stiffness attenuation	147
EVALUATION OF THE TORSIONAL REPAIR DESIGN.....	148
Measured strain in externally bonded CFRP.....	148
Average strain in externally bonded CFRP at each level.....	149
Contribution of externally bonded CFRP and repaired RC column	150
CONCLUDING REMARKS	151
ACKNOWLEDGEMENTS	152
REFERENCES.....	153
V. POST-REPAIR SEISMIC PERFORMANCE OF DAMAGED RC BRIDGE COLUMNS WITH FRACTURED BARS – A NUMERICAL ASSESSMENT ..	171
ABSTRACT	171

1. INTRODUCTION.....	172
2. MODELING OF INDIVIDUAL RC BRIDGE COLUMNS.....	173
2.1 Modeling of Original Column.....	174
2.1.1 Fiber Section Properties.....	174
2.1.2 Column Numerical Model.....	175
2.1.3 Model Validation.....	177
2.2 Modeling of Repaired Column.....	177
2.2.1 Damage Prior to Repair and Repair Program.....	177
2.2.2 Column Numerical Model.....	178
2.2.3 Model Validation.....	179
3. MEASURED COLUMN CAPACITIES.....	179
4. MODELING OF THE RC BRIDGE STRUCTURE.....	180
4.1 Background of the Selected Bridge.....	180
4.2 Bridge Numerical Model.....	181
4.3 Modal Analysis.....	182
5. DYNAMIC TIME HISTORY ANALYSIS OF RC BRIDGES.....	182
5.1 Selection of Ground Motion (GM) Records.....	183
5.2 Demand Results.....	183
5.3 Discussion of the Results.....	184
6. CONCLUSIONS.....	186
7. ACKNOWLEDGMENTS.....	187
REFERENCES.....	187

SECTION

2. SUMMARY, CONCLUSIONS, AND RECOMMENDATIONS.....	210
2.1. SUMMARY OF RESEARCH WORK.....	210
2.2. CONCLUSIONS.....	212
2.3. RECOMMENDATIONS.....	215

APPENDICES

A. EXPERIMENTAL STUDY.....	216
B. REPAIR MATERIALS.....	227
C. REPAIR DESIGN METHODOLOGY.....	256
D. CFRP SURFACE STRAIN ANALYSIS.....	264
E. SELECTED GROUND MOTION RECORDS.....	315

BIBLIOGRAPHY.....	327
-------------------	-----

VITA.....	333
-----------	-----

LIST OF ILLUSTRATIONS

	Page
PAPER I	
Figure 1. Numerical Analysis of Repaired RC Columns.....	39
 PAPER II	
Fig. 1. Geometry and reinforcement details of original columns.	62
Fig. 2. Damage conditions of the original columns after previous tests.....	63
Fig. 3. Test setup for original and repaired columns.	64
Fig. 4. CFRP layout for Column 1-R.....	65
Fig. 5. CFRP layout for Column 2-R.....	66
Fig. 6. CFRP layout for Column 3-R.....	67
Fig. 7. CFRP layout for Column 4-R.....	68
Fig. 8. CFRP layout for Column 5-R.....	69
Fig. 9. Novel anchorage system.....	70
Fig. 10. General behavior of Column 1-R compared to Column 1.....	71
Fig. 11. General behavior of Column 2-R compared to Column 2.	72
Fig. 12. General behavior of Column 3-R compared to Column 3.....	73
Fig. 13. General behavior of Column 4-R compared to Column 4.....	74
Fig. 14. General behavior of Column 5-R compared to Column 5.....	75
Fig. 15. Toque-to-moment ratios for Column 4 and Column 4-R.....	76
Fig. 16. Strength indices for repaired columns.	77
Fig. 17. Stiffness indices of initial state for repaired columns.....	78
Fig. 18. Idealized envelopes for original and repaired columns.	79
Fig. 19. General service stiffness indices for repaired columns.	80
Fig. 20. Ductility indices for repaired columns.	81
 PAPER III	
Fig. 1. Geometry and reinforcement details of original columns.	110
Fig. 2. Damage to Column 1 ($T/M=0$).	111
Fig. 3. Damage to Column 2 ($T/M=0.2$).	112
Fig. 4. Damage to Column 3 ($T/M=0.4$).	113
Fig. 5. Moment-curvature curves for final repair design of Column 1-R ($T/M=0$).	114

Fig. 6. Final repair design for Column 1-R ($T/M=0$).....	115
Fig. 7. Final repair design for Column 2-R ($T/M=0.2$).....	116
Fig. 8. Final repair design for Column 3-R ($T/M=0.4$).....	117
Fig. 9. Details of novel anchorage system.....	118
Fig. 10. U-anchor used on east and west faces of Columns 2-R and 3-R.....	119
Fig. 11. Repair procedure.....	120
Fig. 12. Test setup of repaired column.....	121
Fig. 13. Hysteresis response of repaired Column 1-R ($T/M=0$).....	122
Fig. 14. Failure of repaired Column 1-R ($T/M=0$) - northwest corner.....	123
Fig. 15. Failure of repaired Column 1-R ($T/M=0$) - south side.....	124
Fig. 16. Hysteresis behavior of repaired Column 1-R compared to original Column 1 ($T/M=0$).....	125
Fig. 17. Hysteresis behavior of repaired Column 2-R compared to original Column 2 ($T/M=0.2$).....	126
Fig. 18. Hysteresis behavior of repaired Column 3-R compared to original Column 3 ($T/M=0.4$).....	127
Fig. 19. Location of the strain gauges applied on Column 1-R ($T/M=0$).....	128
Fig. 20. Load-longitudinal surface strain relationship - Column 1-R ($T/M=0$).....	129
Fig. 21. Load-transverse surface strain relationship - Column 1-R ($T/M=0$).....	130
Fig. 22. Force-displacement relationship of original Column 1 ($T/M=0$).....	131
Fig. 23. Force-displacement relationship of repaired Column 1-R ($T/M=0$).....	132
Fig. 24. Force-displacement relationship of Column 2-R ($T/M=0.2$).....	133
Fig. 25. Force-displacement relationship of Column 3-R ($T/M=0.4$).....	134

PAPER IV

Fig. 1 - Details of original column.....	160
Fig. 2 - Damage condition of concrete in original column.....	161
Fig. 3 - Damage condition of reinforcing steel in original column.....	162
Fig. 4 - Test setup for repaired column.....	163
Fig. 5 - Failure of repaired column.....	164
Fig. 6 - Hysteresis behaviors of original and repaired columns.....	165
Fig. 7 - Torsional moment-twist envelopes of repaired column compared to original column.....	166

Fig. 8 - Torsional stiffness attenuation of repaired column compared to original column.....	167
Fig. 9 - CFRP strain gage layout and relation to repaired column damage location	168
Fig. 10 - Average transverse surface strain-torsional moment relationship of repaired column.....	169
Fig. 11 - Average longitudinal surface strain-torsional moment relationship of repaired column	170

PAPER V

Fig. 1. Geometry and reinforcement details of original column.....	193
Fig. 2. Fiber discretization of the cross-section	194
Fig. 3. Comparison of measured and calculated moment-curvature relationships for original column	195
Fig. 4. Numerical model for original column	196
Fig. 5. Comparison of the measured and calculated response for original column	197
Fig. 6. Damage to original column prior to repair	198
Fig. 7. Numerical model for repaired column.....	199
Fig. 8. Comparison of the measured and calculated response for repaired column	200
Fig. 9. Idealized load-displacement envelope for original and repaired columns	201
Fig. 10. Numerical model of bridge structure.....	202
Fig. 11. Details of bent elements	203
Fig. 12. Spectral acceleration for the selected GM records	204
Fig. 13. Drift ratio demand of columns under selected earthquake records for each bridge model	205
Fig. 14. Base shear demand of columns under selected earthquake records for each bridge model	206
Fig. 15. Summary of drift ratio demand of columns under the selected earthquake records for each bridge model.....	207
Fig. 16. Summary of maximum base shear demand of columns under selected earthquakes for each bridge model	208
Fig. 17. Average base shear demand of columns under selected earthquake records for each bridge model	209

LIST OF TABLES

	Page
Table 1.1. Column Number Designation	5
PAPER I	
Table 1. Summary of Studies on Repair of Reinforced Concrete Bridge Columns without Fractured Longitudinal Bars	37
Table 2. Summary of Studies on Repair of Reinforced Concrete Bridge Columns with Fractured Longitudinal Bars	38
PAPER II	
Table 1. Summary of damage to original columns	59
Table 2. Repair mortar properties (provided by the manufacturer)	60
Table 3. Summary of failure modes of repaired columns	61
PAPER III	
Table 1. Summary of damage to original columns	106
Table 2. Idealized response values for original and repaired columns	107
Table 3. Comparison of results	108
Table 4. Response indices for the repaired columns	109
PAPER IV	
Table 1. Properties of repair mortar and CFRP system	156
Table 2. Torsional moment and corresponding twist at cracking, yielding, and maximum states	157
Table 3. Contribution of the transverse and longitudinal CFRP	158
Table 4. Estimation of contribution of repaired RC column	159
PAPER V	
Table 1. Natural frequency of bridge structure models	191
Table 2. Selected earthquake ground motion records	192

1. INTRODUCTION

1.1. BACKGROUND

Damage to bridge structures during an earthquake can have devastating social and economic consequences, particularly for bridges located along key routes that are critical for emergency response and other essential functions. Such bridges are defined as “important” by ATC-18 (1997), which stipulates that damage from an earthquake should be repairable within three days. Thus rapid and efficient repair techniques are required to restore the functionality of the bridge for emergency vehicles to provide timely service and mitigate the impact on the affected community. As such, rapid repair may also be referred as “emergency” repair due to the fact that long term effects are not considered in the repair.

Extensive research has been conducted on seismic *retrofit* of reinforced concrete (RC) structures (e.g., Chai et al. 1991, Priestley et al. 1994, Saadatmanesh et al. 1996, Seible et al. 1997, Saiidi et al. 2001, Laplace et al. 2005). Few studies, however, have focused on seismic *repair* of RC structures (Priestley et al. 1993, Saadatmanesh et al. 1997, Lehman et al. 2001, Cheng et al. 2003, Li and Sung 2003, Saiidi et al. 2004, Belarbi et al. 2008, and Shin et al. 2011). The term *repair* in this study refers to the work to restore a damaged structure to its original capacity in terms of strength and displacement, which is different from *retrofit*, which refers to the work to upgrade the capacity of a structure with inadequate design. The main difference lies in how to consider the contributions of the reinforcing steel and concrete of the host member. The analysis for RC column *retrofit* is based on full contribution of reinforcing steel and concrete, while the damage to the reinforcement and concrete should be considered in RC column *repair*.

In most repair studies, rapid repair has not been emphasized, and the timely reopening of the structure to traffic has not been a primary consideration. Although various techniques have been shown to be effective in restoring the capacity of damaged RC columns, they generally require considerable time, expert workers, and/or specialized equipment during construction. Therefore, most methods in the literature are difficult to accomplish as part of an emergency rapid repair. Recently, some work has been

conducted on rapid repair of RC columns using externally bonded carbon fiber reinforced polymer (CFRP) composites (Vosooghi et al. 2008, 2009, 2010) and other advanced materials such as shape memory alloys (Shin et al. 2011). These studies were focused on columns with circular cross section that were damaged under cyclic bending moment and shear, without the inclusion of torsion. Though some studies have focused on torsional strengthening of RC members (e.g., Matthys and Triantafillou 2011, Ghobarah et al 2002, Panchacharam and Belarbi 2002, and Chalioris 2008), no work has been done on rapid repair of RC columns severely damaged under combined axial, shear, flexural, and torsional loading.

The use of externally bonded strengthening systems can significantly shorten the time required to complete a repair. FRP composites are particularly attractive for this purpose due to their high strength- and stiffness- to-weight ratios and ease of installation compared with other materials. In addition, decades of study have undeniably demonstrated the effectiveness of FRP in repairing and strengthening RC columns.

Local modifications (interventions) from the retrofit or repair of an individual RC column member can change the performance of the member, which in turn can influence the performance of the bridge structure in which the column is included, especially under seismic loading. In general, the seismic performance of a bridge structure will be improved when the retrofit or repair is carried out uniformly for all the members. Modifications to a single member or only some of the members of a bridge structure, on the other hand, may result in a stiffness irregularity, which can result in an unbalanced seismic demand on the members of the structure. To date, most research on seismic repair or retrofit of RC bridges has focused on assessing the response of individual columns (member level), not the bridge structure (system level), considering that columns are the primary source of energy dissipation for a bridge structure during an earthquake and due to limitations in modeling and especially testing of full bridge structures. Thus, the need exists to develop techniques to reflect the effects of the intervention on the entire bridge structure. With the availability of increasingly powerful computers, researchers and engineers are provided an opportunity to implement numerically intensive modeling strategies. In particular, analytical tools based on the fiber element have shown the

effectiveness in simulating the response of RC members under earthquake loadings (e.g. Xiao and Ma 1997, Shao et al. 2005, and Zhu et al. 2006).

1.2. OBJECTIVES AND SCOPE OF WORK

The major objective of this study is to develop a technique to rapidly repair severely damaged RC columns under combined loading effects including torsion. The technique used to repair the columns included externally bonded CFRP composites. In order to evaluate the effectiveness of the developed repair method, both experimental and analytical studies have been conducted in this research. The experimental study included five 1/2-scale RC column specimens subjected to different combined loading conditions. The five columns are designated as Columns 1 to 5 throughout this dissertation and are summarized in Table 1.1. Column 1 was subjected to cyclic uniaxial cantilever bending and shear ($T/M=0$) in addition to constant axial load. Columns 2, 3, and 4 were subjected to constant axial load and a combined cyclic loading effect of uniaxial cantilever bending, shear, and torsion, with torsional moment-to-flexural moment ratios (T/M) of 0.2, 0.4, and 0.6, respectively. Column 5 was tested under pure torsion ($T/M=\infty$) in addition to constant axial load.

To achieve the objective of this study, the scope of work included the following:

- ◆ Evaluate the damage conditions of columns prior to repair;
- ◆ Propose repair design methods for columns damaged under different combined loading with different damage conditions, based on a comprehensive literature review of previous studies on retrofit and repair techniques;
- ◆ Conduct the rapid repair procedure in a three-day period along with the arrangement of instrumentation, and retest the repaired columns under the same combined loading as the corresponding original columns following the repair;
- ◆ Analyze the data collected during the test and compare it to the original response to evaluate the repair performance;
- ◆ Develop nonlinear fiber element models to simulate the response of the original (undamaged) and repaired columns;

- ◆ Conduct a seismic assessment of the post-repair response of an RC bridge with buckled and fractured column bars to evaluate how the repair would influence the response of the entire bridge system, in which the developed models for the original and repaired columns were employed after validation with the experimental results.

1.3. SIGNIFICANCE

This research fills in critical gaps in the literature on repair of RC bridge columns with respect to the severe damage level and the inclusion of torsion. The large scale nature of the test specimens in this study allowed for evaluation of the constructability of the proposed repair technique in practice.

1.4. DISSERTATION OUTLINE

This dissertation includes three sections and five appendices. Section 1 provides a brief introduction to the subject area and explains the need for the current research study. The first section also presents the objectives and scope of work of the investigation.

Section 2 presents three published journal papers and two journal papers under review or in process. The first paper is a detailed literature review to establish the state-of-the-art on the studied topic, which presents a comprehensive summary and review of techniques to repair earthquake-damaged RC bridge columns, as well as numerical analysis methods for repaired columns. The second paper presents the experimental study on rapid repair of the five severely damaged RC columns with different damage conditions included in this study. The third paper focuses on the repair of flexure dominant columns, and the fourth paper focuses on torsional repair. The fifth paper presents a seismic assessment of the post-repair response of an RC bridge with buckled and fractured column bars.

Section 3 summarizes the findings and conclusions of this study and proposes future research.

There are five appendices at the end of this dissertation, which include a detailed discussion of the experimental study in Appendix A; detailed information of the materials used in the rapid repair in Appendix B, in which both the measured results and the data

sheets provided by the manufacturers are provided, in addition to the testing results of bond strength between CFRP and the host concrete; repair design methodology in Appendix C; CFRP surface strain time history results with the locations of the strain gauges applied on the five repaired columns in Appendix D; and the 40 scaled ground motion records in Appendix E.

Table 1.1 Column Number Designation

COLUMN DESIGNATION	LOADING TYPE	T/M	TRANSVERSE REINFORCEMENT RATIO	LONGITUDINAL REINFORCEMENT RATIO
1	Flexure/Shear (no torsion)	0	1.32%	2.13%
2	Flexure/Shear/Torsion	0.2	1.32%	2.13%
3	Flexure/Shear/Torsion	0.4	1.32%	2.13%
4	Flexure/Shear/Torsion	0.6	1.32%	2.13%
5	Torsion	∞	1.32%	2.13%

PAPER

I. SEISMIC REPAIR OF REINFORCED CONCRETE BRIDGE COLUMNS: A REVIEW OF RESEARCH FINDINGS

Ruili He¹; Yang Yang²; and Lesley H. Sneed³

Abstract

Repair has become a viable option for restoring the use of earthquake-damaged reinforced concrete (RC) elements, even those that have been severely damaged. To select and design an appropriate repair system for damaged RC bridge columns, it is important that results from previous research studies are known. This paper presents a comprehensive summary and review of techniques to repair earthquake-damaged RC bridge columns, as well as numerical methods for analyzing the response of repaired columns. Repair of columns without and with fractured longitudinal reinforcing bars are discussed. Studies are reviewed in terms of the apparent damage, repair technique, and performance of the repair. Advantages and disadvantages associated with each repair technique are discussed, and areas in need of future research are explored.

Keywords: Columns, buckled bars, fiber-reinforced polymer composites, fractured bars, jacketing, numerical analysis, reinforced concrete, repair.

Introduction

Seismic repair and retrofit of reinforced concrete (RC) structures has been the subject of much recent investigation. The term *repair* in this paper refers to the work to restore a damaged structure to some extent of its original, or as-built, capacity in terms of strength, stiffness, and/or ductility; while the term *retrofit* refers to the work to upgrade the capacity of a structure that was inadequately designed or detailed to meet the current seismic requirements. The major challenge related to repair, which also differentiates between repair and retrofit, is the need to estimate the residual capacity of the damaged structure, which usually involves many simple and/or conservative assumptions. For seismic design of bridge structures, columns are typically chosen as the location for inelastic deformation, and bridge columns are designed as the primary source of energy dissipation during an earthquake. Accordingly, an extensive number of research studies have been conducted on seismic repair and retrofit of RC bridge columns.

RC bridge columns constructed in the U.S. prior to the 1970s are considered to be sub-standard because they were not adequately detailed to resist seismic loads. They have severely inadequate transverse reinforcement and longitudinal reinforcing bars that are typically lap spliced at the base; thus the common failure modes of these columns are characterized as shear, bond degradation in the lap-splice zone, premature concrete failure due to lack of confinement, or a combination of these. Accordingly, a significant number of research studies have focused on seismic retrofit of existing sub-standard RC columns. Preventing brittle shear failure, preventing splice failure, and providing a target flexural ductility are the three major objectives of seismic retrofit as explained by Seible et al. (1997). The most common seismic retrofit techniques for RC bridge columns involve the application of RC jackets (e.g., Rodriguez and Park 1994; Bett et al. 1988), steel jackets (e.g., Chai et al. 1991; Priestley et al. 1994a, 1994b; Saiidi et al. 2001; Laplace et al. 2005), or fiber reinforced polymer (FRP) composite jackets (e.g., Saadatmanesh et al. 1996; Seible et al. 1997).

According to US seismic design practice after 1971, RC bridge columns are detailed to preclude the brittle failure modes occurring in sub-standard columns mentioned above. Such seismically detailed columns are also expected to experience damage during moderate or strong earthquakes, and they are required to avoid collapse

under the maximum credible earthquake. The level of damage is a function of different factors related to the earthquake loading and the affected bridge structure itself such as ground shaking intensity, earthquake type, and force/deformation demand on individual members. It is cumbersome, time consuming, and expensive to replace damaged RC bridge columns. Therefore, appropriate repair methods are needed to restore the damaged columns. Typical repair techniques for RC bridge columns involve epoxy injection into cracks (French et al. 1990), repair of spalled concrete, and/or application of jackets as external reinforcement. Reinforced concrete (Bett et al. 1988, Fukuyama et al. 2000, Lehman et al. 2001), steel (Chai et al. 1991 et al., Fukuyama et al. 2000, Elsouiri and Harajli 2011), and FRP (Priestly et al. 1993, Saadatmanesh et al. 1997, Sheikh and Yau 2002, Li and Sung 2003, Cheng et al. 2003, Saiidi and Cheng 2004, Chang et al. 2004, Nesheli and Meguro 2006, Belarbi et al. 2008, Vosooghi et al. 2008, Vosooghi and Saiidi 2009, He et al. 2013a,b and 2014, Rutledge et al. 2013) are commonly used as jacketing materials for seismic repair of RC columns with different damage levels, similar to retrofit of RC columns.

Repair objectives vary with the design details of as-built columns. For damaged sub-standard bridge columns, the repair aims not only to restore the structure to its as-built state but also to improve the performance in terms of strength and ductility in a future earthquake; however, for seismically detailed RC bridge columns, the goal of the repair is to restore the structure to its as-built state. In some cases as for bridges located along key routes that are critical for emergency response and other essential functions, defined as “important” by ATC-18 (1997), rapid repair methods are needed to temporarily restore some level of function and prevent damage from extending to other regions. In such a repair, sometimes referred to as an “emergency repair,” a lower limit state (or service level) may be allowed for the structure than the as-built condition.

In all cases, the “*initial*” condition of the column is different for the case of repair than for the case of retrofit because the repair must compensate for loading and damage that have occurred prior to repair. Several additional challenges that differentiate seismic repair from seismic retrofit include the need for estimation of damage and/or inelastic response that has occurred, estimation of the mechanical properties of the base materials (both before and after the seismic event), compatibility of the repair materials with the

base materials, and constructability of the repair. The first two factors must be considered in order to determine the initial state of the column, and all of these factors can complicate the design and/or analysis of repaired RC columns.

This paper summarizes experimental works on seismic repair of RC bridge columns with different damage levels and numerical methods for analyzing the response of repaired RC columns, which make up the two major sections of this paper. In accordance with the different emphases in the repair considerations and unique challenges in repairing damaged RC columns with fractured longitudinal bars, experimental works are organized into separate sections on repair of damaged columns without and with fractured longitudinal reinforcing bars. Each study is reviewed with emphasis on the repair technique and effectiveness. Advantages and disadvantages associated with the repair techniques are also summarized.

Research Significance

The objective of this paper is to collect up-to-date information on repair of both sub-standard and seismically detailed RC bridge columns to facilitate development and improvement of seismic repair methods. This paper also includes a discussion on the recent progress and current challenges with numerical analysis of repaired RC bridge columns. This paper focuses on repair of earthquake-damaged RC bridge columns; the repair of RC building columns or RC bridge columns damaged by other means is outside the scope of this paper.

Background - Earthquake Damage to RC Bridge Columns

RC bridge columns may experience complex combined axial, shear, bending, and torsional loadings during an earthquake. The resulting apparent damage may include cracking or spalling of concrete cover, crushing of the concrete core, and buckling and/or fracture of reinforcement. Recent studies have focused on post-earthquake evaluation of RC bridge columns to correlate the apparent damage and internal and external seismic response parameters, which ultimately can be utilized in the repair design for restoration of service to the bridge. Damage was classified in terms of three damage levels in ATC-32 (1996): minimal; repairable; and significant. Damage is

classified as significant if a permanent offset is apparent, if the reinforcement has yielded, or if major concrete spalling has occurred; repairable damage is not quantitatively defined in ATC-32.

Five distinct damage states were proposed in a study by Vosooghi and Saiidi (2010) based on a review of shake table test data of thirty RC bridge columns: DS-1: flexural cracks; DS-2: first spalling and shear cracks; DS-3: extensive cracks and spalling; DS-4: visible transverse and longitudinal bars; DS-5: imminent failure. The standard columns reviewed were controlled by flexure or flexure/shear, while the sub-standard columns reviewed were mostly controlled by shear.

A study by Belarbi et al. (2010) illustrated that the responses and failure modes of RC columns under combined axial, shear, bending, and torsional loading are highly complex and are affected by the member geometry and sectional details (column aspect ratio, thickness of concrete cover, longitudinal and transverse reinforcement ratios, etc.), material properties (unconfined and confined concrete, longitudinal and transverse reinforcement, etc.), and loading combinations (axial load index, torsional moment-to-bending moment ratio, loading history, etc.). Possible failure sequences under combined loading were identified as: (1) flexural and shear cracking; (2) longitudinal reinforcement yielding; (3) cover spalling; (4) crushing of the diagonal compression strut; (5) yielding of the transverse reinforcement; (6) longitudinal bar buckling, spiral fracture, and longitudinal bar fracture.

The most severe damage is associated with column failure or imminent failure, which has been defined in different ways. Based on the definition given by Lehman et al. (2001), visible evidence of core concrete crushing, longitudinal bar buckling, or longitudinal/transverse reinforcement fracture is classified as severe damage. For the purpose of the PEER Structural Performance Database (Berry et. al 2004), failure is defined as the first occurrence of one of the following: buckling or fracture of a longitudinal bar, fracture of a transverse bar, or loss of axial-load capacity. If experimental test data are available, researchers often consider that failure is reached when a significant reduction in strength is achieved and the stiffness starts degrading (Belarbi et al. 2010). When bar fracture occurs, the reduction in member resistance caused by bar fracture makes itself evident in the force-deformation response of the

member as an abrupt and significant drop in the force. Thus, unless bar fracture occurs in the post-peak response of the member, failure is often considered to be associated with the cycle when fracture occurs.

Repair of RC Bridge Columns

From the discussion in the previous section, it is clear that the existence of fractured longitudinal bars constitutes a severe level of damage to RC columns, and furthermore poses additional challenges associated with treatment of those bars to restore the capacity. Repair techniques for RC bridge columns without or with fractured longitudinal bars are discussed separately in the following sections.

Repair of RC Bridge Columns without Fractured Longitudinal Bars

For damaged RC bridge columns without fractured longitudinal bars, the repair can usually be accomplished by injecting cracks, replacing damaged concrete, and sometimes strengthening the column with supplementary reinforcement to compensate for the strength loss due to softened concrete and/or yielded internal reinforcement and to provide confinement to improve ductility. In cases of repairing RC columns with slight to moderate concrete damage, concrete repair alone may be adequate without application of an external strengthening system, although a lower initial stiffness can be anticipated (French et al. 1990, Lehman et al. 2001). Reinforced concrete (Bett et al. 1988, Fukuyama et al. 2000), steel (Chai et al. 1991., Fukuyama et al. 2000, Elsouiri and Harajli 2011), FRP (Priestly et al. 1993, Saadatmanesh et al. 1997, Sheikh and Yau 2002, Li and Sung 2003, Chang et al. 2004, Nesheli and Meguro 2006, Belarbi et al. 2008, Vosooghi et al. 2008, Vosooghi and Saiidi 2009, He et al. 2013a, 2014, Rutledge et al. 2013), and other materials (Shin and Andrawes 2011) have been used as external strengthening systems in repair applications. This section summarizes experimental works attempting to repair RC columns without fractured longitudinal bars. The studies are presented in terms of type of strengthening system. Aspects including scale of test specimen, damage state of the column prior to repair, repair technique, and effectiveness of repair are discussed for each study and are summarized in Table 1.

Reinforced concrete (RC) jackets

RC jackets have been used to repair earthquake-damaged columns for several decades. RC jackets usually involve enlarging the column cross-section with reinforced concrete along part of or the entire length of the column, and in some cases, connecting the reinforcement in the jacket to the encased damaged column.

Bett et al. (1988) reported the repair of a 2/3-scale square RC column with a RC jacket. The column was subjected to a constant axial load and reversed cycles of lateral displacement. The as-built column was designed as sub-standard and experienced a brittle, shear-dominated failure due to the shear span-to-depth (aspect) ratio and inadequate reinforcement details. The severely damaged column was repaired by encasing the core in a concrete jacket reinforced with closely spaced ties and cross-ties connected to the mid-face longitudinal bars. Test results showed that the repaired column was stiffer and stronger than the original column and performed nearly as well as columns retrofitted using the same technique as the repair.

Fukuyama et al. (2000) reported the repair of a 1/2-scale square RC column. Cyclic lateral load was applied to the column while the axial compressive load was held constant (30% of the axial capacity), which resulted in heavy damage including crushed core concrete. The column was repaired by enlarging the cross-section with a RC jacket with welded wire shear reinforcement and high-fluidity concrete. The crushed concrete within the concrete core was left untreated. Test results showed that the repaired column had a higher shear strength and ductility than the as-built column. Also, the stiffness of the repaired column was increased compared to the original column as determined from the shear force-hysteresis loops.

Steel jackets

Repair of RC columns using steel jackets usually involves casting new concrete to restore the cross-section, installing the steel jacket by in-field welding parts along the length of the jacket, and filling the gap between the jacket and column with cement based grout (Weyers et al. 1993, Ghasemi et al. 1996, and Itani 2003). In some cases, the original cross-section may also be enlarged.

Chai et al. (1991) proposed a repair technique that involved encasing the column plastic hinge region in a bonded steel jacket. A 2/5-scale circular sub-standard RC bridge column with inadequate lap splice lengths of the longitudinal bars had previously been tested to high drift ratio under constant axial load (17% of the axial capacity) and reversed cyclic lateral load. Testing resulted in bond failure of the spliced reinforcement in the plastic hinge region. Tests of the repaired column showed that the repair was able to enhance the strength and ductility compared to the as-built column.

Fukuyama et al. (2000) reported the repair of a 1/2-scale square RC column with a steel jacket. The column was tested under constant axial load (30% of the axial capacity) and cyclic lateral load resulting in crushed core concrete and buckled longitudinal bars. The repair involved arranging additional longitudinal reinforcing bars outside the buckled bars, leaving the crushed concrete in the column untreated, enlarging the cross-section by placing steel plates along the perimeter of the column, and grouting high-fluidity concrete in the gap between the steel plates and crushed concrete. Test results showed that the repaired column had a higher shear strength and ductility than the as-built column. Also, the stiffness of the repaired column was increased as a result of increasing the column cross-section.

Elsouri and Harajli (2011) reported a study on repair of lap splices in RC columns using steel ties and/or FRP wraps for confinement. They tested 3 full-scale rectangular columns with different longitudinal reinforcement ratios. The columns were subjected to cyclic lateral load without axial load. Prior to repair, the columns had experienced bond failure of the starter bars and extensive concrete damage within the splice region. The thickness of confining material was estimated by the method proposed by Darwin et al. (2005). The results showed that the repaired columns achieved considerably larger lateral loads and energy dissipation capacities than the as-built columns. The effectiveness of the method was also confirmed by analytical results assuming perfect bond between lap spliced bars, which were similar to the experimental results.

Fiber-reinforced polymer (FRP) jackets

In recent decades, FRP composites have become increasingly popular in repairing and strengthening RC members. Fibers may be oriented in different directions to

achieve different objectives. FRP with fibers oriented in the hoop direction (transverse to the axis of the column) functions similarly to stirrups and help confine the core concrete so that the shear strength and ductility of the column can be improved. FRP with fibers oriented along the longitudinal axis of the column functions mainly to increase the flexural strength of the repaired column.

In a study by Priestley et al. (1993), a glass FRP (GFRP) jacket and epoxy injection was used to repair a 2/5-scale sub-standard circular RC bridge column without lap splices. The column had been tested to failure under reversed cyclic loading and constant axial load (axial load index of 18%). The damage included open diagonal cracks and spalled concrete. The repair procedure included removing the loose concrete, patching with cement and sand mortar, injecting epoxy in all cracks, and applying a full-height GFRP jacket. The test results indicated that the initial stiffness of the column was fully restored by the repair, and the repaired column reached a higher displacement ductility than that of the as-built column.

Saadatmanesh et al. (1997) conducted a study on repairing earthquake-damaged RC columns with prefabricated GFRP composite straps. The specimens included four 1/5-scale RC columns with seismic deficiencies. Two of the columns had a circular cross-section, and two had a rectangular cross-section. The columns were tested to failure under reversed cyclic lateral loading and constant axial load. At the end of the initial tests, the columns experienced severe damage including debonding of starter bars, spalling and crushing of concrete, buckling of longitudinal reinforcement, and separation of the longitudinal bars from the core concrete. The repair procedure consisted of casting fresh concrete after removing spalled and damaged concrete in the failure regions, and applying active confinement with FRP. To apply active confinement, spacers were bonded to the finished surface of the columns to create a gap. The column was then wrapped with FRP sheets. Epoxy grout was pressurized in the gap between the column and the sheets to apply active confining pressure on the column. Test results indicated that the repair technique was effective in restoring both the flexural strength and displacement ductility, which were higher than those of the as-built columns. In all repaired specimens, the initial stiffness was lower, however, the stiffness deterioration under large loading cycles was lower than that of the corresponding as-built columns.

Sheikh and Yau (2002) repaired two circular RC columns with different damage levels. The columns were tested under cyclic loading and a constant axial load (54% of the axial capacity). The first column was tested until flexural cracks, cover concrete spalling, and longitudinal reinforcement yielding occurred, while the second column was tested until both longitudinal and spiral reinforcement yielding occurred. The repair was conducted while the columns maintained 2/3 of the original applied axial load. After loose concrete was removed and the surface was patched, carbon FRP (CFRP) was wrapped around the first column, and GFRP was wrapped around the second column. Results indicated that the performance of the repaired columns was comparable to undamaged specimens that were strengthened.

Li and Sung (2003) conducted an experimental study on an earthquake-damaged sub-standard bridge column repaired with epoxy and non-shrink mortar and strengthened with CFRP wrap. The circular column was a 2/5-scale model constructed with lap-spliced shear reinforcement. The column was tested under cyclic loading and constant axial load (axial load index of 15%) resulting in shear failure at low displacement ductility. Cracks were observed inside the column core, and concrete spalling was observed outside of the core. Test results showed that the repair significantly improved the seismic performance of the column in terms of strength and ductility. The failure mode of the repaired column was altered from shear failure to flexural failure.

In a study by Chang et al. (2004), the seismic performance of two damaged 2/5-scale rectangular bridge columns was effectively restored with a CFRP jacket. The columns were seismically-detailed with no specific structural deficiency. The columns were tested to failure under pseudo dynamic loading. Flexural failure occurred in the plastic hinge zone without fractured longitudinal reinforcement. The repair included replacing the damaged concrete in the plastic hinge zone with non-shrink mortar, followed by application of the CFRP wrap. Additionally, a single layer of CFRP was wrapped around the remainder of the column to provide external confinement. Test results showed that the strength and ductility of the columns were successfully restored. However, the initial stiffness of repaired columns was less than that of the as-built columns, which was attributed to the fact that the CFRP did not bridge the cracks near

the column-footing joint, and the yielding of longitudinal bars may have penetrated into the footing.

In a study by Nesheli and Meguro (2006), two 1/2-scale damaged square RC columns were repaired with pretensioned carbon or aramid FRP belts, which provided both active and passive confinement. One of the columns had been partially retrofitted with pretensioned FRP belts prior to the initial test. The original columns were tested to brittle shear failure with large diagonal cracks under constant axial load and reversed cyclic lateral load. The repair was performed rapidly without removal of damaged concrete or crack injection. As a result of pretensioning the FRP belts, the initial cracks of the damaged column were closed. Test results indicated that the lateral strength of the damaged columns was partially restored.

Belarbi et al. (2008) repaired a 1/2-scale circular RC bridge column that was severely damaged under constant axial load (axial load index of 7%) and cyclic lateral and torsional loading using externally bonded CFRP. Damage to the column included spalled cover concrete, crushed core concrete, and buckled longitudinal reinforcing bars. The damaged column was repaired using externally bonded CFRP with fibers oriented both in the column longitudinal and transverse directions. A mechanical anchorage system was used in an attempt to anchor the longitudinal CFRP sheets to the footing. It was concluded from the test results that the repair method could restore and enhance the flexural, torsional, and axial capacity of the column. It was also concluded that the longitudinal CFRP sheets may not have been required in the repair since they pulled out from the footing at low load levels.

Vosooghi et al. (2008) used CFRP wrap to repair the middle bent of a 1/4-scale two-span bridge model, which was tested to the condition including visible bars, initial buckling in some longitudinal bars, and initial concrete core damage. The columns had a circular cross-section. The bridge specimen was tested under near-field motions increasing gradually with simulating the fault rupture, followed by static loading to increase the damage level. The damaged columns were repaired by CFRP wrapping after repair of the damaged concrete with a fast-set grout and epoxy injection of the adjacent cracks. Retesting of the repaired columns showed that the lateral load capacity

and the ductility of the bent were fully restored, and the service level stiffness was nearly restored to that of the undamaged bent stiffness.

Vosooghi and Saiidi (2009) reported repairing two high shear, standard RC bridge columns using CFRP jackets. The 1/3-scale seismically detailed circular RC bridge columns with spiral reinforcement were tested to near failure on a shake table. The apparent damage included visible spirals and longitudinal bars, buckled longitudinal bars, and damage of core concrete. For both columns, the damaged concrete was replaced by a fast-set non-shrink mortar, and the cracks were epoxy injected. The two damaged columns were repaired with a different number of CFRP layers and different repair mortar and application methods. Test results indicated that the repair design method fully restored the lateral load and drift capacity of the columns, although the service stiffness was not fully restored. Results also suggested that the spirals were able to contribute to the shear capacity, even though they yielded in the initial tests.

He et al. (2013a) rapidly repaired five 1/2-scale square standard bridge columns with different damage conditions using externally bonded CFRP with fibers orientated in the column longitudinal and transverse directions. The columns had been tested to failure under constant axial load (7% of the axial capacity) and combined cyclic lateral and torsional loading with different bending moment-to-torsional moment ratios (T/M). With increasing T/M, the damage region increased along the column height, and the plastic hinge location shifted away from the base. Damage included concrete cracking, cover concrete spalling, and core concrete crushing, as well as longitudinal reinforcement yielding. Damaged ties failed by yielding and, in some cases, subsequent opening of end hooks. Additionally, longitudinal bars buckled in most of the columns, and longitudinal reinforcing bars fractured in one of the columns tested under lateral loading without torsion (discussed in the next section of this paper). Externally bonded CFRP was used to repair each of the damaged columns, and fractured and buckled bars were left untreated. Retesting of the repaired columns under the same combined loading as the corresponding original columns revealed that the repair method was effective in rapidly restoring the bending and/or torsional strength and ductility if there are no fractured longitudinal bars. The stiffness of the columns was not completely restored, which was attributed to the damage accumulated and the fact that only a portion of the

damaged columns was repaired. Further discussion on torsional repair was discussed in detail in a related paper by He et al. (2014).

Two damaged RC bridge columns containing buckled longitudinal bars were repaired by plastic hinge relocation using CFRP with carbon fiber anchors in a study by Rutledge et al. (2013). The circular columns were tested under a load history corresponding to that of two specific earthquakes by controlling the lateral displacement applied to the top of the column in a static manner. A constant axial load was also applied (axial load ratio of 6%). The first column was damaged with buckled longitudinal bars. Following the initial test, the second column was also subjected to additional cyclic “aftershock” loading in a static manner, which resulted in buckled longitudinal bars. The performance of the second column under the aftershock loading was used to compare the performance of the damaged columns subjected to cyclic loading with and without repair. To repair the first column, the original plastic hinge was strengthened with transverse and longitudinal CFRP anchored to the footing with carbon fiber anchors. Additionally, transverse fibers were wrapped around the expected new plastic hinge region to achieve higher curvature at the new plastic hinge location so that the displacement capacity at the top of the column could be restored. Testing of the first repaired column under constant axial load and reversed cyclic lateral displacements indicated an increase in lateral force capacity compared to that of the original column. However, the plastic hinge region did not form in the intended location, which was attributed to underestimation of the confinement provided by the hoop reinforcement. The repair of the second column was similar to that of the first column, except that no hoop fibers were provided for confinement of the expected new plastic hinge region. Testing of the repaired second column indicated a similar increase in strength with respect to the original column, and the plastic hinge was successfully relocated to the location intended. It was concluded that the repair was able to restore the initial stiffness, as well as increase the strength and displacement capacities.

Shape memory alloys (SMA)

SMA was used in a study by Shin and Andrawes (2011) to rapidly repair a 1/3-scale severely damaged circular RC column. The column was tested under constant

axial load (5% of the axial load capacity) and cyclic lateral loading until problems during testing resulted in an accidental increase in one direction from 1.5% to 7% drift ratio. The resulting damage was localized in the plastic hinge region with complete concrete crushing one side of the cross-section and cracks at the other side. The longitudinal bars buckled but did not fracture. The repair technique included replacing damaged concrete with quick-setting mortar, straightening, cutting and reconnecting the severely buckled longitudinal bars with mechanical couplers, injecting cracks with epoxy, and wrapping the damaged region with prestained SMA wires. Retesting of the repaired column showed that lateral strength, stiffness, and flexural ductility were restored or improved, which was attributed to the ability of the SMA spirals to apply and maintain active confinement on the damaged region of the column and delay the progression of damage.

Repair of RC Bridge Columns with Fractured Longitudinal Bars

Longitudinal bar fracture is often experienced at high ductility levels in flexure-dominant RC columns that are seismically detailed. It appears to be quite challenging to restore the ductility of RC columns containing fractured bars to that of the as-built condition without treatment of the damaged bars, while the objective of restoring the strength is relatively easier. Fewer studies have been conducted on repair of RC columns with fractured longitudinal bars than those without. Techniques that have been investigated include connecting the fractured bars with couplers (Shin and Andrawes 2011), placing new longitudinal bars anchored in the footing as reinforcement of enlarged cross-sections (Lehman et al. 2001), splicing steel plates to existing bars (Cheng et al. 2003), and applying externally bonded longitudinal reinforcement (such as FRP) to the repaired concrete surface (Saiidi and Cheng 2004, He et al. 2013, and Rutledge et al. 2013). Studies on repair of RC columns with fractured longitudinal bars are summarized below and in Table 2.

Lehman et al. (2001) reported repair methods for three severely damaged circular RC columns using mechanical couplers, headed bars, or a RC jacket. The columns were 1/3-scale and had different longitudinal reinforcement ratios of 0.75% (407S), 1.5% (415S), and 3% (430S). The as-built columns were tested under a constant axial load

(7% of the axial capacity) and cyclic lateral load with increasing levels of displacement until failure. The columns sustained damage to the concrete, the longitudinal reinforcement, and the spiral reinforcement. Three different repair schemes were used considering the nature of damage and details of the as-built columns. Column 407S was repaired by removing and replacing the damaged region, which involved mechanically severing the damaged region, splicing new longitudinal reinforcing bars to the existing bars in both the column and footing with mechanical couplers, placing new spiral reinforcement, and casting new concrete. The repaired column developed comparable stiffness and exhibited higher strength and deformation capacities than the as-built column. Column 415S was repaired by casting a concrete jacket reinforced with headed longitudinal bars along the damage region, so that the flexural plastic hinge was relocated from the base of the column to the region immediately above the jacketed region. The stiffness and strength of the repaired column were comparable to those of the as-built column; however the deformation capacity was reduced, which was attributed to the shorter effective column length. For Column 430S, the repair scheme also included a RC jacket but with the plastic hinge remaining within the jacket at the base of the column. All existing bars were severed at the base of the column, and new reinforcement was provided in the jacket. Tests showed that flexural hinging occurred at the column base, as intended. The deformation capacity of the column, however, was less than that of the as-built column, which may have been due to the reduced longitudinal reinforcement ratio at the base after the jacket was installed.

Cheng et al. (2003) reported a method to repair RC columns with fractured longitudinal bars using dog-bone shaped steel plates and a FRP jacket. Their study included two full-size hollow columns with a circular cross-section. The columns were tested to failure under cyclic lateral load with increasing levels of displacement and a constant axial load (10% of the axial capacity). One of the columns failed in flexural with concentrated damage including fractured outer layer longitudinal bars, buckled inner layer bars, and crushed concrete through the thickness of the column wall. The other column was damaged with the outer layer bars fractured at the column hinge and diagonal shear cracks across the mid-height of the column wall, which indicated a flexural-shear failure mode. Dog-bone shaped bars were used to replace the fractured

and buckled longitudinal bars in outer layer of cross-sections within the plastic hinge, and FRP wrap was used to enhance the deformation capacity of columns. The repair upgraded the failure mode of flexural-shear to flexure-dominant failure mode. The strength of the repaired columns was lower than that of the as-built columns since the inner layer of buckled longitudinal reinforcing bars was not repaired. The ductility of the repaired columns was also lower than that of the as-built columns, although the displacement capacity was increased.

Saiidi and Cheng (2004) proposed a rapid repair method for RC columns containing fractured longitudinal bars using externally bonded FRP with fibers oriented in both the longitudinal and transverse directions of the column. In their study, two 0.4-scale flared columns with different reinforcement ratios were repaired. The cross-sectional dimensions varied along the height of the columns. The columns had been retrofitted with steel jackets and tested to failure under cyclic loading in a previous study. The two columns were tested under cyclic lateral load with increasing levels of displacement and a constant axial load corresponding to 16% of the axial capacity of the columns. Because of the flared shape of the columns, the longitudinal bars fractured a distance away from the base of the column. To repair the columns, damaged concrete within and near the plastic hinge was removed and replaced with high-strength, low-shrinkage grout. The fractured longitudinal reinforcing bars were left untreated, and unidirectional GFRP and CFRP sheets with fibers orientated along the longitudinal axis of the column were applied to compensate for the flexural strength loss of the fractured bars. The longitudinal FRP was designed to provide the same tensile strength as the yield force of the fractured bars and divided equally between GFRP and CFRP laminates. Because the critical section was located a distance away from the base of the column, adequate length was available to develop the FRP. GFRP sheets were also wrapped around the column to provide shear strength and confinement. Test results showed that the repaired columns developed strength comparable to that of similar undamaged RC columns retrofitted with steel jackets; however, the ductility of the repaired columns was lower than that of similar retrofitted columns.

Shin and Andrawes (2011) reported a repair method for RC columns with fractured longitudinal bars using couplers to connect the fractured bars followed by application of

shape memory alloys (SMA) spirals at the repaired region. The test specimen was a 1/3-scale circular RC column that was tested under constant axial load (5% of the axial load capacity) and cyclic lateral load. The damage after the original test included crushed concrete, fractured longitudinal bars, and excessive opening of transverse reinforcement. The repair was accomplished by replacing the damaged concrete with quick-setting mortar, injecting epoxy in the cracks, connecting the fractured bars using rebar couplers, and wrapping the SMA spirals at the repaired region. Retesting the repaired column revealed that the lateral strength was fully restored, and the stiffness was higher than that of the original column. The overall displacement ductility was increased, though the displacement capacity was lower than that of the as-built column.

He et al. (2013a & b) rapidly repaired a 1/2-scale square RC bridge column with buckled and fractured longitudinal bars using externally bonded CFRP without any treatment to the damaged reinforcement. The column was subjected to reversed cyclic loading resulting and a constant axial load (7% of the axial load capacity), which resulted in buckled and fractured bars within the plastic hinge region at the base of the column, and crushed concrete. The repair procedure involved removing loose concrete, applying quick-setting non-shrink mortar, and installing unidirectional CFRP sheets in both the column longitudinal and transverse directions. Because the critical section was located at the base of the column, an anchorage system was developed in an attempt to anchor the longitudinal CFRP to the footing. The flexural strength was not completely restored, which was attributed to limitations in anchoring the longitudinal CFRP and developing the design force required at the critical section. This study highlighted some of the challenges in using this system when the fractured bars are located at the column base.

In addition to repairing two damaged large-scale circular RC columns with buckled bars as discussed in the previous section, Rutledge et al. (2013) also repaired a severely damaged column with fractured bars by plastic hinge relocation using externally bonded CFRP anchored to the footing with carbon fiber anchors. The circular column was tested under a specific earthquake load history by controlling the lateral displacement applied to the top of the column in a static manner. A constant axial load was also applied (axial load ratio of 6%). Damage included buckled and fractured bars on one side of the

column and crushed concrete. Test results showed that the repaired column had an increased force and displacement capacity compared to the original column, and the initial stiffness was restored. However, rupture of the carbon fiber anchors was observed during testing. Therefore, the researchers recommended that application of this technique should be limited to columns without fractured bars.

Summary

For damaged RC columns without fractured longitudinal bars, the reviewed studies indicate that concrete repair and application of jackets are able to restore and even enhance the strength and ductility compared to the as-built columns, even for columns with severe damage. Generally, the RC, steel, and FRP jackets described previously provide passive confinement to the concrete encased within. New materials, such as SMA, have been used to provide active confinement. Steel and FRP jackets can also provide active confinement to the concrete by pressurizing grout or epoxy in the gap between the columns and jacket as was shown by the study by Saadatmanesh et al. (1997). Comparing the different systems for repairing the damaged RC bridge columns without fractured longitudinal bars, it should be noted that RC jackets require a relatively long time to cure as well as considerable labor. Furthermore, RC jackets increase the member size and stiffness, as was shown in the studies by Bett et al. (1988), and Fukuyama et al (2000), which can change the dynamic characteristics of the member and cause increased demands at other locations of the structure. Steel jackets may also increase the initial stiffness due to increased cross-section, as indicated in the study by Fukuyama et al. (2000). The use of steel jackets can also reduce the construction time compared to RC jackets, although specialized equipment is needed to install the jacket. Additional treatment may also be needed to protect the steel from corrosion. The use of FRP jackets is becoming increasingly popular because of their light weight, high strength- and stiffness-to-weight ratios, corrosion resistance, and ease of installation. Repair with FRP jackets can maintain the original cross-section, although as was shown in the studies by Saadatmanesh et al. (1997) et al., Vosooghi and Saiidi (2009), and He et al. (2013a), decreased stiffness may be expected due to untreated damage in the column.

For damaged RC bridge columns with fractured longitudinal bars, replacing damaged longitudinal bars with new bars spliced by mechanical couplers has been shown successful in restoring both the strength and ductility of damaged RC columns with fractured bars (Lehman et al. 2001, Cheng et al. 2003). Jacketing the damaged region with reinforced concrete and well-anchored longitudinal bars has also been successful, although this method may potentially change the behavior of the column by increasing the cross-section, relocating the plastic hinge, changing the failure mode, and/or lowering the deformation capacity (Lehman et al., 2001). Plastic hinge relocation has been used as shown in the study by Rutledge et al. (2013), however, the displacement capacity cannot be restored unless the new plastic hinge region is also strengthened to provide more rotational capacity compared to the as-built condition. Since most of the methods to repair damaged RC columns with fractured longitudinal bars require a significant amount of time and labor, it should be noted that many of them are generally not suitable for rapid repair. Although the use of externally bonded FRP has been attempted for rapid repair of damaged columns with fractured longitudinal bars (He et al. 2013a&b, Saiidi and Cheng 2004), this technique may be limited to RC columns with bar fracture occurring away from the ends of the column due to the large force demands on the FRP anchorage system. Otherwise, a lower limit state (or service level) may be expected. Other methods, such as the use of SMA spirals at the repaired region (Shin and Andrawes 2011) are currently being explored.

It should be noted that repair may increase the capacity of a damaged RC column beyond its original as-built capacity and/or cause the plastic hinge region to form at a different location (e.g., Rutledge et al. 2013). Therefore, repair of damaged columns may cause damage to other capacity-protected components of a bridge such as piles, column-cap beam connections, etc. These issues can be addressed without any special modification to the structure if overstrength factors were used in design of the original structure. For structures designed without using overstrength factors, or if higher strength or displacement is required after considering the overstrength factors, the capacity-protected components must also be repaired as discussed by Saiidi et al. (2013).

Numerical Analysis of Repaired RC Bridge Columns

Studies reviewed in the previous section demonstrate that the seismic behavior of repaired RC columns may be altered from the original as-built condition in terms of initial stiffness, strength, and/or ductility. Accordingly, it is of interest of researchers and engineers to determine how such changes will influence the seismic performance of the individual repaired column, as well as the entire bridge structure.

Tools for analyzing the response of RC columns have been developed and widely used in seismic analysis during recent decades, especially with the advances made in the application of the finite element method. Some of these methods can be modified to enable the analysis of retrofitted and/or repaired RC columns jacketed with different materials.

Quantitative evaluation of repaired RC columns presents several challenges. As discussed in the study by Vecchio and Bucci (1999), the following issues must be considered: change in column configuration due to the repair; superposition of loaded and damaged unrepaired segments of the column with newly-placed unloaded repaired segments; appropriate constitutive modeling of loaded and repair materials; proper consideration of residual stresses and strain differentials at the interface of existing and newly-placed materials; and proper consideration of the chronology of the loading, damage, and repair sequences.

Modeling of Repaired RC Columns

Two different general procedures have been reported in the literature to model repaired RC columns, which are referred to in this paper as the two-phase method and the damage-index method. In the two-phase method (see Figure 1a), the elements for both the original column and the repairing portions are built at the beginning of the modeling procedure. The first phase of the analysis is conducted without activation of the elements representing the repair materials (e.g., repair concrete, external strengthening system) to simulate the loading of the original column (Region O-A in Figure 1a). In the second phase, the damaged and/or removed portions of the column are deleted in the model and are replaced by different material properties representing the repair concrete (Region A-B in Figure 1a). The repairing elements are then activated to

simulate the repair sequence before reloading of the repaired columns (Region B-C in Figure 1a).

This two-phase procedure was first reported by Vecchio and Bucci (1999) for analysis of repaired RC structures. In their study, a procedure was developed by modifying nonlinear fiber-element algorithms to consider the effects of chronology of the loading, damage, and repair, which makes it possible to analyze retrofitted, repaired, and sequentially constructed concrete structures. Using this technique, elements can be engaged and disengaged at various stages of loading, and strain measures representing previous loading and damage conditions can be carried forward by using the concept of plastic strain offsets in the context of the smeared rotating crack model. In this procedure, nonlinear material models were used for the concrete, reinforcement, and repair materials. Different RC structures were modeled as 2D models and analyzed using this method, and results were found to be accurate for both flexure- and shear-dominated structures in terms of strength, stiffness, and failure mode. The method was also proved to be numerically stable and efficient at all stages of loading.

Lee et al. (2011) developed a beam-column repair element with death and birth features to model repaired RC columns. The finite element of the repaired column included elements to represent both original and repaired portions. The simulation of the repaired column involved two phases. First, the original column was analyzed with deactivating the repair element (death), and then the repaired column was analyzed with activating the repair element (birth). The death and birth time of the repair element can be arbitrarily set, which allows the unrepaired damage to columns to be conveniently reflected in the analysis. The developed repair element was then incorporated into the general fiber element program ZeusNL. The method was used to simulate the cyclic response of two RC columns repaired with steel or FRP jackets, and the results were in reasonable agreement with the experimental results in terms of strength and the softening branch of strength. However, the method overestimated the energy dissipation.

The damage-index method, illustrated in Figure 1b, is based on assumptions to account for the damage condition prior to repair. The damaged/repaired condition of the column is defined as the initial condition in the model (Point B in Figure 1b). For example, in a study by Duarte et al. (2014), material parameters of repaired RC

members were modified to consider the effect of damage and repair. The experimental study included two RC members damaged with cracked concrete that were repaired by epoxy injection followed by applying an external CFRP strengthening system. The repaired members were analyzed using the program ATENA. In order to consider the effect of the epoxy injection in the model, the equivalent material parameters (e.g. fracture energy) were modified, and the values of the parameters were determined by parametric study. Though the numerical and experimental ultimate strengths were slightly different, the global structural response obtained with the numerical model was similar to the experimental behavior.

Vosooghi and Saiidi (2013) proposed a method to analyze rapidly repaired RC columns that were severely damaged with yielded reinforcement by reducing the steel stiffness corresponding to different damage states to represent the influence of yielded bars from previous tests. Each repaired column was modeled as a beam-column element, and a shear deformation spring and bond slip spring were used to incorporate the deformation due to shear and bond slip near the column-footing joint, respectively. To model the influence of yielded bars that were not replaced in the repair, a constitutive model was proposed for existing degraded steel reinforcement with reduced stiffness corresponding to different damage levels. They also reported a confined concrete model including the confinement from FRP jacket and excluding the contribution from yielded spirals. Their model successfully predicted a decreased initial stiffness of repaired RC columns compared to the original columns, which was consistent with experimental results.

Other Considerations

As discussed previously, unique challenges exist for the case of repaired columns relative to as-built or retrofitted columns, and very few studies have reported numerical analysis of repaired RC columns. Considering the seismic repair methods discussed in the first part of this paper, this section summarizes some studies focusing on related issues that may be important in simulating the response of repaired RC columns, such as modeling of bond slip of lap splices (Xiao and Ma 1997), modeling of the distributed bond interface between external strengthening system and concrete column (Shao et al.

2005, Zhu et al. 2006), modeling bond slip in mechanical couplers (Billah and Alam 2012). The studies presented in this section are not intended to be inclusive, but rather to provide guidance on how such issues can be incorporated into the model of a repaired RC column.

In the study by Xiao and Ma (1997), link elements were developed to model the lap splice in a sub-standard RC column with deficient lap splices that was retrofitted with a prefabricated GFRP jacketing system in the plastic hinge region. The distribution length of the link elements was related to the lap splice length and a proposed bond-slip relationship that was a function of the material properties and measured strains of the concrete, steel, and FRP. The link elements connected the plastic hinge region of the column with the starter bars and the upper portion of the column with the spliced longitudinal reinforcement, both of which were modeled as beam-column elements. The model was successful in simulating the behavior of the columns under static pushover loading. The strength and ductility indicated by the model were in good agreement with the experimental results.

Bond between concrete and an external strengthening system has been simulated in different ways. In the study by Shao et al. (2005), a distributed bond interface element was used to represent the slip between the concrete core and an FRP tube, which were both modeled as beam-column elements using the fiber element method. In another study by Zhu et al. (2006), perfect bond between the concrete core and FRP was modeled by sharing the same nodes. The concrete core was modeled as a solid RC beam-column element, and the FRP was modeled as a beam-column element with a hollow section. Though these studies were focused on concrete filled FRP tubes, the findings may be extrapolated to model repaired RC columns with an externally bonded FRP system.

In repairing severely damaged RC columns with fractured longitudinal bars, mechanical bar couplers have been used to splice new bars to existing bars (Lehman et al. 2001, Cheng et al. 2003). Though there are no reported studies on simulating such repaired RC columns, studies focused on as-built RC bridge columns reinforced with hybrid bars spliced with bar couplers may be extrapolated to model repaired columns with replacement bars spliced with bar couplers. For example, Billah and Alam (2012)

reported an analytical study on RC columns reinforced with stainless steel (SS) or shape memory alloy (SMA) bars within the plastic hinge region and stainless steel or FRP bars in regions outside the plastic hinge region, which were spliced with mechanical bar couplers. Their study is significant in incorporating the influence of bar couplers on the seismic behavior of RC columns. Stress-slip relationships within the couplers measured from coupon tests were used to determine the parameters in the rotational spring in the model, which were used to simulate the bond slip at the column-footing joint.

Summary

In summary, two different methods have been reported for numerical analysis of repaired RC bridge columns: a two-phase method, and a damage-index method. The two-phase method can consider the chronology of the loading, damage, and repair, although the initial state of the repaired column (Point B in Figure 1a) is dependent upon the accuracy of modeling the as-built column, including its post-peak response. The damage-index, on the other hand, can be used to define the initial state of the repaired column (Point B in Figure 1b). Considering the repair methods described in the first part of this paper, treatment of related issues such as bond-slip of lap splices, slip within mechanical couplers, and the bond interface between the external strengthening system and concrete column that have been reported in the literature for simulation of as-built or retrofitted RC columns can be extrapolated to model repaired RC columns.

Concluding Remarks

This paper summarizes studies on repair of earthquake-damaged RC bridge columns including damage description, repair procedures, repair effectiveness, and analysis of repaired RC columns. Based on the information summarized from the previous studies, the following concluding remarks are made:

1. For earthquake-damaged RC columns without fractured longitudinal bars, jacketing with reinforced concrete, steel, FRP, SMA, or other materials has been shown to work well to restore both strength and ductility; however, a change in initial stiffness can be expected for each of the jacketing techniques, and the influence on the global seismic response of the bridge needs further study.

2. For earthquake-damaged RC columns with fractured longitudinal bars, repair techniques including replacement of damaged bars or application of supplementary reinforcement have been developed. Among these techniques, replacing damaged bars and connecting them with mechanical couplers and jacketing with reinforced concrete has been shown to be successful in restoring strength, ductility, and initial stiffness. Application of FRP with fibers oriented along the longitudinal axis of the column may be limited to columns in which the bar fracture has occurred away from the column end or to cases where a lower limit state (or service level) is accepted. Further research is needed to investigate methods to restore the ductility and initial stiffness using FRP jackets.

3. Unique challenges exist for the case of repaired columns relative to as-built or retrofitted columns, and very few studies have reported numerical analysis of repaired RC columns. Two general methods have been reported in the literature for numerical analysis of repaired RC columns: a two-phase method, and a damage-index method. The two-phase method can consider the chronology of the loading, damage, and repair, although the initial state of the repaired column is dependent upon the accuracy of modeling the as-built column, including its post-peak response. The damage-index method, on the other hand, can be used to define the initial state of the repaired column. Treatment of specific issues related to some of the repair methods discussed in this paper, such as bond-slip of lap splices or mechanical couplers, and modeling of the bond interface between the external strengthening system and concrete column, have been reported in the literature for simulation of as-built or retrofitted RC columns and can be extrapolated to repaired RC columns.

Acknowledgements

The authors would like to express their appreciation to the University of Missouri Research Board and National University Transportation Center (NUTC) at Missouri S&T for their financial support for this study.

References

- Applied Technology Council (ATC) (1997). "Seismic Design Criteria for Bridges and Other Highway Structures: Current and Future." *ATC-18*, Redwood City, CA.
- Applied Technology Council (ATC) (1996). "Improved Seismic Design Criteria for Bridges: Provisional Recommendations." *ATC-32*, Redwood City, CA.
- Belarbi, A., Silva, P. F., Bae, S. W. (2008). "Retrofit of RC Bridge Columns Under Combined Axial, Shear, Flexure, and Torsion Using CFRP Composites." *Challenges for Civil Engineering (CCC)*, Porto.
- Belarbi, A., Prakash, S., and Silva, P. F. (2010). "Incorporation of Decoupled Damage Index Models in Performance-Based Evaluation of RC Circular and Square Bridge Columns under Combined Loadings." *Structural Concrete in Seismic Design of Bridges*, SP-271, 79-102.
- Berry, M., Parrish, M., and Eberhard, M. (2004). "PEER Structural Performance Database User's Manual (Version 1.0)." *Pacific Earthquake Engineering Research Center*, University of California, Berkeley.
- Bett, B. J., Klingner, R. E., and Jirsa, J. O. (1988). "Lateral Load Response of Strengthened and Repaired Reinforced Concrete Columns." *ACI Structural Journal*, September-October, 499-508.
- Billah, A.H.M. M, Alam, M. S. (2012). "Seismic Performance of Concrete Columns Reinforced with Hybrid Shape Memory Alloy (SMA) and Fiber Reinforced Polymer (FRP) Bars." *Construction and Building Materials*, 28(1), 730-742.
- Chai, Y. H., Priestley, M. J. N., Seible, F. (1991). "Seismic Retrofit of Circular Bridge Columns for Enhanced Flexural Performance." *ACI Structural Journal*, 88(5), 572-584.

- Chang, S. Y., Li, Y. F., and Loh, C. H. (2004). "Experimental Study of Seismic Behaviors of As-Built and Carbon Fiber Reinforced Plastics Repaired Reinforced Concrete Bridge Columns." *Journal of Bridge Engineering*, ASCE July-August, 391-402.
- Cheng, C. T., Yang, J. C., Yeh, Y. K., and Chen S. E. (2003). "Seismic Performance of Repaired Hollow-Bridge Piers." *Construction and Building Materials*, 17, 339-351.
- Darwin, D., Lutz, L. A., and Zuo, J. (2005). "Recommended Provisions and Commentary on Development and Lap Splice Lengths for Deformed Reinforcing Bars in Tension." *ACI Structural Journal*, 102(6), 892-900.
- Duarte, P., Correia, J. R., Ferreira, J.G., Nunes, F., and Arruda M. R. T. (2014). "Experimental and Numerical Study on the Effect of Repairing Reinforced Concrete Cracked Beams Strengthened with Carbon Fiber Reinforced Polymer Laminates." *Canadian Journal of Civil Engineering*. 41: 222-231. (Dx.doi.org/10.1139/cjce-2013-0124).
- Elsouri, A. M. and Harajli, M. H. (2011). "Seismic Repair and Strengthening of Lap Splices in RC Columns: Carbon Fiber-Reinforced Polymer versus Steel Confinement." *Journal of Composites for Construction*, 15(5), 721-731.
- French, C. W., Thorp, G. A., and Tsai, W. J. (1990). "Epoxy Repair Techniques for Moderate Earthquake Damage." *ACI Structural Journal*, 87(4), 416-424.
- Fukuyama, K., Higashibata, Y., and Miyauchi, Y. (2000). "Studies on Repair and Strengthening Methods of Damaged Reinforced Concrete Columns." *Cement & Concrete Composites*, 22, 81-88.
- Ghasemi, H., Otsuka, H., Cooper, J. D., and Nakajima, H. (1996). "Aftermath of the Kobe Earthquake." *FHWA Public Roads*, 60(2).
- He, R., Sneed, L. H., and Belarbi, A. (2013a). "Rapid repair of Severely Damaged RC Columns with Different Damage Conditions – An Experimental Study." *International Journal of Concrete Structures and Materials*, 7(1), 35-50.

- He, R., Grelle, S., Sneed, L. H., and Belarbi, A. (2013b). "Rapid Repair of a Severely Damaged RC Column Having Fractured Bars Using Externally Bonded CFRP." *Journal of Composite Structures*, 101, 225-242.
- He, R., Sneed, L. H., and Belarbi, A. (2014). "Torsional Repair of Severely Damaged Column Using Carbon Fiber-Reinforced Polymer." *ACI Structural Journal*, 111, 12 pp. (DOI:10.14359.51686627).
- Itani, R. and Liao X. (2003). "Effects of Retrofitting Applications on Reinforced Concrete Bridges." *Technical Report No. WA-RD 570.1*, Washington State Transportation Center (TRAC), Washington State University, Pullman, Washington.
- Laplace, P. N., Sanders, D., Saiidi, M., Douglas, B., and El-Azazy, S. (2005). "Retrofitted Concrete Bridge Columns under Shake Table Excitation." *ACI Structural Journal*, 102(4), 662-628.
- Lee, D. H., Park, J., Lee, K. and Kim, B. H. (2011). "Nonlinear Seismic Assessment for the Post-repair Response of RC Bridge Piers." *Composites Part B*, 42(5), 1318-1329.
- Lehman, D. E., Gookin, S. E., Nacamuli, A. M., and Moehle, J. P. (2001). "Repair of Earthquake-Damaged Bridge Columns." *ACI Structural Journal*, 98(2), 233-242.
- Li, Y. F. and Sung Y. Y. (2003). "Seismic Repair and Rehabilitation of a Shear-Failure Damaged Circular Bridge Column Using Carbon Fiber Reinforced Plastic Jacketing." *Canadian Journal of Civil Engineering*, 30, 819-829.
- Nesheli, K. N. and Meguro, K. (2006). "Seismic Retrofitting of Earthquake-Damaged Concrete Columns by Lateral Pre-Tensioning of FRP Belts." *Proceedings of the 8th U.S. National Conference on Earthquake Engineering*, April 18-22, San Francisco, California, USA, Paper No. 841.
- Priestley, M. J. N. and Seible, F. (1993). "Repair of Shear Column Using Fiberglass/Epoxy Jacket and Epoxy Injection." Report No. 93-04, Job No. 90-08, *Seqad Consulting Engineer*, July.

- Priestley, M. J. N., Seible, F., Xiao, Y., and Verma, R. (1994a). "Steel Jacket Retrofitting of Reinforced Concrete Bridge Columns for Enhanced Shear Strength-Part 1: Theoretical Considerations and Test Design." *ACI Structural Journal*, 91(4), 394-405.
- Priestley, M. J. N., Seible, F., Xiao, Y., and Verma, R. (1994b). "Steel Jacket Retrofitting of Reinforced Concrete Bridge Columns for Enhanced Shear Strength-Part 2: Test Results and Comparison with Theory." *ACI Structural Journal*, 91(5), 537-551.
- Rodriguez, M., and Park, R. (1994). "Seismic Load Tests on Reinforced Concrete Columns Strengthening by Jacketing." *ACI Structural Journal*, 91(2), 150-159.
- Rutledge, S. T., Kowalsky, M. J., Seracino, R., and Nau, J. M. (2013). "Repair of Reinforced Concrete Bridge Columns Containing Buckled and Fractured Reinforcement by Plastic Hinge Relocation." *Journal of Bridge Engineering*, ASCE, A4013001, 1-10.
- Saadatmanesh, H., Ehsani, M. and Jin, L. (1996). "Seismic Strengthening of Circular Bridge Pier Models with Fiber Composites." *ACI Structural Journal*, 93(6), 639-647.
- Saadatmanesh, H., Ehsani, M. and Jin, L. (1997). "Repair of Earthquake-Damaged RC Columns with FRP Wraps." *ACI Structural Journal*, 94(2), 206-215.
- Saiidi, M. S. and Cheng, Z. (2004). "Effectiveness of Composites in Earthquake Damage Repair of RC Flared Columns." *Journal of Composites for Construction*, ASCE, 8(4), 306-314.
- Saiidi, M., Wehbe, N., Sanders, D., and Caywood, C. (2001). "Shear Retrofit of Flared RC Bridge Columns Subjected to Earthquake." *Journal of Bridge Engineering*, ASCE, 6(3), 189-197.
- Seible, F., Priestley, M. J. N., Hegemier, G., and Innamorate, D. (1997). "Seismic Retrofit of RC Columns with Continuous Carbon Fiber Jackets." *Journal of Composites for Construction*, ASCE, 1(2), 52-62.

- Shao, Y., Aval, S. and Mirmiran, A. (2005). "Fiber-Element Model for Cyclic Analysis of Concrete-Filled Fiber Reinforced Polymer Tubes." *Journal of Structural Engineering*, 131(2), 292-303.
- Sheikh, S. A., and Yau, G. (2002) "Seismic Behavior of Concrete Columns Confined with Steel and Fiber-Reinforced Polymers." *ACI Structural Journal*, 99(1), 72-80.
- Shin, M., and Andrawes, B. (2011). "Emergency Repair of Severely Damaged Reinforced Concrete Columns Using Active Confinement with Shape Memory Alloys." *Smart Materials and Structures*, 20, 9 pp.
- Vecchio, F. J. and Bucci, F. (1999). "Analysis of Repaired Reinforced Concrete Structures." *Journal of Structural Engineering*, 125(6), 644-652.
- Vosooghi, A, Saiidi, M. S., and Gutierrez, J. (2008). "Rapid Repair of RC Bridge Columns Subjected to Earthquakes." *Proceedings of 2nd International Conference on Concrete Repair, Rehabilitation, and Retrofitting (ICCRRR)*, Cape Town, South Africa, 24-26 November, 1113-1119.
- Vosooghi, A., and Saiidi, M. S. (2009). "Rapid Repair of High-Shear Earthquake-Damaged RC Bridge Columns." *Proceedings of the 25th US-Japan Bridge Engineering Workshop*, Tsukuba, Japan, Session 7, October.
- Vosooghi, A., and Saiidi, M. S. (2010). "Seismic Damage States and Response Parameters for Bridge Columns." *Structural Concrete in Seismic Design of Bridges*, SP-271, 29-46.
- Vosooghi, A., and Saiidi, M. S. (2010). "Post-Earthquake Evaluation and Emergency Repair of Damaged RC Bridge Columns Using CFRP Materials." Report Number CCEER-10-05, September.
- Vosooghi, A. and Saiidi, M. S. (2013). "Design Guidelines for Rapid Repair of Earthquake-Damaged Circular RC Bridge Columns Using CFRP." *Journal of Bridge Engineering*, 18(9), 827-836.

Weyers, R. E., Prowell, B. D., Sprinkel, M. M., and Vorster, M. (1993). "Concrete Bridge Protection, Repair, and Rehabilitation Relative to Reinforcement Corrosion: A Methods Application Manual," *Technical Report*, State Highway Research Program Contract C-103, National Academy of Science, Washington, D.C.

Xiao, Y. and Ma, R. (1997). "Seismic retrofit of RC circular columns using prefabricated composite jacketing." *Journal of Structural Engineering*, 123(10), 1357-1364.

Zhu, Z., Ahmad, I. and Mirmiran, A. (2006). "Fiber Element Modeling for Seismic Performance of Bridge Columns Made of Concrete-Filled FRP Tubes." *Engineering Structures* 28(14), 2023-2035.

List of Tables

Table 1. Summary of Studies on Repair of Reinforced Concrete Bridge Columns without Fractured Longitudinal Bars

Table 2. Summary of Studies on Repair of Reinforced Concrete Bridge Columns with Fractured Longitudinal Bars

List of Figures

Figure 1. Numerical Analysis of Repaired RC Columns

Table 1. Summary of Studies on Repair of Reinforced Concrete Bridge Columns without Fractured Longitudinal Bars

Reference	Scale	Cross-Section Shape	Axial Load Index	Loading Type	Brief Description of Apparent Damage/Failure	Repair Method	Strength	Displacement Ductility	Stiffness
Bett et al. (1988)	2/3	Square (Sub-Standard)	7%	Cyclic lateral loading	Badly damaged with brittle shear failure	Installed RC jacket with closely-spaced ties and cross-ties connected to mid-face longitudinal bars	Enhanced	Not reported	Enhanced
Fukuyama et al. (2000)	1/2	Square	30%	Cyclic lateral loading	Heavily damaged with crushed core concrete	Installed RC jacket with welded wire shear reinforcement	Enhanced	Enhanced	Enhanced
Chai et al. (1991)	2/5	Circular (Sub-Standard)	17%	Cyclic lateral loading	Bond failure of the spliced reinforcement in plastic hinge region	Removed loose concrete; installed steel jacket; installed external pre-stressing on footing	Restored	Enhanced	Not reported
Fukuyama et al. (2000)	1/2	Square	30%	Cyclic lateral loading	Crushed core concrete; buckled longitudinal bars	Installed steel plates around column; grouted between steel plates and concrete with added longitudinal bars	Enhanced	Enhanced	Enhanced
Elsouri and Harajli (2011)	Full	Rectangular (Sub-Standard)	-	Cyclic lateral loading	Bond failure of the starter bars; concrete damaged in the splice zone	Replaced concrete; installed steel ties and/or FRP wraps	Enhanced	Enhanced	Not reported
Priestley et al. (1993)	2/5	Circular (Sub-Standard)	18%	Cyclic lateral loading	Open diagonal cracks; spalled concrete cover	Removed loose concrete; patched with mortar; applied full height GFRP jacket; injected epoxy through the jacket	Restored	Enhanced	Restored
Saadatmanesh et al. (1997)	1/5	Circular & Rectangular (Sub-Standard)	-	Cyclic lateral loading	Debonding of starter bars; spalling and crushing of concrete; buckling of longitudinal bars; separation of the main bars from core concrete	Replaced spalled concrete; installed GFRP strap around failure zone; pressurized gap between GFRP and column with epoxy grout	Restored	Restored	Lower
Sheikh & Yau (2002)	-	Circular	54%	Cyclic lateral loading	Flexural cracks; cover concrete spalling; longitudinal and spiral reinforcement yielding	Removed loose concrete; patched the column; installed EB transverse FRP (either CFRP or GFRP)	Enhanced	Enhanced	Not reported
Li & Sung (2003)	2/5	Circular	15%	Cyclic lateral loading	Shear failure at low displacement ductility	Replaced damaged concrete with non-shrinkage mortar; high-pressure epoxy injection; installed EB transverse CFRP	Enhanced	Enhanced	Not reported
Chang et al. (2004)	2/5	Rectangular	-	Cyclic lateral loading	Flexural failure in the plastic hinge zone	Removed damaged concrete cover; placed non-shrink mortar; installed EB transverse CFRP	Restored	Restored	Lower
Nesheli & Meguro (2006)	1/2	Square	20%	Cyclic lateral loading	Brittle shear failure with large diagonal cracks	Repaired damaged concrete; wrapped EB transverse carbon fiber belts; pretensioned fiber belts	Lower	1 Lower, 1 Not reported	Lower
Belarbi et al. (2008)	1/2	Circular	7%	Combined cyclic lateral loading and torsion	Concrete cover appalled; core concrete crushed; longitudinal reinforcing bars buckled	Removed damaged concrete; placed low viscosity grout; applied EB longitudinal CFRP with mechanical anchorage; applied EB transverse CFRP	Enhanced	Not reported	Not reported
Vosooghi et al. (2008)	1/4	Circular	-	Shake table testing and additional static loading	Visible bars; initial buckling in longitudinal bars; initial concrete core damage	Removed loose concrete; injected epoxy into cracks; patched concrete with quickset grout; wrapped with EB CFRP	Restored	Restored	Lower
Vosooghi & Saïidi (2009)	1/3	Circular	-	Shake table testing	Visible spirals and longitudinal bars; buckled longitudinal bars; concrete core damage	Replaced loose concrete with non-shrink mortar; injected epoxy into cracks; wrapped with EB CFRP	Restored	Restored	Lower
He et al. (2013a)	1/2	Square	7%	Cyclic lateral load and twist	Spalled cover concrete; crushed core concrete; buckled longitudinal bars; yielded and/or opened ties	Removed and replaced loose concrete; applied EB longitudinal CFRP sheets with anchorage system; installed EB transverse CFRP	Restored	Restored	Lower
Rutledge et al. (2013)	-	Circular	6%	*Cyclic lateral loading	Buckled longitudinal bars	Relocated the plastic hinge by using EB CFRP in longitudinal direction with CFRP anchors; installed EB transverse CFRP	Enhanced	Enhanced	Restored
Shin & Andrawes (2011)	1/3	Circular	5%	Cyclic lateral loading	Crushed and cracked concrete; buckled longitudinal bars	Removed loose concrete; straightened, cut, and coupled buckled bars; injected epoxy into cracks; applied mortar; wrapped pre-strained SMA	Enhanced (in one direction)	Enhanced (in one direction)	Enhanced (in one direction)

Note: * The loading history used in the original study corresponded to specific earthquake load history, applied by controlling the lateral displacement applied to the top of the column in a static manner

Table 2. Summary of Studies on Repair of Reinforced Concrete Bridge Columns with Fractured Longitudinal Bars

Reference	Scale	Cross-Section Shape	Axial Load Index	Lateral Load Type	Brief Description of Apparent Damage/Failure	Repair Method	Strength	Displacement Ductility	Stiffness
Lehman et al. (2001)	1/3	Circular	7%	Cyclic lateral loading	Buckled longitudinal bars; fractured longitudinal and spiral bars	Severed damaged region; spliced new longitudinal bars connected to the footing and column with mechanical couplers; placed new spirals; cast new concrete	Enhanced	Enhanced	Restored
						Installed RC jacket reinforced with headed longitudinal bars (relocation of the plastic hinge)	Restored	Lower	Restored
						Severed all existing bars in the plastic hinge to maintain plastic hinge location; provided RC jacket with replacement bars	Lower	Lower	Not reported
Cheng et al. (2003)	Full	Hollow circular	10%	Cyclic lateral loading	Buckled and fractured longitudinal bars; crushed concrete	Repaired concrete; repaired fractured longitudinal bars with dog-bone welded steel plate; replaced transverse bar; installed EB transverse FRP	Lower	Lower	Not reported
Saiidi & Cheng (2004)	2/5	Flared	16%	Cyclic lateral loading	Fractured longitudinal bars; crushed concrete	Repaired concrete; installed EB longitudinal CFRP and GFRP; installed EB transverse GFRP	Restored or enhanced	Lower	Not reported
Shin and Andrawes (2011)	1/3	circular	5%	Cyclic lateral loading	Buckled and fractured longitudinal bars; crushed concrete	Repaired concrete; reconnected longitudinal bars with mechanical couplers; installed SMA wrap	Restored or enhanced	Enhanced	Enhanced
He et al. (2013a&b)	1/2	Square	7%	Cyclic lateral loading	Buckled and fractured longitudinal bars; crushed concrete	Repaired concrete; installed EB longitudinal CFRP with anchorage system; installed EB transverse CFRP	Lower	Lower	Lower
Rutledge et al. (2013)	-	Circular	6%	*Cyclic lateral loading	Buckled and fractured longitudinal bars; crushed concrete	Repaired concrete; relocated the plastic hinge using EB longitudinal CFRP with CFRP anchors, installed EB transverse CFRP	Enhanced	Restored	Restored

Note: * The loading history used in the original study corresponded to specific earthquake load history, applied by controlling the lateral displacement applied to the top of the column in a static manner.

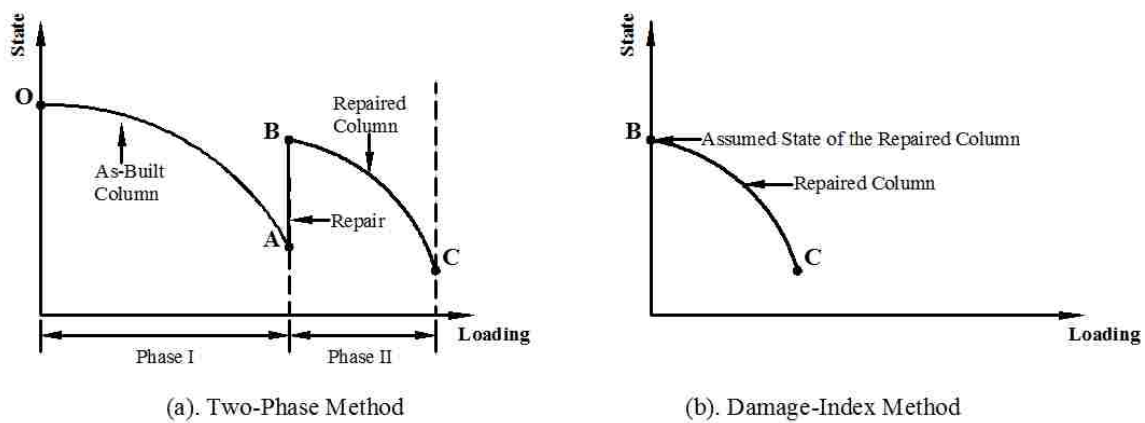


Figure 1. Numerical Analysis of Repaired RC Columns

II. RAPID REPAIR OF SEVERELY DAMAGED RC COLUMNS WITH DIFFERENT DAMAGE CONDITIONS: AN EXPERIMENTAL STUDY

Ruili He¹, Lesley H. Sneed², Abdeldjelil Belarbi³

Abstract

Rapid and effective repair methods are desired to enable quick reopening of damaged bridges after an earthquake occurs, especially for those bridges that are critical for emergency response and other essential functions. This paper presents results of tests conducted as a proof-of-concept in the effectiveness of a proposed method using externally bonded carbon fiber reinforced polymer (CFRP) composites to rapidly repair severely damaged RC columns with different damage conditions. The experimental work included five large-scale severely damaged square RC columns with the same geometry and material properties but with different damage conditions due to different loading combinations of bending, shear, and torsion in the previous tests. Over a three-day period, each column was repaired and retested under the same loading combination as the corresponding original column. Quickset repair mortar was used to replace the removed loose concrete. Without any treatment to damaged reinforcing bars, longitudinal and transverse CFRP sheets were externally bonded to the prepared surface to restore the column strength. Measured data were analyzed to investigate the performance of the repaired columns compared to the corresponding original column responses. It was concluded that the technique can be successful for severely damaged columns with damage to the concrete and transverse reinforcement. For severely damaged columns with damaged longitudinal reinforcement, the technique was found to be successful if the damaged longitudinal reinforcement is able to provide tensile resistance, or if the damage is located at a section where longitudinal CFRP strength can be developed.

Keywords: CFRP composite; Cyclic loading; Rapid repair; RC columns; Severely damaged.

1. Introduction

Damage to bridge structures during an earthquake can have devastating social and economic consequences, particularly for bridges located along key routes that are critical for emergency response and other essential functions. Such bridges are defined as “important” by ATC-18 [1], which stipulates that full access to “important” bridges should be possible within three days after an earthquake. In order to restore access to essential traffic in affected areas, rapid and effective repair methods are desired for varying levels of damage to minimize the impact on the community.

Decades of study have demonstrated the effectiveness of externally bonded fiber reinforced polymer (FRP) in strengthening and repairing reinforced concrete (RC) columns. Most studies have focused on flexural or shear strengthening or repair application of various types of members or providing confinement in case of columns. Among the studies on repair, most have focused on columns with slight or moderate damage in which concrete, steel, or FRP jacketing was used to restore the strength and displacement capacity [2-6]. Few studies, however, have focused on repairing severely damaged ductile RC bridge columns, especially those with buckled or fractured longitudinal reinforcing bars [2,6]. Although these techniques have been shown to be effective in restoring the strength and displacement capacity, rapid repair was not emphasized, and timely reopening of the bridge was not a consideration. To address this issue, Vosooghi and Saiidi [7] recently developed guidelines for rapid repair of damaged bridge columns with carbon FRP (CFRP). Their studies focused on circular RC bridge columns under flexural and shear loading conditions without ruptured longitudinal reinforcing bars.

Bridge columns may experience complex axial, shear, bending, and torsional loading during an earthquake. As shown by Prakash et al. [8], interaction between loading actions influences the location and type of damage. Therefore, it is of interest to develop a repair technique for damaged columns with different damage conditions resulting from combined loading effects.

The present study was conducted as a proof-of-concept with the objective of determining the feasibility and effectiveness of a proposed technique to rapidly repair severely damaged RC bridge columns with different damage conditions using externally-

bonded CFRP for emergency service use after an earthquake. The term “rapid” in the context of this study refers to a three-day time period as defined by ATC-18 [1] and other researchers [9]. This research will fill in critical gaps in the literature with respect to the severe damage level and inclusion of torsional loading effects and will help guide future research efforts in this area. This experimental study included five half-scale square bridge columns that were tested to complete failure under different combined loading effects of axial, shear, bending, and torsion in a previous study [8]. After the previous tests, the columns were severely damaged with different damage conditions. Each column was repaired within a three-day period and retested on the fourth day under the same combined loading as the corresponding original column. The performance of the repaired columns was evaluated by comparing the response with that of the corresponding original columns. The large scale nature of the test specimens in this study allowed for evaluation of the constructability of the developed repair technique in practice.

2. Original Columns

Five square RC columns were tested in a previous study, each with the same nominal geometry and material properties. The columns were 1/2 scale bridge columns designed based on CALTRANS [10] and ACI 318 [11] seismic provisions. The column specimen was simulated as a cantilever, and the aspect ratio (H/B) was 6, where H and B are the height of the column and the cross-section dimension, respectively. Figure 1 shows the column geometry and reinforcement details. The column was 22 in. (560 mm) square reinforced with four No. 9 (29 mm dia.) deformed bars in the corners and eight No. 8 (25 mm dia.) intermediate bars, with a longitudinal reinforcement ratio of 2.13%. Tie reinforcement consisted of square and octagonal No. 3 (10 mm dia.) deformed bars spaced at 3.25 in. (82 mm), with a transverse reinforcement ratio of 1.32%. The measured yield strength of the longitudinal bars was 76 ksi (524 MPa) for No. 8 (25 mm dia.) bars and 67 ksi (462 MPa) for No. 9 (29 mm dia.) bars. For the ties, the measured yield strength was 74 ksi (510 MPa). Yield strength of the reinforcing bars was determined in accordance with ASTM A 370 [12]. The target 28-day cylinder compressive strength of

the concrete was 5,000 psi (34 MPa). Additional information including measured concrete properties is provided in Prakash et al. [8].

The previous research studied the seismic performance of square RC bridge columns under combined loading effects including torsion. The study was focused on the interaction between bending and torsion, and the primary variable was the torque-to-moment ratio (T/M). All five columns were tested to failure under cyclic lateral loading and a constant axial load of approximately 150 kips (667 kN) to simulate the dead load from the superstructure. Column 1 was subjected to cyclic uniaxial cantilever bending and shear ($T/M=0$) in addition to the constant axial load. Columns 2, 3, and 4 were subjected to the constant axial load and a combined cyclic loading effect of uniaxial cantilever bending, shear, and torsion, with torque-to-moment ratios (T/M) of 0.2, 0.4, and 0.6, respectively. Column 5 was tested under pure torsion ($T/M=\infty$) in addition to the constant axial load.

3. Column Damage Conditions

After the original tests, the columns were severely damaged with different damage conditions due to the different combined cyclic loading effects (T/M). The overall damage conditions were classified based on both visual observations and measured response data. According to previous work [13], any visible evidence of core concrete crushing, longitudinal bar buckling, or longitudinal/transverse reinforcement fracture is classified as severe damage. Damage is classified as significant according to ATC 32 criteria if a permanent offset is apparent, if the reinforcement has yielded, or if major concrete spalling has occurred [14]. The terms “*significant*” and “*severe*” are used interchangeably in this paper when referring to the column damage.

The damaged columns after the original tests are shown in Figure 2, which illustrates the difference in the visible damage extent and the plastic hinge location. Generally, the damage region extended farther along the column height and the plastic hinge location shifted away from the base with increasing torque-to-moment ratio. For instance Column 1, which was tested under cyclic shear and bending, sustained cover concrete spalling 25 in. (635 mm) above the column base, and the plastic hinge was located approximately 10 in. (260 mm) above the base. Column 5, which was subject to

cyclic torque moment, exhibited concrete damage that extended almost the entire column length, and the core concrete crushed through the cross section 64 in. (1,620 mm) above the column base. The damage to Columns 1, 2, and 3 was concentrated near the base of the column at the location of maximum moment due to flexure-dominant behavior in columns with low T/M ratios ($T/M < 0.5$). Columns 4 and 5 were torsion-dominant with high T/M ratios ($T/M > 0.5$), which resulted in higher plastic hinge location and larger damage extent as illustrated in Figure 2.

Measured data acquired during testing were used to monitor changes in load-displacement response and determine locations at which the reinforcement yielded. At completion of testing, the load-displacement responses showed that the stiffness of each column decreased significantly, and the residual strength was less than 50% of the peak load. Some of the columns were completely damaged without any resistance to the applied loading [8].

A detailed description of the damage to the original columns is summarized in Table 1. Damage to each column included concrete cracking, cover concrete spalling, and core concrete crushing, as well as longitudinal reinforcement yielding. Damaged ties failed by yielding and, in some cases, subsequent straightening of the end hooks. Additionally, longitudinal bars buckled in Columns 1-4, and two longitudinal reinforcing bars fractured in Column 1 near the base of the column at the northwest and southeast corners of the cross-section (see Figure 1).

4. Rapid Repair of Damaged Columns

4.1 Repair Materials

In view of the short time frame for the rapid repair, the repair materials used were selected for ease of installation, compatibility with the other materials, and capability of achieving their desired strengths within the timeframe. A quickset repair mortar and unidirectional CFRP strengthening system were used in this study. The repair mortar was used to replace the removed damaged concrete, while the CFRP strengthening system was used to compensate for the loss in strength due to material degradation during the previous column tests.

The repair mortar was a shrinkage-compensating micro concrete that had high bond strength, high early strength, and self-compacting properties. Material properties provided by the manufacturer are given in Table 2. The compressive strength was monitored by casting 2 in. (51 mm) cubes on the same day as replacing the removed concrete. The compressive strength was measured one day after casting, at test day, and at 28 days after casting. The compressive strength of the repair mortar measured at test date was nearly 5 ksi (28 MPa) for each column.

The CFRP strengthening system consisted of unidirectional carbon fiber sheets. Putty was used to fill the voids on the column surface, while primer was used to facilitate the bond between the concrete and the CFRP system. The properties of the dry carbon fiber fabric provided by manufacturer were: tensile strength of 550 ksi (3,800 MPa); tensile modulus of 33,000 ksi (227 GPa); ultimate rupture strain of 0.0167; and nominal thickness of 0.0065 in. (0.165 mm) per ply. The carbon fiber was linear elastic.

Bond between the host concrete and externally applied CFRP is critical for flexural, shear, and torsional strengthening, so bond strength testing of the CFRP-to-concrete bond was performed in accordance with ASTM D7234 [15]. A representative sample of CFRP was bonded to the concrete surface that was prepared using the same techniques and at the same time as the CFRP application. The test was performed at the time of testing of the repaired column. For each column, the bond strength test results met the CFRP system manufacturer's and ACI 440.2R [16] minimum specified bond strength of 200 psi (1,380 kPa).

4.2 Repair Procedure

The entire repair process took approximately 30 man-hours over three days and involved the following seven steps: 1) straightening the column; 2) removing loose concrete; 3) placing repair mortar; 4) preparing the column surface; 5) installing longitudinal and transverse CFRP; 6) arranging instrumentation; and 7) retesting repaired columns. The axial load was not applied during the repair procedure considering that shoring systems can be used to support the self-weight of the superstructure in practice during the repair. Straightening of the column was challenging and time-consuming due to limited equipment available in the lab; therefore the time for straightening was not

included in the three-day period here. On the first day, the damaged loose concrete was removed and formwork erected, then quickset mortar was placed. The mortar was allowed to set approximately 12 hours before the formwork was removed on the second day. Then the column surface was prepared for installation of the CFRP system. The surface was smoothed and corners were rounded with a hand grinder, and then putty and primer were applied. The longitudinal CFRP was applied, followed by transverse CFRP. The transverse CFRP was applied after the longitudinal CFRP to help preventing the debonding of the longitudinal CFRP from the host concrete. For the longitudinal CFRP, fibers were aligned along the longitudinal axis of the column. For the transverse CFRP, fibers were oriented transverse to the longitudinal axis of the column. Detailing of the CFRP systems is discussed in a subsequent section. No special technique was used to cure the CFRP system except for Columns 1 and 2 in which a plastic sheet and a small heater were used to facilitate curing because the temperature in the laboratory was unusually low. Cracks on the concrete surface outside the region with CFRP were not repaired. An unexpected delay occurred during the repair of Column 1, which resulted in testing on the 5th day.

4.3 Test Setup and Loading Protocol

The experimental setup is shown in Figure 3. In the original tests, the columns were anchored to the strong floor with four DYWIDAG bars with 50 kips (222 kN) prestressing force in each bar (Figure 3a and b), which is discussed in Prakash et al. [8]. The system used to anchor the repaired columns to the strong floor was modified due to damage to the anchors. Two steel wide flange beams were used with two steel double channel beams to anchor the repaired column specimens (Figure 3c and d). Because of the position of the wide flange beams and resulting space limitations, some of the instrumentation used in the original tests was not used in the repaired column tests.

The repaired columns were tested under the same initial combined loading effects as the original columns. Similar to the procedure used for testing the original columns, the testing procedure for repaired columns was initiated in force control and then continued in displacement control. In testing the original columns, testing shifted to displacement control when first yield of the reinforcing steel occurred [8]. For the

repaired columns, yielding of the steel had occurred during the previous test, and monitoring the strain was not always possible due to damage to the strain gages mounted to the reinforcement. Therefore, testing was shifted to displacement control when significant reduction of the stiffness was observed. In addition, different procedures were used to maintain the torque-to-moment ratio (T/M) during the displacement control testing. In the original tests, an iterative feedback system was used to control the torque-to-moment [8], whereas in the present program, a trial-and-error method was used based on values recorded from the previous cycle. As a result, some differences existed in the loading protocol details.

5. CFRP Layouts

The CFRP layouts are summarized in this section. The CFRP design procedures will be described in detail elsewhere by the authors. In general, the externally bonded CFRP strengthening system for each damaged column was designed to restore the column strength in terms of shear, bending, and torsion associated with the peak load in the original test. It should be noted that in the case of a permanent repair, the repair system should also be capable of restoring the ductility, although this aspect was not explicitly accounted for in the design due to the inclusion of torsion. The transverse CFRP wrap was designed to provide confinement to the concrete and to restore the strength in terms of torsion and shear, in which the CALTRANS provisions for RC column retrofit were used [18,19]. The longitudinal CFRP was designed to compensate for the flexural and torsional strength loss due to the damaged reinforcement and softened concrete. Interaction between bending and torsion was considered in the design [20].

The CFRP layout for each repaired column is shown in Figures 4-8. Repaired columns are denoted in this paper with the extension “-R”. The CFRP layout for each column was designed and detailed considering the nature of damage to the column, the damage location, and the peak applied loading. As a result, each column had a different repair region and CFRP layout. To maximize the time efficiency, only the regions of the column at and adjacent to the plastic hinge were repaired. Adjustments were made to the designs based on lessons learned during testing of previous repaired columns within the

series as discussed below. (Repaired columns were repaired and tested in sequential order from Column 1-R to 5-R).

For Columns 1-R, 2-R, and 3-R, the repair regions were located in the lower half of the columns since the damage was concentrated near the base of the columns. This was the case because Columns 1, 2, and 3 were flexure dominant. The increasing number of transverse CFRP sheets at the bottom level of Column 3-R compared to Column 2-R, and Column 2-R compared to Column 1-R, is due to the fact that the damage in Columns 1-R and 2-R was concentrated near the base of the column, and damage did not spread to the adjacent region. Longitudinal CFRP was installed only on the north and south sides of Column 1-R because the column was subjected to uniaxial bending and no torsion, and because space limitations did not allow for installation of an appropriate anchorage system to anchor longitudinal sheets on the east and west faces. However, transverse CFRP splitting observed on the east and west sides at early stages of testing Column 1-R prompted the use of longitudinal CFRP sheets on all four sides of Columns 2-R and 3-R. Thus one longitudinal sheet was provided on the east and west sides that was anchored at the base by U-anchors, which required minimal space for installation. The longitudinal CFRP sheets on the north and south faces were anchored with an anchorage system consisting of a steel plate welded to a quarter-section of steel pipe reinforced with stiffeners and fastened to the concrete with threaded steel anchor rods that were embedded using a chemical adhesive. The anchorage system is sketched at the base of the columns in Figures 4-6. A photo of the anchorage system is shown in Figure 9, and details of the anchorage system design are described by Grelle [17].

For Columns 4-R and 5-R, the repair regions extended along most of the column length. Column 4 was repaired along most of its height except for the top 12 in. (305 mm) because of lack of damage in the top region as well as difficulty of applying formwork and placing the repair mortar along the full height of the column. However, shifting of the plastic hinge location of Column 4-R prompted the full height repair of Column 5-R.

6. Test Results

6.1 Summary of Failure Modes

The failure modes of the repaired columns are summarized in Table 3. Column 1-R experienced premature failure due to the detailing of the anchorage system used to anchor the longitudinal CFRP sheets to the base of the column [17]. During testing, the top of the quarter-pipe section of the anchorage system came into contact with the CFRP system, which led to CFRP rupture on both the south and north sides of the column due to the bearing of the corner of the anchorage system. It must be noted that because Column 1 had fractured longitudinal bars, the repair needed to compensate for the strength loss of the fractured bars. This resulted in a large demand on the longitudinal CFRP relative the other repaired columns, and also resulted in a large force in the CFRP that needed to be anchored to the base at the critical section for bending moment. Column 2-R, which had the plastic hinge at the base of column after the previous test similar to Column 1, failed due to CFRP rupture and crushing of concrete in plastic hinge region near the base of the column. No further damage was observed in the unrepaired region of Column 2-R. Also, the detailing problems with the anchorage system were avoided by maintaining a gap between the repaired column and the anchorage system. For Column 3-R, the test was terminated due to limitations of the actuators. No damage was observed in the repaired region; however the plastic hinge relocated just above the repaired region. The concrete cover just beyond the repaired region spalled off, and the cover spalling progressed upwards until testing was terminated. The plastic hinge was also relocated in Column 4-R from the location in Column 4, For Column 4-R, the plastic hinge shifted to the unrepaired region just above the repaired region. The failure mode was concrete crushing in the unrepaired region followed by CFRP rupture near the unrepaired region. The failure mode of Column 5-R was rupture of the CFRP. Rupture of the external CFRP on Column 5-R first occurred at the south-west corner of the column approximately 65 in. (1,650 mm) above the column base, which coincides with the interface of the unrepaired concrete and the newly placed repair mortar. Rupture progressed to the upper west side of the column, and then to the lower south side. Finally, the ruptured CFRP peeled away with a thin layer of concrete bonded underneath, and crushed mortar fell out.

6.2 General Behavior of Repaired Columns

The general response of each repaired column relative to the corresponding original column is described in this section. The measured load-displacement and torque-twist relationships of the repaired columns compared to the corresponding original columns are shown in Figures 10 to 14, in which both the hysteresis and envelope responses are provided. As illustrated in the figures, the repaired columns behaved asymmetrically in the positive and negative cycles. This response can be attributed to the unsymmetrical damage in the original column, the unsymmetrical removal and replacement of loose concrete during the repair procedure, and possibly some original displacement at the beginning of testing the repaired columns, which was due to the fact that the repaired column was not perfectly straightened.

The measured lateral load and displacement in Column 1-R did not reach that of Column 1, which is due to premature failure associated with longitudinal CFRP anchorage as discussed in the previous section. A moment-curvature analysis of the repaired cross-section confirms that the lateral load associated with the predicted moment capacity after failure of the longitudinal CFRP was close to the peak lateral load measured during the test. It must be noted that anchorage of externally bonded longitudinal CFRP sheets is a crucial issue to ensure that the tensile force can be developed at the critical section. When the plastic hinge is located near a joint, the situation is even more complicated by the interaction between the column and the anchorage system, which was the situation of Column 1-R. Therefore careful attention must be paid to detailing of both the FRP and its anchorage system.

Figures 11 and 12 show that both the flexural strength and ductility of Columns 2-R and 3-R were mainly restored to Columns 2 and 3, although the maximum torque of Column 2-R did not reach that of original column. Similarly for Column 4-R, Figure 13 shows that the torsional strength was improved compared to Column 4, but the measured lateral load and displacement did not reach the original state. To explain the differences in bending and torsional strength restoration for each repaired column, the difference in the loading protocol details between the repaired column and corresponding original column must be noted. As discussed previously, it was difficult to maintain the torque-to-moment ratio after shifting to displacement control, which resulted in the applied load

with different torque-to-moment ratios for the repaired and original columns. For instance Figure 15 shows the torque-to-moment ratios (T/M) for the applied load on Column 4-R and Column 4. The torque-to-moment ratio of Column 4 reduced significantly after shifting from load control to displacement control at a lower load level compared to Column 4-R. This resulted in higher bending moment in Column 4 compared to Column 4-R, since this bending moment was reached at a lower torque compared to Column 4-R. Therefore, it can be concluded that the bending-torque interaction played a role in the level of strength restored.

Comparison of the applied torque-twist envelopes of Column 5 and Column 5-R in Figure 14 indicates that the torsional strength and twist at maximum torque were enhanced by the repair. For Column 5, the torsional strength reduced rapidly after the maximum torque was achieved because the core concrete crushed and thus could not provide further torsional resistance. The post-peak response of Column 5-R was characterized by a reduction in torsional strength with increasing applied torque, but not as rapidly as that of Column 5. This phenomenon can be explained in part by the confinement provided by the transverse CFRP wrap.

In general, Figures 10-14 also show that the rate of stiffness deterioration of the repaired columns under large reversed cyclic loading was lower than that of the corresponding original columns. However, the initial stiffness of repaired columns was lower than that of corresponding original columns.

6.3 Evaluation of the Repair Technique

Comparison of the repaired column performances in this study is complicated by the different damage conditions of the corresponding original columns and the different repair profiles. Thus non-dimensional response indices were developed to compare the repaired column to the corresponding original column in terms of strength, stiffness, and ductility, which were the extension of previous work by Vosooghi and Saiidi [21]. The indices were then used to compare the performance of the repaired columns.

6.3.1 Strength Index

The strength of a column is defined as the maximum measured applied load during the test [22]. The ratio of the repaired column strength to the original column strength is defined as the strength index *STRI*, which was determined by Eq. (1).

$$\begin{aligned} STRI &= \frac{V_r}{V_o} \\ &= \left(\frac{T_r}{T_o} \right) \end{aligned} \quad (1)$$

$V_r (T_r)$ and $V_o (T_o)$ in Eq. (1) represent the maximum lateral load (torque moment) measured in the repaired and original columns, respectively.

The strength indices for the columns are provided in Figure 16, which illustrates that the repair method is effective in restoring the bending and/or torsional strength. The flexural strength restoration ranged from 63-111%, and torsional strength restoration ranged from 83-118%. Although Column 1-R was restored to 75% of its original flexural strength, the results can be misleading since the strength restoration was limited by the flexural capacity of the repaired cross-section section with fractured bars, because the longitudinal CFRP failed prematurely. For Columns 2-R, 3-R, and 4-R, which were subjected to combined bending and torsion, either the flexural strength, the torsional strength, or both, were fully restored. Bending-torque interactions played a role in the level of bending and torsional strength restored as discussed in the previous sections. For Column 5-R subjected to pure torsion, the torsional strength was fully restored.

6.3.2 Stiffness Index

The stiffness of columns can be expressed by the initial stiffness and the general service stiffness, which were determined by the following methods. The initial stiffness was determined by the ratio of the summation of absolute values of positive and negative peak lateral load (torque for torsion) in the first cycle of the test to the summation of corresponding absolute values of positive and negative displacement (twist for torsion) [23], which was calculated by Eq. (2). The ratio of the repaired column initial stiffness to the original column initial stiffness is defined as the stiffness index *STFI*, which was computed by Eq. (3).

$$K_i = \frac{V_{p1} + V_{n1}}{D_{p1} + D_{n1}} = \left(\frac{T_{p1} + T_{n1}}{TW_{p1} + TW_{n1}} \right) \quad (2)$$

$$STFI_1 = \frac{K_{ir}}{K_{io}} \quad (3)$$

In Eq. (2), V_{p1} (T_{p1}) is the measured positive peak lateral load (torque moment) during the first cycle, and D_{p1} (TW_{p1}) is the corresponding lateral displacement (twist). V_{n1} (T_{n1}) is the absolute value of measured negative peak lateral load (torque), and D_{n1} (TW_{n1}) is the absolute value of the corresponding lateral displacement (twist).

The initial stiffness indices for the repaired columns are illustrated in Figure 17. The initial bending stiffness indices ranged from 39-112%, and initial torsional stiffness indices ranged from 32-81%. With the exception of the bending stiffness of Column 4-R/4, the initial stiffness of the repaired columns was lower than that of the corresponding original columns. This reduction in initial stiffness is due to the unrepaired cracked portions of the repaired columns and material degradation during the original tests.

The general service stiffness index was determined based on an idealized envelope representing an elasto-plastic curve [9]. For the original columns, the envelopes were idealized by setting the initial slope to pass through the first yield point and adjusting the plastic portion so that areas under the measured curve and idealized curve were equal. For the repaired columns, the elastic part of the idealized curve was obtained by connecting the origin to the point on the measured envelope at which the applied load (torsional moment) was one-half of the peak measured value. The yield level was established by equalizing the area between the measured and idealized curves. The idealizations of the envelopes of the original and repaired columns are illustrated in Figure 18.

The general service stiffness index $STFI_2$ is defined as the ratio of the service stiffness of the repaired column K_r to that of the original column K_o as shown in Eq. (4). The service stiffnesses K_r and K_o are determined from the ratio of the plastic base shear (torque) to the effective yield displacement (twist), which were obtained from the idealized curves (see Figure 18).

$$STFI_2 = \frac{K_r}{K_o} \quad (4)$$

As shown in Figure 19, the general service stiffness indices for bending ranged from 85-189%, and general service stiffness indices for torsion ranged from 69-138%.

It should be noted that the general service stiffness indices for the repaired columns are dependent on the idealization of the measured envelopes of both original and repaired columns. Results are sensitive to assumptions used in developing the idealized curves. Thus these index values are presented herein to compare the global behaviors of the repaired and corresponding original columns. Also, the torque-bending interaction should be kept in mind in evaluating these indices. In general, the general service stiffness was restored more effectively than the initial stiffness.

6.3.3 Ductility Index

The ductility index DI is defined as the ratio of the ductility capacity of the repaired column D_r to that of the original column D_o (see Eq. (5)). The ductility capacity is defined as the ratio of the ultimate displacement (twist) to the effective yield displacement (twist), which can be obtained from the idealized curves in Figure 18.

$$DI = \frac{D_r}{D_o} \quad (5)$$

The ductility indices in terms of both bending and torsion are illustrated in Figure 20. The ductility indices for bending ranged from 68-250%, and torsional strength restoration ranged from 69-170%.

Similar to the general service stiffness indices, the ductility indices for the repaired columns are dependent on the idealization of the measured envelopes of both original and repaired columns. However, results are encouraging and suggest that the ductility can be restored to an extent that can meet the needs of a temporary repair and allow emergency service use after an earthquake. More work is needed to determine whether this method can be used for permanent repair, in which case the ductility should be considered in design and should be fully restored.

7. Conclusions

This paper discusses the results of five large-scale tests conducted as a proof-of-concept in the effectiveness of a proposed method to rapidly repair severely damaged RC columns with different damage conditions. While the original geometric and material properties were nominally the same for each column, the location of plastic hinge and nature of damage were different because of different loading conditions. The repair procedure involved removal and replacement of loose concrete, followed by installation of longitudinal and transverse CFRP sheets. Because of the rapid nature of the repair, damaged reinforcing bars were left untreated. The repair of each column was designed to restore the strength associated with the peak load in the original test. While further study needs to be conducted to completely understand the design and performance of repaired RC columns subjected to combined loading effects including torsion, the following conclusions can be made from this study:

1. The developed repair procedure was practical and achievable as an emergency repair;
2. The repair method is effective in restoring the bending and/or torsional strength. Factors such as bending-torque interaction, failure mode, and repair detailing played a role in the level of strength restored;
3. Results suggest that the repair method can restore the stiffness and ductility capacity of the columns to levels that can meet the needs of a temporary repair and allow emergency use after an earthquake;
4. In this study, for the flexural dominant columns with damage concentrated near the base, only the portion of the columns with severe damage, and the region immediately adjacent to it, were repaired. Results confirmed that the strength can be restored or even enhanced for columns without fractured longitudinal bars. These findings are significant in terms of time that can be saved in completing a temporary emergency repair;
5. The rapid repair method used in this study did not include repair of fractured longitudinal reinforcing bars. When fractured longitudinal bars (and critical section) are located near the base of the column, as was the case for Column 1 in this study, a large force demand is required of the CFRP strengthening system, as well as a substantial anchorage system to develop it. The method utilized in this study was

- found to be only partial unsuccessful in this case, since premature failure of the strengthening system limited the strength restoration; and
6. Though initial stiffnesses of the repaired columns were lower than that of original columns due to the unrepaired cracked portions, the general service stiffnesses were restored to a higher level. Also, the rate of stiffness deterioration under large reversal cyclic loading was lower for the repaired columns than that of the corresponding original columns.

Acknowledgements

The research was performed at Missouri S&T. The authors would like to express their appreciation to the University of Missouri Research Board for the financial support for this project. BASF is gratefully acknowledged for providing the repair materials. Thanks are also due to research specialist, Jason Cox, research/lab technician, John Bullock, electronics technicians, Brian Swift and Gary Abbott, and the group members, Stephen Grelle, Corey Grace, Qian Li, and Yang Yang, for their help throughout the repair and testing processes.

References

- ACI Committee 318. (2008). *Building code requirements for structural concrete and commentary (ACI318-08)*. Farmington Hills, MI: American Concrete Institute.
- ACI Committee 440. (2008). *Guide for the design and construction of externally bonded FRP systems for strengthening concrete structures. ACI 440.R-08*. Farmington Hills, MI: American Concrete Institute.
- Applied Technology Council (ATC). (1997). *Seismic design criteria for bridges and other highway structures: Current and future. ATC-18*, Redwood City.
- ASTM. (2005). *Standard test method for pull-off adhesion strength of coatings on concrete using portable pull-off adhesion testers. D7234-05*. West Conshohocken, PA: ASTM International.

- ASTM. (2012). *Test methods and definitions for mechanical testing of steel products. A370-12a*. West Conshohocken, PA: ASTM International.
- California Department of Transportation. (2004). *Caltrans bridge design specification*. Sacramento, CA: California Department of Transportation.
- California Department of Transportation. (2006). *Seismic design criteria (SDC), version 1.4*. Sacramento, CA: Engineering Service Center, Earthquake Engineering Branch.
- California Department of Transportation. (2007). *Memo to designers 20-4, attachment B*. Sacramento, CA: Engineering Service Center, Earthquake Engineering Branch.
- Chai, Y. H., Priestley, M. J. N., & Seible, F. (1991). Seismic retrofit of circular bridge columns for enhanced flexural performance. *ACI Structural Journal*, 88(5), 572-584.
- Cheng, C. T., Yang, J. C., Yeh, Y. K., & Chen, S. E. (2003). Seismic performance of repaired hollow-bridge piers. *Construction and Building Materials*, 17(5), 339-351.
- Elkin, S. J., Nacamuli, A. M., Lehman, D. E., & Moehle, J. P. (1999). Seismic performance of damaged bridge columns. *Earthquake Engineering and Engineering Seismology*, 1(1), 39-50.
- Grelle, S. V. (2011). *Categorization and experimental evaluation of anchorage systems for FRP laminates bonded to reinforced concrete structures*. Master's Thesis, Missouri University of Science and Technology, Rolla, MO.
- Jing, M., Raongjant, W., & Li, Z. (2007). Torsional strengthening of reinforced concrete box beams using carbon fiber reinforced polymer. *Composite Structures*, 78(2), 264-270.
- Lehman, D. E., Gookin, S. E., Nacamuli, A. M., & Moehle, J. P. (2001). Repair of earthquake-damaged bridge columns. *ACI Structural Journal*, 98(2), 233-242.
- Park, R. & Paulay, T. (1975). *Reinforced concrete structures*. New York: Wiley.

- Prakash, S. S., Li, Q., & Belarbi, A. (2012). Behavior of circular and square reinforced concrete bridge columns under combined loading including torsion. *ACI Structural Journal*, 109(3), 317-327.
- Rojahn, C., Mayer, R., Anderson, D. G., Clark, J., Hom, J. H., Hutt, R. V., & O'Rourke, M. J. (1997). *Seismic design criteria for bridges and other highway structures*. Redwood City, CA: Applied Technology Council.
- Saadatmanesh, H., Ehsani, M. & Jin, L. (1997). Repair of earthquake-damaged RC columns with FRP wraps. *ACI Structural Journal*, 94(2), 206-215.
- Stoppenhagen, D. R., Jirsa, J. Q., & Wyllie, Jr., L.A. (1995). Seismic repair and strengthening of a severely damaged concrete frame. *ACI Structural Journal*, 92(2), 177-187.
- Vosooghi, A., & Saiidi, M. (2009). Rapid repair of high-shear earthquake-damaged RC bridge columns. In *Proceedings of 25th US-Japan Bridge Engineering Workshop*, Tsukuba, Japan, Session 7.
- Vosooghi, A., & Saiidi, S. (2012). Design guidelines for rapid repair of earthquake-damaged circular RC bridge columns using CFRP." *Journal of Bridge Engineering*. doi: 10.1061/(ASCE) BE. 1943-5592.0000426.
- Vosooghi, A., & Saiidi, M. (2013). Shake-table studies of repaired reinforced concrete bridge columns using carbon fiber-reinforced polymer fabrics. *ACI Structural Journal*, 110(91), 105-114.
- Vosooghi, A., Saiidi, M., & Gutierrez, J. (2008). Rapid repair of RC bridge columns subjected to earthquakes. In *Proceedings of 2nd international conference on concrete repair, rehabilitation, and retrofitting (ICCRRR 2008)*, Cape Town, South Africa, pp. 397-398.

Table 1 Summary of damage to original columns.

Column	T/M	Concrete Damage		Reinforcing Bar Damage			
				Longitudinal			Ties ^a
		Cover Spall	Core Crush	Yield	Buckle	Fracture	
Column 1	0	25 in. (635 mm) above column base	10 in. (260 mm) above column base	All bars	All bars, 10 in. (260 mm) above column base	2 bars; 10 in. (260 mm) above column base (see Fig.1)	4 ties
Column 2	0.2	37 in. (950 mm) above column base	20 in. (500 mm) above column base	All bars	10 bars, 20 in. (500 mm) above column base	None	3 ties
Column 3	0.4	58 in. (1,470 mm) above column base	30 in. (760 mm) above column base	All bars	10 bars, 30 in. (760 mm) above column base	None	1 tie
Column 4	0.6	94 in. (2,380 mm) above column base	40 in. (1,020 mm) above column base	All bars	10 bars, 40 in. (1,020 mm) above column base	None	1 tie
Column 5	∞	120 in. (3,050 mm) above column base	64 in. (1,620 mm) above column base	2 bars	None	None	0 tie

^a Values in this column refer to the number of ties removed during repairing.

Table 2 Repair mortar properties (provided by the manufacturer).

Property	Results	Test Method
Fresh wet density, lb/ft ³ (kg/m ³)	142 (2,275)	ASTM C 138
Compressive strength, psi (MPa); 2 in. (51 mm) cubes		ASTM C 109
1 day	2,500 (17.2)	
7 days	5,000 (34.5)	
28 days	6,000 (41.4)	
Compressive strength, psi (MPa); 3 by 6 in. (76 by 152 mm) cylinders, at 28 days.	5,000 (34.5)	ASTM C 39
Flexural strength, psi (MPa), at 28 days	1,150 (7.9)	ASTM C 348
Slant shear bond strength, psi (MPa), at 28 days	3,000 (20.7)	ASTM C 882 (modified)
Splitting tensile strength, psi (MPa), at 28 days	500 (3.4)	ASTM C 496

Table 3 Summary of failure modes of repaired columns.

Repaired Column	Failure Mode	
Column 1-R (T/M=0)	Premature failure related to the detailing of the longitudinal CFRP anchorage system, followed by fracture of two additional longitudinal reinforcing steel bars	Flexure Dominant
Column 2-R (T/M=0.2)	Rupture of CFRP (flexure), crushing of concrete in the repaired region	
Column 3-R (T/M=0.4)	Testing terminated due to limitations of the actuators	
Column 4-R (T/M=0.6)	Crushing of concrete in the unrepaired region (torsion) followed by CFRP rupture next to the unrepaired region	Torsion Dominant
Column 5-R (T/M= ∞)	Rupture of CFRP, crushing of concrete (torsion)	

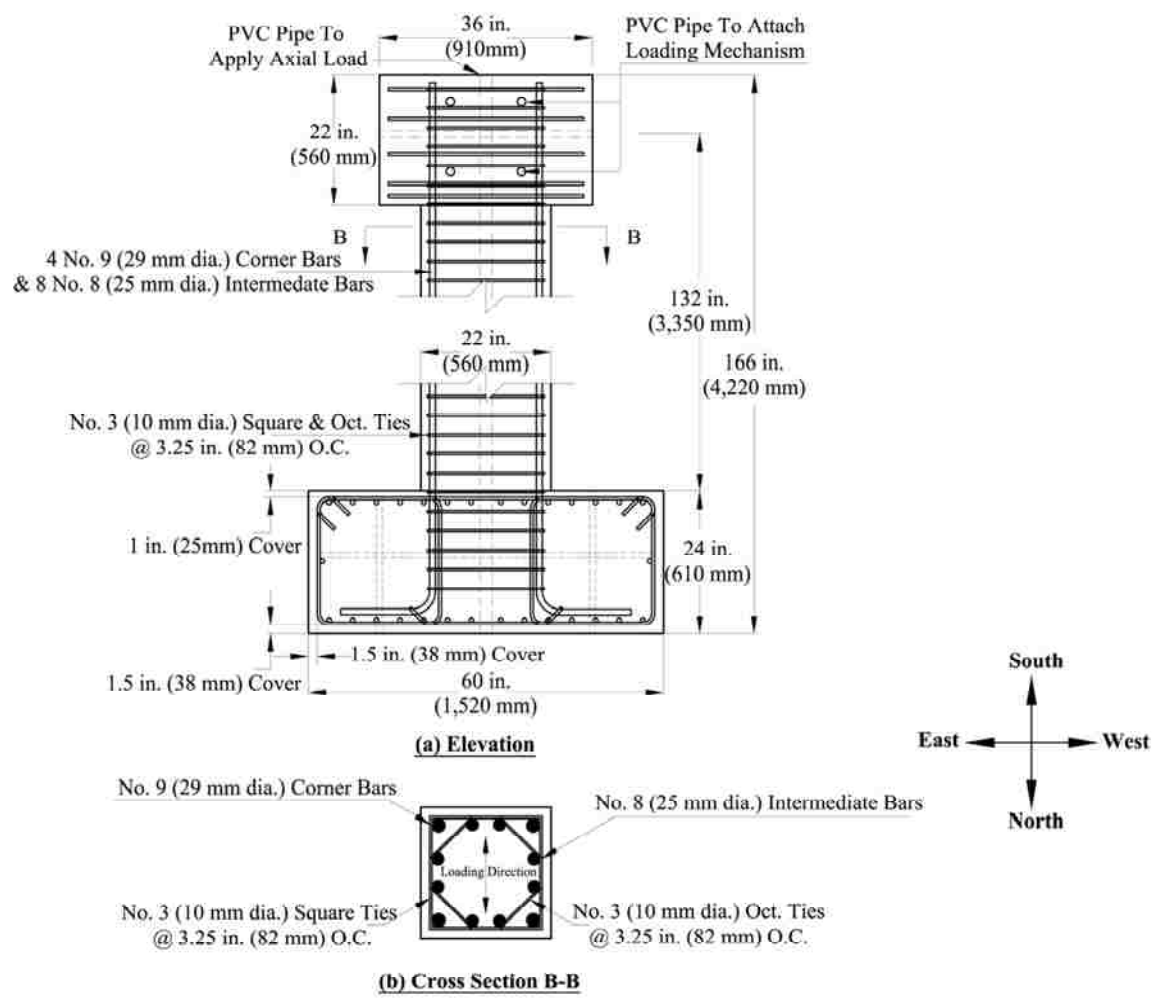


Fig. 1 Geometry and reinforcement details of original columns.

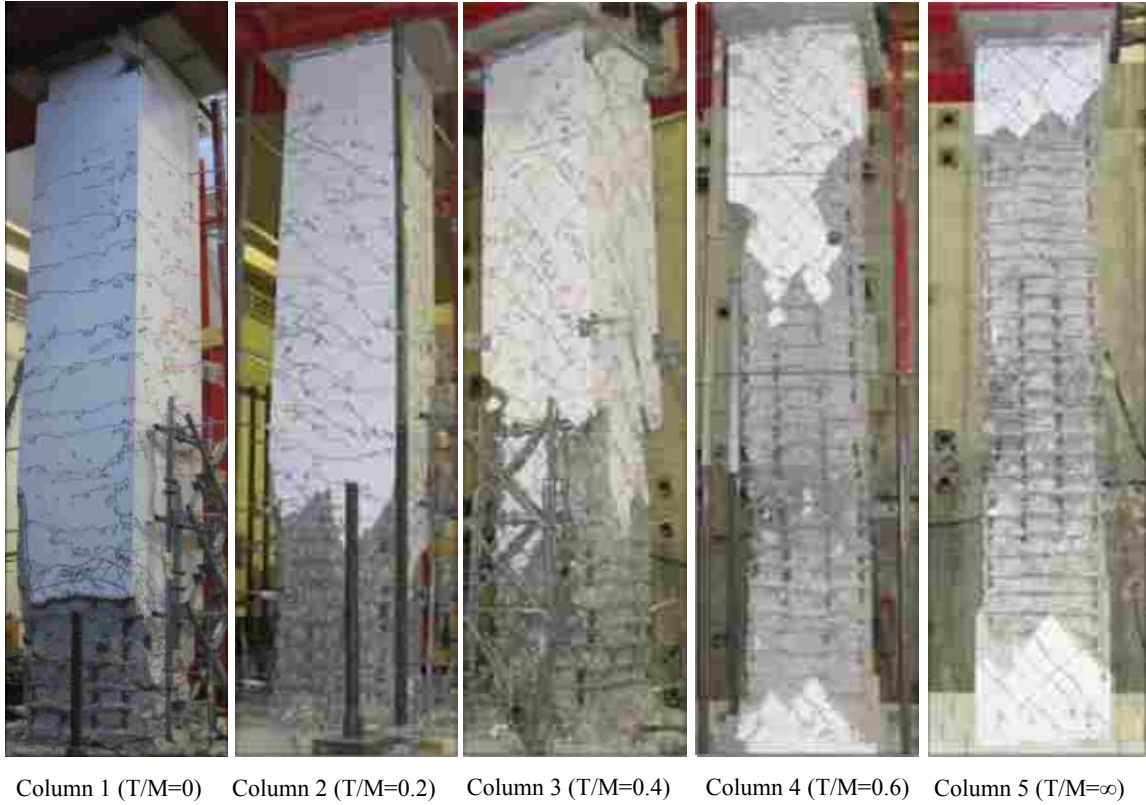


Fig. 2 Damage conditions of the original columns after previous tests.

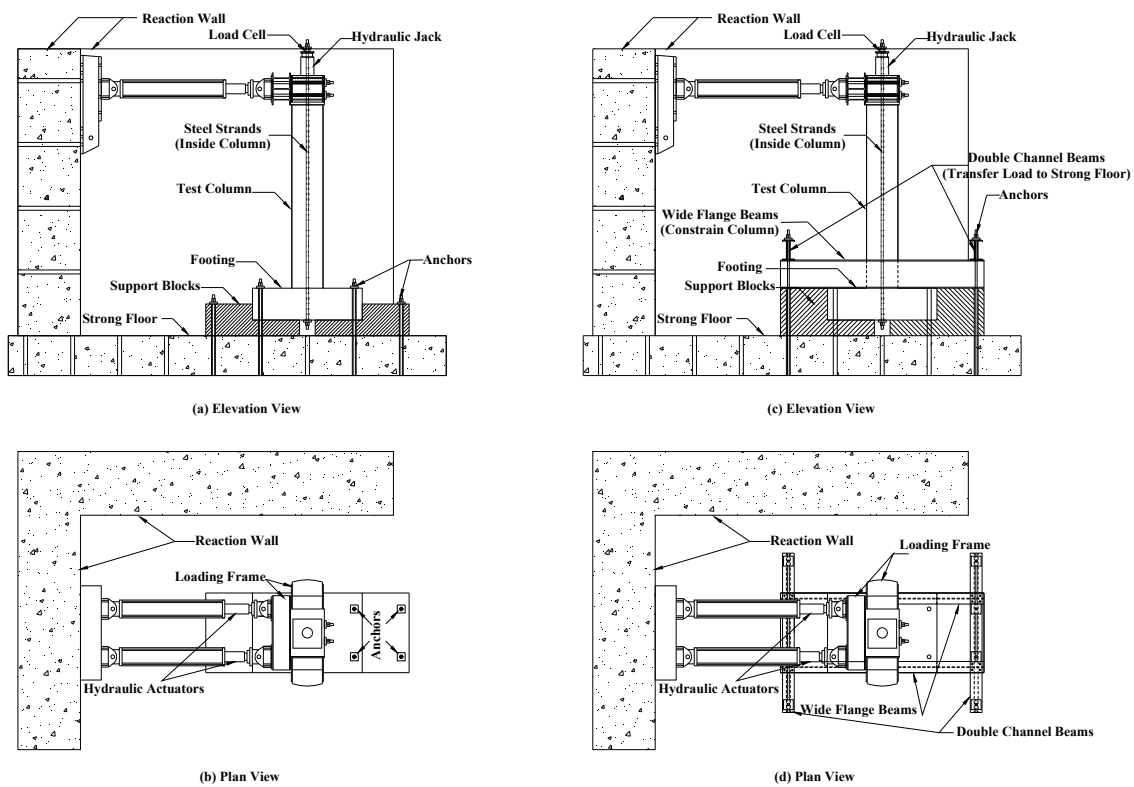


Fig. 3 Test setup for original and repaired columns.

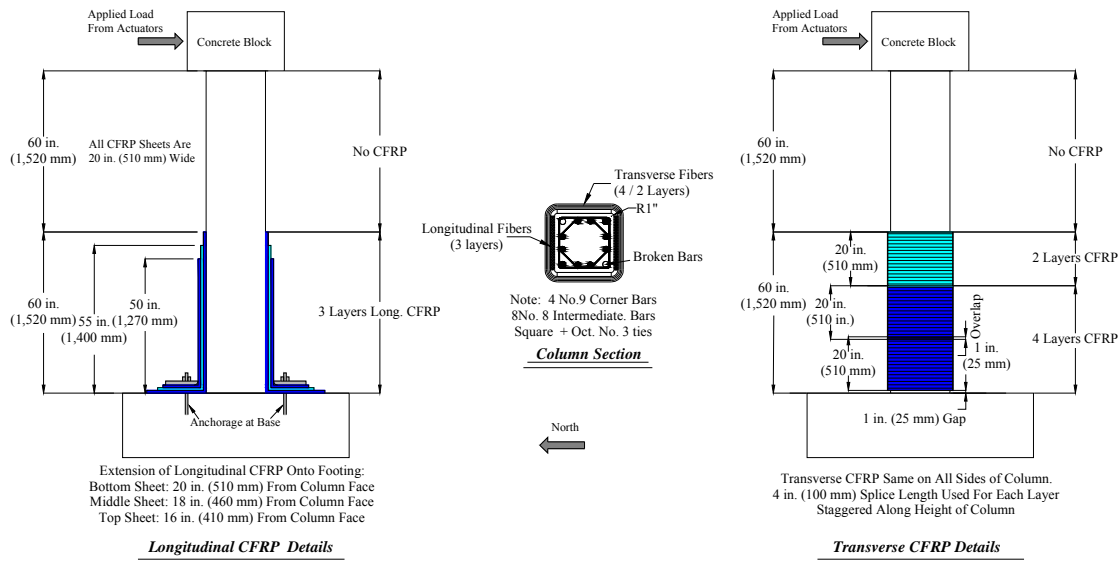


Fig. 4 CFRP layout for Column 1-R.

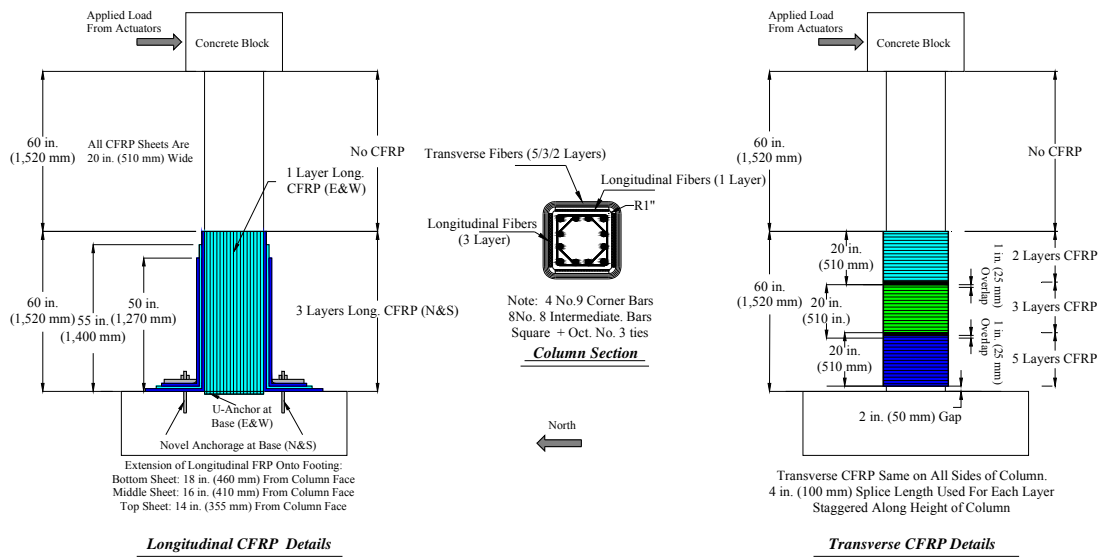


Fig. 5 CFRP layout for Column 2-R.

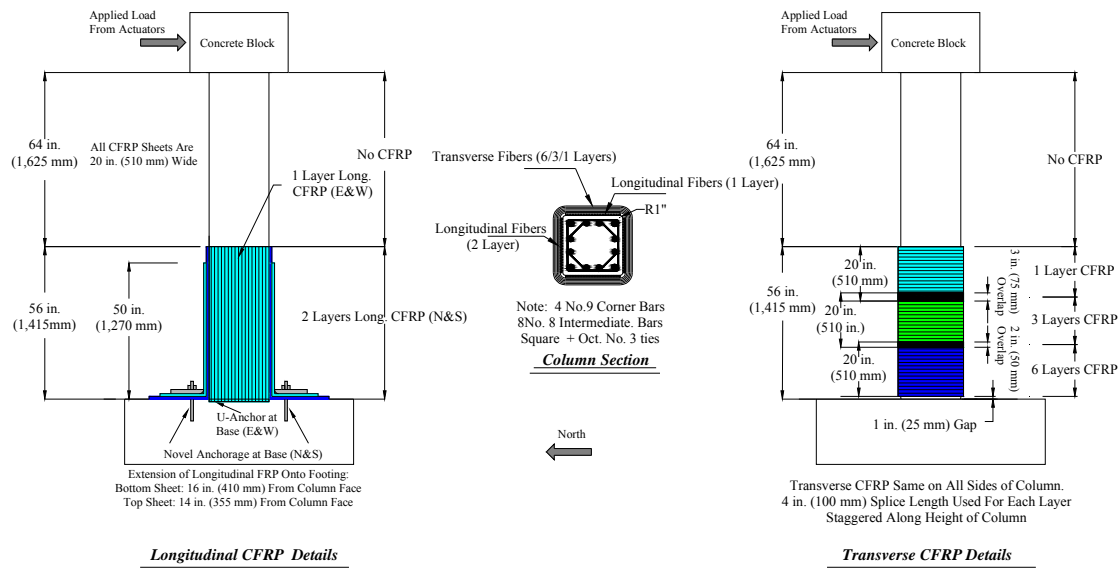


Fig. 6 CFRP layout for Column 3-R.

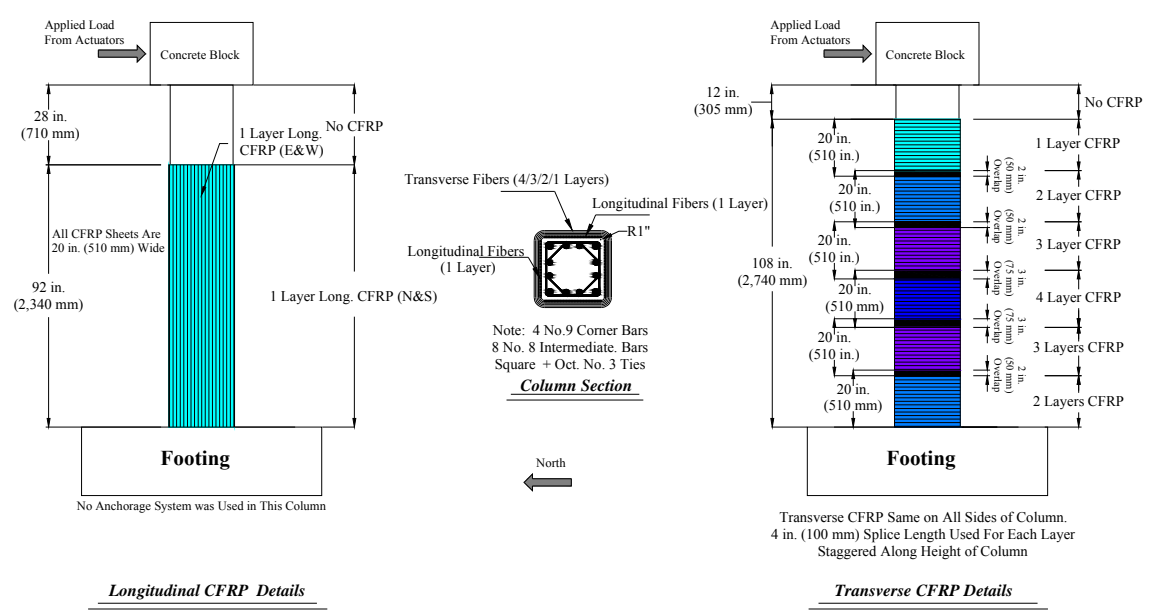


Fig. 7 CFRP layout for Column 4-R.

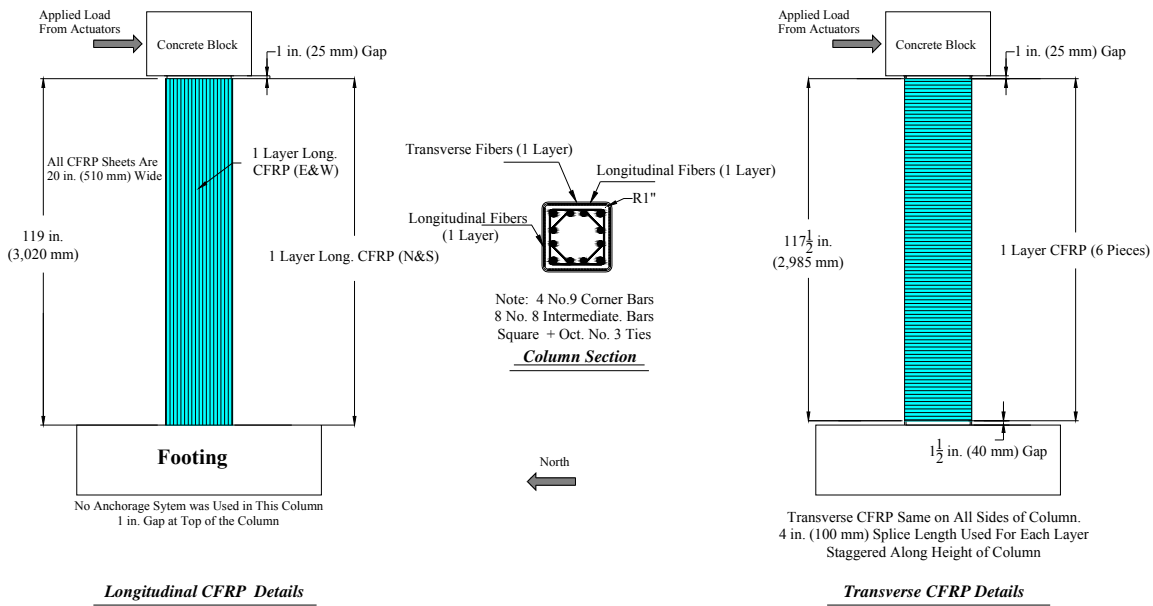


Fig. 8 CFRP layout for Column 5-R.



Fig. 9 Novel anchorage system.

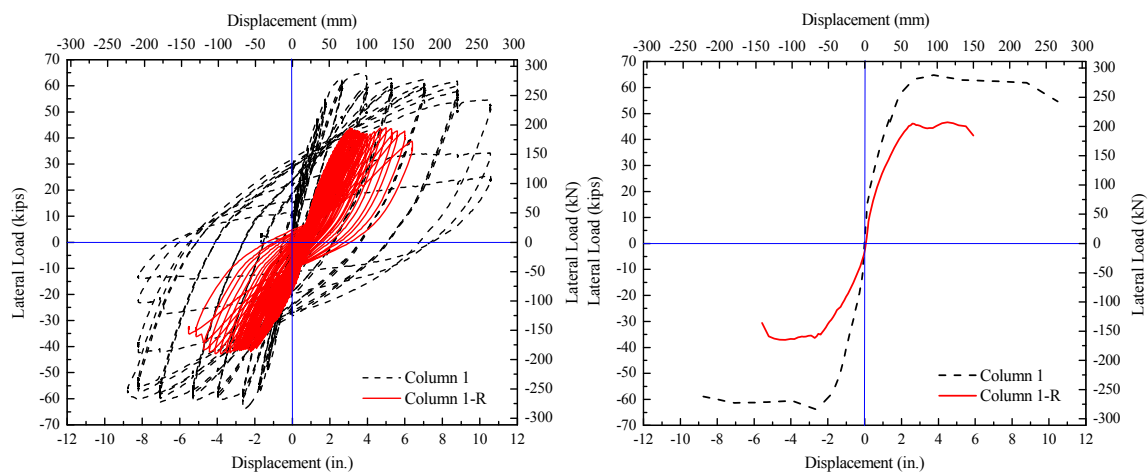


Fig. 10 General behavior of Column 1-R compared to Column 1.

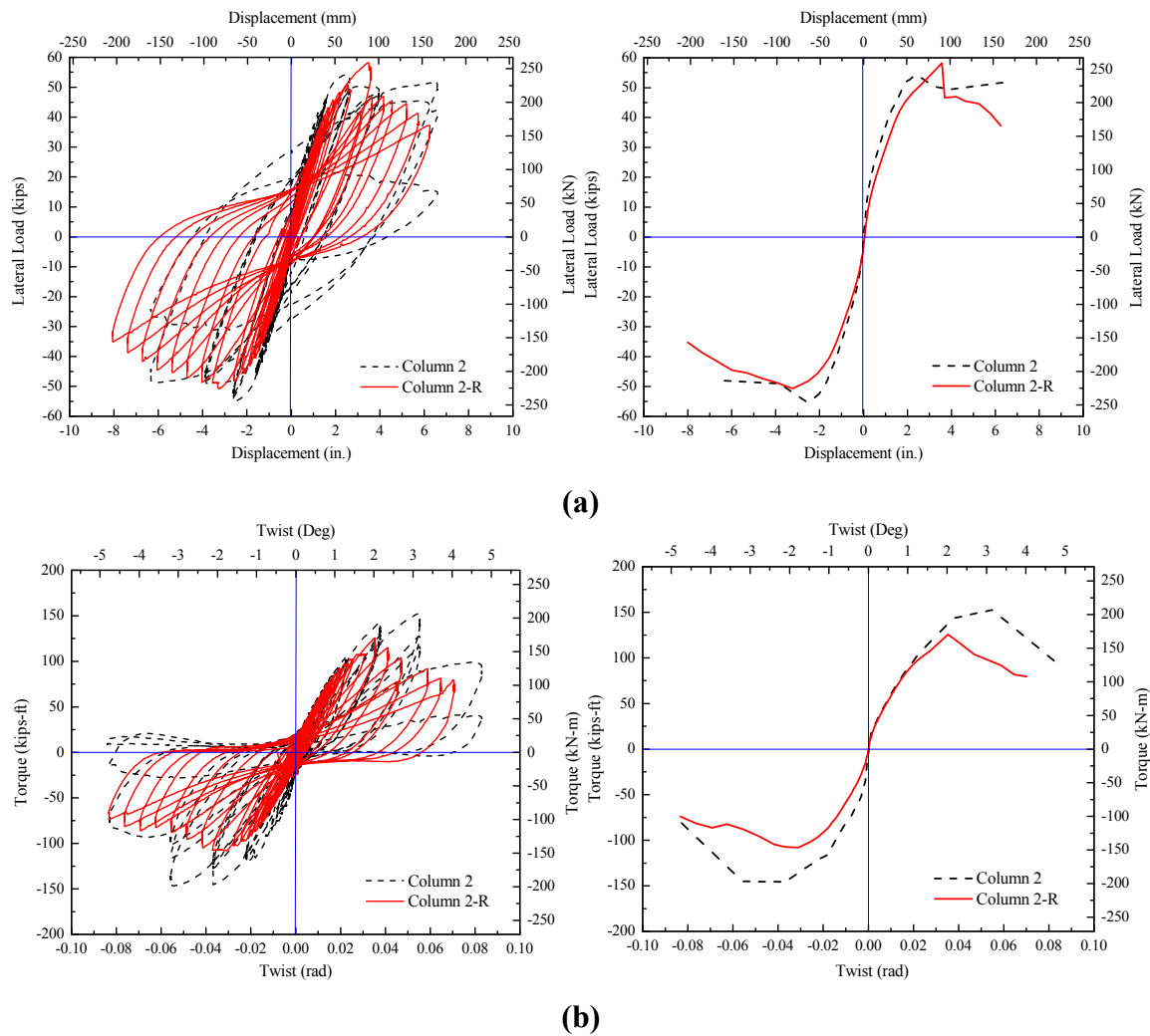


Fig. 11 General behavior of Column 2-R compared to Column 2. **a** Bending behavior. **b** Torsional behavior.

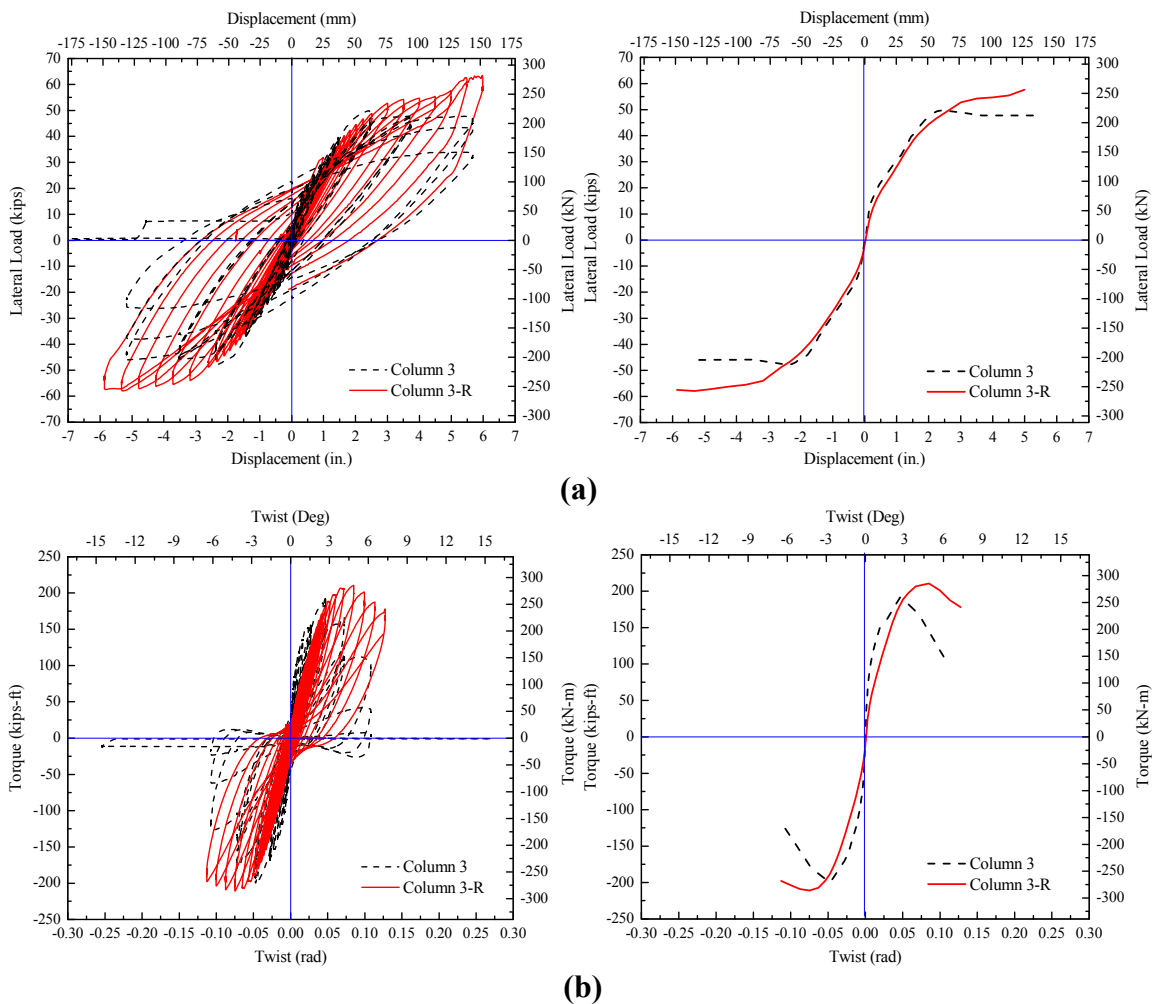
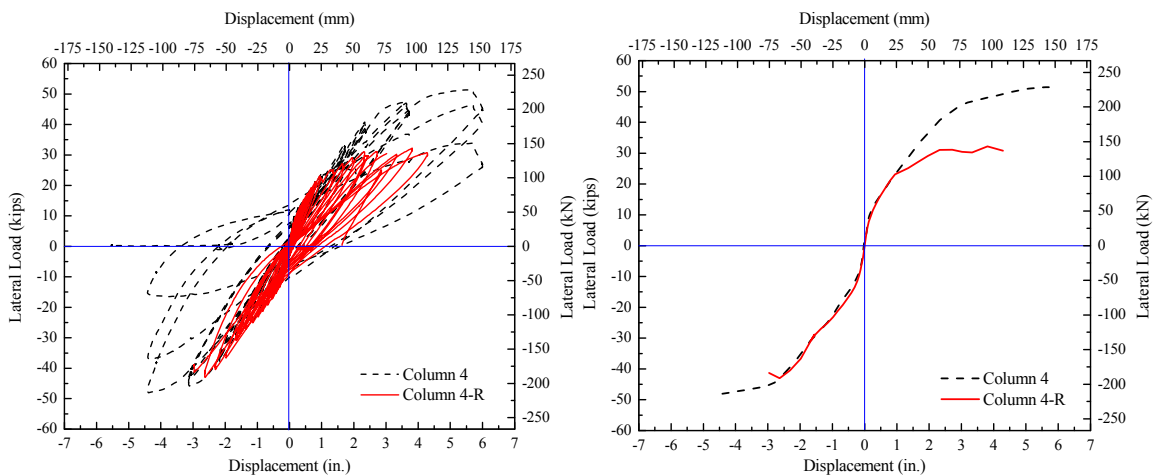
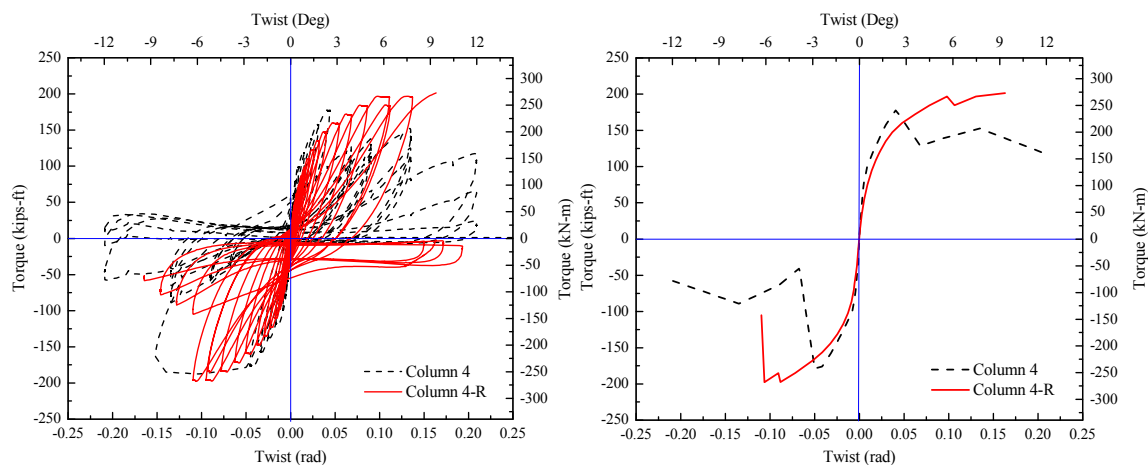


Fig. 12 General behavior of Column 3-R compared to Column 3. **a** Bending behavior. **b** Torsional behavior.



(a)



(b)

Fig. 13 General behavior of Column 4-R compared to Column 4 **a** Bending behavior. **b** Torsional behavior.

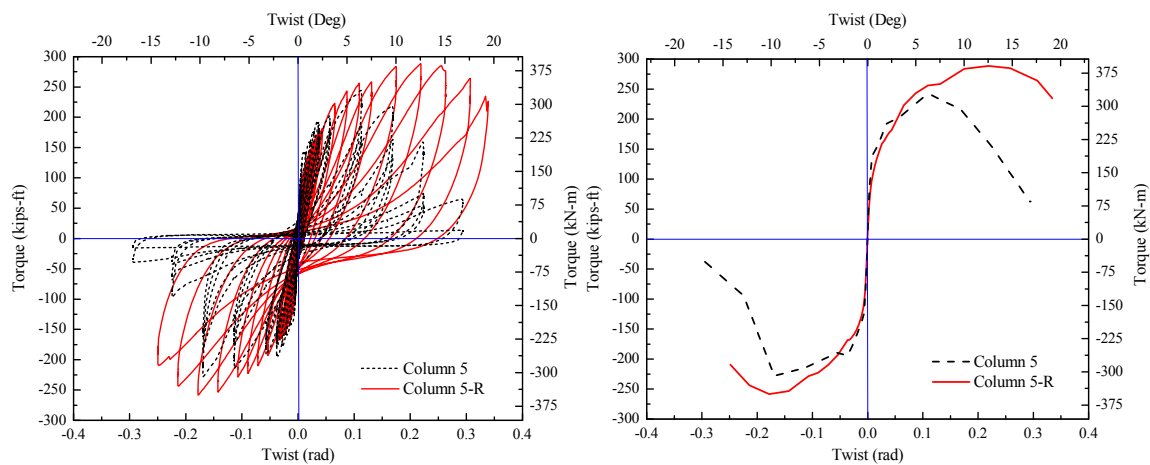


Fig. 14 General behavior of Column 5-R compared to Column 5.

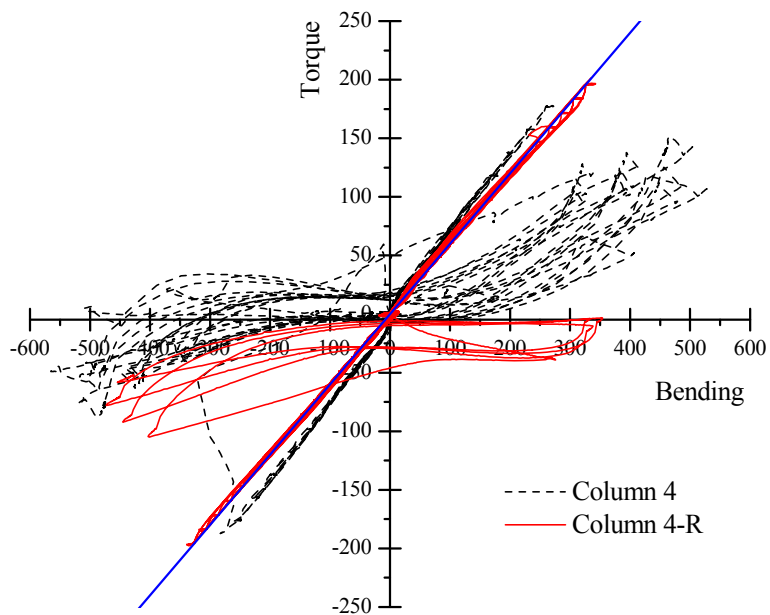


Fig. 15 Torque-to-moment ratios for Column 4 and Column 4-R.

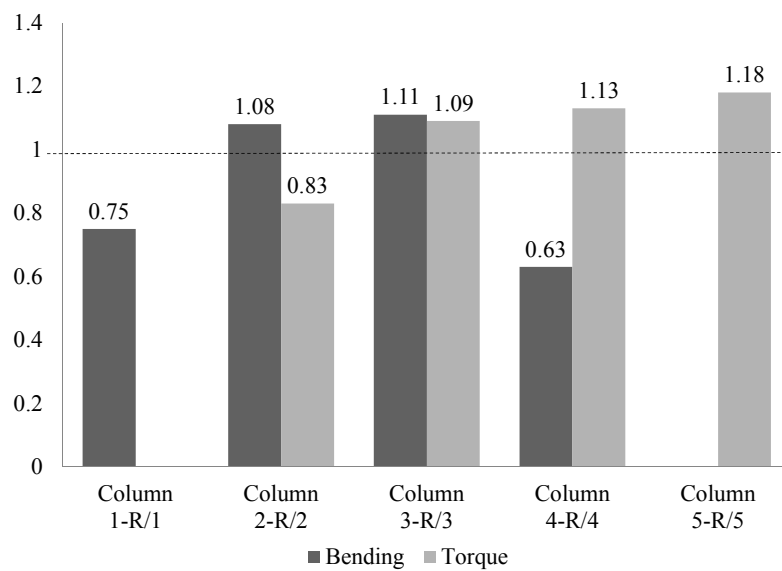


Fig. 16 Strength indices for repaired columns.

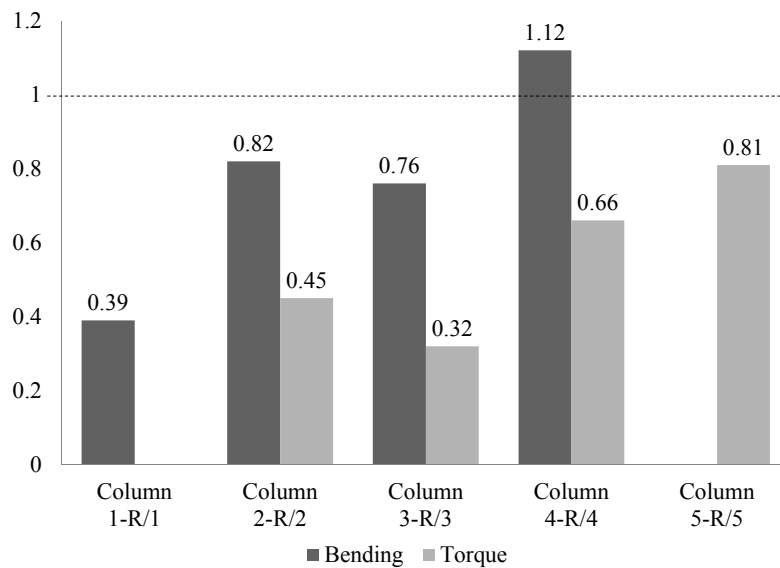


Fig. 17 Stiffness indices of initial state for repaired columns.

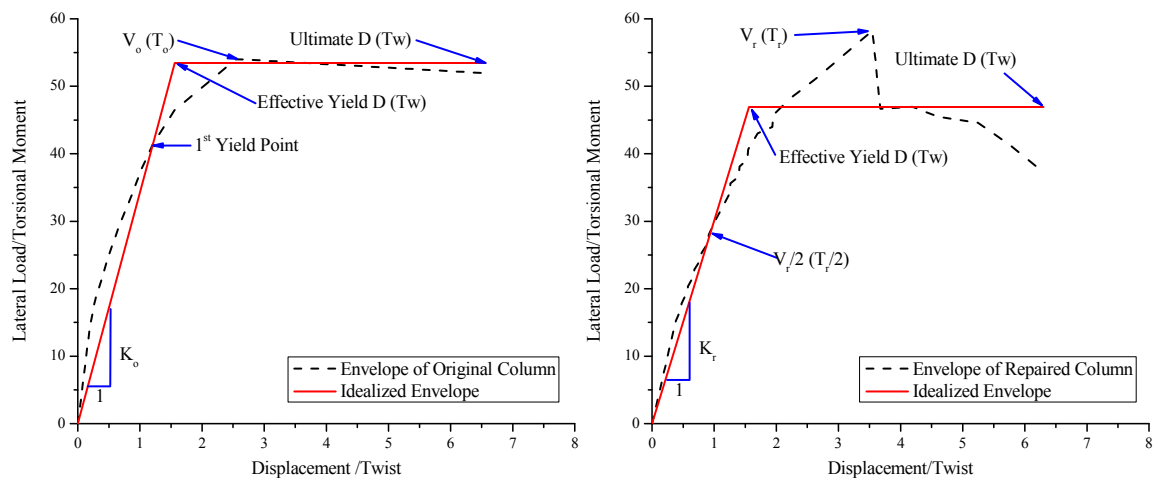


Fig. 18 Idealized envelopes for original and repaired columns.

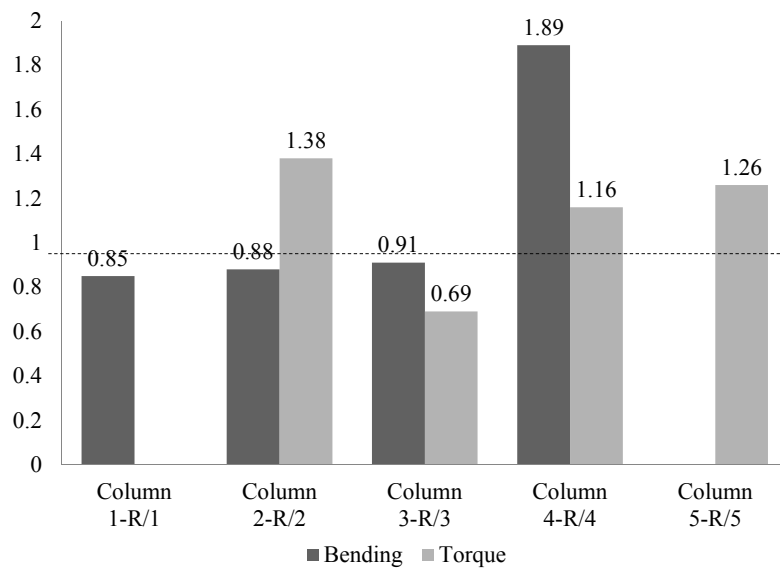


Fig. 19 General service stiffness indices for repaired columns.

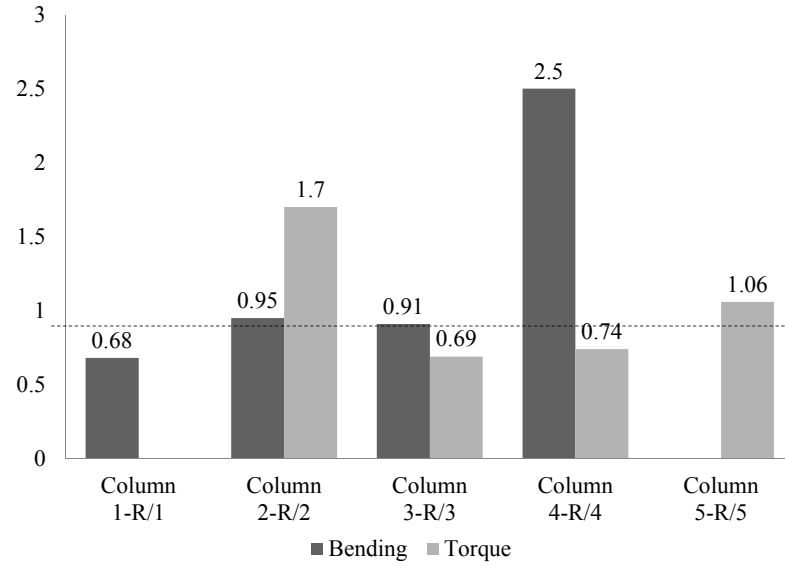


Fig. 20 Ductility indices for repaired columns.

III. RAPID REPAIR OF A SEVERELY DAMAGED RC COLUMN HAVING FRACTURED BARS USING EXTERNALLY BONDED CFRP

Ruili He¹, Stephen Grelle², Lesley H. Sneed^{3,*}, Abdeldjelil Belarbi⁴

ABSTRACT

Research on rapid repair of reinforced concrete (RC) columns has been limited to columns with slight or moderate damage. Moreover, few studies have been conducted on repair of severely damaged columns, particularly with buckled or fractured reinforcing bars. In those studies, however, the techniques used involve considerable time and effort and are not considered “rapid”. The goal of this study was to develop an effective technique to rapidly repair severely damaged RC columns for temporary service use with externally bonded carbon fiber reinforced polymers (CFRP). This paper describes the repair and retest of three half-scale severely damaged square RC bridge columns within four or five days. Damage to each column included buckled longitudinal bars, and one column had fractured bars near the column base. The repairs were designed to restore the column strength using longitudinal and transverse CFRP. A novel anchorage system was designed to anchor the longitudinal CFRP to the column footing. This study illustrates the effectiveness and limitations of this repair technique. The technique was found to be successful in restoring the strength of the columns without fractured bars, but only partially successful for the column with fractured bars located near the base because of CFRP anchorage limitations.

Key words: Anchorage, Bridge Column, Carbon Fiber Reinforced Polymer (CFRP), Fractured Bars, Reinforced Concrete (RC), Rapid Repair

1. Introduction

Based on current seismic design criteria, reinforced concrete (RC) bridge columns are designed to undergo concrete cracking, concrete cover spalling, and yielding of reinforcing steel and to provide a significant rotation capacity at plastic hinges without collapse. Damage to bridge structures during an earthquake can have devastating social and economic consequences, particularly for those that are located along key routes that are critical for emergency response and other essential functions. Such bridges are defined as “important” by ATC-18 [1], which stipulates that damage from an earthquake should be repairable within three days. Thus rapid and effective repair methods for varying levels of damage are needed to enable quick reopening of these bridges to minimize the impact on the community of affected areas. For columns with slight or moderate damage, extensive research has been conducted in which concrete, steel, or fiber reinforced polymer (FRP) jacketing was used to restore the strength and ductility of the column [2-5]. Few studies, however, have focused on the repair of severely damaged ductile RC bridge columns, especially those with buckled or fractured longitudinal reinforcing bars [6-8]. To compensate for the loss of strength due to fractured bars, most traditional repair methods have focused on the replacement or addition of internal steel reinforcement [6,7] Although these techniques have been shown to be effective in restoring the strength and ductility of severely damaged RC columns, they generally require considerable time to implement, making them difficult to accomplish as part of an emergency repair that can be achieved in a short timeframe. In a study by Saiidi and Cheng [8], glass and carbon FRP sheets with fibers in the axial direction of the column were used to compensate for the flexural strength loss due to the ruptured bars.

FRP jacketing has been used extensively to retrofit substandard RC columns that were not adequately detailed to resist seismic loads due to its high strength- and stiffness-to-weight ratios and ease of installation compared with other materials. Because installation and handling time is a critical factor in a rapid repair, FRP is a potential option in rapidly repairing severely damaged columns, although compensating for loss of strength due to fractured or buckled bars can be challenging. In such case, FRP with fibers oriented in both the column transverse (jacketing) and longitudinal directions might be considered. Depending on the damage location, an appropriate anchorage

system may be required to anchor the longitudinal FRP to the column or adjacent member when there is not enough bond length to develop its strength. In general, FRP anchorage systems are used to allow the anchored FRP to reach a higher design strength than would be possible without its inclusion. Moreover, in some cases anchorage systems provide a force transfer mechanism that is critical to the strength of the FRP system [9]. When the critical section is located near the end of a member, such as in the case of cantilever column bending, the performance of the anchorage system becomes critical to ensure that the tensile load in the FRP can be transferred to the supporting member. Otherwise, premature failure of the strengthening system can occur [5].

This paper describes the results of three half-scale severely damaged square RC bridge columns that were rapidly repaired for temporary service use. Each column had buckled longitudinal bars, concrete cover spalling, and significant crushing of the concrete core. One of the columns, which is emphasized in this paper, was unique as it had fractured longitudinal bars located near the footing at the column base. This study is the first attempt to rapidly repair severely damaged columns using an externally bonded carbon FRP (CFRP) system without any treatment of the damaged reinforcing bars. Both longitudinal and transverse CFRP sheets were used to repair the columns. Especially for the column with fractured bars, the design of a novel anchorage system was necessary to develop the longitudinal CFRP strength [10]. The overall goals of this paper are to demonstrate proof of concept and to establish the details on the repair procedure, design philosophy, and FRP anchorage detailing. The experimental results of the repaired columns and anchorage system are also discussed, and recommendations are made for future use and improvements of this system.

2. Background

2.1. Design of original columns

Fig. 1 shows the geometry and reinforcement details of the RC columns that were the focus of this investigation. The columns were 22 in. (560 mm) square reinforced with four deformed No. 9 ($\phi = 29$ mm) bars in the four corners and eight No. 8 ($\phi = 25$ mm) intermediate bars. They were 166 in. (4,220 mm) tall with 132 in. (3,350 mm) effective height measured from the column base to the centerline of applied loading. Square and

octagonal No. 3 ($\phi = 10$ mm) deformed bars were used as the tie reinforcement spaced at 3.25 in. (82 mm). The tie bars were anchored using 135 degree bent hooks with a development length of 2.5 in. (64 mm). The longitudinal and transverse reinforcement volumetric ratios were 2.13% and 1.32%, respectively. The measured yield strengths of the No. 8 ($\phi = 25$ mm) and No. 9 ($\phi = 29$ mm) longitudinal bars were 76 ksi (524 MPa) and 67 ksi (462 MPa), respectively. The measured yield strength of the No. 3 ($\phi = 10$ mm) ties was 74 ksi (510 MPa). The concrete compressive strength measured at the original test date ranged from 5,260 psi (36.3 MPa) to 5,880 psi (40.5 MPa).

2.2. Damage evaluation of original columns

The columns were originally tested to failure under cyclic lateral loading and a constant axial load of approximately 150 kips as part of a separate study [11]. Column 1 was subjected to cyclic uniaxial cantilever bending and shear in addition to the constant axial load. Columns 2 and 3 were subjected to the constant axial load and a combined cyclic loading effect of uniaxial cantilever bending, shear, and torsion, with torque-to-moment ratios (T/M) of 0.2 and 0.4, respectively. All tests were conducted at the High Bay Structural Engineering Research Laboratory (SERL) at Missouri University of Science and Technology (Missouri S&T) in Rolla, MO.

Figs. 2-4 show the damaged columns after the original tests. Damage to all three columns included concrete cracking, cover spalling, and core crushing and longitudinal reinforcement yielding and buckling. Additionally, two longitudinal reinforcing bars fractured in Column 1 near the base of the column at the northwest and southeast corners of the cross section (see Figure 2). The damage to all three columns was concentrated near the base of the column at the location of maximum moment due to flexure-dominant behavior in columns with low T/M ratios ($T/M < 0.5$). The damage is summarized in Table 1 in which measurements are included to provide insight into the damage extent and plastic hinge location of each column. Damaged ties failed by yielding and, in some cases, subsequent straightening of the end hooks.

ATC-32 defines three general damage states for RC members: slight, moderate, and significant [12]. Some recent studies have also attempted to refine these damage states by correlating the apparent damage to seismic response parameters [13-15].

Considering the damage conditions of the original columns as described previously, the damage observed was classified as significant according to ATC-32 criteria. The terms “significant” and “severe” are used interchangeably in this paper when referring to the column damage.

3. Column repair materials

Because this was a rapid repair, the timeframe from repair initiation to test initiation was critical and closely monitored to demonstrate that the repair materials used were compatible and capable of achieving their required strengths within the timeframe. The CFRP strengthening system was comprised of carbon fiber tow sheets consisting of unidirectional fibers with the following properties given by manufacturer: ultimate tensile strength of 550 ksi (3,800 MPa); tensile modulus of 33,000 ksi (227 GPa); ultimate rupture strain of 0.0167; and nominal thickness of 0.0065 in. (0.165 mm) per ply. The CFRP sheets were 20 in. (508 mm) wide. The stress-strain relationship of the fibers is linear-elastic until rupture.

The material used to replace the removed damaged concrete was selected given the following considerations: (1) design strength can be achieved in two to three days after placement; (2) surface moisture is minimal a short time after placement; and (3) fluidity can minimize voids present after placement. A pre-extended micro concrete was chosen as the repair mortar. The average compressive strength of the repair mortar at test date based on the results of three tests measured in accordance with ASTM C109 [16] was 5,410 psi (37.3 MPa) for Column 1-R, 5,855 psi (40.4 MPa) for Column 2-R, and 5,455 psi (37.6 MPa) for Column 3-R. Note the designation –R indicates the repaired column.

Bond strength testing of the CFRP-to-concrete bond was performed in accordance with ASTM D7234 [17]. A representative sample of CFRP was bonded to the concrete surface that was prepared using the same techniques and at the same time as the CFRP application. The test was performed at the time of retesting of the repaired column. The average bond strength based on the results of three tests was 380 psi (2.6 MPa), 230 psi (1.6 MPa), and 580 psi (4.0 MPa) for Columns 1-R, 2-R, and 3-R, respectively. The bond

strength test results met the CFRP system manufacturer's and ACI 440.2R [18] minimum specified bond strength of 200 psi (1.4 MPa).

4. Repair design

4.1. CFRP design

The repair of each column was designed to restore the column strength associated with the peak load in the original test. In the case of a permanent repair, the strengthening system should also restore the column stiffness and ductility, although these aspects were not explicitly accounted for in this design. To maximize the time efficiency, only the regions of the columns at and adjacent to the plastic hinge were repaired. A primary region was defined as the region where the damage was concentrated, and a secondary region was the region adjacent to the primary region with the same length. Portions of the column outside these regions exhibited slight cracks on the concrete surface but were not repaired. The repair design objective was accomplished by utilizing the CFRP sheets in both the transverse and longitudinal directions. The following assumptions were made during the design process: 1) longitudinal reinforcing bars that had buckled in the original test would only provide tensile strength, 2) the design compressive strength of the repair mortar was 4,000 psi (27.6 MPa) at test date, and 3) failure of the FRP anchorage system would not occur.

4.1.1. Column 1-R

The preliminary designs of the longitudinal and transverse CFRP were conducted separately first, then a sectional analysis was used to finalize the design. The transverse CFRP was preliminarily designed with the objective of restoring the shear strength and the confinement, then the larger number of layers from each those designs was selected as the preliminary design result.

To compensate for the strength loss due to the fractured longitudinal reinforcing bars, the longitudinal CFRP was preliminarily designed to provide the same tensile strength as the yield force of the fractured bars [8]. Considering that the column was subjected to uniaxial bending in the north and south directions, and that limited space was

available for anchorage application on the east and west sides of the column (due to the test setup), longitudinal CFRP was applied only to the north and south faces.

In RC members that are fully wrapped by FRP, loss of aggregate interlock of the concrete has been observed to occur before the FRP wrap reaches its ultimate strain. To preclude this failure mode, the maximum strain used for the design of transverse FRP is usually limited to a specific value, which is known as the effective strain [18]. The effective strain of the transverse CFRP wrap in this design was chosen as 0.004, which is based on testing and experience [19]. Therefore, in determining the thickness of the transverse CFRP required to restore the shear strength, the stress in the CFRP was limited to $0.004E_j$, where E_j is the elastic modulus of the CFRP. According to California Department of Transportation (Caltrans) criteria for seismic shear design for ductile concrete members [20], the required thickness for the jacketing, t_j , is determined as:

$$t_j = \frac{V_0/\phi - (V_c + V_s)}{2 \times 0.004 \times E_j \times b} \quad (1)$$

in which V_0 is the over-strength shear, V_c is the concrete shear capacity, V_s is the shear strength provided by the transverse reinforcing steel, ϕ is a strength reduction factor taken as 0.85 for shear, and b is the column dimension in the loading direction. V_0 was taken as the shear corresponding to the maximum moment achieved in the original test. Since four ties in the plastic hinge were opened and removed during placement of the formwork for the repair mortar, which resulted in a larger tie spacing within the plastic hinge, V_s was conservatively neglected. V_c was calculated based on the estimated compressive strength of the repair mortar at test date, which considered the confinement effect of the transverse CFRP wrap.

The thickness of the transverse CFRP required to restore the confinement from the damaged stirrups was preliminarily designed according with the provisions for RC column retrofit given by Caltrans [21] as Eq. (2):

$$t_j = \frac{f_l D}{2\alpha_j E_j \varepsilon_j} \quad (2)$$

in which f_l is the confinement stress, and D is the equivalent dimension for the square column. α_j is reduction factor for FRP modulus of elasticity, E_j is the CFRP modulus of elasticity, and ε_j is the dilating strain estimated to be 0.004 [21].

Based on the preliminary designs of the longitudinal and transverse CFRP, a sectional analysis was made to finalize the design. Moment-curvature analysis was conducted using a layer-by-layer approach in which the cross section was divided into a number of discrete layers. Each layer contained a quantity of concrete confined by CFRP, steel ties, or both, longitudinal reinforcing steel, and CFRP. The stresses in the concrete, reinforcing steel, and CFRP in each layer were determined from the average strain in each layer and the stress-strain relationships. The model by Lam and Teng [22], which is adopted by ACI Committee 440 [18], was used to describe the compressive stress-strain relationship of the CFRP-confined concrete in this study. Though this model has not been verified for damaged concrete confined with FRP, it was used in this design because the damaged concrete would be removed and replaced with repair mortar at the critical cross section where the sectional analysis was conducted. The theoretical moment-curvature relationship for the constant axial load P of 7% of the axial strength was determined by incrementally increasing the concrete strain in the extreme compression layer. For each value of the concrete strain in the extreme compression layer, the neutral axis depth was determined by satisfying force equilibrium as shown in Eq. (3):

$$P = \sum_{i=1}^n f_{ci} A_{ci} + \sum_{i=1}^n f_{si} A_{si} + \sum_{i=1}^n f_{Fi} A_{Fi} \quad (3)$$

where f_{ci} , f_{si} , and f_{Fi} represent the stresses of concrete, steel, and CFRP in the i th layer, A_{ci} , A_{si} , and A_{Fi} are the areas of concrete, steel, and fiber in the i th layer, and n is the number of layers. Then the moment M corresponding to the given concrete strain in the extreme compression layer was determined by taking the moments of the internal forces about a suitable axis using Eq. (4):

$$M = \sum_{i=1}^n f_{ci} A_{ci} d_{ci} + \sum_{i=1}^n f_{si} A_{si} d_{si} + \sum_{i=1}^n f_{Fi} A_{Fi} d_{Fi} - P \cdot \frac{h}{2} \quad (4)$$

where d_i represents the distance of the centroid of i th layer from the extreme compression fiber, and h is the section depth. The curvature was determined by dividing the concrete strain in the extreme compression layer by the neutral axis depth.

Fig. 5 shows the result of the moment-curvature analysis. The predicted decrease in moment capacity from points A to B in the figure is due to rupture of the longitudinal CFRP. It should be noted that results were based on the assumption that the longitudinal

CFRP anchorage could transfer the force required from the column to the footing. Design of the system used to anchor the longitudinal CFRP is discussed in the next section.

The final repair design for Column 1-R consisted of three layers of longitudinal CFRP on the north and south faces of the column. A varying number of layers of transverse CFRP wraps were placed around the column to a height of 60 in. (1,524 mm) from top of footing, which is the height of the sum of primary and secondary regions mentioned previously. Half the number of transverse layers provided in the primary region was provided in the secondary region. No longitudinal or transverse CFRP was placed above this height. The final repair design is shown in Fig. 6.

4.1.2. Columns 2-R and 3-R

The repair design was modified for Column 2-R based on the performance of repaired Column 1-R and to include the design for torsion ($T/M = 0.2$). Similarly, the repair design for Column 3-R was modified based on the performance of repaired Columns 1-R and 2-R and to include the design for torsion ($T/M=0.4$). The torsion was designed based on a space truss model [23]. For both Columns 2-R and 3-R, the longitudinal CFRP design included the designs for flexure and for torsion, which were assumed to be additive. In designing the transverse CFRP, shear and torsion were assumed to be additive.

The final repair designs for Columns 2-R and 3-R are shown in Figs. 7 and 8, respectively. In addition to providing reinforcement on the north and south faces (the extreme tension and compression fibers in the direction of bending), 1 layer of longitudinal CFRP was provided on the east and west faces for torsion, as well as to prevent crack initiation on these two faces for both Columns 2-R and 3-R. Column 3-R had the least amount of longitudinal CFRP because the design bending moment was smaller than that of Columns 1-R and 2-R. For Columns 2-R and 3-R, the layers of transverse CFRP were adjusted based on the performance of the previous repaired column responses. The number of layers of transverse CFRP in the repair region 20 in. (510 mm) to 60 in. (1,525 mm) above the footing was reduced on Columns 2-R and 3-R because the damage observed in the repaired Column 1-R test was concentrated in the

first 20 in. (510 mm) region, and there was no visible damage in the repaired region above.

4.2. Anchorage

4.2.1. Column 1-R

Based on the repair design for Column 1-R described in the previous section, a significant force in the CFRP was required to be anchored to the column footing in order to compensate for the tensile strength of the fractured reinforcing bars. This presented a challenge for the design of the anchorage system, as the systems reported upon in literature are generally not designed to resist forces of such magnitude. Therefore, an extensive review of anchorage systems was conducted [9], based upon which a novel anchorage system was designed for the column repair.

The anchorage system used to anchor the longitudinal CFRP sheets on the north and south faces consisted of a steel plate welded to a quarter-section of steel pipe reinforced with stiffeners and fastened to the concrete with threaded steel anchor rods that were embedded using a chemical adhesive. Fig. 9 shows the details of the anchorage system. Placement of the anchor bolts was dictated by the reinforcement layout in the column footing, as well as the existing cracks in the footing near the plastic hinge location. The quarter-section of pipe was placed at the column-to-footing interface in order to resist the force that was expected to develop as the CFRP debonded at the 90-degree joint, as well as to reduce local stress concentrations in the CFRP due to this reaction. Load cells were installed on select anchor rods, and strain gages were installed on the steel plate to monitor the behavior of the anchorage system. Details of the anchorage system design and observed behavior are described at length elsewhere [10].

4.2.2. Columns 2-R and 3-R

The longitudinal CFRP on the north and south faces of Columns 2-R and 3-R was anchored using the same anchorage system used in Column 1-R. A 0.25 in. (6 mm) gap was provided between the edge of the quarter-pipe and the column face as shown in Fig. 9 to avoid premature failure due to the bearing of the column onto the edge of anchorage. The longitudinal CFRP sheet on the east and west faces of Columns 2-R and 3-R was

anchored using U-anchors placed in the footing at the column-footing joint (see Fig. 10) due to space limitations in these areas (wide flange beams in the test setup in Fig. 12).

5. Repair procedure

The damaged columns were repaired and retested within five days for Column 1-R and within four days for Columns 2-R and 3-R. The repair procedure consisted of seven steps (including instrumentation application) shown in Fig. 11. Before the repair began, the damaged columns were straightened to ensure that they were capable of being repaired and retested. Initial straightening was challenging due to limited equipment available, and this step was not included in the repair time. The rapid repair started with removing loose concrete, followed by erecting formwork, and placing repair mortar on the first day. After the mortar set approximately 12 hours, the formwork was removed, and the surface of the concrete was prepared for CFRP applications. Column corners were rounded with a hand grinder to provide a radius of 0.5 in. (12 mm). The CFRP composite strengthening system was applied on the third day for Column 1-R and on the second day for Columns 2-R and 3-R. All longitudinal CFRP sheets were installed first, followed by installation of the transverse CFRP wrap. No special curing process was used, although a plastic sheet was provided to keep in heat for Columns 1-R and 2-R due to the low temperature in the lab (see Fig. 11f). Before retesting, a significant amount of instrumentation was installed on the repaired column to evaluate the behavior. Instrumentation took place on the fourth day for Column 1-R and on the third day for Columns 2-R and 3-R. The repaired columns were retested at the beginning of the following day.

6. Test procedure

The testing setup that was used to provide fixity of the footing during testing involved a reinforced concrete test bed. Hydrostone® was placed in gaps between the footing and the test bed to eliminate the potential for movement. Two steel wide flange beams were placed over the surfaces of the footing and the test bed to resist the forces generated by the rotation of the footing when the lateral force was applied to the top of the column. The wide flange beams reacted against a double-channel built-up steel

section placed on each end of the test bed that transferred the reaction to the reaction floor using four Dywidag bars on each end. Hydrostone® was also placed under the wide flange beams to ensure a uniform bearing surface on the beam flanges. Resistance to shear forces applied to the column was provided by two Dywidag bars that passed through each end of the test bed and into the reaction floor.

The test was completed in one day. Lateral load was applied to the column using two hydraulic actuators that were mounted to the column cap and reacted against a reaction wall. Torsion was applied to Columns 2-R and 3-R by adjusting the forces or displacement of the two actuators. As with the original column, a constant axial load of approximately 150 kips (670 kN) was applied with seven steel prestressing strands through a PVC pipe in center of the column. This load corresponds to approximately 7% of the original column axial strength, which is representative of the axial load from a bridge superstructure. The strands were fixed at the top of the column cap and at the bottom of footing. The axial load was applied using a hydraulic jack. The applied axial load was monitored during the test, and the maximum variation due to the lateral displacement was 5%. The test setup is shown in Fig. 12.

Load was applied to the repaired columns under slow cyclic loading in a manner similar to the original columns. One exception was that only one cycle was applied at each load stage to the repaired columns, while three cycles were applied at each load stage to the original columns after yielding. The other difference was that the specified T/M ratio was maintained during loading within each cycle more successfully with the repaired columns than the original columns, which varied after yielding occurred. The testing procedure was initiated in force control and was increased in small increments until the applied load neared 50% of the estimated capacity of Column 1-R and 80% of Columns 2-R and 3-R. Afterwards, the testing procedure was continued in displacement control. Positive shear force and bending moment were defined as when the actuators were pushing the column in the south direction. Likewise, negative shear force and bending moment were defined as when the actuators were pulling the column in the north direction. Positive torsion was defined when the column twisted in counterclockwise direction.

7. Discussion of test results

7.1. Overall behavior and observed damage

For Column 1-R, little observable behavior occurred while the specimen was tested under force control. After several cycles of displacement control testing, some unusual shear cracks were observed on the east and west vertical faces of the footing directly beneath the column. These cracks initiated in the cycle from A to A' shown in Fig. 13. The cracks continued to open wider until the applied load reached the cycle from B to B'. Following, further opening and closing of the cracks was not observed for the remainder of the test. Also, the forces measured from the load cells on the anchorage system anchor rods on both sides of the column decreased significantly and remained small for the remainder of the test.

As the test progressed, it was observed that the CFRP near the base of the column came into contact with the top of the quarter-pipe section of the anchorage system. At the same time, tapping on the CFRP surface revealed that the CFRP directly above the anchorage had debonded from the surface of the column. Ultimately, CFRP rupture was noted on both the south and north sides of the column at the same height due to the bearing of the corner of the anchorage system. Splitting of the transverse CFRP on the east and west sides of the column was also observed prior to failure due to opening and closing of cracks in the concrete within. The test was terminated when the lateral load-carrying capacity had diminished. This occurred after a sound was heard from the column that indicated fracture of longitudinal reinforcing bars. Fig. 14 shows the northwest corner of the column at failure. Rupture of CFRP can be seen adjacent to the quarter-pipe section of the anchorage, while splitting of the transverse CFRP is shown on the west face. After removing the CFRP at completion of testing, crushing of the cover concrete was observed on the north side of the column near the point of contact between the column and the anchorage. Fig. 15 shows the southeast corner of the column after testing in which rupture of CFRP on the south side adjacent to the anchorage edge and splitting of the transverse CFRP on the east side are shown. After removing the CFRP, two intermediate No. 8 ($\phi = 25$ mm) longitudinal bars on the south side were found to have fractured during the test.

For Column 2-R, pullout of the U-anchors applied on the east and west sides of the column was observed during the test as expected. As the column was loaded cyclically, the tested column dilated in the plastic hinge region, which was located slightly higher than that of Column 1-R due to the influence of torsion applied. Rupture of the CFRP was also observed during the test, but because a gap was provided between the anchorage system and column (Fig. 9), the contact failure that occurred in the Column 1-R test was avoided. All damage was localized within the region 20 in. (510 mm) directly above the column footing.

For Column 3-R, no damage was observed in the repaired region during testing. Throughout the initial stages of loading, existing cracks in the concrete located directly above the repaired region were observed to open and close. As the test progressed, the concrete cover just above the repaired region spalled off, and the cover spalling progressed upwards until testing was completed. Formation of damage occurred slightly above the repaired region because the T/M ratio (and particularly the applied torsion) was maintained after yielding, which was not the case during the original test as mentioned previously. Testing was terminated because the orientation of the actuators prevented further rotation of the column.

The failure mode of each repaired column was different due to several reasons. First, the initial damage condition of each column was different. Because Column 1-R had fractured reinforcing bars, the demand on the longitudinal CFRP and its anchorage system were larger than for Columns 2-R and 3-R. Also, the plastic hinge from the original test was located slightly higher above the base on Columns 2 and 3 than on Column 1 due to the applied torsion. Additionally, problems resulting from detailing of the longitudinal CFRP anchorage system on Column 1-R were addressed in the repair of Columns 2-R and 3-R.

7.2. Load-deformation response

Fig. 16 shows the measured hysteresis load-displacement relationship of repaired Column 1-R compared to original Column-1. As shown in the figure, the column behaved asymmetrically in the positive cycle (displaced to the south) and the negative cycle (displaced to the north). This can be attributed to the unsymmetrical damage in the

original column and the unsymmetrical removal and replacement of loose concrete during the repair procedure. In the positive direction, the applied load was increased to 46.14 kips (205 kN) at a displacement of 2.6 in. (66 mm), while in the negative direction the applied load was increased to -36.55 kips (-162 kN) at a displacement of -2.7 in. (-69 mm). Then the load resisted by the column remained nearly constant with increasing displacement. The applied load reached its maximum value of 46.64 kips (208 kN) at a displacement of 4.5 in. (114 mm) in the positive direction and -37.10 kips (-165 kN) at a displacement of -4.3 in. (-109 mm) in the negative direction. Following the maximum load, the applied load decreased with increasing displacement until failure of the repaired column associated with fracture of two additional longitudinal bars.

As discussed in the previous section, the applied lateral load ceased to increase when the load measured from the anchorage load cells dropped, which indicates that the tensile force in the longitudinal CFRP could not be transferred to the support. This is because the anchorage system was critical to developing the force in the longitudinal CFRP at the location of maximum moment (the column-footing interface). In the predicted moment-curvature response shown in Fig. 5 used for designing the repair, Point B represents the predicted moment capacity of the section after failure of the longitudinal CFRP. The value of Point B is approximately 460 kip-ft (625 kN-m), which corresponds to an applied lateral load of approximately 42 kips (187 kN). This value is close to the peak lateral load measured in the positive cycle.

Figs. 17 and 18 show the measured hysteresis load-displacement relationship of repaired Columns 2-R and 3-R, respectively, compared to original Columns 2 and 3. Both the strength and displacement were restored or even improved compared to the original columns. However, during testing of Column 3-R, large rotations caused by the torsion loads caused the swivels on the actuator heads to become bound. The binding of these swivels may have caused false readings in the internal actuator load. The onset of binding was not apparent during testing, so it was estimated by analyzing the data from the two actuators (see Fig. 18). It is clear that the maximum load before the onset of binding is higher than the maximum resisted by the original column.

7.3. Load-surface strain response

In order to study the performance of the externally bonded CFRP, strain gages were installed to the surface of the CFRP in five levels as shown in Fig. 19. Ten total strain gages were applied in longitudinal direction, and twenty were applied in the transverse direction. The measured strain for Column 1-R is discussed in this section.

Fig. 20 shows the applied load versus longitudinal strain relationships on the CFRP faces in which positive strain values indicate tensile strains. This figure shows that the surface strain history measured at Levels 2 and 3, which were located near the plastic hinge region of the original column, is more complex than that in other regions of the column (strain gages at Level 1 were damaged during testing). The magnitude of the compressive strains measured was greater than the magnitude of the tensile strains near the plastic hinge (Levels 2 and 3 of Fig. 19), which indicates that the applied longitudinal CFRP did not function as expected near the plastic hinge. This is attributed to the complex behavior and interaction between the CFRP, column, and anchorage system. At levels farther away from the plastic hinge, the measured tensile and compressive surface strains were nearly symmetric. The maximum measured tensile strain was approximately $2,440 \mu\epsilon$, which is much less than the CFRP rupture strain of $16,700 \mu\epsilon$. In addition, longitudinal strains decreased with increasing height from the column base since they are further from the plastic hinge.

Fig. 21 shows the applied load versus transverse strain relationships on the CFRP faces. The maximum transverse strain reached $2,340 \mu\epsilon$ at Level 1, which is much smaller than the CFRP rupture strain. As expected, the magnitude of the measured strains decreased with increasing distance from the column-footing joint. The strain measured in the plastic hinge zone was higher than that measured elsewhere because the CFRP acted as replacement of removed or opened stirrups to provide shear strength and confinement for the concrete in this location. The transverse strains measured away from the plastic hinge were very small, which shows that the reinforcing steel stirrups in these regions could still work well to provide adequate shear strength and confinement. It should be noted that all strain gauges were installed on the center of the column faces, and strains at the column corners are expected to be larger than the measured values.

Based on the measured strains on the surface of the CFRP, the tensile strength of the CFRP was not fully utilized in either the longitudinal or transverse directions. This observation supports the conclusion that the longitudinal CFRP system in Column 1-R failed prematurely primarily due to anchorage as discussed previously. Additionally, the transverse CFRP continued to play a role in confining the column until complete failure of the repaired column due to fracture of two additional longitudinal bars.

7.4. Comparison of the repaired and original columns

Strength, stiffness, and ductility capacity are three important parameters to describe the performance of a structure. Although restoration of the column stiffness and ductility were not included in the repair design, the results are compared here to describe the overall repair performance. In order to compare the response of the repaired columns to the original columns with respect to these three parameters, envelopes based on the peak base shears and corresponding displacements were developed, which were then idealized by elasto-plastic curves [15, 24]. For the original columns, the envelopes were idealized by setting the initial slope to pass through the first yield point and adjusting the plastic portion so that areas under the measured curve and idealized curve were equal. For the repaired columns, the elastic part of the idealized curve was obtained by connecting the origin to a point on the measured envelope at which the force was one-half of the peak measured value. The yield level was established by equalizing the area between the measured and idealized curves. For example, the idealized elasto-plastic curves for Column 1 are shown in Figs. 22 and 23 for the original and repaired columns, respectively. The same analysis was conducted for Columns 2 and 3, which are shown in Figs. 24 and 25. The idealized response values for the original and repaired columns are summarized in Table 2. From the idealized elasto-plastic curves, three non-dimensional response indices [24-26] were developed as follows.

Strength Index (STRI) - The strength index is defined as the lateral strength ratio of the repaired and original column, which is calculated in Eq. (5). The lateral strength of the column is defined as the maximum measured applied load, which is given in Table 3.

$$STRI = \frac{V_r}{V_o} \quad (5)$$

In Eq. (5), the terms V_r and V_o represent the maximum base shear measured in the repaired and original columns, respectively.

Stiffness Index (STFI) - The stiffness index in Eq. (6) is defined as the ratio of the service stiffness of the repaired column K_r to that of the original column K_o . The ratio of the plastic base shear to the effective yield displacement is defined as the service stiffness, which can be obtained from the idealized curves. Service stiffness values are shown in Table 3.

$$STFI = \frac{K_r}{K_o} \quad (6)$$

Ductility Index (DI) - The ductility index in Eq. (7) is defined as the ratio of the ductility capacity of the repaired column (D_r') to that of the original column (D_o). The ratio of ultimate displacement to effective yield displacement is defined as ductility capacity, which can be obtained from the idealized curves (D_r and D_o). The ultimate displacement was defined as the displacement corresponding to a significant drop in the load carrying capacity in bending (for Column 1-R) or in both bending and torsion (for Columns 2-R and 3-R) due to fracture of the embedded reinforcing steel, rupture of the externally bonded CFRP, or failure of the unrepaired portion of the column as described previously. In order to account for the different initial stiffnesses of the original and repaired columns, the ductility of the repaired column (D_r') was modified as shown in Eq. (8) [26]. Ductility capacity values are shown in Table 3.

$$DI = \frac{D_r'}{D_o} \quad (7)$$

$$D_r' = D_r \times \frac{K_o}{K_r} = D_r \times \frac{1}{STFI} \quad (8)$$

The response indices for the repaired columns are summarized in Table 4. The strength index for all three columns varies between 75.0% and 111.2%. It should be noted for Column 1 that the strength index (75.0%) was limited by the anchorage-related failure of the longitudinal CFRP as discussed previously. For Columns 2 and 3, which did not have fractured longitudinal reinforcing bars, the strength was restored or even

enhanced compared to that of the original column. The stiffness index ranged from 85.2% to 90.8%. The stiffness of the repaired columns was not fully restored due to stiffness degradation of the reinforcing steel bars and concrete cracking in the unrepaired portion of the column. The ductility index ranged from 79.0% to 107.3%. With regard to the ductility index for Column 1 (79.0%), it should be noted that the ductility of the repaired column (Column 1-R) was associated with the strength of the repaired column, which again was limited by anchorage-related failure of the longitudinal CFRP. Thus this ductility is attributed to the behavior of the repaired column confined with transverse CFRP and reinforced with the unfractured longitudinal bars (similar to Columns 2 and 3). If the peak load associated with the design moment had been achieved for Column 1-R, however, it is expected that the behavior of the column would not be ductile because of the brittle nature of CFRP, as indicated in the predicted moment-curvature response in Fig. 5. The ductility index for Columns 2 and 3, on the other hand, ranged from 107.3% to 100.0%. Given each of these results, it can be concluded that the repairs would be appropriate for temporary service use associated with the serviceability limit state repair, but may not be appropriate for the ultimate limit state, especially for Column 1 with fractured bars near the column base.

8. Conclusions

In this study, a technique was developed to rapidly repair severely damaged RC columns with externally-bonded CFRP for emergency service use. Three half-scale square RC bridge columns, severely damaged in a previous study, were repaired and retested to evaluate the repair performance. Damage to the columns included cracked, spalled, and crushed concrete, and yielded and buckled longitudinal reinforcement. Damage to Column 1 also included fractured longitudinal reinforcement near the base of the column. In addition to constant axial load, Column 1-R was subjected to cyclic uniaxial cantilever bending and shear, while Columns 2-R and 3-R were subjected to constant axial load and combined cyclic uniaxial cantilever bending, shear and torsion, with T/M of 0.2 and 0.4, respectively. The repairs were designed to restore the column strength using longitudinal and transverse CFRP. A novel anchorage system was

designed to anchor the longitudinal CFRP to the footing. Based on the findings of this study, the following conclusions are made:

1. Overall, the repair procedure developed was practical and achievable as a rapid emergency repair.
2. In this study, only the portion of the columns with severe damage, and the region immediately adjacent to it, were repaired. Results confirmed that the strength can be restored or even enhanced for the columns without fractured longitudinal bars, although a reduction in stiffness was observed due to stiffness degradation of the reinforcing steel and concrete cracking in the unrepaired portion of the column. The displacement capacity of the repaired columns without fractured bars was restored nearly to that of the original condition, although smaller displacement ductility was obtained. These findings are significant in terms of time that can be saved in completing a temporary emergency repair.
3. For the column with fractured longitudinal bars, the flexural strength was only partially restored by providing longitudinal and transverse CFRP in the plastic hinge region. Without adding additional steel reinforcement, full restoration is difficult to achieve and requires very careful detailing and adequate anchorage strength to ensure that the tensile force in the CFRP can be transferred to support at the location of maximum moment.
4. Use of longitudinal CFRP on all four sides of the column improved the performance of the repaired columns by mitigating cracking and improving the flexural strength of the repaired column.
5. A novel anchorage system was designed and used to anchor the longitudinal CFRP at the column-footing interface. Problems resulting from detailing of the anchorage system as well as the large force demands, however, contributed to the failure of the column with fractured bars. Detailing improvements, including providing a gap between the anchorage plates to the column face, improved the performance of the anchorage system.

Acknowledgements

The research was performed at Missouri S&T. The authors would like to express their appreciation to the University of Missouri Research Board for the financial support for this project. BASF is gratefully acknowledged for providing the repair materials. Thanks are also extended to research specialist, Jason Cox, research/lab technician, John Bullock, electronics technicians, Brian Swift and Gary Abbott, and the group members, Stephen Grelle, Corey Grace, Qian Li and Yang Yang, for their help throughout the repair and testing processes.

References

- [1] Applied Technology Council (ATC). Seismic Design Criteria for Bridges and Other Highway Structures: Current and Future. ATC-18, Redwood City, Calif; 1997.
- [2] Stoppenhagen DR, Jirsa JQ, and Wyllie Jr LA. Seismic repair and strengthening of a severely damaged concrete frame. *ACI Structural J* 1995; 92(2): 177-87.
- [3] Chai YH, Priestley MJN, Seible F. Seismic Retrofit of Circular Bridge Columns for Enhanced Flexural Performance. *ACI Struct J* 1991; 88(5): 572-84.
- [4] Saadatmanesh H, Ehsani M, Jin L. Repair of Earthquake-Damaged RC Columns with FRP Wraps. *ACI Struct J* 1997; 94(2): 206-15.
- [5] Belarbi A, Silva PF, Bae SW. Retrofit using CFRP Composites of RC Bridge Columns under Combined Axial, Shear, Flexure, and Torsion. In: Torres Marques et al., editors. *Challenges for civil construction*. Porto: FEUP; 2008. p. 10.
- [6] Lehman DE, Gookin SJ, Nacamuli AM, Moehle JP. Repair of Earthquake-Damaged Bridge Columns. *ACI Struct J* 2001; 98(2): 233-42.
- [7] Cheng CT, Yang JC, Yeh YK, Chen SE. Seismic Performance of Repaired Hollow-Bridge Piers. *Constr Build Mater* 2003; 17(5): 339-51.
- [8] Saiidi M, Cheng Z. Effectiveness of Composites in Earthquake Damaged Repair of RC Flared Columns. *J Compos Constr ASCE* 2004; 8(4): 306-14.

- [9] Grelle SV, Sneed LH. An Evaluation of Anchorage Systems for Fiber-Reinforced Polymer (FRP) Laminates Bonded to Reinforced Concrete Elements. ASCE structural congress. Las Vegas, NV: ASCE; 2011. P. 12.
- [10] Grelle SV. Categorization and Experimental Evaluation of Anchorage Systems for FRP Laminates Bonded to Reinforced Concrete Structures. Master's Thesis, Missouri University of Science and Technology, Rolla, MO.; 2011. p. 159.
- [11] Prakash SS, Li Q, Belarbi A. Behavior of Circular and Square Reinforced Concrete Bridge Columns under Combined Loading Including Torsion. ACI Struct J 2012; 109(3): 317-27.
- [12] Rojahn C, Mayes R, Anderson DG, Clark J, Hom JH, Nutt RV, et al. Seismic Design Criteria for Bridges and Other Highway Structures. New York, USA: John Wiley & Sons; 1997. P. 198.
- [13] Belarbi A, Prakash SS, Silva PF. Incorporation of Decoupled Damage Index Models in Performance-based Evaluation of RC Circular and Square Bridge Columns under Combined Loadings. Structural concrete in performance-based seismic design of bridges, SP-271, American Concrete Institute; 2010, p. 79-102.
- [14] Vosooghi A, Saiidi M. Seismic Damage States and Response Parameters for Bridge Columns. Structural concrete in performance-based seismic design of bridges, SP-271, American Concrete Institute; 2010. p. 29-46.
- [15] Vosooghi A, Saiidi M. Post-Earthquake Evaluation and Emergency Repair of Damaged RC Bridge Columns Using CFRP Materials. Center for Civil Engineering Earthquake Research, Department of Civil and Environmental Engineering, University of Nevada, Reno, Nevada, Report No. CCEER-10-05; 2010. p. 636.
- [16] ASTM C109-11/C109M-11. Standard Test Method for Compressive Strength of Hydraulic Cement Mortars (Using 2in. or 50 mm Cube Specimens). ASTM International; 2011. p. 9.

- [17] ASTM D 7234-05. Standard Test Method for Pull-Off Adhesion Strength of Coatings on Concrete Using Portable Pull-Off Adhesion Testers. ASTM International; 2005.p. 8.
- [18] ACI 440.2R-8. Guide for the Design and Construction of Externally Bonded FRP Systems for Strengthening Concrete Structures. American Concrete Institute: Farmington Hills, MI; 2008. p. 76.
- [19] Priestley MJN, Seible F, Calvi GM. Seismic Design and Retrofit of Bridges. New York, USA: John Wiley & Sons; 1996. p. 686.
- [20] California Department of Transportation. Seismic Design Criteria (SDC), version 1.4. California, USA: Engineering service center, earthquake engineering branch; 2006.
- [21] California Department of Transportation. Memo to Designers 20-4, Attachment B. California, USA: Engineering service center, earthquake engineering branch; 2007.
- [22] Lam L, Teng J. Design-Oriented Stress-Strain Model for FRP-Confined Concrete in Rectangular Columns. J Reinforced Plast Compos 2003; 22(13): 1149-86.
- [23] ACI Committee 318 Building Code Requirements for Structural Concrete and Commentary (ACI318-11). American Concrete Institute, Farmington Hills, MI; 2011. p. 503.
- [24] Vosooghi A, Saiidi M, Gutierrez J. Rapid Repair of RC Bridge Columns Subjected to Earthquakes. In: Proc of 2nd international conference on concrete repair, rehabilitation, and retrofitting (ICCRRR 2008), Cape Town; 2008. p. 397-8.
- [25] Vosooghi A, Saiidi M. Rapid Repair of High-Shear Earthquake-Damaged RC Bridge Columns. In: Proc of 25th US-Japan bridge engineering workshop, Tsukuba, Japan, Session 7; 2009. p. 10.

- [26] Vosooghi A, Saiidi M. Design Guidelines for Rapid Repair of Earthquake-Damaged Circular RC Bridge Columns Using CFRP. J Bridge Eng 2012.
[http://dx.doi.org/10.1061/\(ASCE\) BE: 1943-5592.0000426](http://dx.doi.org/10.1061/(ASCE)BE:1943-5592.0000426).

Table 1

Summary of damage to original columns.

Column	<i>T/M</i>	Concrete damage		Reinforcing bar damage			Ties removed
		Cover spall	Core crush	Yield	Buckle	Fracture	
Column 1	0	25 in. (635 mm) above column base	10 in. (260 mm) above column base	All bars	All bars, 10 in. (260 mm) from column base	2 bars; 10 in. (260 mm) above column base (see Fig. 1)	4 ties
Column 2	0.2	37 in. (950 mm) above column base	20 in. (500 mm) above column base	All bars	10 bars, 20 in. (305 mm) from column base	None	3 ties
Column 3	0.4	58 in. (1470 mm) above column base	30 in. (760 mm) above column base	All bars	10 bars, 30 in. (760 mm) from column base	None	1 tie

Table 2

Idealized response values for original and repaired columns.

	Plastic base shear kips (kN)		Effective yield displacement inches (mm)		Ultimate displacement inches (mm)	
	Original	Repaired	Original	Repaired	Original	Repaired
Column 1	62.3 (277)	43.7 (194)	1.7 (43)	1.4 (36)	10.6 (269)	5.9 (150)
Column 2	53.5 (238)	46.9 (209)	1.6 (41)	1.6 (41)	6.6 (168)	6.3 (160)
Column 3	48.8 (217)	52.6(234)	1.6 (41)	1.9 (48)	5.6 (142)	6 (152)

Table 3

Comparison of results.

	Lateral strength kips (kN)		Service stiffness kips/inch (kN/mm)		Ductility capacity inch/inch (mm/mm)	
	Original	Repaired	Original	Repaired	Original	Repaired
Column 1	64.76 (288)	48.54 (216)	36.6 (6.4)	31.2 (5.4)	6.2 (6.2)	4.2 (4.2)
Column 2	54.05 (240)	58.23 (259)	33.4 (5.8)	29.3 (5.1)	4.1 (4.1)	3.9 (3.9)
Column 3	49.84 (222)	55.42 (247)	30.5 (5.3)	27.7 (4.9)	3.5 (3.5)	3.2 (3.2)

Table 4
Response indices for the repaired columns.

INDEX	STRI (%)	STFI (%)	DI (%)
Column 1	75.0	85.2	79.0
Column 2	107.7	87.7	107.3
Column 3	111.2	90.8	100.0

Fig. 1. Geometry and reinforcement details of original columns.

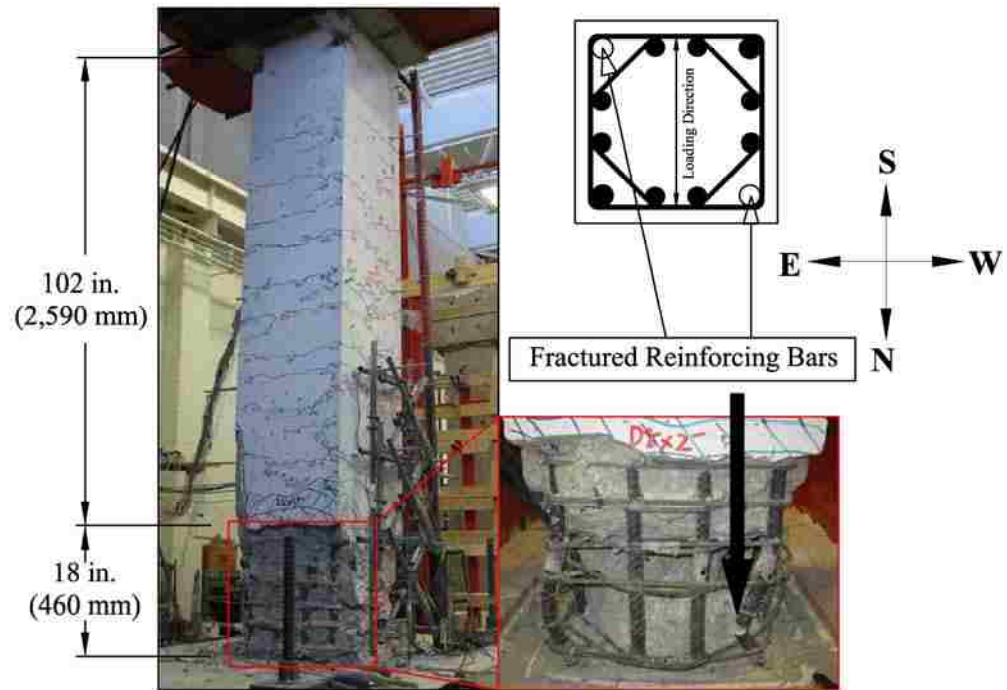


Fig. 2. Damage to Column 1 ($T/M=0$).

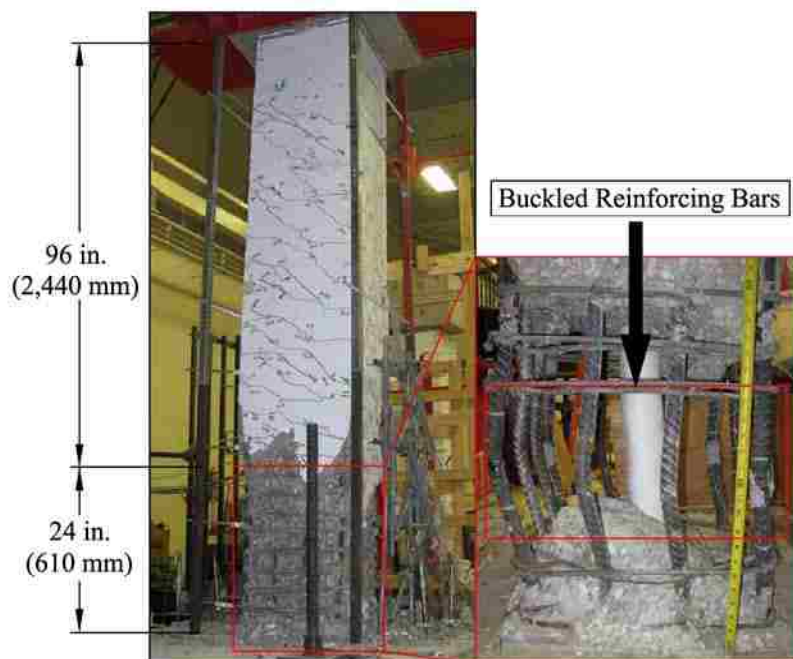


Fig. 3. Damage to Column 2 ($T/M=0.2$).

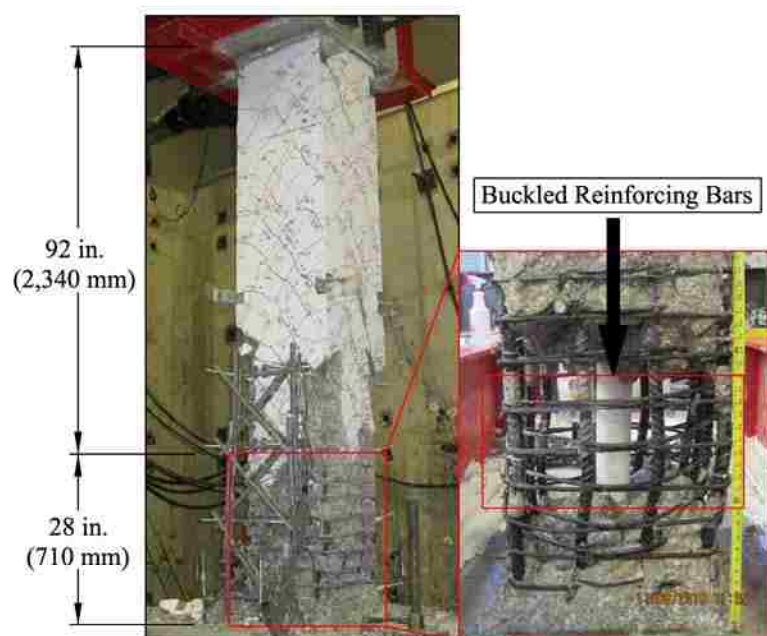


Fig. 4. Damage to Column 3 ($T/M=0.4$).

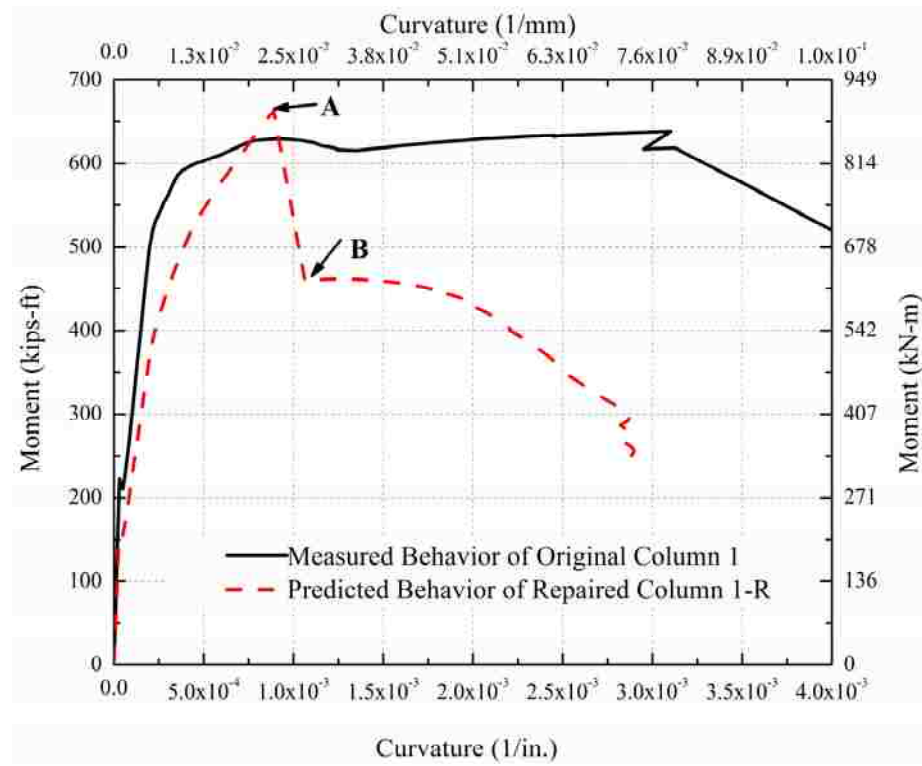


Fig. 5. Moment-curvature curves for final repair design of Column 1-R ($T/M=0$).

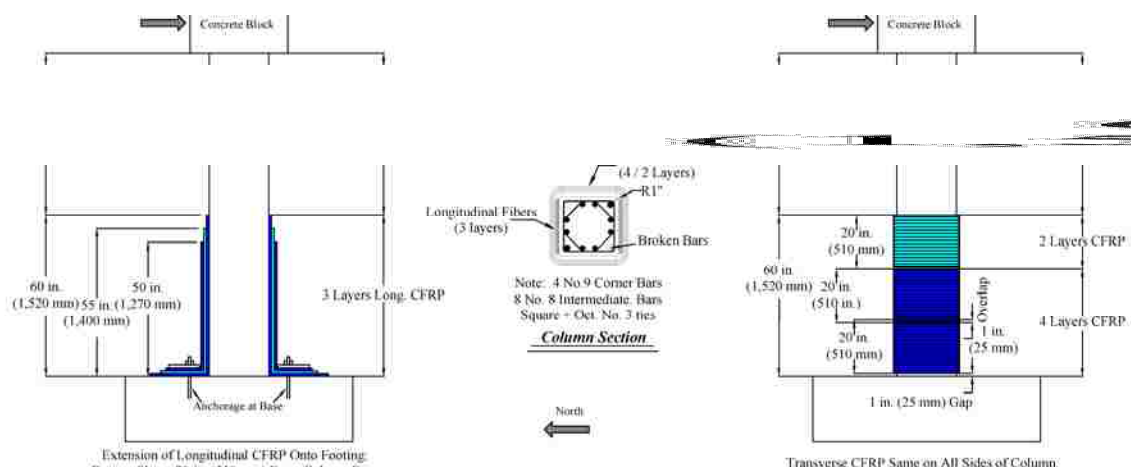


Fig. 6. Final repair design for Column 1-R ($T/M=0$).

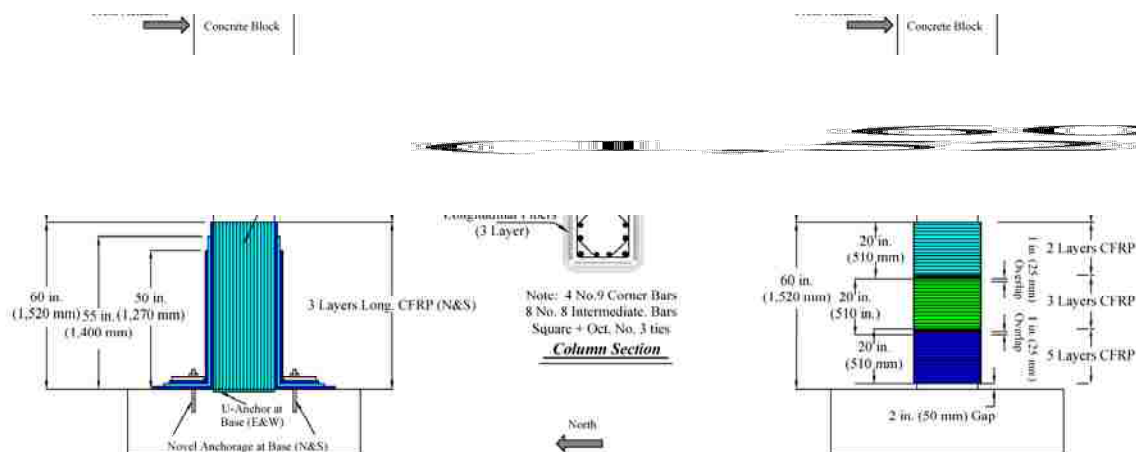


Fig. 7. Final repair design for Column 2-R ($T/M=0.2$).

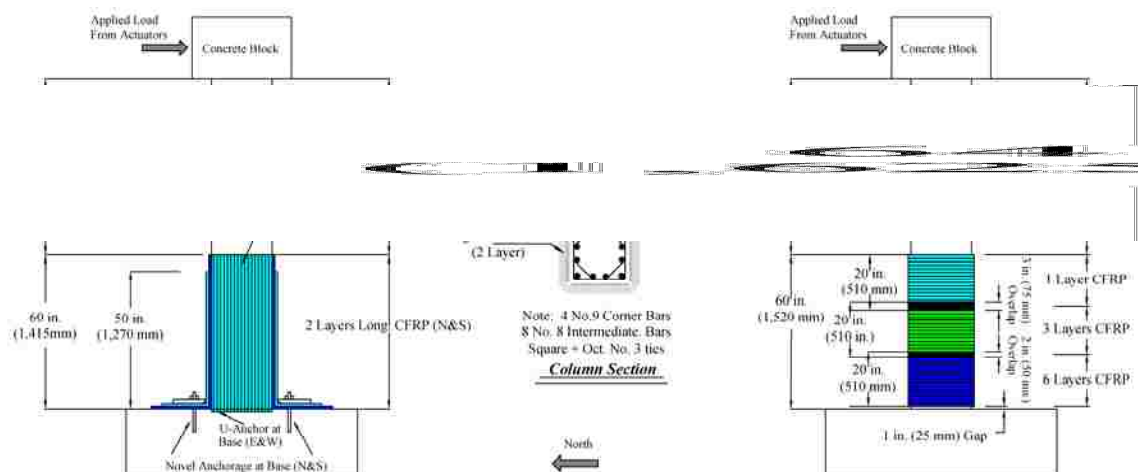


Fig. 8. Final repair design for Column 3-R ($T/M=0.4$).

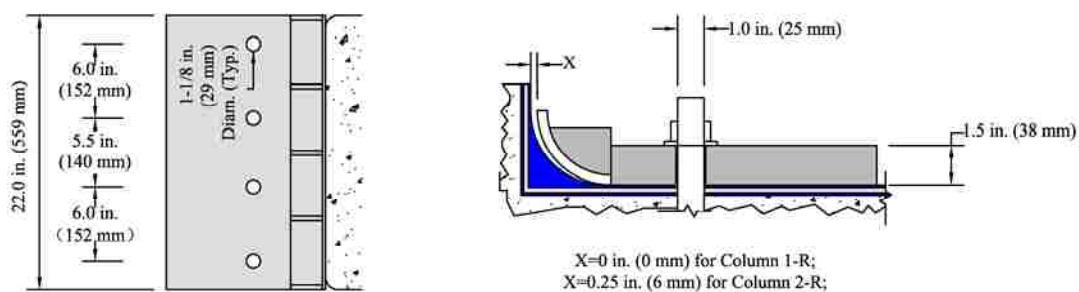


Fig. 9. Details of novel anchorage system.

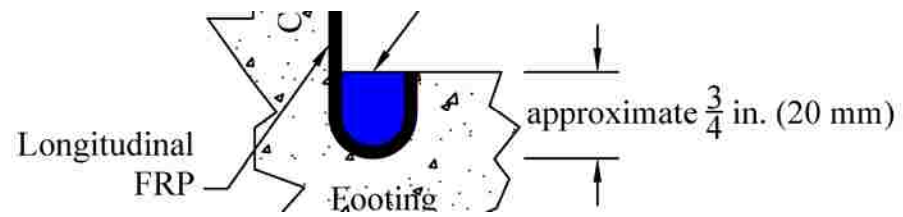


Fig. 10. U-anchor used on east and west faces of Columns 2-R and 3-R.



Fig. 11. Repair procedure. (a) Column after straightening, (b) column after loose concrete removal, (c) repair mortar placement, (d) surface preparation, (e) CFRP application, (f) curing process.

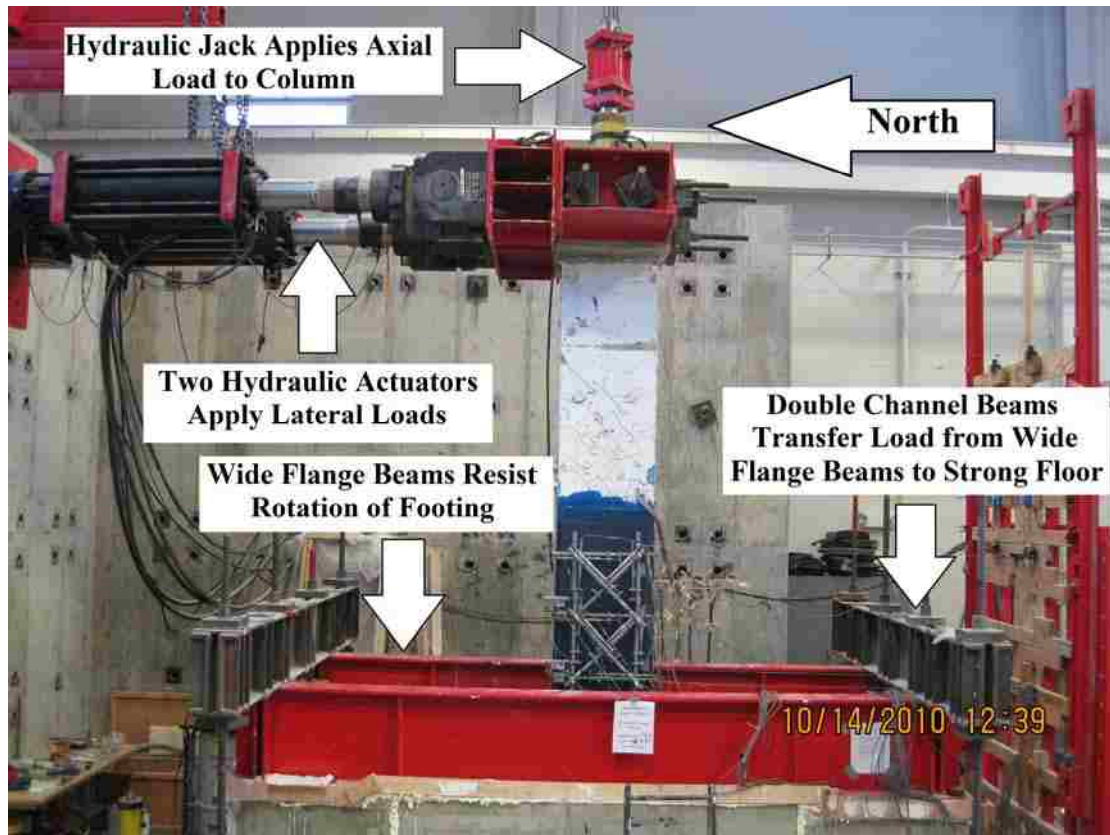


Fig. 12. Test setup of repaired column.

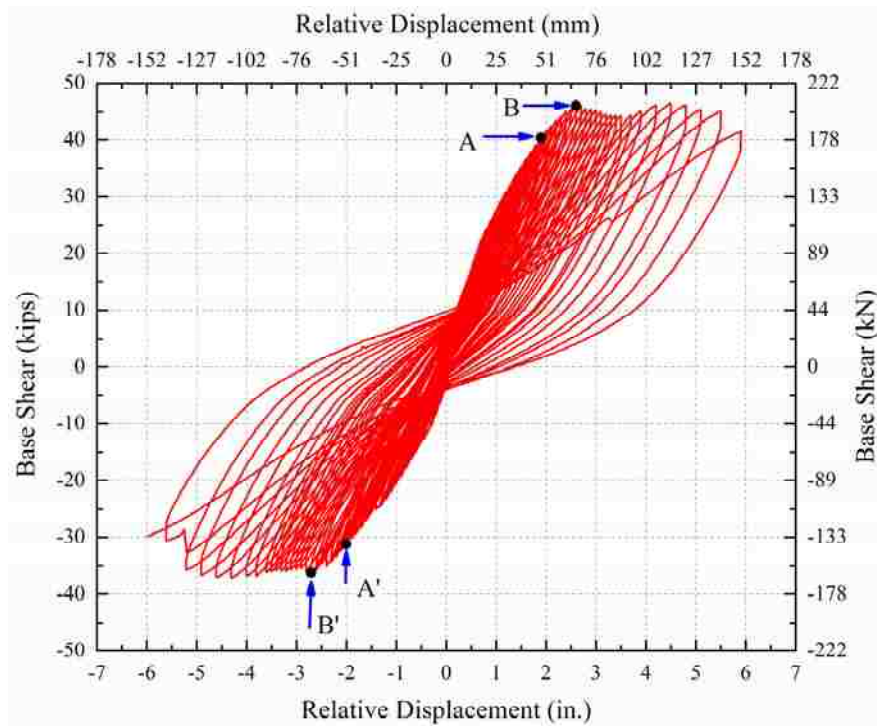


Fig. 13. Hysteresis response of repaired Column 1-R ($T/M=0$).



(a)

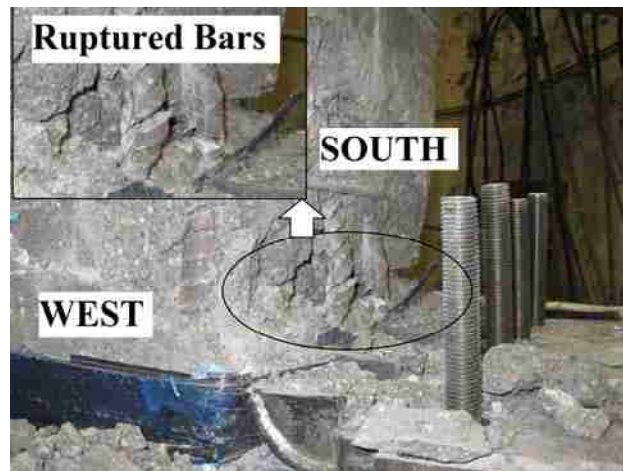


(b)

Fig. 14. Failure of repaired Column 1-R ($T/M=0$) - northwest corner.



(a)



(b)

Fig. 15. Failure of repaired Column 1-R ($T/M=0$) - south side.

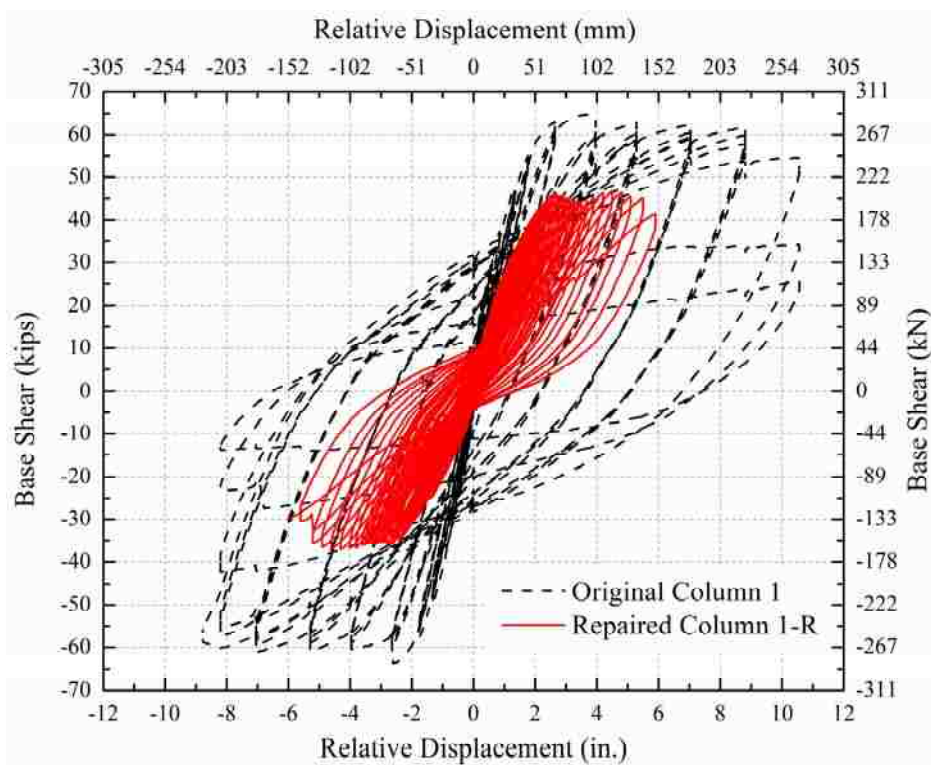


Fig. 16. Hysteresis behavior of repaired Column 1-R compared to original Column 1 ($T/M=0$).

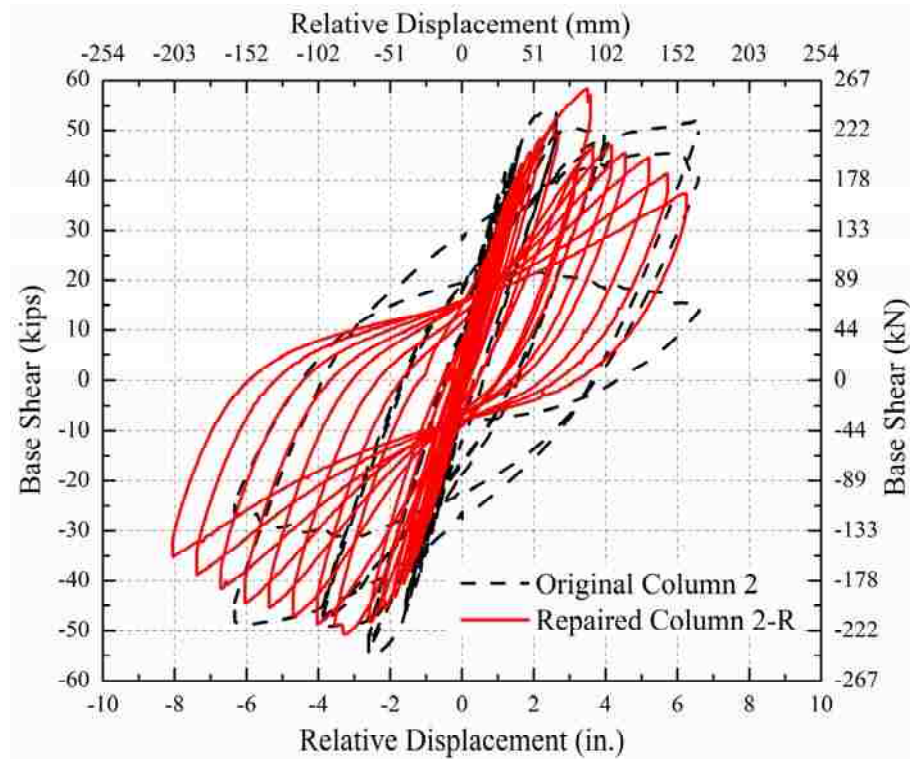


Fig. 17. Hysteresis behavior of repaired Column 2-R compared to original Column 2 ($T/M=0.2$).

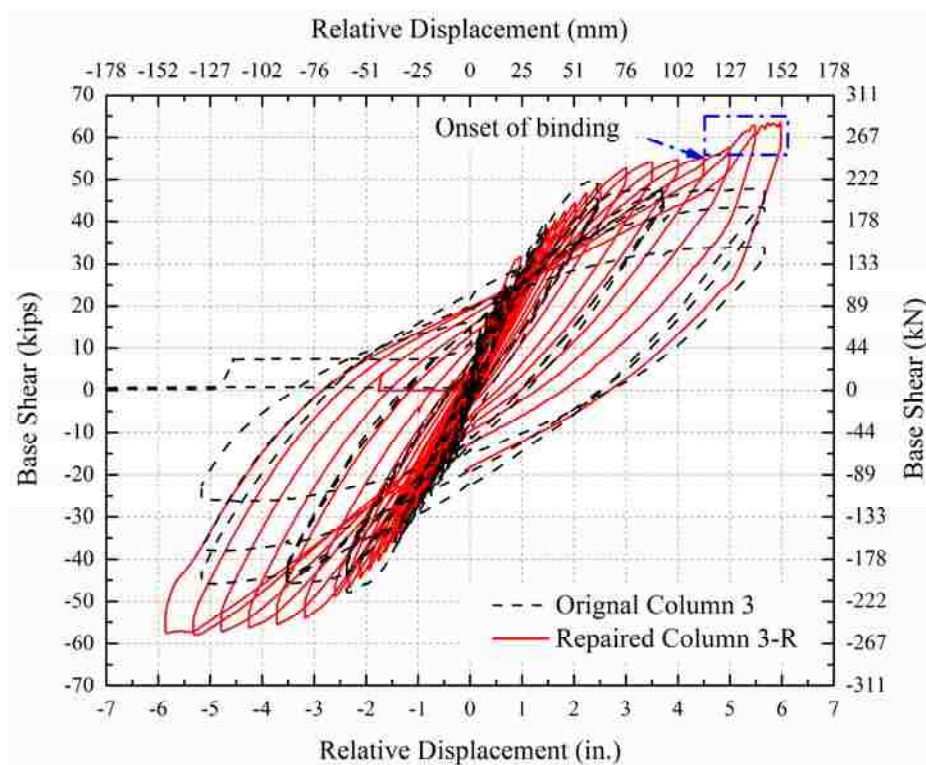


Fig. 18. Hysteresis behavior of repaired Column 3-R compared to original Column 3 ($T/M=0.4$).

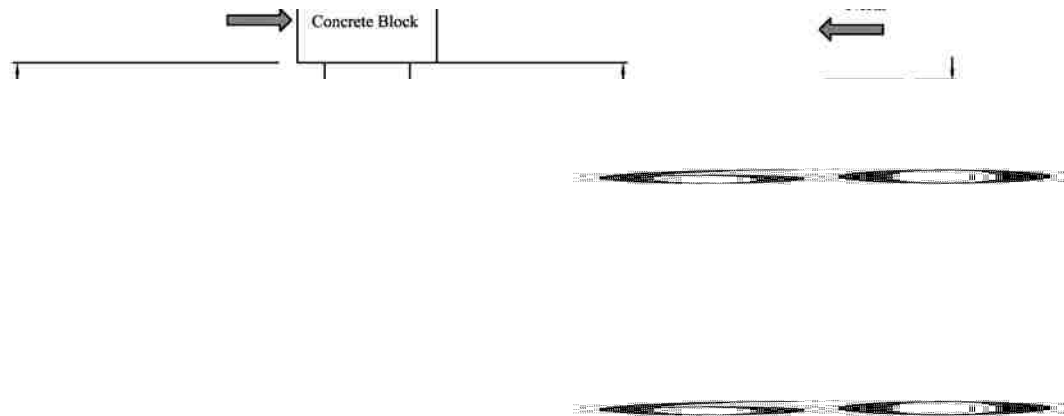


Fig. 19. Location of the strain gauges applied on Column 1-R ($T/M=0$).

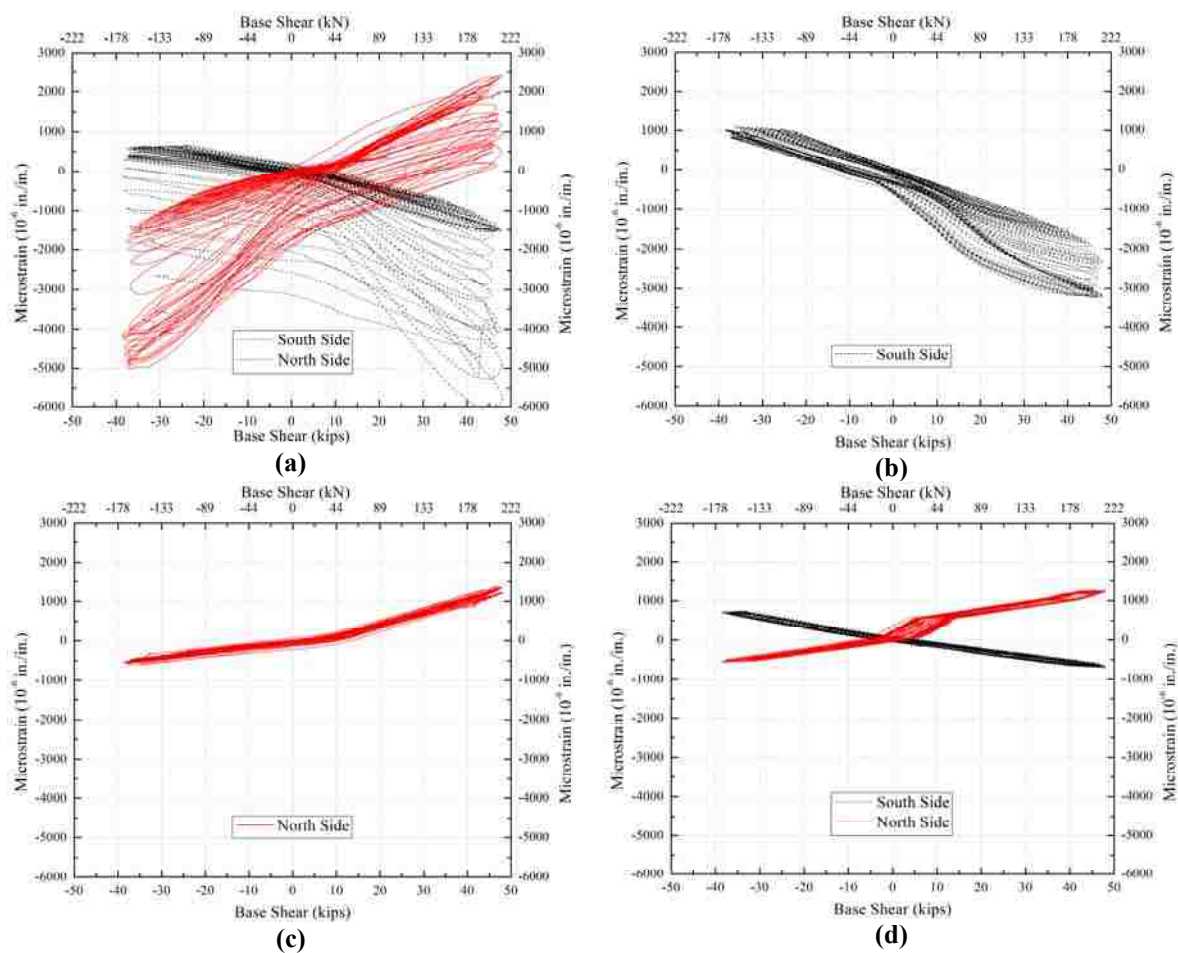


Fig. 20. Load-longitudinal surface strain relationship - Column 1-R ($T/M=0$) (a) Level 2, (b) Level 3, (c) Level 4, (d) Level 5.

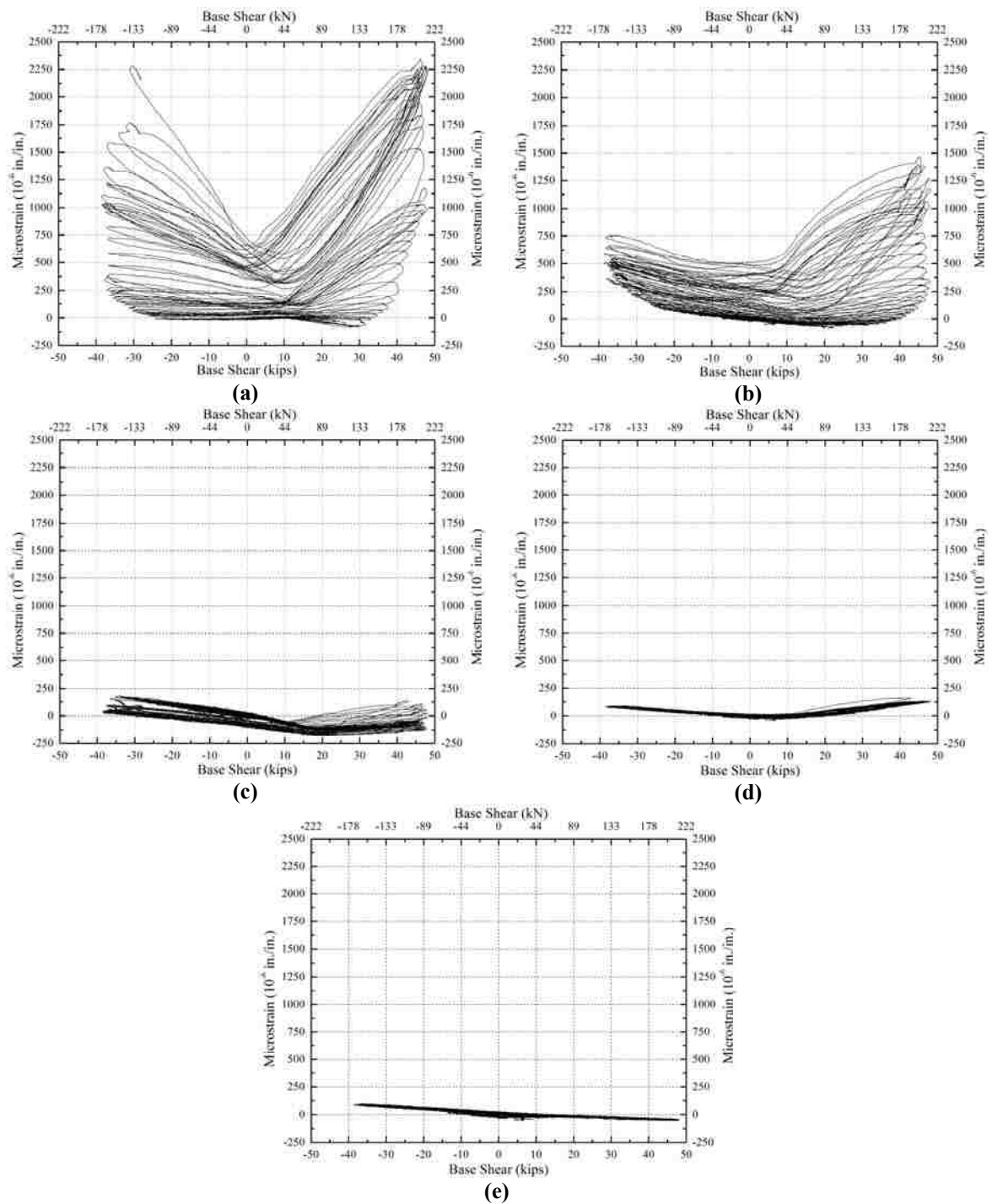


Fig. 21. Load-transverse surface strain relationship - Column 1-R ($T/M=0$) (a) Level 1 - north side, (b) Level 2 – north side, (c) Level 3 – north side, (d) Level 4 – north side, (e) Level 5 – north side.

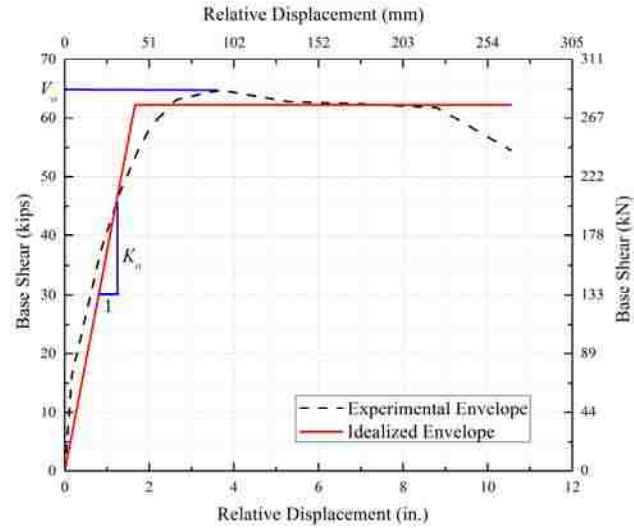


Fig. 22. Force-displacement relationship of original Column 1 ($T/M=0$).

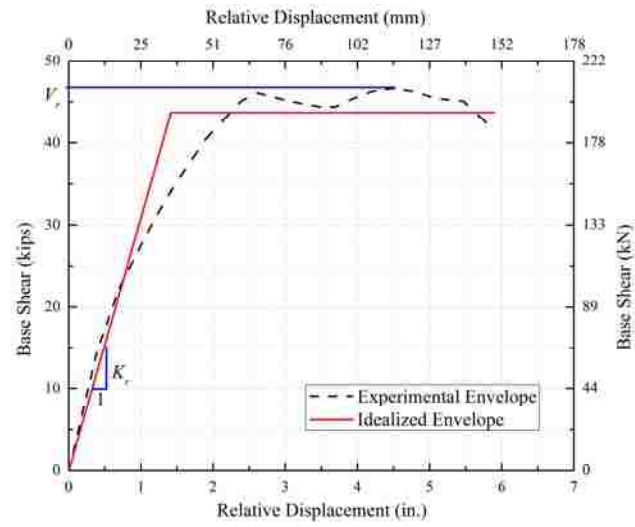


Fig. 23. Force-displacement relationship of repaired Column 1-R ($T/M=0$).

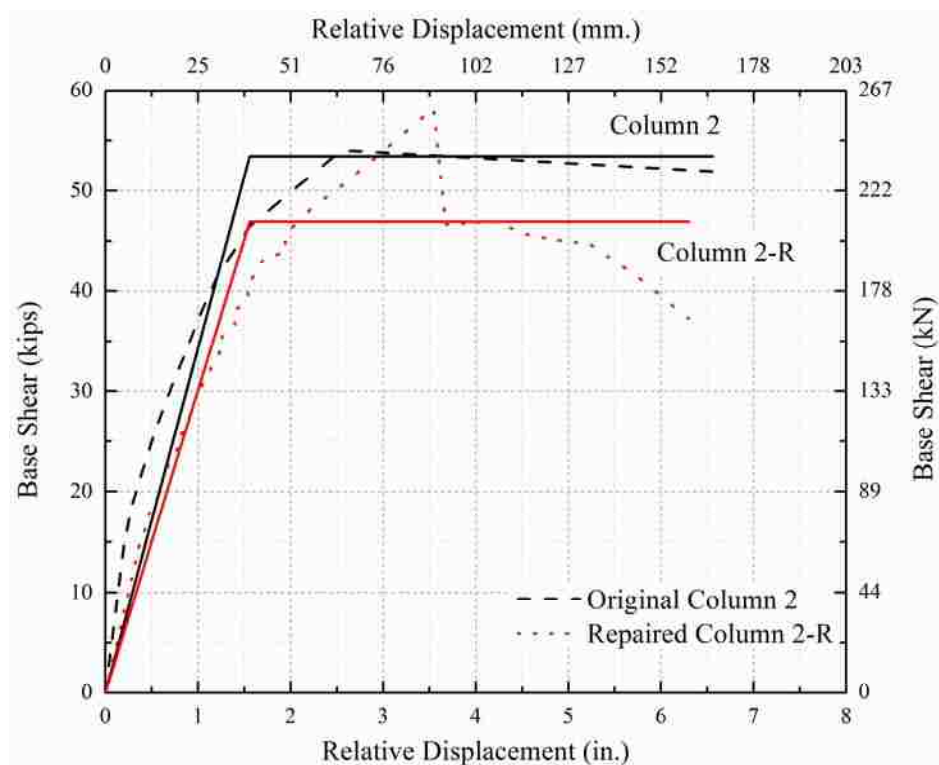


Fig. 24. Force-displacement relationship of Column 2-R ($T/M=0.2$).

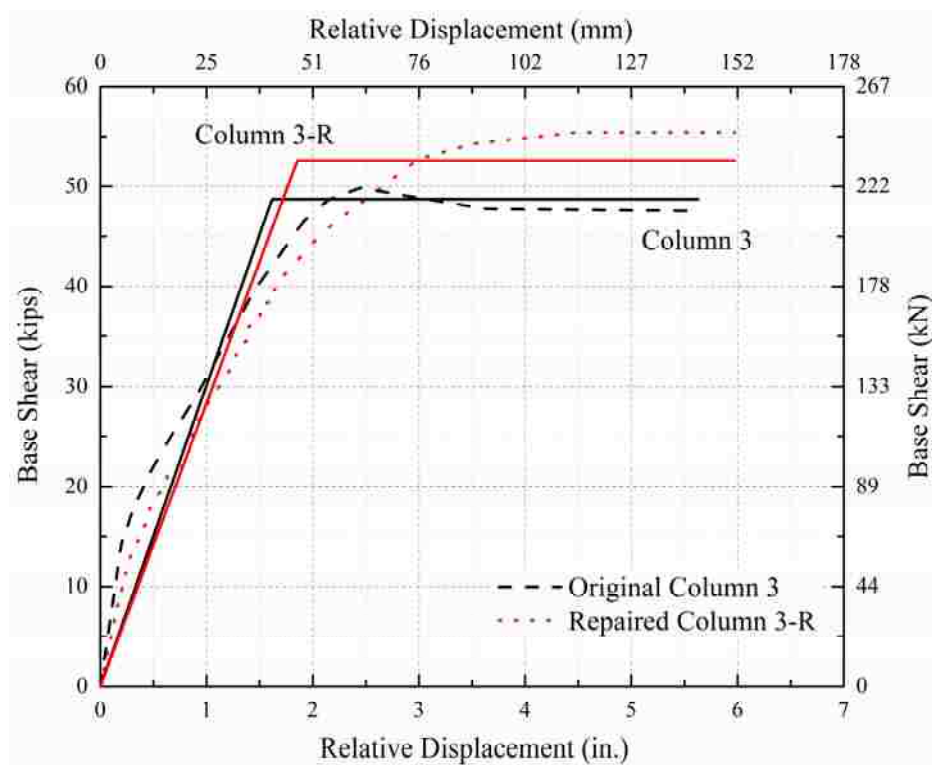


Fig. 25. Force-displacement relationship of Column 3-R ($T/M=0.4$)

IV. TORSIONAL REPAIR OF SEVERELY DAMAGED COLUMN USING CARBON FIBER-REINFORCED POLYMER

Ruili He, Lesley H. Sneed, and Abdeldjelil Belarbi

ABSTRACT

Although a limited number of studies have been conducted on the use of externally bonded composites for torsional retrofit or strengthening of RC members, very few are available on torsional repair. This paper evaluates a method for repairing severely damaged RC columns subjected to torsional moment using externally bonded carbon fiber-reinforced polymer (CFRP) composites. A half-scale RC column that was previously tested to failure under constant axial load and cyclic torsional moment was repaired with externally bonded CFRP using a rapid methodology. CFRP sheets with fibers oriented in both the transverse and longitudinal directions were applied to restore the strength and ductility of the damaged column to its original condition. This study demonstrates that this method can be used to restore the torsional performance of severely damaged RC columns. Contributions of the transverse and longitudinal CFRP sheets to the torsional resistance are evaluated, and repair design for torsional moment using this method is discussed.

Keywords: Columns; cyclic loading; fiber-reinforced polymer (FRP) composites; repair; torsional moment.

INTRODUCTION

The use of externally bonded fiber reinforced polymer (FRP) composites has been studied extensively in repair and/or strengthening of reinforced concrete (RC) members. Most studies have focused on flexural or shear strengthening applications of various types of members or providing confinement for columns. Research on strengthening of RC members for torsion, however, has been limited, particularly for bridge structures. RC bridge members are not usually designed to resist torsional loads, which are considered to be secondary in nature. However, bridge columns may experience torsional loads due to wind, seismic, and other lateral loads. Torsional loads can even be critical if bridges are constructed with geometric irregularities or certain structural constraints, such as curved and skewed superstructure, unequal column heights, rigid decking, or abutment restraints¹.

A detailed review of the literature on torsional strengthening reveals that externally bonded FRP can significantly enhance the torsional capacity and deformation capacity of RC members²⁻¹³. The contribution of FRP to the torsional capacity is related to an effective strain in the FRP, which is generally lower than the FRP ultimate strain². Even at relatively low FRP strain levels, however, the torsional strength of FRP-strengthened RC members can be increased⁷. For members subjected to pure torsion, the most effective orientation of fibers in externally bonded FRP has been found to be 45 deg. relative to the longitudinal axis of the member since the fibers are aligned with the principal tensile stresses, which also maximizes the FRP efficiency⁵. Comparison of the effectiveness of various wrapping configurations has shown that members that are fully wrapped with continuous FRP sheets performed better than those with discrete strips or U-wrap^{4,5}. Full wrapping, however, is not always practical such as in the case of T-beams. Though most researchers have pointed out that a continuous loop is necessary to increase the torsional strength, research findings suggest that discontinuous laminates or even laminates with fibers oriented along the member longitudinal axis also improve the torsional capacity and performance⁷. For example, longitudinal laminae applied to the face of RC spandrel beams were reportedly found to help maintain the torsional stiffness by controlling concrete crack widths. Attention should be paid to the amount of FRP to

avoid brittle failure since test results revealed that excessive amounts can reduce the ductility of the member⁹.

The present research program by the authors aims to develop a rapid repair method for severely damaged RC columns with different damage conditions. The experimental work was focused on a series of half-scale RC bridge columns that were severely damaged from a previous study¹⁴. Five columns with the same nominal geometry and material properties were tested under constant axial load in addition to cyclic flexure, shear, and/or torsion in varying proportions. The applied torsional moment-to-flexural moment ratios were $T/M = 0$ (no torsion), 0.2, 0.4, 0.6, and ∞ (no flexure). The location of plastic hinge and nature of damage were different for each column because of the different loading conditions. To restore the damaged columns to their original condition, CFRP sheets were applied to the external surface with the fibers orientated both transverse to and along the column axis. Performance was evaluated by comparing the global response of the repaired columns to that of the corresponding original columns in terms of strength, ductility, and stiffness, which are discussed in detail by He et al.^{15,16}. This paper focuses on one column in the series that was subjected to constant axial load and pure cyclic torsional moment ($T/M=\infty$), which provides a unique opportunity to explore torsional repair design and performance and further understanding of torsional behavior of FRP strengthened members.

RESEARCH SIGNIFICANCE

This paper evaluates a method for repairing severely damaged columns subjected to torsion using externally bonded CFRP. Rapid repair methods are needed for different types of damage due to an extreme event to enable quick reopening of important structures and minimize impact on the community. While limited studies have been conducted on the use of FRP for torsional retrofit or strengthening of RC members, no prior research has focused on torsional repair. Findings show that externally bonded CFRP can be used to restore or even improve the torsional performance of severely damaged RC columns. Contributions of transverse and longitudinal CFRP to the torsional resistance are evaluated.

EXPERIMENTAL PROGRAM

Description of original column

The original column was a half-scale RC bridge column that was designed based on CALTRANS¹⁷ and ACI 318¹⁸ seismic provisions. The column aspect ratio (H/B) was 6, where H and B are the height of the column and the cross-section width respectively. Fig. 1(a) shows the column geometry and reinforcement details. The total height of the column specimen was 166 in. (4,220 mm) with an effective height of 132 in. (3,350 mm) measured from the column base to the centerline of applied lateral load. The column was 22 in. (560 mm) square reinforced with four No. 9 (29 mm dia.) deformed bars in the four corners and eight No. 8 (25 mm dia.) bars on the column faces. Tie reinforcement consisted of square and octagonal No. 3 (10 mm dia.) deformed bars with 3.25 in. (82 mm) spacing. The tie bars were anchored using 135 deg. bent hooks with a hook length of 2.5 in. (64 mm). The longitudinal and transverse reinforcement ratios were 2.13% and 1.32%, respectively. The measured yield strength of the longitudinal reinforcing bars was 76 ksi (524 MPa) for the No. 8 (25 mm dia.) bars and 67 ksi (462 MPa) for the No. 9 (29 mm dia.) bars. The measured yield strength of the ties was 74 ksi (510 MPa). The measured cylinder compressive strength of the concrete was 4,730 psi (32.6 MPa) at test date.

Loading protocol of original column

A constant axial load of approximately 150 kips (670 kN), which corresponded to 7% of the nominal axial capacity, was applied to the column to simulate the dead load from the bridge superstructure. A hydraulic jack on top of the load stub was used to apply the axial load with seven steel prestressing strands through a PVC pipe in center of the column cross section. The strands were anchored at the top of the load stub and at the bottom of the column footing. Cyclic torsional moment was applied through equal but opposite directional forces in two hydraulic actuators mounted to the load stub that reacted to a strong wall. Testing was conducted in force-control until first yielding of the transverse reinforcing bars and then continued in displacement-control until failure of the column. One cycle was applied at 10% increments of the estimated yield torsional moment in force-control, then three cycles were applied at each load stage in

displacement-control as illustrated in Fig. 1(b). The twist corresponding to first yield of the transverse reinforcing bars was defined as ductility D1 ($\mu_\theta=1$).

Damage evaluation of original column

The damage to the original column after the original test is shown in Fig. 2, which illustrates significant crushing of the core concrete. The concrete cover spalled along almost the entire column length, and the core concrete crushed through the cross-section in the region from 45 in. (1,140 mm) to 65 in. (1,650 mm) above the column base (see Fig. 2). No buckled or fractured reinforcing bars were observed in the original damaged column. Strains were measured in the longitudinal and transverse reinforcing steel bars at locations shown in Fig. 3. Although several strain gages were damaged during testing, Fig. 3 shows that yielding of transverse reinforcement occurred along the full height of the column except Gage Elevation 3, which was 2 in. (50 mm) above the column base. Yielding of longitudinal reinforcement occurred in the north-west corner No. 9 (29 mm dia.) bar at Gage Elevations 7 and 8. Considering the damage conditions, the damage observed was classified as significant according to ATC-32¹⁹. The terms “significant” and “severe” are used interchangeably in this paper when referring to the column damage.

Repair scheme

In this study, the overarching goal of the repair was to rapidly and temporarily restore the column integrity for emergency service use. ATC 18²⁰ criteria state that full access to bridge structures located along key routes that are important to emergency response and other essential functions should be possible within three days after an earthquake. Therefore, the repair scheme was developed based on the condition that it can be accomplished in a three-day period. Because of the temporary nature of the repair, restoration of strength was the main objective, and durability aspects were not considered in the repair design. The short timeframe in which to complete the repair was a significant challenge when choosing the repair scheme, especially considering the severity of damage to the original column and implementation of the repair procedure. Based on ease of installation, an externally bonded CFRP system was selected for the repair scheme in this study.

Repair Materials - A shrinkage-compensating micro concrete with graded aggregate was used to replace the removed damaged concrete. The repair mortar selected has high bond strength, high early strength, and self-compacting properties. Material properties provided by the manufacturer are listed in Table 1, and the average cube compressive strength at test day measured in accordance with ASTM C109²¹ was 6,260 psi (43.2 MPa). The CFRP strengthening system included unidirectional high strength carbon fiber fabric with material properties shown in Table 1. A 12 in. (300 mm) cube block was constructed of the repair mortar at the same time the mortar was used to replace the removed column concrete. A representative sample of CFRP was bonded to the block surface using the same technique and at the same time as the CFRP application. The bond strength testing of the CFRP-to-concrete interface was performed in accordance with ASTM D7234²² at the time of testing the repaired column. The average measured bond strength was 310 psi (2.1 MPa), which met the CFRP system manufacturer's and ACI 440.2R²³ minimum requirements of 200 psi (1.4 MPa).

Repair Procedure - The damaged column was repaired by replacing the damaged concrete with the selected repair mortar and then applying CFRP sheets in both the longitudinal and transverse directions. A wet lay-up process was used to apply the CFRP sheets. The repair process was completed in a 3-day period and included the following steps: 1) straightening the damaged column; 2) removing the loose concrete; 3) preparing the formwork for repair mortar placement; 4) placing the repair mortar; 5) applying the longitudinal CFRP sheets; and 6) applying the transverse CFRP sheets. The axial load that was imposed during the original test was not applied during the repair procedure, since a shoring system is commonly used in practice. All repair work was conducted in the High Bay Structural Engineering Research Laboratory (SERL) at Missouri University of Science and Technology (Missouri S&T) in Rolla, MO. Details of the repair procedure are discussed elsewhere¹⁶.

Loading protocol of repaired column

The repaired column was tested at the beginning of the fourth day after repair initiation, which corresponded to one day after application of the CFRP strengthening system. Fig. 4 shows the test setup in which a constant axial load of 150 kips (670 kN)

was applied using a hydraulic jack on top of the column, and cyclic torsional moment was applied with two hydraulic actuators mounted to the load stub. The repaired column was twisted under slow cyclic loading. The same loading protocol that was used for the original column was used for the repaired column with the exception that one cycle was applied at each load stage after shifting to displacement control since there was no specific yield point for the repaired column.

TORSIONAL REPAIR DESIGN USING EXTERNALLY BONDED CFRP

As discussed previously, the repair system was designed to restore the torsional strength of the original column. Especially in the case of a permanent repair, the repair system should also restore the stiffness and ductility, although these aspects were not explicitly accounted for in the repair design, and little guidance exists in the literature with respect to torsion. The repair design is described below, based on the assumption that the RC column with newly-placed repair mortar and yielded reinforcing steel can provide a reduced amount of its original torsional strength²⁴, and the deficiency is compensated by the contribution of the CFRP strengthening system.

Predicting torsional strength of RC members with externally bonded FRP

The torsional strength T of an RC member strengthened with externally bonded FRP is usually estimated by adding the individual torsional strength contributions of the RC member T_{RC} and the externally bonded FRP strengthening system T_f as given in Eq. (1)^{10,12}. In this equation, it is assumed there is no interaction between the RC member and externally bonded FRP system.

$$T = T_{RC} + T_f \quad (1)$$

Torsional Strength Contribution of RC Member, T_{RC} - RC members subject to pure torsion fail due to either concrete crushing or reinforcement yielding. In order to exhibit ductile failure, torsional members are commonly designed such that steel yielding will occur prior to crushing of the concrete compression diagonals. This is also the basis of the ACI 318 code¹⁸ approach to calculate the torsional strength of RC members, where the space truss analogy is used with the assumptions that concrete carries no tension and

behaves as compression diagonals at an angle θ with respect to the longitudinal axis, and the reinforcement yields at failure. With this approach, T_{RC} is computed using Eq. (2):

$$T_{RC} = \frac{2A_o A_t f_{yt}}{s} \cot \theta \quad (2)$$

where A_o is the gross area enclosed by the shear flow path, s is the center-to-center spacing of transverse reinforcement, A_t is the area of one leg of a closed stirrup resisting torsion within spacing s , f_{yt} is the specified yield strength of transverse reinforcement, and θ is the angle of diagonal crack with respect to the column axis (usually assumed as 45 deg.).

Torsional Strength Contribution of Externally Bonded FRP System, T_f - Most models available to determine the FRP contribution T_f to the torsional capacity of strengthened RC members are based on the condition that a continuous loop is provided for the formation of the thin tube approach and the stress transfer around the member for the circulatory shear flow^{25,26}. Therefore, only the contribution of FRP that is wrapped fully around (or in some cases, partially around and properly anchored to) the cross-section is considered to contribute to T_f in Eq. (1). FRP that is wrapped around the cross-section is referred to as “transverse FRP” in this paper. It should be noted that test results have suggested that externally bonded FRP with fibers oriented along the RC member longitudinal axis (termed “longitudinal FRP” in this paper) can also increase the torsional strength⁷, although continuity of fibers is not provided in this case. However, longitudinal FRP is generally less effective than transverse wrapping, and the contribution to the torsional strength is difficult to quantify.

FRP with unidirectional fibers that is transversely wrapped around the RC member is considered to behave similarly to closed stirrups; thus a similar approach can be used to account for the contribution of FRP wrap to the torsional strength as for traditional RC members. Predicting the torsional strength of RC members depends on the accuracy in determining the location of the shear flow centerline (A_o in Eq. (2)). For FRP that is wrapped around an RC member, the shear flow centerline is usually estimated as the outside dimensions of the RC member^{25,26}. It is a challenge, however, to determine the maximum strain that can be achieved in the FRP system at the ultimate state, termed the effective strain. As mentioned previously, the effective strain is usually less than the

ultimate fiber strain and is governed by the failure mode of either the FRP system or the strengthened RC member²³. In models presented by FIB²⁵ and NCHRP Report 655²⁶, an equation similar to that used to calculate the RC column contribution (Eq. (2)) is used to calculate the contribution of externally bonded FRP to the torsional strength. The major difference between these models lies in the calculation of the effective strain according to various failure modes. In a model by Salom et al.⁷, the equation used to calculate the RC column contribution (Eq. (2)) is combined with the formula in the ACI Committee 440 report²³ used to estimate the shear capacity of FRP jackets applied to concrete members.

Design of CFRP system for repaired column

The column repaired in this study had crushed concrete through the entire cross section, yielded longitudinal reinforcement in the north-west corner in the plastic hinge zone, and yielded tie reinforcement along nearly the full height. Existing analytical models for torsional strengthening cannot be applied directly to torsional repair design because they are based on full contribution of concrete and tie reinforcement to the column torsional strength. Therefore, it was necessary to estimate the contribution of yielded tie reinforcement and softened concrete to the torsional strength of the repaired column. Based on previous research involving repair of damaged RC members²⁴, it was assumed that the repaired RC column (without the externally bonded CFRP strengthening system) would provide 50% of the original column torsional strength T_{RC-O} after replacing the removed loose concrete with repair mortar. The original column torsional strength was 244 kip-ft (330.8 kN-m).

For a square column that is fully wrapped FRP with fibers orientated perpendicular to the longitudinal column axis, the FIB²⁵ and NCHRP Report 655²⁶ models reduce to the expression shown in Eq. (3). The expression in Eq. (3) is similar to Eq. (2) for internal transverse reinforcing steel ties with the exception of how the effective strain is determined. In this repair design, Eq. (3) was used in designing the number of layers of transverse CFRP required, and the NCHRP Report 655²⁵ method was used to determine the effective strain in the CFRP, ε_{fe} given in Eq. (4):

$$T_f = \frac{2A_0 A_f f_{fe}}{s_f} \quad (3)$$

$$\varepsilon_{fe} = 0.004 + \frac{1}{2} \left(\frac{1}{2} \varepsilon_{fu} - 0.004 \right) \quad (4)$$

where A_f is the area of CFRP external reinforcement, f_{fe} is the effective CFRP stress = $E_f \varepsilon_{fe}$, s_f is the center-to-center spacing of the applied CFRP sheets, ε_{fe} is the effective CFRP strain, E_f is the modulus of elasticity of CFRP, and ε_{fu} is the ultimate strain of the CFRP system.

One layer of transverse CFRP was applied to the repaired column, which according to Eq. (3) contributes 106 kip-ft (143.7 kN-m) to the column torsional strength. Additionally, one layer of longitudinal CFRP was provided for several reasons: 1) to minimize changes to the ratio of the stiffness in the longitudinal and transverse directions due to the application of the CFRP strengthening system; 2) to control concrete crack widths and help maintain the torsional stiffness of the repaired column; and 3) to compensate for the strength discrepancy between the design strength and the estimated strength of the repaired column with only one layer of transverse CFRP. The final design of the CFRP system included one layer in each of the transverse and longitudinal directions. CFRP in both directions was provided the full height of the column, with a 1 in. (25 mm) gap between the top of the column and the load stub.

EXPERIMENTAL RESULTS

Observed behavior and failure mode of repaired column

At the beginning of testing the repaired column, there was no visually apparent twist or damage with increasing torsional moment applied to the column. A wrinkle in the CFRP was observed on the west face orientated from lower north to upper south as shown in Fig. 5a when the torsional moment was applied at the cycle from -192.4 kip-ft (-260.9 kN-m) at the twist of -3.09 deg. (Point A'' in Fig. 6b) to 226.7 kip-ft (307.4 kN-m) at the twist of 3.72 deg. (Point B' in Fig. 6b). The wrinkle was located approximately 45 in. (1,145 mm) above the column base. When torsional moment was applied in the opposite direction, the wrinkle flattened. With increasing number of cycles, more wrinkles appeared above and below the first wrinkle, and the wrinkles did not flatten when the torsional moment was applied in the opposite direction (see Fig. 5(b)). This phenomenon can be explained by the occurrence of concrete cracking, which caused the

initiation of localized debonding of the fiber sheets at the crack locations. The failure mode of the repaired column was rupture of the CFRP, which was a progressive process. Initial rupture of the CFRP is shown in Fig. 5(c). Rupture of the CFRP first occurred at the south-west corner of the column approximately 65 in. (1,650 mm) above the column base, which coincides with the interface of the unrepaired concrete and the newly placed repair mortar. Rupture progressed to the upper west side of the column, and then to the lower south side. Finally, the ruptured CFRP peeled away with a thin layer of concrete bonded underneath, and crushed mortar fell out. Initiation and propagation of CFRP rupture were attributed to localized stress concentrations near cracks in the mortar or concrete substrate, which were due to the non-ductility of CFRP. CFRP rupture occurred when the most highly stressed location reached the ultimate strength of the CFRP system, which was also confirmed by the measured strain values discussed later.

Torsional moment versus twist response

Fig. 6(a) and Fig. 6(b) show the applied torsional moment versus twist hysteresis curves of the original and repaired columns, respectively. By joining together the peak value of each cycle in the same load direction, envelopes for the original and repaired columns were developed as shown in Fig. 7. Comparison of the applied torsional moment-twist envelopes shows that the torsional strength and twist at maximum torsional moment were enhanced by the repair.

At the beginning of testing the original column, the response was linear with increasing applied torsional moment until the concrete cracked at a torsional moment of 141.6 kip-ft (192.0 kN-m). Then, the torsional moment continued to increase but at a reduced stiffness. First yielding of the ties was measured when the applied torsional moment reached 203.2 kip-ft (275.5 kN-m) corresponding to a twist of 3.21 deg. The maximum applied torsional moment was measured at the first cycle after shifting to displacement-control when yielding occurred in the longitudinal bar at the north-west corner of the cross section. The maximum torsional moment resisted by the original column was 244.4 kip-ft (331.4 kN-m) corresponding to a twist of 6.47 deg. The torsional strength reduced rapidly after the maximum torsional moment was achieved because the core concrete crushed, and thus the column could not provide further torsional resistance.

The repaired column exhibited nearly the same tangential stiffness as the original column at the beginning of the test. However, the stiffness decreased with increasing applied torsional moment. No visible damage occurred until the appearance of the first wrinkle when the applied torsional moment reached 226.7 kip-ft (307.4 kN-m) at a twist of 3.72 deg. Then, the repaired column continued to resist increasing applied torsional moment until initial rupture of the CFRP occurred at the maximum torsional moment of 295.6 kip-ft (400.7 kN-m) and twist of 12.49 deg. The post-peak response was characterized by a reduction in torsional strength with increasing twist, but initially not as rapidly as that of the original column. The phenomenon that the repaired column was able to provide torsional resistance after reaching the maximum torsional moment can be explained in part by the confinement provided by the CFRP transverse wrap even after some localized rupture. It must also be noted that one cycle was applied to the repaired column at each load stage after shifting to displacement-control as opposed to three cycles for the original column, which likely resulted in less accumulated damage and provided better energy absorption in the repaired column.

The applied torsional moment at concrete cracking, tie yielding, and maximum torsional moment for the original and repaired columns are summarized in Table 2 with the corresponding twists. Cracking values are not given for the repaired column, since cracks were not visible during the test because of the presence of the CFRP wrap. The point at which the first wrinkle appeared and sudden increases in strains were measured in the transverse direction was defined as the yield point of the repaired column (Point B' in Fig. 6(b) and Fig. 7). The maximum torsional moment T_{max} resisted by the repaired column was 20% larger than that of the original column. This increase is attributed to the contribution of the externally bonded CFRP, which functioned as external reinforcement. The torsional ductility μ_{θ} of the original and repaired columns was calculated as the ratio of the twist at maximum torsional moment θ_{max} to the twist at yield torsional moment θ_y . Table 2 shows that the rotational ductility of the repaired column was also enhanced compared to that of the original column by using the externally bonded CFRP system.

Stiffness attenuation

Torsional stiffness was determined by the ratio of the summation of absolute values of positive and negative peak torsional moment in each cycle to the summation of corresponding absolute values of positive and negative twist⁹. Stiffness attenuation of the original and repaired columns is shown by the relation of G_i/G_o versus twist in Fig. 8. G_i denotes the torsional stiffness at the i th loading cycle for the original or repaired column. G_o denotes the initial torsional stiffness (determined from the loading first cycle) of the original column, which was used in order to compare the stiffness attenuation of the original and repaired columns in the same graph. The vertical step in the relation of the original column shows the effect of three cycles applied at the same twist, which indicates that the stiffness of the original column decreased slightly with increasing number of cycles applied.

Fig. 8 shows the stiffness of the repaired column was restored initially to approximately 80% of the original column. Full stiffness restoration was not achieved due to core concrete damage accumulated in the previous test. Generally, the repaired column exhibited a similar trend in torsional stiffness attenuation as the original column. The torsional stiffness of both the original and repaired columns decreased rapidly with increasing twist until a twist of approximately 1.7 deg., which is due to internal damage such as concrete cracking. With further increases in applied twist, the stiffness attenuation became slower until the maximum torsional moment was reached. The attenuation of stiffness of the original column after the maximum torsional moment was reached is due to reduction in cross-section due to cover spalling and to crack opening, as well as yielding of transverse reinforcement. For the repaired column, application of the CFRP strengthening system resulted in relatively slower stiffness attenuation prior to column failure. Additionally, some stiffness was maintained at the ultimate state. Therefore it can be concluded that the externally bonded CFRP system not only acted as external reinforcement, but also helped to restore and maintain the torsional stiffness, which is attributed to the CFRP system's ability to provide some confinement and restrain crack development.

EVALUATION OF THE TORSIONAL REPAIR DESIGN

Measured strain in externally bonded CFRP

To examine the behavior of the CFRP strengthening system and evaluate its efficiency on restoring the torsional strength of the repaired column, strain gages were installed on the surface of the CFRP at six levels along the column height on the different column faces. A total of 44 strain gages were applied, 22 in the longitudinal direction and 22 in the transverse direction, as shown in Fig. 9.

Transverse strains recorded on the north and south faces of the column exhibited a similar trend with respect to the applied torsional moment; similarly, transverse strains recorded on the east and west faces exhibited a similar trend. Generally, transverse strains measured on the east and west faces were slightly larger than those measured on north and south faces. It should be noted that the two hydraulic actuators used to apply the cyclic torsional moment were mounted to the load stub on north face as shown in Fig. 4.

The relationship between local transverse strains at the maximum torsional moment and damage of the repaired column is shown in Fig. 9. Strains measured at Level 3, where the plastic hinge was located in the original column and new repair mortar was placed, ranged from 25% to 55% of the CFRP ultimate strain. This response is consistent with observations that the concrete did not crush and little dilation was observed at this level. Measured strains reached the CFRP ultimate strain at locations adjacent to, and at the same level of, regions of concrete crushing. For example, rupture of the CFRP system initiated at the south-west corner approximately 5 in. (125 mm) below Level 4, and concrete crushed at that location during the test. This is confirmed from the large strain value measured on west side at Level 4. Strains measured on the east and west faces at Level 5 reached the ultimate strain, while the strain on south side did not reach ultimate because of the release after concrete crushing that occurred at on the south face. At Level 2, the strain on the east side also reached the CFRP ultimate strain, which is attributed to localized deformation because strains measured on other three sides were approximately 30% of the ultimate strain. Also, the strain measured in this location increased with increasing cycles even after the maximum torsional moment was reached. Large strains measured at Level 6 indicate that the unrepaired concrete inside the CFRP cracked and the cross-section dilated during the test.

Tensile strains were measured in the longitudinal direction of the column irrespective of the direction of twist, which confirmed that the longitudinal CFRP contributed to the torsional resistance. Compressive strain values measured are likely the result of localized deformation of the CFRP due to damage of the concrete. In general, the longitudinal strain at each level was largest on the south side of the column except at Levels 4 (west face) and 5 (east face). This can be explained by the observation that rupture and peel off of the CFRP system occurred on the south side of the column, and CFRP rupture occurred on the west side at Level 4. The largest strain at Level 5 was measured on the east face, not the south face, which can be explained by the observation that the concrete crushed in that location so the strain at the region released.

Average strain in externally bonded CFRP at each level

The average strains at each level were determined from the values measured on the four column faces at the corresponding level. The average transverse and longitudinal strains at each level are shown versus applied torsional moment in Figs. 10 and 11 respectively, in which positive values indicate tensile strains. Generally, the average measured transverse strain was smallest at Level 1, followed by Level 2, Level 3, and Level 4. The relatively small strains measured at Levels 1 and 2 are attributed to the constraint provided by the column footing. It should be noted that Level 3 is within the region in which all of the crushed concrete was removed and replaced by the repair mortar. Level 4 is adjacent to the concrete replacement region and is also the region where CFRP rupture initiated. Accordingly, this level was of particular interest in this analysis.

Values of the average measured transverse strain at each level corresponding to the maximum applied torsional moment, indicated by markers shown in Fig. 10, are given in Table 3. The average measured transverse strains at Levels 5 and 6 reached around 66% of the CFRP ultimate strain (1.67%). The average measured strain at Level 4 where CFRP rupture initiated was 7549 microstrain. For comparison, the value of the effective strain used to design the transverse CFRP was approximately 6125 microstrain (from Eq. (4)). Thus the NCHRP Report 655 method²⁶ was reasonable for determining the effective strain in designing the transverse CFRP for this column.

Compared to the transverse strains, the average measured longitudinal strain values were smaller, which can be seen from Figs. 10 & 11, even though the same amount of CFRP was applied in each direction (1 layer). This confirms that the transverse CFRP was more effective than the longitudinal CFRP in providing torsional resistance and thus restoring the torsional capacity. The average measured longitudinal strain values at each level corresponding to the maximum applied torsional moment are given in Table 3, and they are indicated by markers in Fig. 11.

Contribution of externally bonded CFRP and repaired RC column

Based on the average strain values corresponding to the maximum applied torsional moment (indicated in Figs. 10 and 11), the contribution of the transverse CFRP to the repaired column torsional resistance was calculated according to Eq. (3) and is summarized in Table 3. T_{ft} in Table 3 represents the torsional moment resisted by transverse CFRP, ε_{fe} is the average measured strain at each level corresponding to the maximum torsional moment, and f_{fe} is the calculated stress in the CFRP determined by Eq. (5).

$$f_{fe} = E_f \varepsilon_{fe} \quad (5)$$

Although the longitudinal CFRP was not continuous around the cross-section, it was anchored by the transverse CFRP wrap and fully developed along most of the column length. As discussed previously, the FIB²⁵ and NCHRP Report 655²⁶ models are not applicable for longitudinal FRP. Therefore, the contribution of the longitudinal CFRP T_{fl} to the repaired column torsional resistance was calculated based on the model given by Salom et. al.⁷, which is based on principles applied to strengthening in shear. It should be noted that in the case of the CFRP layout used in this study, the same equation was deduced from this model for calculating the contribution of longitudinal CFRP as that used to calculate the contribution of transverse CFRP (Eq. (3)). Calculated values of T_{fl} are summarized in Table 3. The individual contributions of transverse and longitudinal CFRP were then added together to estimate the total contribution of the externally bonded FRP system T_f as shown in Eq. (6).

$$T_f = T_{ft} + T_{fl} \quad (6)$$

Finally, the contribution of the repaired RC column (without external CFRP) $T_{RC,R}$ to the total torsional resistance of the repaired column was estimated by subtracting T_f determined from Eq. (6) from the maximum applied torsional moment resisted by the repaired column, $T_{max,R}$ given in Table 4. In this table, $T_{RC,O}$ is the measured torsional capacity of the original column. The ratio $T_{RC,R}/T_{RC,O}$ represents the torsional strength attributed to the RC column component that was restored in the repair. As shown in Table 4, the ratio $T_{RC,R}/T_{RC,O}$ ranges from 32% to 78%. Between Levels 2 and 4, corresponding to locations of severe damage (concrete crushing through the core and yielding of transverse reinforcement), the ratio varies from 50% to 77%. These results confirm that the assumptions made during the repair design were reasonable, namely that the CFRP would rupture and the original repaired RC column without external CFRP would provide approximately 50% of the original column capacity.

CONCLUDING REMARKS

In this study, torsional repair of a severely damaged RC column was explored. A half-scale square RC bridge column, severely damaged in a previous study, was repaired and retested to evaluate the repair performance. The column was subjected to constant axial load and cyclic torsional moment. Unidirectional CFRP sheets with fibers oriented in both the column transverse and longitudinal directions were bonded to the column after the damaged concrete was removed and replaced with repair mortar. The torsional behavior and failure mode of the repaired column were investigated and compared with those of the original column. Also, the contribution of the CFRP to the torsional resistance was evaluated. Although only one column was evaluated which may limit the quantitative evaluation of the results, the study and pertaining results provide qualitative understanding of repairing for torsion and form the basis for the following conclusions to guide further research on torsional repair of RC members using this system:

1. The failure mode of the repaired column was rupture of the CFRP system, which occurred at an average stress level less than the ultimate strength of the CFRP due to stress concentration. The CFRP functioned as external reinforcement and also confined the RC column and inhibited the propagation of torsional concrete cracking.

- Consequently, the maximum torsional moment was increased compared to the original column;
2. The rotational deformation capacity of the repaired RC column was enhanced compared to that of the original column. Additionally, the rotational ductility was increased;
 3. The post-peak response of the repaired column was initially more gradual compared to the immediate steep post-peak response of the original column due to the confinement provided by the CFRP. This behavior is beneficial for seismic repair in terms of better energy absorption capability;
 4. Comparison of the torsional stiffness attenuation of the original and repaired columns indicates that the CFRP system helped provide confinement and restrain torsional crack development so that limited torsional stiffness can be maintained in the post-peak state;
 5. Strains measured on the surface of the CFRP confirmed that transverse and longitudinal sheets both contributed to the torsional resistance of the repaired column. The transverse sheets, however, were more efficient than the longitudinal sheets; and
 6. Analysis of strains measured on the surface of the CFRP sheets confirmed that the repair design assumption that the RC column can provide approximately 50% of the original torsional capacity was reasonable. Additionally, the value of the effective strain determined by NCHRP Report 655 was reasonable in designing the transverse CFRP for this column.

ACKNOWLEDGEMENTS

The authors would like to express their appreciation to the University of Missouri Research Board for the financial support for this project. BASF is gratefully acknowledged for providing the repair materials. Thanks are also to research specialist, Jason Cox, research/lab technician, John Bullock, electronics technicians, Brian Swift and Gary Abbott, and Stephen Grelle, Corey Grace, Qian Li, and Yang Yang for their help throughout the repair and testing processes.

REFERENCES

1. Hsu, T. T. C., *Torsion of Reinforced Concrete*, Van Nostrand Reinhold, Inc., New York, 1984, 516 pp.
2. Matthys, S., and Triantafillou, T. (2001). "Shear and Torsion Strengthening with Externally Bonded FRP Reinforcement," *Proceedings of the International Workshop on Composites in Construction: A Reality*, E. Cosenza, G. Manfredi, and A. Nanni, eds., Capri, Italy, 2001, pp. 203-210.
3. Zhang, J. W., Lu, Z. T., and Zhu, H. (2001). "Experimental Study on the Behavior of RC Torsional Members Externally Bonded with CFRP." *Proceedings FRP Composites in Civil Engineering. CICE2001*, Hong Kong, pp. 713-722.
4. Panchacharam, S., and Belarbi, A. (2002). "Torsion Behavior of Reinforced Concrete Beams Strengthened with FRP Composites" *Proceedings 1st FIB Congress*, Osaka, Japan, pp. 1-10.
5. Ghobarah, A., Ghorbel, M. N., and Chidiac, S. E. (2002). "Upgrading Torsional Resistance of Reinforced Concrete Beams Using Fiber-reinforced Polymer." *Journal of Composites for Construction*, ASCE, Vol. 6, No. 4, pp. 257-263.
6. Hii, A. K. Y., and Al-Mahaidi, R. (2004). "Torsional Strengthening of Reinforced Concrete Beams Using CFRP Composites." *Proceedings, 2nd Int. Conf. on FRP Composites in Civil Engineering*, CICE2004, Adelaide, Australia, pp. 551-559.
7. Salom, P. R., Gergely, J., and Young, D. T. (2004). "Torsional Strengthening of Spandrel Beams with Fiber-reinforced Polymer Laminates." *Journal of Composites for Construction*, ASCE, Vol. 8, No. 2, pp. 157-162.
8. Hii, A. K. Y., and Al-Mahaidi, R. (2006). "An Experimental and Numerical Investigation on Torsional Strengthening of Solid and Box-section RC beams Using CFRP Laminates." *Composite Structures*, Vol. 75, No. 1-4, pp. 213-221.

9. Jing M., Raongjant, W., and Li, Z. (2007). "Torsional Strengthening of Reinforced Concrete Box Beams Using Carbon Fiber Reinforced Polymer." *Composite Structures*, Vol. 78, No. 2, pp. 264-270.
10. Hii, A. K. Y., and Al-Mahaidi, R. (2007). "Torsional Capacity of CFRP Strengthened Reinforced Concrete Beams." *Journal of Composites for Construction*, ASCE, Vol. 11, No. 1, pp. 71-80.
11. Ameli, M. Ronagh, H. R., and Dux, P. F. (2007). "Behavior of FRP Strengthened Concrete Beams Under Torsion." *Journal of Composites for Construction*, ASCE, Vol. 11, No. 2, pp. 192-200.
12. Mohammadizadeh, M. R., Fadaee, M. J., Ronagh, H. R., and Ahmadinezhad, A. (2008). "Behavior of High-strength Concrete Beams Strengthened with CFRP Sheets in Torsion." *4th International Conference on FRP Composites in Civil Engineering*, CICE2008, Zurich, Switzerland, pp. 1-6.
13. Chalioris, C. E. (2008). "Torsional Strengthening of Rectangular and Flanged Beams Using Carbon Fiber-reinforced-polymers - Experimental Study." *Construction and Building Materials*, Vol. 22, No. 1, pp. 21-29.
14. Prakash, S. S., Li, Q., and Belarbi, A. (2012). " Behavior of Circular and Square Reinforced Concrete Bridge Columns under Combined Loading Including Torsion." *ACI Structural Journal*, Vol. 109, No. 3, pp. 317-327.
15. He, R., Sneed, L. H., and Belarbi, A. (2013). "Rapid Repair of Severely Damaged RC Columns with Different Damage Conditions: An Experimental Study." *International Journal of Concrete Structures and Materials*, Vol. 7, No. 1, pp. 35-50.
16. He, R., Grelle, S., Sneed, L.H., and Belarbi, A. (2013). "Rapid Repair of a Severely Damaged RC Column Having Fractured Bars Using Externally Bonded CFRP." *Journal of Composite Structures*, Vol. 101, pp. 225-242.
17. CALTRANS (2004). "Caltrans Bridge Design Specification." California Department of Transportation, Sacramento, CA.

18. ACI Committee 318 (2008). "Building Code Requirements for Structural Concrete and Commentary (ACI318-08)." American Concrete Institute, Farmington Hills, MI, 456 pages.
19. Rojahn, C., Mayer, R., Anderson, D. G., Clark, J., Hom, J. H., Hutt, R. V., and O'Rourke, M. J. (1997). "Seismic Design Criteria for Bridges and Other Highway Structures." Redwood City, CA., 166 pages.
20. Applied Technology Council (ATC) (1997). "Seismic Design Criteria for Bridges and Other Highway Structures: Current and Future." ATC-18, Redwood City, CA.
21. ASTM (2011). Standard Test Method for Compressive Strength of Hydraulic Cement Mortars (Using 2-in. or [50-mm] Cube Specimens). *C109/C109M-11*, ASTM International, 9 pages.
22. ASTM (2005). Standard Test Method for Pull-Off Adhesion Strength of Coatings on Concrete Using Portable Pull-Off Adhesion Testers. *D7234-05*, ASTM International, 8 pages.
23. ACI Committee 440 (2008). Guide for the Design and Construction of Externally Bonded FRP Systems for Strengthening Concrete Structures. *ACI 440.2R-08*, American Concrete Institute: Farmington Hills, MI.
24. Vosooghi, A., Saiidi, M. (2012). "Design Guidelines for Rapid Repair of Earthquake-Damaged Circular RC Bridge Columns Using CFRP." *Journal of Bridge Engineering*, (ASCE) BE. 1943-5592.0000426.
25. FIB (CEB-FIP) (2001). Technical Report: Externally Bonded FRP Reinforcement for RC Structures. Bulletin 14, 59-68.
26. Zureick, A. H., Ellingwood, B. R., Nowak, A. S., Mertz, D. R., and Triantafillou, T. C. (2010). "Recommended Guide Specification for the Design of Externally Bonded FRP Systems for Repair and Strengthening of Concrete Bridge Elements." NCHRP Report 655, 28-43.

Table 1 - Properties of repair mortar and CFRP system

Repair Mortar		
Property	Results	Test Method
Fresh wet density, lb/ft ³ (kg/m ³)	142	ASTM C 138
Compressive strength, psi (MPa), 2 in. (50 mm) cubes		ASTM C 109
1 day	2,500	
7 days	5,000	
28 days	6,000	
Compressive strength, psi (MPa), 3 by 6 in. (75 by 150 mm) cylinders at	5,000	ASTM C 39
Flexural strength, psi (MPa) at 28 days	1,150	ASTM C 348
Slant shear bond strength, psi (MPa) at 28 days	3,000	ASTM C 882
Splitting tensile strength, psi (MPa) at 28 days	500	ASTM C 496
CFRP System		
Property	Requirement	
Fiber material	High strength carbon	
Fiber tensile strength, ksi (MPa)	720 (4,950)	
Areal weight, lb/ft ² (g/m ²)	0.062 (300)	
Fabric width, in. (mm)	20 (500)	
Nominal thickness, in./ply (mm/ply)	0.0065 (0.165)	
Ultimate tensile strength, ksi (MPa)	550 (3,800)	
Tensile modulus, ksi (GPa)	33,000 (227)	
Ultimate rupture strain, %	1.67	

Table 2 - Torsional moment and corresponding twist at cracking, yielding, and maximum states

		Original	Repaired
Cracking	T_{cr} , kip-ft (kN-	141.6	
	θ_{cr} , deg.	0.52	
Yielding	T_y , kip-ft (kN-	203.2	226.7 (307.4)
	θ_y , deg.	3.21	3.72
Maximum	T_{max} , kip-ft (kN-	244.4	295.6 (400.7)
	θ_{max} , deg.	6.47	12.49
Torsional	$\mu_{\theta} (\theta_{max}/\theta_y)$	2.02	3.36

Table 3 - Contribution of the transverse and longitudinal CFRP

Contribution of Transverse CFRP						
Level	ϵ_{fe} 10 ⁻⁶	E_f ksi (GPa)	f_{fe} ksi (MPa)	A_0 in. ² (mm ²)	t_f in. (mm)	T_{ft} kip-ft (kN-m)
1	3,776		125 (859)			65.3 (88.6)
2	4,876		161 (1,110)			84.4 (114.4)
3	4,995	33,000 (227)	165 (1,136)	484 (312.3E3)	0.0065 (0.165)	86.4 (117.2)
4	7,549		249 (1,718)			130.6 (177.1)
5	10,588		349 (2,409)			183.2 (248.4)
6	10,757		355 (2,448)			186.1 (252.4)
Contribution of Longitudinal CFRP						
Level	ϵ_{fe} 10 ⁻⁶	E_f ksi (GPa)	f_{fe} ksi (MPa)	A_0 in. ² (mm ²)	t_f in. (mm)	T_{ft} kip-ft (kN-m)
1	2,335		77.0 (531.2)			40.4 (54.8)
2	2,954		97.5 (672.0)			51.1 (69.3)
3	1,170	33,000 (227)	38.6 (266.2)	484 (312.3E3)	0.0065 (0.165)	20.2 (27.5)
4	2,527		83.4 (574.9)			43.7 (59.3)
5	2,013		66.4 (458.0)			34.8 (47.2)
6	1,682		55.5 (382.7)			29.1 (39.4)

Table 4 - Estimation of contribution of repaired RC column

Level	$T_{max,R}$ kip-ft (kN-m)	T_f kip-ft (kN-m)	$T_{RC,R}$ kip-ft (kN-m)	$T_{RC,O}$ kip-ft (kN-m)	$T_{RC,R}/T_{RC,O}$ %
1		105.7 (143.4)	189.8 (257.4)		78
2		135.5 (183.7)	160.1 (217.0)		65
3		106.7 (144.6)	188.9 (256.1)		77
4	295.6 (400.7)	174.4 (236.4)	121.2 (164.3)	244.4 (331.4)	50
5		218.0 (295.6)	77.5 (105.1)		32
6		215.2 (291.8)	80.3 (108.9)		33

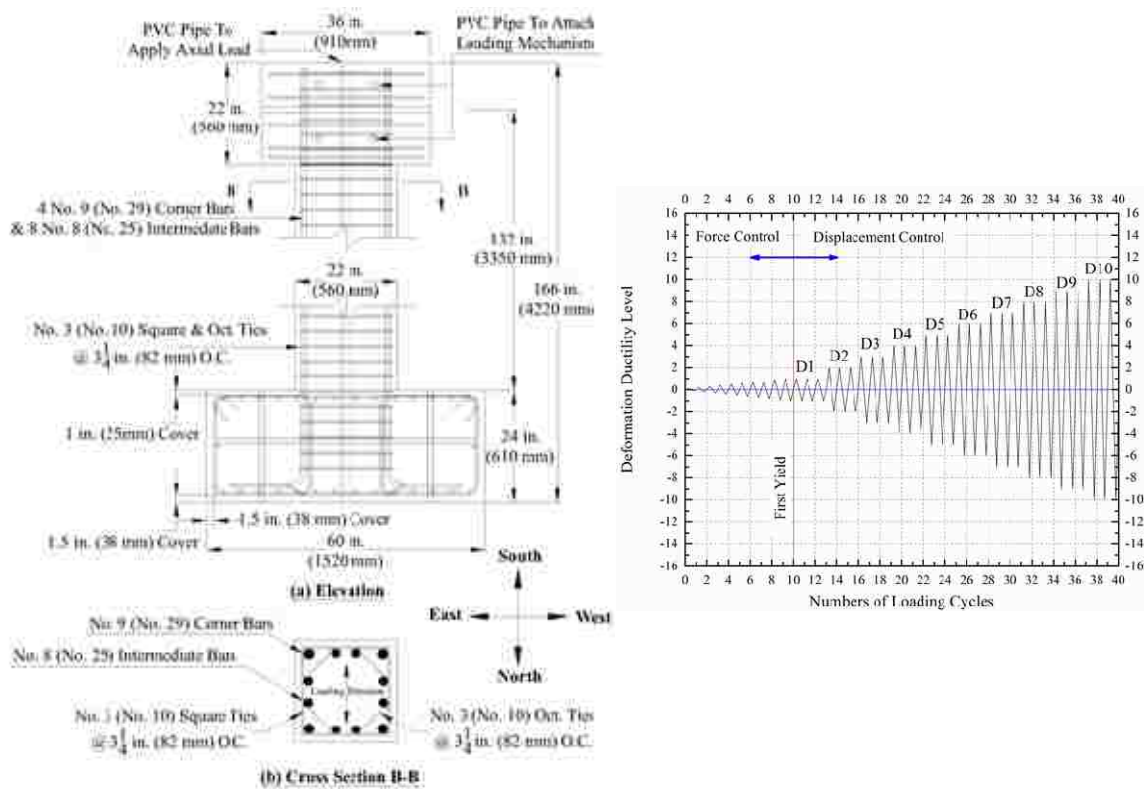


Fig. 1 - Details of original column.

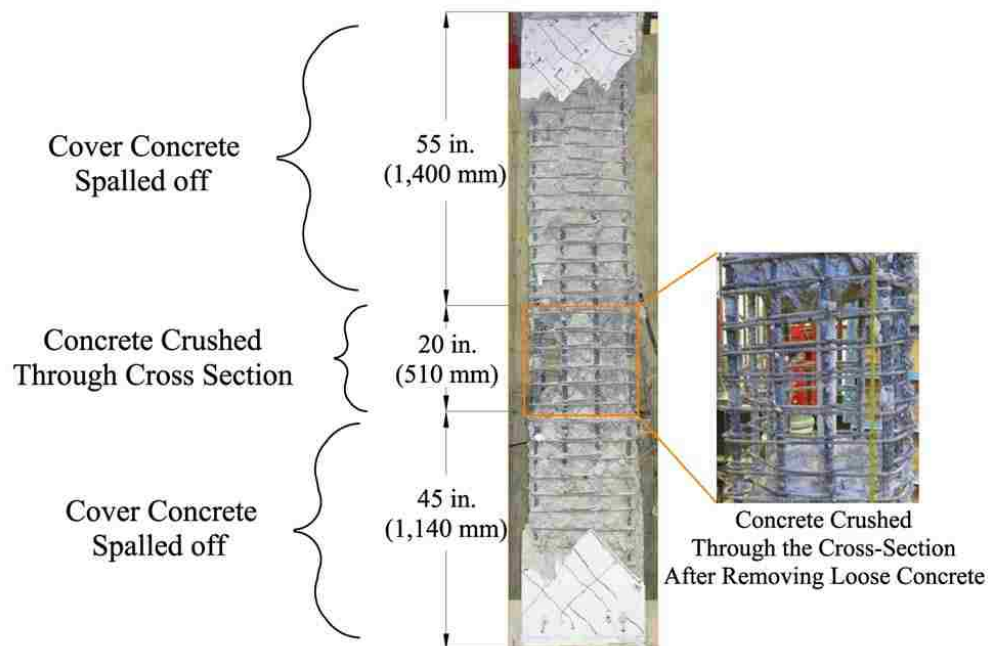


Fig. 2 - Damage condition of concrete in original column.

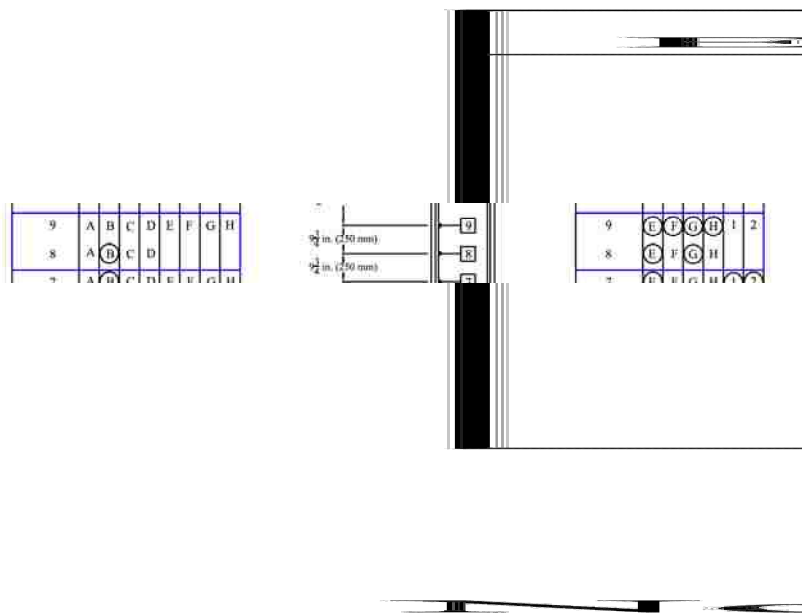


Fig. 3 - Damage condition of reinforcing steel in original column.

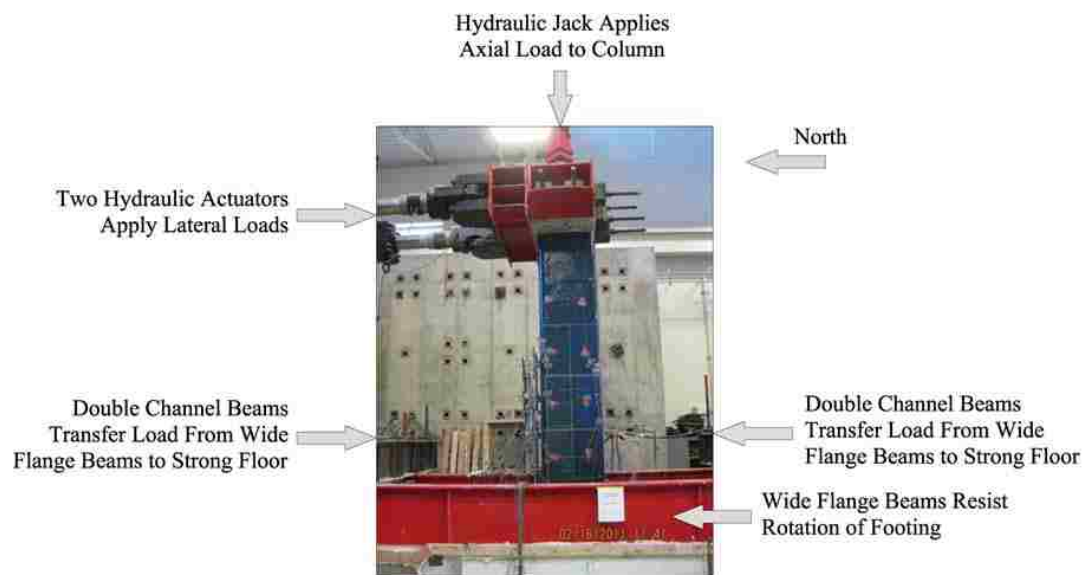
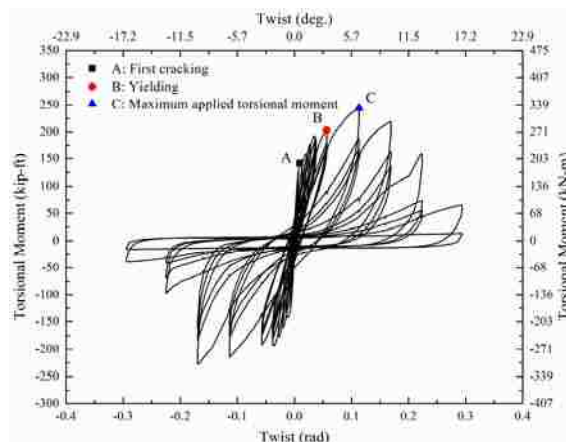


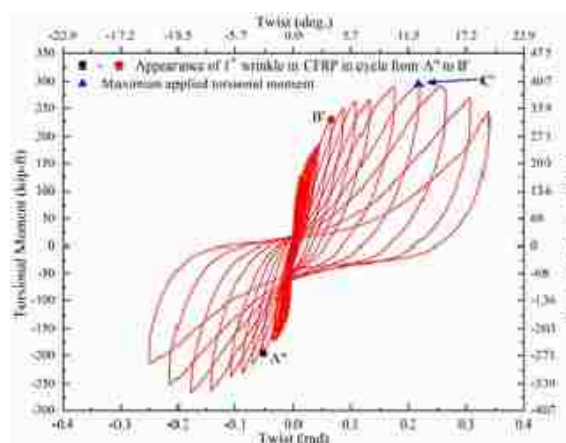
Fig. 4 - Test setup for repaired column.



Fig. 5 - Failure of repaired column.



(a) Original Column



(b) Repaired Column

Fig. 6 - Hysteresis behaviors of original and repaired columns.

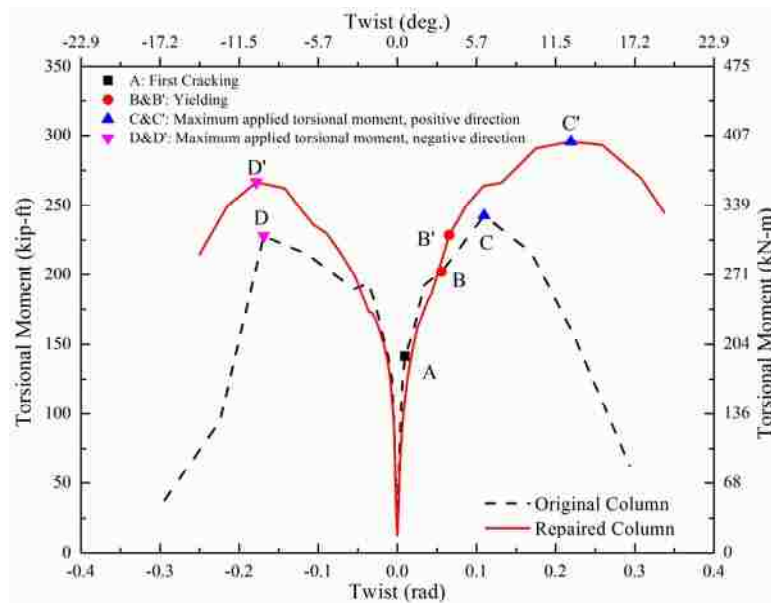


Fig. 7 - Torsional moment-twist envelopes of repaired column compared to original column.

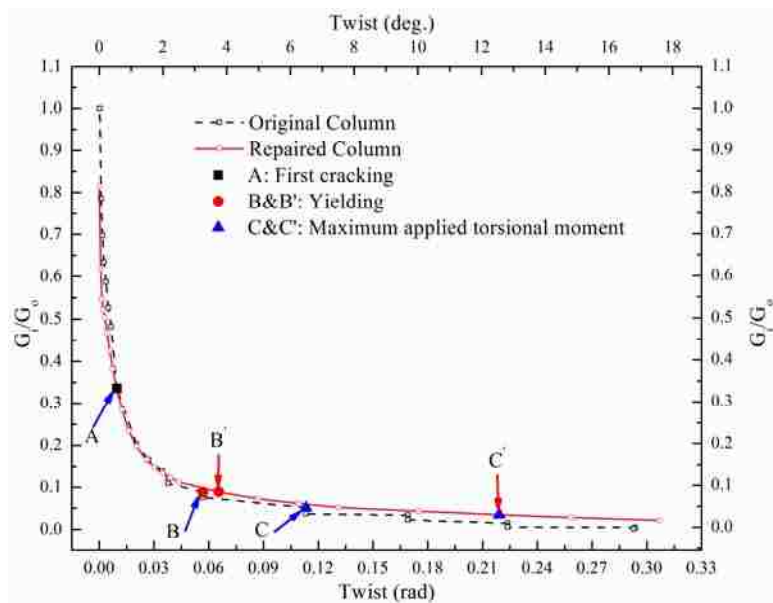


Fig. 8 - Torsional stiffness attenuation of repaired column compared to original column.

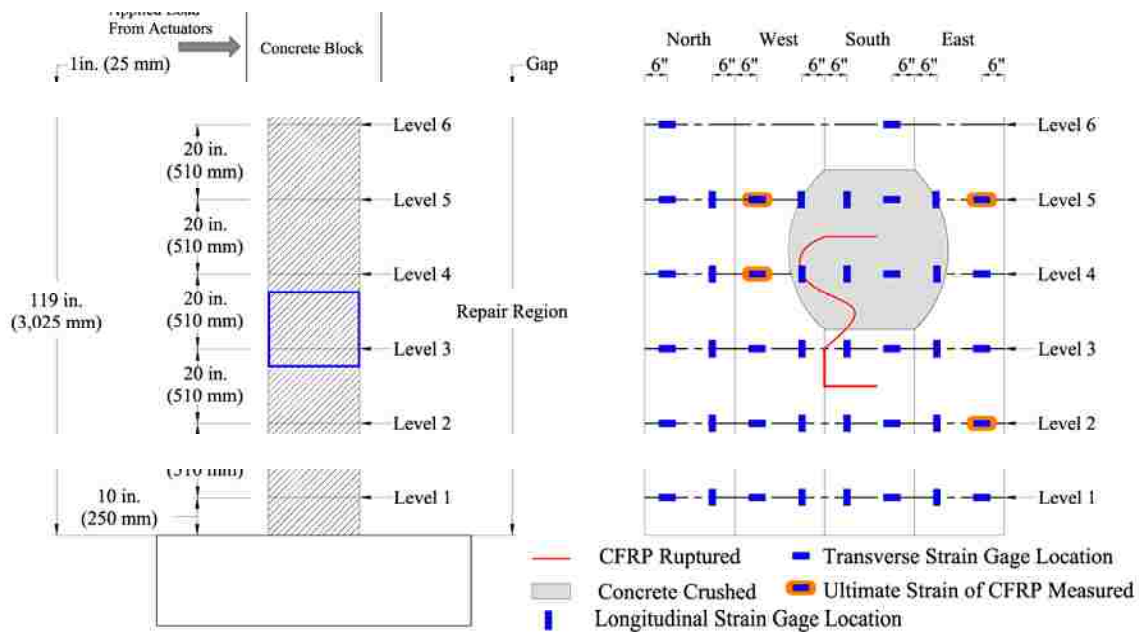


Fig. 9 - CFRP strain gage layout and relation to repaired column damage location.

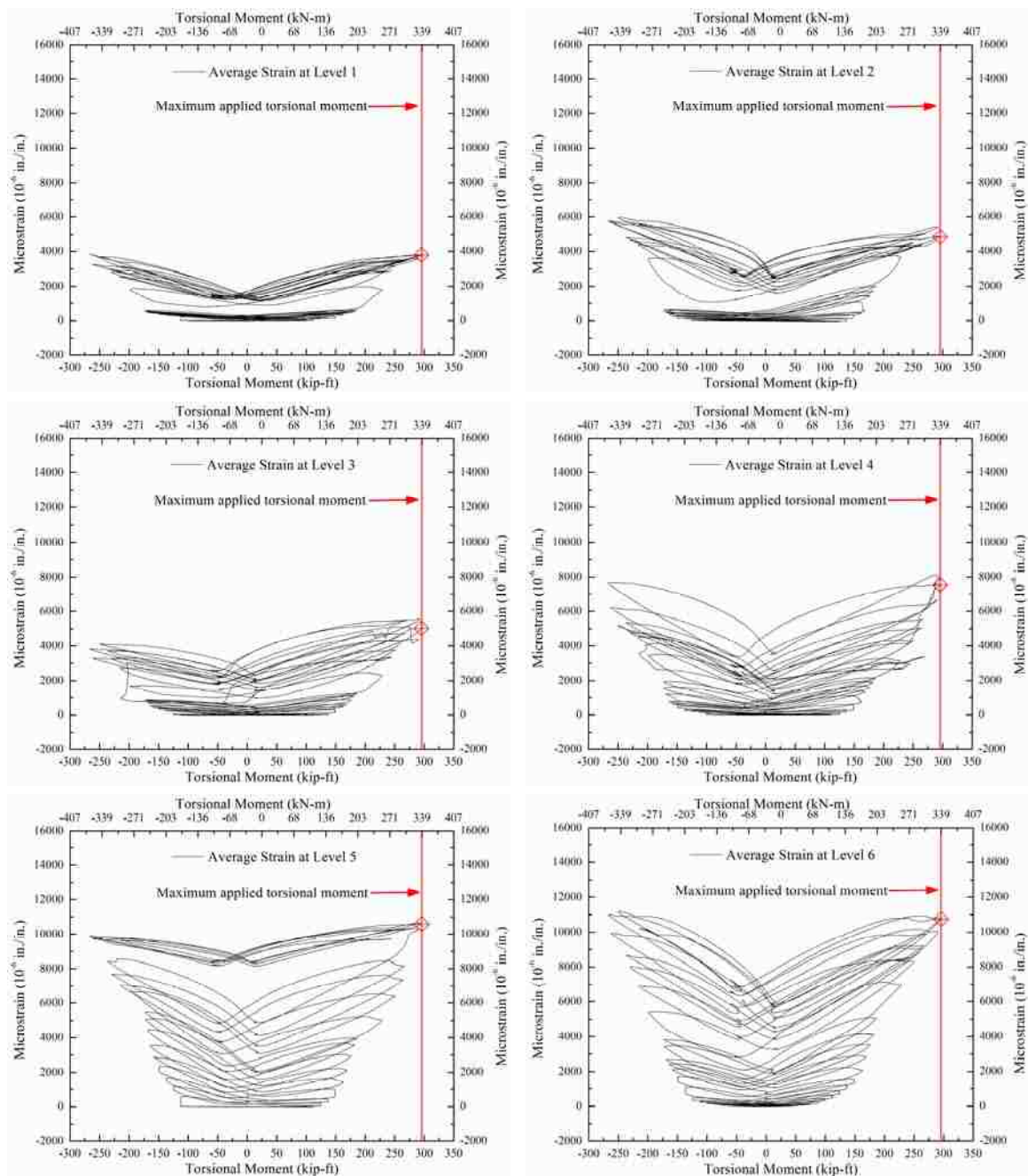


Fig. 10 - Average transverse surface strain-torsional moment relationship of repaired column.

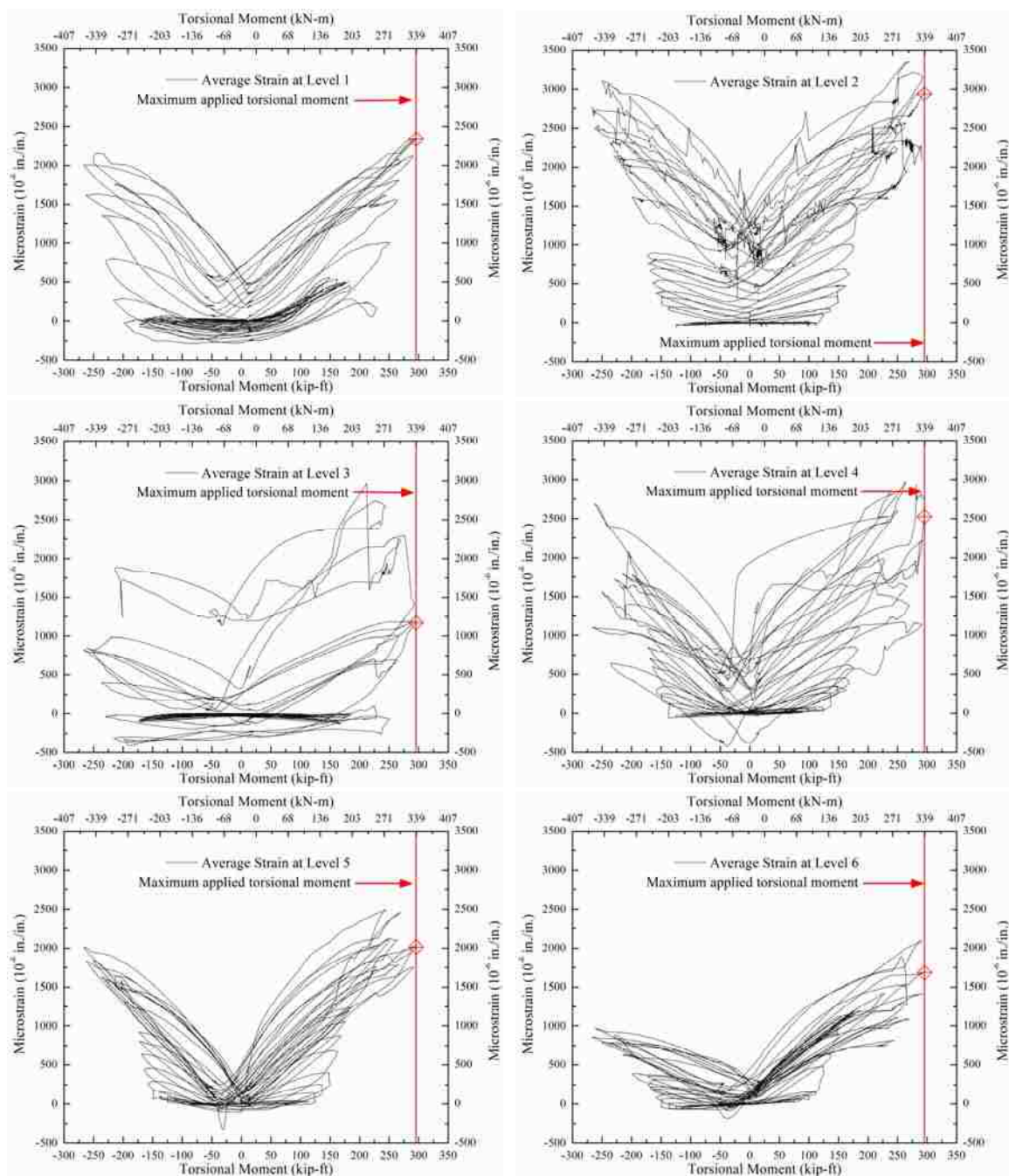


Fig. 11 - Average longitudinal surface strain-torsional moment relationship of repaired column.

V. POST-REPAIR SEISMIC PERFORMANCE OF DAMAGED RC BRIDGE COLUMNS WITH FRACTURED BARS – A NUMERICAL ASSESSMENT

Ruili He, Yang Yang, and Lesley H. Sneed

ABSTRACT

Seismic repair of bridge columns has been studied extensively during past decades; however, few studies were conducted on the influence of the column (member) repair to bridge structures (system). This paper presents a developed method to fill this gap through a case study. In this study, an earthquake-damaged RC column with fractured longitudinal reinforcement was rapidly repaired with externally bonded carbon fiber reinforced polymer (CFRP) sheets. Test results showed that the lateral strength and drift capacity of the column were partially restored. Nonlinear fiber element models were developed using Open System for Earthquake Engineering Simulation (OpenSees) software to simulate the response of the undamaged and repaired columns. The undamaged column was modeled using currently available techniques, while a technique was developed to model the repaired column. Analytical results were validated with experimental results. A three-span RC bridge structure was selected and modeled with the developed column models, based on which dynamic time history analysis was conducted. Seven scenarios of different combinations of undamaged and repaired columns were analyzed employing 40 ground motion (GM) records. The seismic demand on drift ratio and base shear of each column were determined and compared with the drift capacity and lateral strength of the undamaged and repaired columns determined from the experimental results. The results illustrated that the bridge models with one or more of the repaired columns were capable to resist the base shear and drift demand by the 40 GM records selected according to the target design spectrum.

Keywords: Bridge system; dynamic analysis; fiber-reinforced polymer; fractured bars; reinforced concrete columns; repair.

1. INTRODUCTION

An extensive number of studies have been conducted on seismic repair and retrofit of reinforced concrete (RC) bridge columns, considering that they are the primary source of energy dissipation for a bridge structure during an earthquake. Seismic retrofit is conducted for RC bridge columns constructed in the U.S. prior to 1970s since they are not detailed to resist seismic loads. Methods commonly used to retrofit RC bridge columns include applying RC jackets [1], steel jackets [2], or fiber reinforcement polymer (FRP) composite jackets [3]. More recently, efforts have been focused on detailing of RC bridge structures to prevent collapse during an earthquake. RC bridge columns are designed to undergo cracking, spalling or crushing of concrete, yielding or bucking of reinforcing bars, or even fracture of some of the reinforcing bars during a strong earthquake. Repair techniques for earthquake-damaged RC bridge columns typically involve epoxy injection into concrete cracks [4], repair of spalled and crushed concrete, and/or application of jackets as external reinforcement. Similar to retrofit of RC bridge columns, reinforced concrete [5], steel [6], and FRP [7] are commonly used as jacketing materials for repair of RC bridge columns with different damage levels.

Local modifications (interventions) from the retrofit or repair of an individual RC column member can change the performance of the member, which in turn can influence the performance of the bridge structure in which the column is included, especially under seismic loading. In general, the seismic performance of a bridge structure will be improved when the retrofit or repair is carried out uniformly for all the members. Modifications to a single member or only some of the members of a bridge structure, on the other hand, may result in a stiffness irregularity, which can result in an unbalanced seismic demand on the members of the structure. To date, most research on seismic repair or retrofit of RC bridges has focused on assessing the response of individual columns (member level), not the bridge structure (system level), due to limitations in modeling and especially testing of full bridge structures. Thus, the need exists to develop techniques to reflect the effects of the intervention on the entire bridge structure. The availability of increasingly powerful computers has provided an opportunity to implement numerically intensive modeling strategies. In particular, analytical tools based

on the fiber element method have been developed to model the nonlinear behavior of RC structures under cyclic loading, and studies have shown that the fiber element method can be effective in simulating the response of RC members under seismic loading [8-10].

The objective of this paper was to investigate the influence of repair to individual columns on the post-repair seismic performance of the bridge system by developing a method to model repaired RC bridge columns. A method was previously developed by the authors to rapidly repair earthquake-damaged RC bridge columns using externally bonded carbon FRP (CFRP) sheets with fibers oriented in both the column transverse and longitudinal directions [11-13]. Five severely-damaged 1/2-scale RC columns with different damage conditions were repaired using the developed repair method. As discussed in the work by He et al. [12], the repair method proved effective in repairing damaged columns without fractured longitudinal bars, though factors such as bending-torsion interaction and failure mode played a role in the level of restoration. However, the method was only partially successful in repairing a column with fractured longitudinal bars located near the base of the column, in which case a large force demand was required for the CFRP strengthening system, as well as a substantial anchorage system to develop it. In the present study, a nonlinear dynamic analysis of the post-repair response of an RC bridge structure that included this repaired column was conducted. First, models of the undamaged (original) and repaired columns were developed and validated with the experimental results. Then, a prototype bridge structure was selected and modeled with the developed column models, and a dynamic time history analysis was conducted employing 40 ground motion (GM) records. Seven models of the bridge structure with different numbers and locations of repaired columns were analyzed and compared. The results of the analysis were discussed in terms of base shear and top drift ratio demand of the columns.

2. MODELING OF INDIVIDUAL RC BRIDGE COLUMNS

The analytical models for both the undamaged (original) and repaired columns were described in this section. Open System for Earthquake Engineering Simulation (OpenSees) software was utilized in this study. Currently available techniques were used

to model the undamaged column, while a technique was developed to model the repaired column. The developed models were validated by comparing the calculated responses with measured test data from different studies [11, 12, 14]. The original column test specimen was tested to failure under quasi-static reversed cyclic lateral load and a constant axial load of approximately 150 kips (667 kN) (7% of the axial load capacity) [14]. The column was then repaired and retested under the same load protocols [11, 12].

2.1 Modeling of Original Column

2.1.1 Fiber Section Properties

The original column section was constructed as a fiber section object, which is composed of fibers, with each fiber containing a prescribed uniaxial material, an area, and a location. The details of the column geometry and reinforcement are shown in Figure 1 and are discussed in detail elsewhere by the authors [11, 12]. The fiber discretization of the cross-section is shown in Figure 2. The core concrete was discretized to 25 strips in both directions. The cover concrete was discretized to 25 strips along the edge direction and two strips in the thickness direction. For the longitudinal reinforcing steel bars, the analysis was based on one mesh size. The core concrete, cover concrete, and longitudinal steel fibers were each defined by a uniaxial stress-strain model corresponding to the material they represent.

The Linear Tension Softening Concrete02 material in OpenSees was used to model both the unconfined and confined concrete. Mander's model [15] was used to determine the material properties of the confined concrete. The compressive stress-strain relationship of this material model is based on the uniaxial Kent-Scoff-Park concrete material model [16, 17]. The tensile stress-strain relationship is bilinear with the same modulus as the compression stress-strain relationship in the increasing region.

The reinforcing steel is modeled using the Giufre-Menegotto-Pinto constitutive model [18] available in OpenSees. The model has a bilinear backbone curve with a post-yield stiffness proportional to the modulus of elasticity of the steel, $E_{sh}=b \cdot E$, and accounts for the Bauschinger effect in the cyclic response of the material. Despite the simplicity of

the model, it does not account for the yield plateau of the reinforcing steel or the degradation of the steel strength due to bar buckling or rupture.

Moment-curvature relationship from the fiber section was compared to the measured data from the experiment as shown in Figure 3, which illustrated the effectiveness of the discretization scheme with the chosen material models.

2.1.2 Column Numerical Model

The numerical model developed for the original column is illustrated in Figure 4. The column member was modeled as a nonlinear beam-column element with a fiber discretized section shown in Figure 3. For a RC column subjected to a lateral load, it is well established that the total lateral deflection can be attributed to deformations due to flexure, shear, and bond slip [19]. In this model, the shear and bond slip deformations were considered by adding zero-length springs.

The equation proposed by Correal et al. [20] was used to calculate the shear stiffness of column in the zero-length spring for shear

$$K_v = \frac{K_{v,45}}{n_{pr} L_{pz}} \quad (1)$$

where n_{pr} is the number of plastic hinge regions (1 for cantilever columns), and L_{pz} is the length of each plastic hinge zone. L_{pz} was estimated as 1.5 times the column cross-section dimension based on Caltrans [21]. $K_{v,45}$ is the shear stiffness of RC members with 45° diagonal cracks, which was computed by Eq. (2) [22]:

$$K_{v,45} = \frac{\rho_v}{1+4n\rho_v} E_c b_w d \quad (2)$$

where ρ_v is the transverse reinforcement ratio calculated as A_v/sb_w , and n is the modular ratio calculated as E_s/E_c , A_v is the transverse reinforcement area, s is the tie pitch, E_s is the elastic modulus of steel, E_c is Young's modulus of concrete, and $b_w d$ is the web area to resist shear.

The shear stiffness calculated by Eq. (1) was converted to an equivalent rotational stiffness due to difficulties in achieving numerical convergence in dynamic analysis. Eq. (3) [23] was used to determine the equivalent rotational stiffness:

$$K_{v\theta} = \frac{K_v H^2}{n_{pr}} \quad (3)$$

in which H is the column height, and the other parameters were defined in the previous equations.

To consider the bond slip from strain penetration effects, the bond-slip spring model [24] was added to the model. In their model, the relationship of bar stress versus loaded-end slip was proposed as a linear relationship for the elastic region and a curvilinear relationship for the post-yield region. The curvilinear relationship was represented by Eq. (4):

$$\tilde{\sigma} = \frac{\frac{\tilde{s}}{\mu - \tilde{s}}}{\left[\left(\frac{1}{\mu \cdot b} \right)^{R_e} + \left(\frac{\tilde{s}}{\mu - \tilde{s}} \right)^{R_e} \right]^{1/R_e}} \quad (4)$$

where $\tilde{\sigma}$ is the normalized bar stress defined as $\tilde{\sigma} = (\sigma - f_y) / (f_u - f_y)$, \tilde{s} is the normalized bar slip as defined as $\tilde{s} = (s - s_y) / s_y$, μ is the ductility coefficient defined as $\mu = (s_u - s_y) / s_y$, b is the stiffness reduction factor that represents the ratio of the initial slope of the curvilinear portion at the onset of yielding to the slope in the elastic region, f_y and f_u are the yield and ultimate strengths of the steel reinforcing bars, respectively, s_y and s_u are the loaded-end slips when the bar stresses are f_y and f_u , respectively, and the value of factor R_e should be slightly greater than one in order to maintain a zero slope near ultimate strength of the bar.

The bond-slip rotation can be assumed to occur about the neutral axis of the column cross-section at the connection interface [25]. The neutral axis location and the stress in the extreme tension reinforcement corresponding to the desired lateral load are determined from moment-curvature analysis of the section. The rotation occurring at the

interface was obtained as the ratio between the slippage [24] and the distance from the extreme steel bar to the neutral axis. Therefore, the relationship between the applied moment and rotation was developed, which was then applied in the analytical model as a zero-length spring.

2.1.3 Model Validation

Both pushover and cyclic loading analysis were conducted using the developed analytical model of the original column. Axial load was applied along the axis of the column linearly up to 150 kips (667 kN) prior to application of the lateral load and then kept constant during the loading process. Results were validated through comparison of the measured and calculated load-displacement relationships. Figure 5a shows the measured envelope of load-displacement results and the calculated pushover results, in which the effects of shear deformation and strain penetration were included in different combinations. It can be seen that the shear deformation is negligible compared to the flexural deformation since the aspect ratio of the column (6.0) was relatively large [26]. The calculated pushover curve of the model with shear deformation and strain penetration implemented was comparable to the envelope of measured data in terms of initial stiffness and base shear capacity. However, the model could not predict the failure of the column associated with fracture of longitudinal bars due to limitations of the steel material model. Figure 5b shows the comparison of calculated and measured hysteresis behavior of the original column. The model predicted results very close to the measured data in terms of the base shear capacity and initial stiffness. However, the model could not well predict the degraded unloading stiffness and pinching effect.

2.2 Modeling of Repaired Column

2.2.1 Damage Prior to Repair and Repair Program

Figure 6 shows the damaged column after the original test. Damage included cracking and spalling of concrete, yielding and straightening of the end hooks in the reinforcing steel ties, and buckling of ten of the twelve longitudinal bars. Additionally, two longitudinal reinforcing bars fractured near the base of the column on opposite corners. The damaged column was repaired by removing and replacing the crushed

concrete, and then installing three layers of CFRP sheets on the tension faces of the column with fibers oriented in the longitudinal direction of the column. Then, CFRP was wrapped transversely around the column with a varying number of layers to a height of 60 in. (1524 mm) from top of footing. Above this height, no longitudinal or transverse CFRP was placed, and no repair was made to the concrete. Additional details regarding the damage description and repair of the original column are discussed elsewhere by authors [11, 12].

2.2.2 Column Numerical Model

Unique challenges exist for the case of modeling the behavior of repaired RC columns compared with undamaged or retrofitted RC columns. Several aspects complicate the simulation such as accounting for the initial damage condition and estimating the mechanical properties of the materials etc. In this study, a new modeling method was developed to simulate the behavior of the repaired RC column, in which prior damage and repair was accounted for according to different damage states and repairs along the column length.

It was illustrated in the study [23] that the reinforcing steel properties should be modified to account for column softening due to earthquake damage. In their study, the elastic modulus of the longitudinal bars was reduced to account for the Bauschinger effect due to the cyclic loading from the previous testing. Five column damage states were defined in their study: flexural cracks (DS1); first spalling and shear cracks (DS2); extensive cracks and spalling (DS3); visible lateral and longitudinal bars (DS4); and imminent failure (DS5). Different reduction factors were proposed to modify the elastic modulus of the longitudinal bars in repaired columns corresponding to the different damage states.

In modeling the repaired column in this study, the modified steel properties, the confinement provided by the CFRP wrap and the longitudinal CFRP in the repaired region, and the cracked concrete in the unrepaired region were considered. Determination of the damage states along the column length is illustrated in Figure 6d, which was used to determine the reduction factors employed for the longitudinal reinforcing bars. The

repaired column member was modeled as a nonlinear beam-column element with a fiber discretized section as shown in Figure 7, in which different fiber sections were used to represent the different damage states and repairs along the length. In addition, the same shear stiffness used for original column was used in the repaired column model. Bond-slip deformations from the strain penetration effects were included in the analytical model, in which the damage to the pretested reinforcing bars was considered.

2.2.3 Model Validation

The calculated load-displacement relationship from the pushover analysis is compared to the measured data in Figure 8a. Results in Figure 8a illustrated that the developed model can simulate the initial stiffness and the lateral strength capacity of the repaired column with acceptable discrepancy. Figure 8b compares the measured and calculated hysteresis behaviors of the repaired column. The asymmetry of the measured data during testing is due to the unsymmetrical damage from the original testing. The calculated results of the developed analytical model are symmetric for the reason that the unsymmetrical unrepaired damage was not modeled. The behavior of the repaired column in the direction of positive displacement was well-predicted by the developed analytical model. Although the analytical prediction shows slightly larger energy dissipation capacity, good agreement in terms of both lateral strength and initial stiffness is observed. Moreover, pinching of the hysteresis loops observed in the experimental data is also reflected in the analysis.

3. MEASURED COLUMN CAPACITIES

The main emphasis of this study is to estimate seismic demand on critical bridge components through the implementation of nonlinear analysis procedures. The experimental data from the test specimen were used to validate the developed models as discussed in the previous section. In addition, the experimental data were utilized to estimate the capacities of the original and repaired columns in terms of lateral strength and top drift ratio, which were used in the nonlinear dynamic time-history analyses discussed later in this paper.

The capacity values were obtained from idealized load-displacement envelopes for the original and repaired columns shown in Figure 9 with the values of lateral strength and drift ratio capacities shown in the figure. The idealization of the envelopes was described elsewhere by the authors [11, 12]. The base shear capacity was defined as the equivalent yield base shear in the idealized elasto-plastic curves in Figure 9. The base shear capacity of the original and repaired columns was 62.3 kips (277 kN) and 43.7 kips (194 kN), respectively. The top drift ratio capacity of the original and repaired columns was 4.5% and 8.0%, respectively.

4. MODELING OF THE RC BRIDGE STRUCTURE

4.1 Background of the Selected Bridge

Example No. 4 of Seismic Design of Bridges provided by the Federal Highway Administration [27] was selected for evaluating the effects of the column repair. The bridge was designed for seismic loading using the Standard Specifications for Highway Bridges [28]. This bridge was selected because the columns of the bents have similar cross-sectional dimensions, aspect ratio, and reinforcement ratios to those included in the experimental program of this study, which were 1/2-scale prototype specimens. The bridge was designated to be built in the western United States in a seismic zone with an acceleration coefficient of 0.30g. The superstructure had a 30-degree skew to the bents with continuous spans of 100 ft. (30.5 m), 120 ft. (36.6 m), and 100 ft. (30.5 m). The superstructure was a cast-in-place (CIP) concrete box girder with two interior webs and a depth of 8 ft. (2440 mm). Columns of the bents were designated to be cast monolithically with the CIP box girder, which results in nearly fixed joints between the superstructure and substructure in both the longitudinal and transverse directions. The columns had a height of 20 ft. (6100 mm) from the top of the footing to the soffit of the box girder and a circular cross-section with a 48 in. (1220 mm) diameter. The effective height of the columns was 23.38 ft. (7130 mm) from the top of the footing to the centroid of the gross cross-section of the box girder, which resulted in an aspect ratio of 5.85 for the columns. Thirty-four ASTM 706 Grade 60 No. 11 (35 mm dia.) bars were used as longitudinal reinforcement, and No. 5 (16 mm dia.) spirals at a spacing of 3.5 in. (89 mm) were used as transverse reinforcement with a concrete cover of 2 in. (50 mm). The resulting

longitudinal and transverse reinforcing ratios were 2.79% and 0.8%, respectively. In this study, a 1/2-scale prototype bridge was modeled, in which the square columns tested in this research study were used instead of circular columns. The skew was removed since the effect from the skew was not the focus of this study. The intermediate bents had a cross beam integral with the box girder and two columns that were pinned at the top of spread footings.

4.2 Bridge Numerical Model

Figure 10 shows the numerical model of the scaled bridge structure in OpenSees. The superstructure was modeled with a total of twelve elements located in a single line along the centerline of the bridge structure, with four elements per span. Determination of moments of inertia and torsional stiffness of the superstructure was based on gross cross-sectional properties. The mass density of the superstructure used for the dynamic analysis was adjusted so that the fundamental frequency was the same as that of the full-scaled bridge structure. The bents were modeled with 3-D elements to represent the cap beams and columns. Figure 11 shows the actual bent and the bent model used in the analysis, in which the forces were transferred from the superstructure to the columns at the points of intersection. In order to better represent the load distribution, the moments of inertia and the torsional stiffness used for the cap beam were increased. In addition, rigid link elements were used between the column top at the soffit of the box girder and the cap beam located at the superstructure centroid. The previously developed original and repaired column models were used for the column elements, including the shear deformation and strain penetration effects as discussed previously. The bottom node of the column was released for rotation in both plan directions to model the pinned column base. The footing was eliminated in this simplified model. This model allows longitudinal translational response at the abutment, which is conservative and more desirable for design of the substructure.

The analysis was conducted for the selected bridge structure with seven different models to consider different scenarios of repaired columns. The original bridge structure model without repaired columns was used as the control and is referred to as model Orig. in the following discussion. The bridge structure models with different scenarios of

repaired columns are referred as models R-1, R-12, R-13, R-14, R-123, and R-1234, where R indicates the bridge structure model included repaired column elements, and the numbers after the dash identify the repaired columns in the model by column number. Column numbers are defined in Figure 10. The remaining columns in each model were represented by original (undamaged) columns. It should be noted that in a real bridge structure, fully damaged/repaired columns may not coexist with undamaged columns within the same structure. However, the methodology used in this study can be extended in the future to consider different levels of damage and/or repair in individual members.

4.3 Modal Analysis

Modal analysis was conducted for the seven bridge models described in the previous section. The natural frequencies corresponding to the first three modes of vibration are summarized in Table 1 with the corresponding modal shapes. The modal shapes obtained in this analysis were the same as those given in the file [27]. The fundamental frequency of the model including only original columns, Orig., determined from the modal analysis was 1.2060 Hz, which is similar to the value calculated for the full-scaled bridge in the file (1.2022 Hz). The frequency of the second mode was much larger than the fundamental frequency due to the simplification that no interaction between the structure and soil was modeled in the bent supports and the abutments. The displacement corresponding to the first mode was in the longitudinal direction, which indicates that significant longitudinal response was expected to occur; thus analysis results discussed in this paper are focused on the longitudinal response.

5. DYNAMIC TIME HISTORY ANALYSIS OF RC BRIDGES

Dynamic time history analyses were conducted to assess the performance of the bridge with varied configurations of repaired RC columns subjected to ground motion records during earthquakes. The earthquake records were obtained according to the target design spectrum related to the site condition where the selected bridge is designated to be built. The selected earthquake records were then adjusted to reflect the scale factors for the geometry and mass density of the models.

5.1 Selection of Ground Motion (GM) Records

Twenty data sets of GM records during seven earthquakes were selected according to the target design spectrum, which was determined according to the standards [29, 30]. Each data set included subsets of data in two orthogonal directions recorded from the same event and record station (FN & FP). Accordingly, a total of 40 GM records were employed in the analyses. The selected GM records are presented in Table 2. The GM records were obtained from the GM database provided by the Pacific Earthquake Engineering Research Center (PEER) [31]. The records were selected from a bin of relatively large magnitudes of 6.5-7.0 and belong to moderate epicentral distances of 15-32 km (9.3-20.0 miles). The ratio of the peak ground acceleration (PGA) to the peak ground velocity (PGV) shown in the table is an indicator of the frequency content of seismic motion. The selected GM records were then scaled to match the target design spectrum created previously that corresponds to the structure location, and the values of PGA reported in Table 2 are the scaled values. Figure 12 shows the spectral acceleration for the selected earthquake records after scaling and the target design spectrum. The scaled earthquake records were then scaled appropriately to apply them to the 1/2-scale bridge models.

5.2 Demand Results

Results of the dynamic time history analyses are presented in Figure 13 in terms of top drift ratio demand. Figure 13 shows the top drift ratio demand for each column in each bridge model under the 40 selected GM records. Under each GM record, the four columns in the same bridge model experienced nearly the same drift ratio demand. However, under the same earthquake record, the top drift ratio demands for the columns varied in different bridge models, which shows that the existence of one or more repaired columns influenced the drift ratio demand on all columns in the bridge structure. It is also worthy to note that the drift ratio demand for the columns in models R-12, R-13, and R-14 was similar under the same GM record. This is attributed to the similar structural dynamic properties of the bridge models that included the same number of repaired columns, which was also shown by the modal analysis conducted in the previous section.

Results of the dynamic time history analyses are presented in terms of base shear demand in Figure 14, which shows the base shear demand for each of the four columns in each bridge model under the 40 selected GM records. Under the same GM record, Figure 14 shows that the existence of one or more repaired columns changed the base shear demand to the original columns. Under the same GM record, the base shear demand to the repaired columns was smaller than that to the original columns in the same bridge model, which can be explained by the fact that the columns had almost the same displacement, and the original columns had a higher stiffness. Figure 14 also shows that the base shear demand on the same type of column (original or repaired) was nearly the same under the same GM record for models R-12, R-13, and R-14. This result indicates that the location of the repaired columns did not play a significant role in the displacement and strength demand in such a bridge structure.

5.3 Discussion of the Results

The maximum drift ratio demand on the columns under the selected 40 GM records is summarized for each of the different models in Figure 15a. It is important to note that the maximum drift ratio demand on the columns of the bridge models with repaired columns (R-1, R-12, R-13, R-14, R-123, and R-1234) was larger than that of the bridge model with only original columns (Orig.). However, an increasing number of repaired columns did not strictly correlate with increasing maximum drift ratio demand. The largest maximum drift ratio demand (around 1.5%) occurred in the models with two original and two repaired columns (R-12, R-13, and R-14). Considering all seven bridge models, the maximum top drift ratio demand on the repaired and original columns was 33% and 19% of the corresponding top drift ratio capacities (4.5% for the repaired column, and 8.0% for the original column, see Figure 9). In summary, the maximum drift ratio demands of all the original and repaired columns were less than the corresponding top drift ratio capacities under the 40 GM records selected based on the target design spectrum.

The average top drift ratio demand on the columns in each bridge model is shown with the standard deviation in Figure 15b, which illustrates the influence of the random characteristics of the GM records considered. The average value for each bridge model

was calculated by averaging the drift ratio demand on all four columns under the 40 selected GM records. As shown in Figure 15b, the bridge model with only original columns (Orig.) had the lowest average top drift ratio demand (approximately 0.4%), and the bridge models with repaired columns had higher values, among which the bridge structures with two repaired columns (R-12, R-13, and R-14) had the highest average drift ratio demand (0.6%). Additionally, the difference in average drift ratio demands on bridge models with repaired columns was relatively small. This may be explained by the pattern of the design displacement spectrum for structures with relatively small periods. According to the design displacement spectrum, structures with larger frequency will experience smaller displacement demand; thus, the bridge model with only original columns (with a frequency of 1.2 Hz) had smallest drift ratio demand as shown in the analysis results. However, the trends of average drift ratio demand on the models with repaired columns were not the same as the trends of design displacement spectrum for two reasons: 1) average response displacement spectrum of the 40 GM records is not as smooth as the design spectrum; 2) the frequencies of bridge structures with repaired columns were similar (between 0.6 and 0.7 Hz).

The maximum base shear demands on the original and repaired columns for each bridge model under the selected GM records are summarized in Figure 16a; and the maximum base shear D/C ratios were calculated by dividing the capacity measured in the experiment and are shown in Figure 16b. The maximum base shear demands on the original and repaired columns both occurred in the models with two original and two repaired columns, and the demands were approximately 90% of the lateral strength capacity of the columns. In summary, the maximum base shear demands on all the original and repaired columns were less than the corresponding lateral strength capacities under the 40 GM records selected based on the target design spectrum.

The average base shear demand for the original and repaired columns in each bridge model is shown with the standard deviation in Figure 17a. The average base shear demand value for each bridge model was calculated by averaging the base shear demands from 40 selected GM records, maintaining the distinction between original and repaired columns. As shown in Figure 17a, the columns in the model with only original columns (Orig.) experienced the highest average base shear demand. The existence of repaired

columns decreased the average base shear demand on the original columns as shown in models R-1, R-12, R-13, R-14, and R-123. The average base shear demand on the repaired columns was larger in models including both original and repaired columns than that in the model with only repaired columns (R-1234). The ratios of average base shear demand to capacity (D/C) and the standard deviations are shown in Figure 17b. As shown in this figure, the highest average base shear D/C ratio (approximately 0.48) for the original columns was in the model with only original columns (Orig.). The existence of repaired columns reduced the average base shear D/C ratio for the original columns. The lowest D/C ratio (approximately 0.20) for the repaired columns was in the model with only repaired columns (R-1234).

6. CONCLUSIONS

To evaluate the influence of RC column repair on the post-repair response of bridge system and to assess the effectiveness of a developed rapid repair method, the response of a prototype bridge structure was analyzed under dynamic earthquake loadings with consideration of varied numbers and locations of columns repaired with the proposed method. Both repaired and original column models were developed in OpenSees and validated against experimental data. The original column was modeled with beam-column elements with fiber section and nonlinear springs incorporating effects of shear deformation and strain penetration. A new technique was developed to model the repaired column, considering the variation of cross-sectional properties along the length of the column depending on the varied damage and repair conditions. The developed column models were validated against corresponding measured data by pushover and cyclic analysis. The response of a prototype three-span RC bridge model that incorporated the proposed column model was analyzed employing 40 GM records, which were selected and scaled according to the target design response spectrum. Based on the study presented in this paper, the following conclusions can be drawn.

1. The response of the original column can be predicted by conventional modeling methods with negligible discrepancy; the new technique developed to model the repaired column can reasonably predict the performance of the repaired column;

2. The calculated drift ratio demand on the columns of the bridge models with repaired columns was larger than that of the bridge model with only original columns, however the increasing number of repaired columns did not strictly correlate with increasing drift ratio demand. The drift ratio demands on the columns in the seven bridge models under the GM records selected and scaled based on the target design spectrum were less than the drift ratio capacities of the original and repaired columns;

3. The base shear demands on the columns in the seven bridge models under the GM records selected and scaled based on the target design spectrum were less than the lateral strength capacities of the original and repaired columns;

4. Though the repair method was not able to restore the base shear and drift capacities to the original condition for columns with fractured longitudinal bars near the base, the bridge models with one or more of the repaired columns were found to be capable of resisting the base shear and drift demand by the 40 GM records selected and scaled according to the target design spectrum;

5. Based on the above remarks, it can be concluded that the developed rapid repair method was effective for repairing the damaged column with fractured bars in the prototype bridge selected in this paper. However, further research is in need for the applicability of this repair method to damaged columns in other types of bridge structures with different configurations.

7. ACKNOWLEDGMENTS

The authors would like to express their appreciation to the University of Missouri Research Board and National University Transportation Center (NUTC) at Missouri S&T (Grant No. DTRT06-G-0014) for their financial support for this study.

REFERENCES

1. Rodriguez M, Park R. Seismic load tests on reinforced concrete columns strengthening by jacketing. *ACI Structural Journal* 1994; **91**(2): 150-159.

2. Saiidi M, Wehbe N, Sanders D, Caywood C. Shear retrofit of flared RC bridge columns subjected to earthquake. *Journal of Bridge Engineering* ASCE 2001; **6**(3): 189-197.
3. Seible F, Priestley MJN, Hegemier G, Innamorate D. Seismic retrofit of RC columns with continuous carbon fiber jackets. *Journal of Composites for Construction*, ASCE 1997; **1**(2): 52-62.
4. French CW, Thorp GA, Tsai WJ. Epoxy repair techniques for moderate earthquake damage. *ACI Structural Journal* 1990; **87**(4): 416-424.
5. Lehman DE, Gookin SE, Nacamuli AM, Moehle JP. Repair of earthquake-damaged bridge columns. *ACI Structural Journal* 2001; **98**(2): 233-242.
6. Fukuyama K, Higashibata Y, Miyauchi Y. Studies on repair and strengthening methods of damaged reinforced concrete columns. *Cement & Concrete Composites* 2000; **22**: 81-88.
7. Vosooghi A, Saiidi MS. Rapid repair of high-shear earthquake-damaged RC bridge columns. *Proceedings of the 25th US-Japan Bridge Engineering Workshop* 2009; Tsukuba, Japan, Session 7, October.
8. Xiao Y, Ma R. Seismic retrofit of RC circular columns using prefabricated composite jacketing. *Journal of Structural Engineering* 1997; **123**(10): 1357-1364.
9. Shao Y, Aval S, Mirmiran A. Fiber-element model for cyclic analysis of concrete-filled fiber reinforced polymer tubes. *Journal of Structural Engineering* 2005; **131**(2): 292-303.
10. Zhu Z, Ahmad I, Mirmiran A. Fiber element modeling for seismic performance of bridge columns made of concrete-filled FRP tubes. *Engineering Structures* 2006; **28**(14): 2023-2035.
11. He R, Sneed LH, Belarbi A. Rapid repair of severely damaged RC columns with different damage conditions – an experimental study. *International Journal of Concrete Structures and Materials* 2013a; **7**(1): 35-50.
12. He R, Grelle S, Sneed LH, Belarbi A. Rapid repair of a severely damaged RC column having fractured bars using externally bonded CFRP. *Journal of Composite Structures* 2013b; **101**: 225-242.

13. He R, Sneed LH, Belarbi A. Torsional repair of severely damaged column using carbon fiber-reinforced polymer. *ACI Structural Journal* 2014; **111**, 12 pp. DOI: 10.14359.51686627.
14. Prakash SS, Li Q, Belarbi A. Behavior of circular and square reinforced concrete bridge columns under combined loading including torsion. *ACI Structural Journal* 2012; **109**(3): 317-327.
15. Mander JB, Priestley MJN, Park R. Theoretical stress-strain model for confined concrete. *Journal of Structural Engineering* 1988; **114**(8): 1804-1826.
16. Kent DC, Park P. Inelastic behavior of reinforced concrete members with cyclic loading. *Bulletin of the New Zealand Society for Earthquake Engineering* 1971; **4**(1): 108-125.
17. Scott BD, Park R, Priestley MJN. Stress-strain behavior of concrete confined by overlapping hoops at low and high strain rates. *ACI Journal Proceedings* 1982; **79**(1): 13-27.
18. Taucer F, Spacone E, Filippou F. A fiber beam-column element for seismic response analysis of reinforced concrete structure. *UCB/EERC-91/17*, Earthquake Engineering Research Center 1991, Berkeley, CA.
19. Paulay T, Priestley, MJN. *Seismic Design of Reinforced Concrete and Masonry Building*. Wiley: New York, 1992.
20. Correal J, Saiidi M, Sanders D, El-Azazy S. Analytical evaluation of bridge columns with double interlocking spirals. *ACI Structural Journal* 2007; **104**(4): 393-401.
21. California Department of Transportation. *Seismic Design Criteria (SDC). Version 1.4* 2006, Sacramento, CA.
22. Park R, Paulay T. *Reinforced Concrete Structures* . Wiley: New York, 1975.
23. Vosooghi A, Saiidi MS. Post-earthquake evaluation and emergency repair of damaged RC bridge columns using CFRP materials. *Center for Civil Engineering Earthquake Research*, Department of Civil and Environmental Engineering, University of Nevada, Reno, Nevada, Report No. CCEER-1-05, September 2010.
24. Zhao J, Sritharan S. Modeling of strain penetration effects in fiber-based analysis of reinforced concrete structures. *ACI Structural Journal* 2007; **104**(2): 133-141.

25. Wehbe IN, Saiidi MS, Sanders DH. Seismic performance of rectangular bridge columns with moderate confinement. *ACI Structural Journal* 1999; **96**(2): 248-259.
26. Priestley MJN, Calvi GM, Kowalsky MJ. *Displacement-Based Seismic Design of Structures*. IUSS PRESS: Pavia, Italy, 2007
27. FHWA. *Seismic Design of Bridges – Design Example No. 4: Three-Span Continuous CIP Concrete Bridge*. FHWA-SA-97-009 1996, Washington, D. C.
28. American Association of State Highway and Transportation Officials, Inc. *Standard Specifications for Highway Bridges, 15th edition 1995*. As amended by the Interim Specifications-Bridges-1993 through 1995.
29. AASHTO . *Standard Specifications for Highway Bridge, 16th edition*. American Association of Highway Transportation Officials 1996, Washington, D.C.
30. American Society of Civil Engineers. *ASCE Standard Minimum Design Loads for Buildings and Other Structures*. ASCE 7-05. American Society of Civil Engineers, 2005.
31. < http://peer.berkeley.edu/peer_ground_motion_database>. [Accessed 02.28.14].

Table 1 Natural frequency of bridge structure models

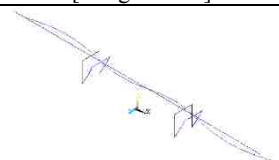
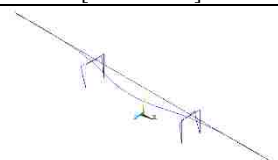
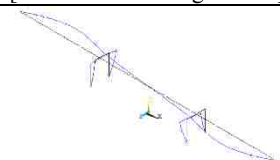
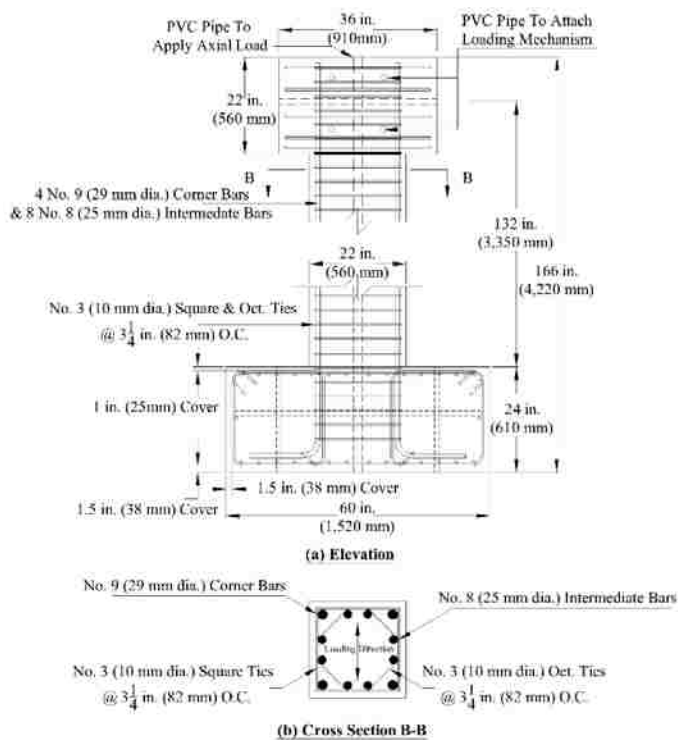
	Bridge Model	Frequencies (Hz)		
		Mode 1 [Longitudinal]	Mode 2 [Transverse]	Mode 3 [Transverse & Longitudinal]
				
Original	Orig.	1.206	14.406	29.647
Repaired	R-1	0.704	14.387	29.641
	R-12	0.636	13.332	27.508
	R-13	0.662	14.386	29.640
	R-14	0.662	14.386	29.640
	R-123	0.616	14.384	29.640
	R-1234	0.568	14.383	29.640

Table 2 Selected earthquake ground motion records

(Source: PEER ground motion database)

Earthquake set	Record No. ^a	Event	Year	Station	Mag	R _{rup} ^b (km)	PGA ^c (g)	PGA/PGV
1	1	Northridge-01	1994	LA - Wadsworth VA Hospital North	6.69	23.6	0.2638	0.00846
	2						0.2496	0.01055
2	3	Northridge-01	1994	Playa Del Rey - Saran	6.69	24.4	0.1559	0.00722
	4						0.1518	0.00698
3	5	Imperial Valley-06	1979	Cerro Prieto	6.53	15.2	0.1746	0.00835
	6						0.1950	0.01502
4	7	Imperial Valley-06	1979	Delta	6.53	22.0	0.1366	0.00922
	8						0.1809	0.01158
5	9	Imperial Valley-06	1979	El Centro Array #12	6.53	17.9	0.1274	0.00523
	10						0.1598	0.00784
6	11	Imperial Valley-06	1979	El Centro Array #13	6.53	22.0	0.2082	0.01034
	12						0.1766	0.00772
7	13	Irpinia- Italy-01	1980	Bisaccia	6.90	21.3	0.1901	0.00685
	14						0.0958	0.00391
8	15	San Fernando	1971	LA - Hollywood Stor FF	6.61	22.8	0.1751	0.00949
	16						0.2232	0.01157
9	17	Superstition Hills-02	1987	El Centro Imp. Co. Cent	6.54	18.2	0.1870	0.00594
	18						0.1353	0.00618
10	19	Superstition Hills-02	1987	Kornbloom Road (temp)	6.54	18.5	0.1572	0.00742
	20						0.2052	0.00417
11	21	Superstition Hills-02	1987	Wildlife Liquef. Array	6.54	23.9	0.1322	0.00758
	22						0.1184	0.00653
12	23	Spitak- Armenia	1988	Gukasian	6.77	24.0	0.2672	0.01054
	24						0.2274	0.00919
13	25	Loma Prieta	1989	Agnews State Hospital	6.93	24.6	0.1652	0.00642
	26						0.1379	0.00808
14	27	Loma Prieta	1989	Coyote Lake Dam (Downst)	6.93	20.8	0.2079	0.01549
	28						0.2412	0.00819
15	29	Loma Prieta	1989	Coyote Lake Dam (SW Abut)	6.93	20.3	0.1703	0.00995
	30						0.4219	0.01085
16	31	Loma Prieta	1989	Hollister - South & Pine	6.93	27.9	0.1456	0.00478
	32						0.1620	0.0073
17	33	Loma Prieta	1989	Hollister Diff. Array	6.93	24.8	0.1744	0.00595
	34						0.1812	0.00762
18	35	Loma Prieta	1989	Palo Alto - 1900 Embarc.	6.93	30.8	0.1751	0.00598
	36						0.1526	0.00692
19	37	Loma Prieta	1989	Palo Alto - SLAC Lab	6.93	30.9	0.2192	0.00581
	38						0.1290	0.0092
20	39	Loma Prieta	1989	Sunnyvale - Colton Ave.	6.93	24.2	0.148	0.00428
	40						0.1274	0.00796

^a Both earthquake records in the two orthogonal directions (FN & FP) are used in this study.^b Closest distance to rupture plane^c The peak ground acceleration was scaled by the modified scale factor discussed in the text



Cross-Section	22 in. × 22 in. (560 mm × 560 mm)
Height	132 in. (3350 mm)
Longitudinal Reinforcing Steel Bars	4 No. 9 (29 mm dia.) & 8 No. 8 (25 mm dia.) ($\rho=2.13\%$) $f_y=76 \text{ ksi}$ (524 MPa) (No. 8) $f_y=67 \text{ ksi}$ (462 MPa) (No. 9)
Transverse Reinforcing Steel Bars	No. 3 (10 mm dia.) @ 3.25 in. (80 mm) ($\rho_t=1.32\%$) $f_y=74 \text{ ksi}$ (510 MPa)
Concrete	$f'_c=5 \text{ ksi}$ (34.5 MPa)

Fig. 1. Geometry and reinforcement details of original column

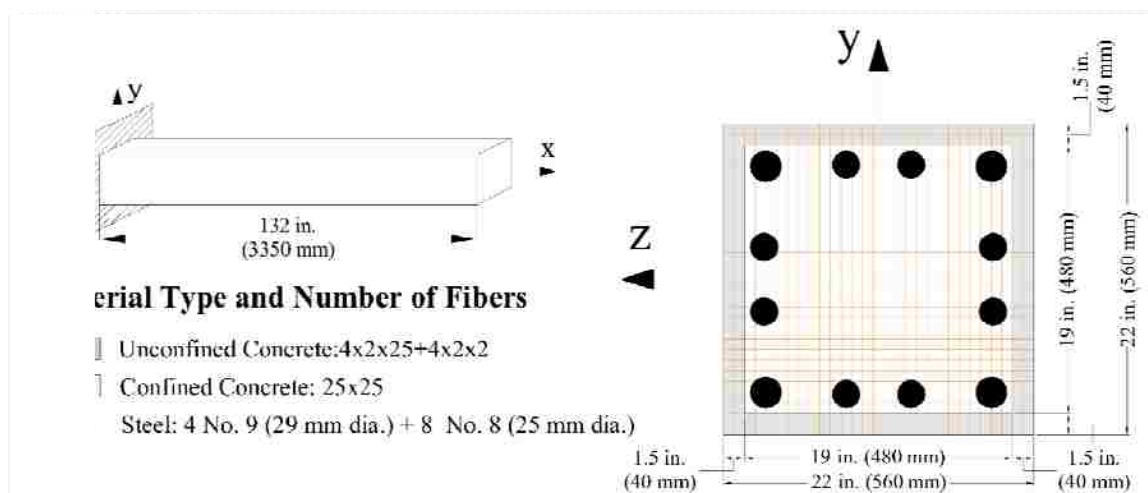


Fig. 2. Fiber discretization of the cross-section

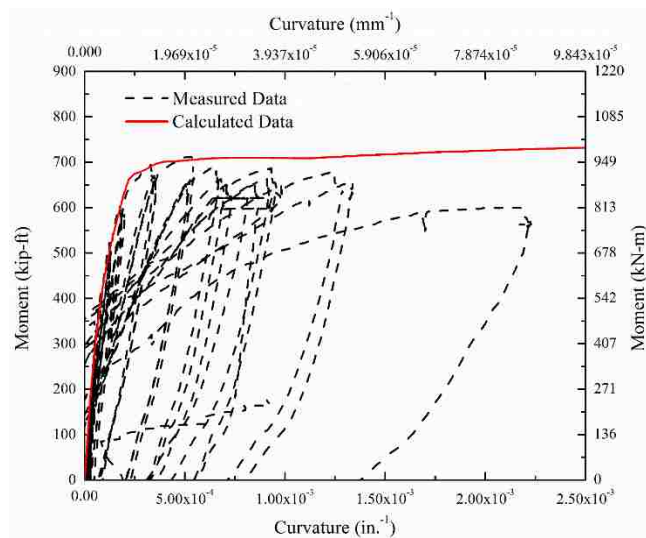


Fig. 3. Comparison of measured and calculated moment-curvature relationships for original column

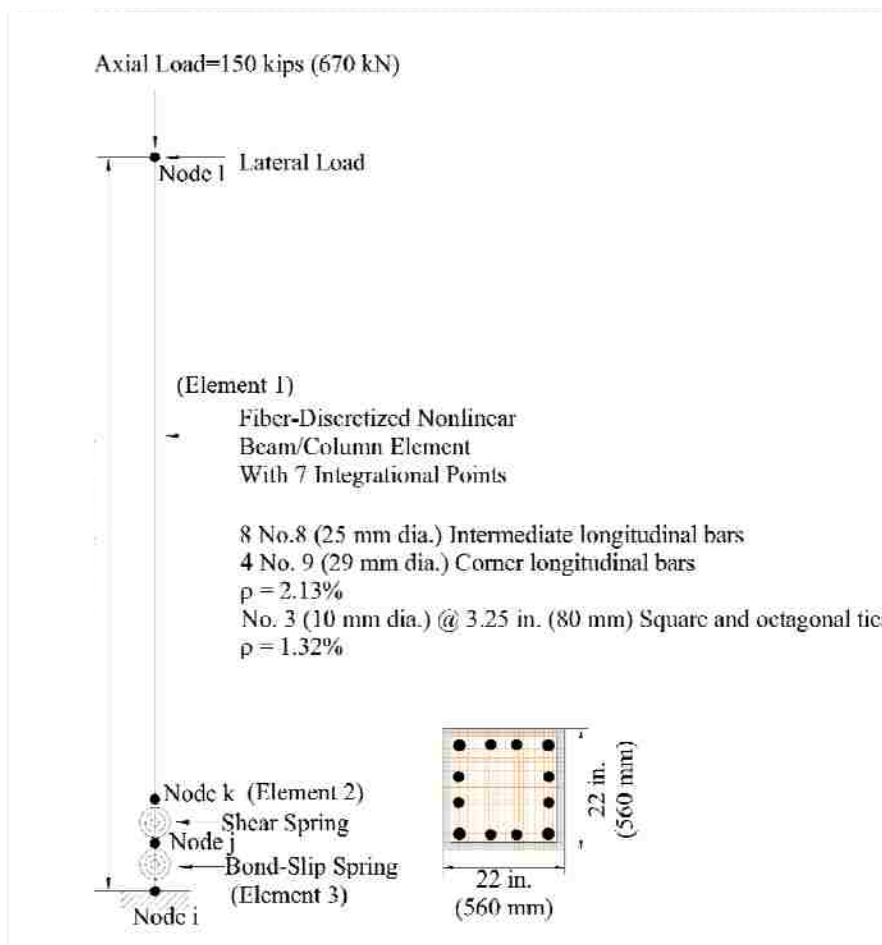
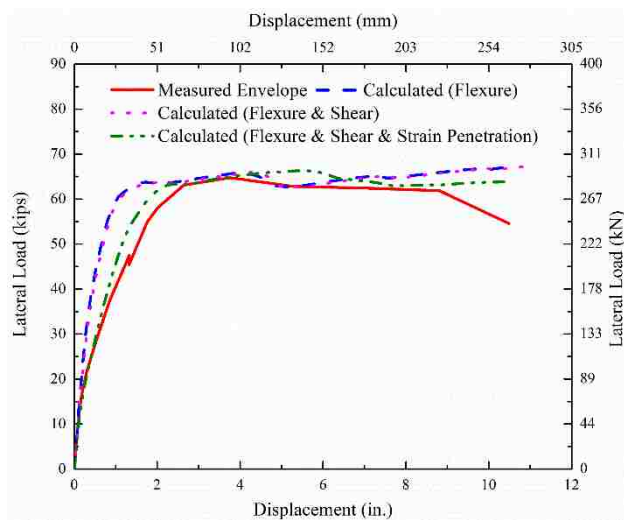
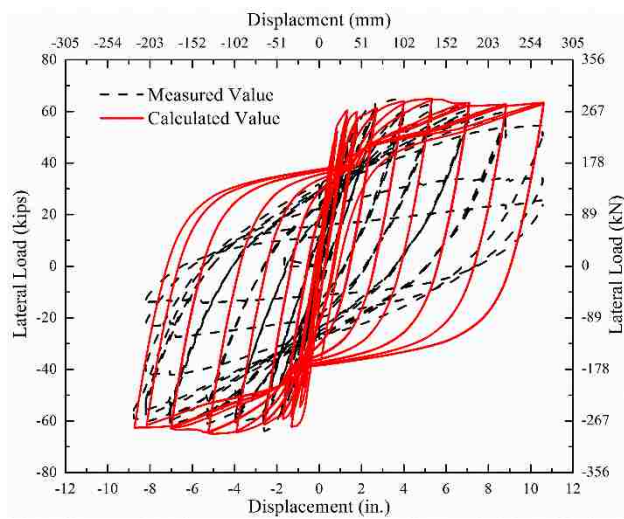


Fig. 4. Numerical model for original column

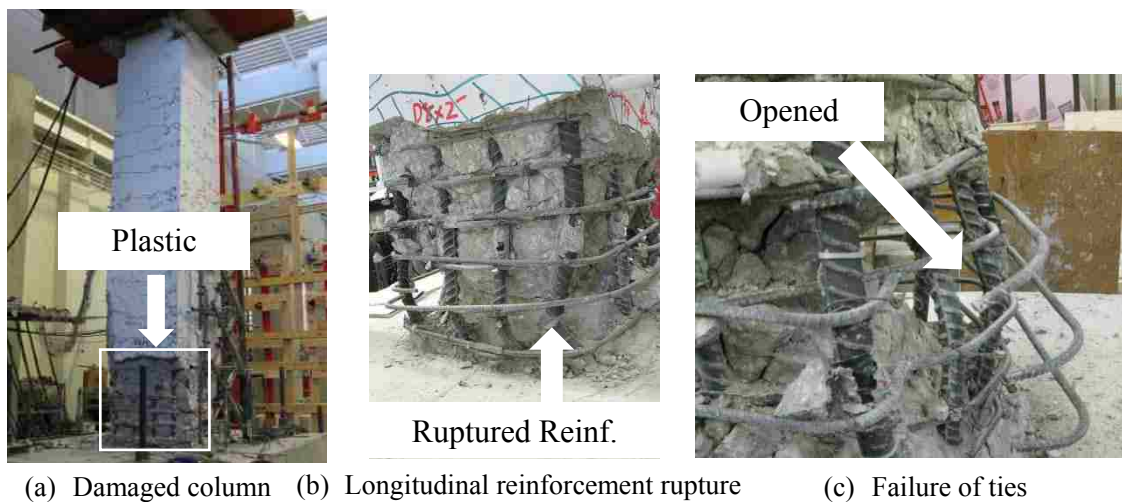


(a) Pushover analysis

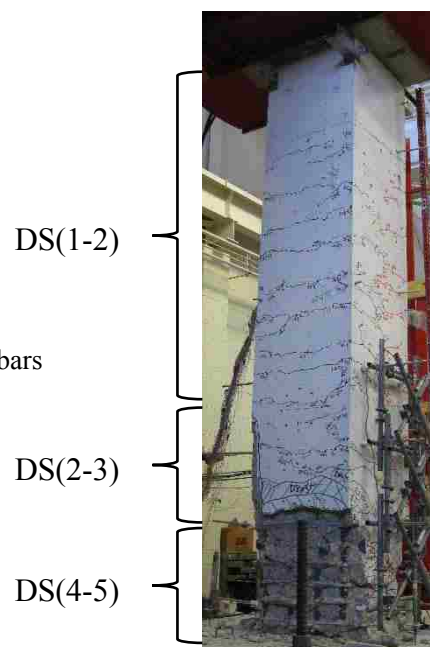


(b) Hysteresis analysis

Fig. 5. Comparison of the measured and calculated response for original column. (a) Pushover analysis; (b) Hysteresis analysis



- DS1: Flexural cracks
- DS2: First spalling and shear cracks
- DS3: Extensive cracks and spalling
- DS4: Visible lateral and longitudinal bars
- DS5: Imminent failure



(d) Determination of damage condition prior to

Fig. 6. Damage to original column prior to repair

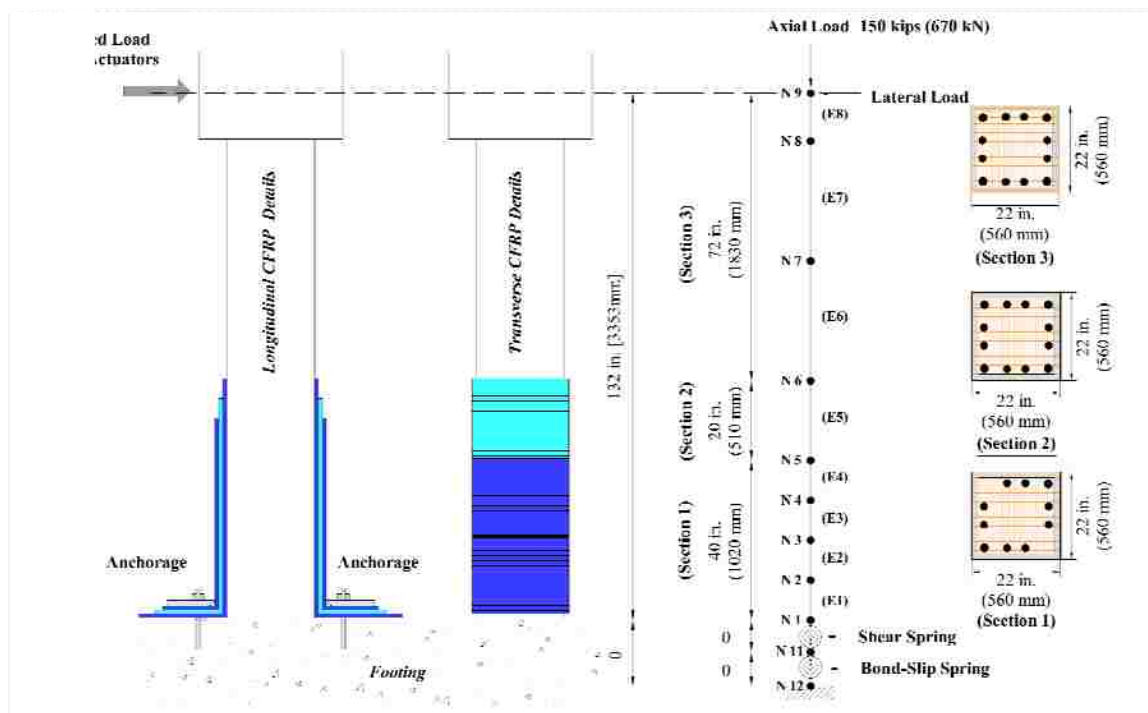
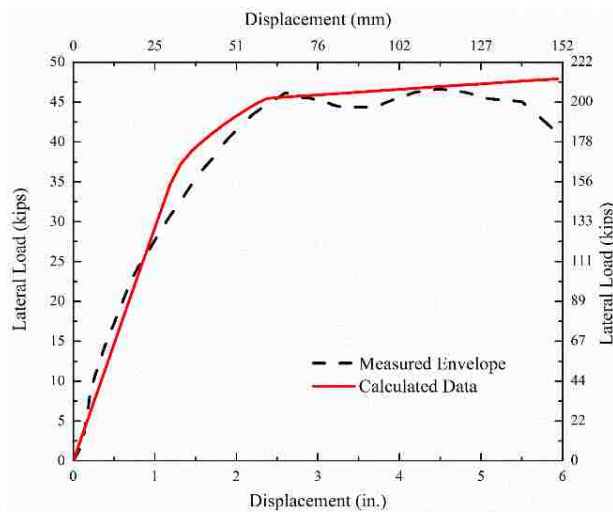
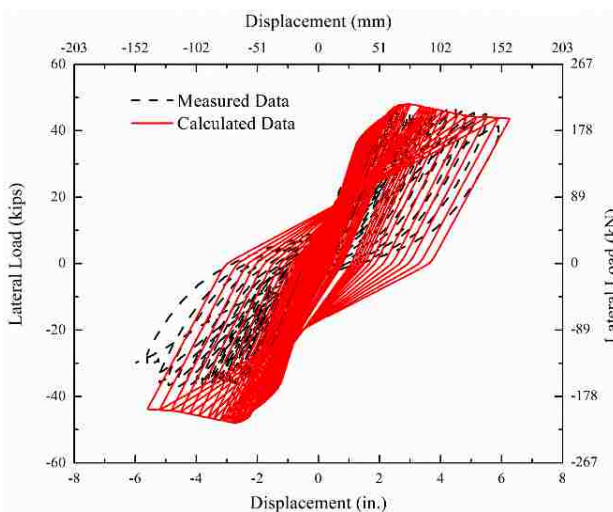


Fig. 7. Numerical model for repaired column



(a) Pushover analysis



(b) Hysteresis analysis

Fig. 8. Comparison of the measured and calculated response for repaired column

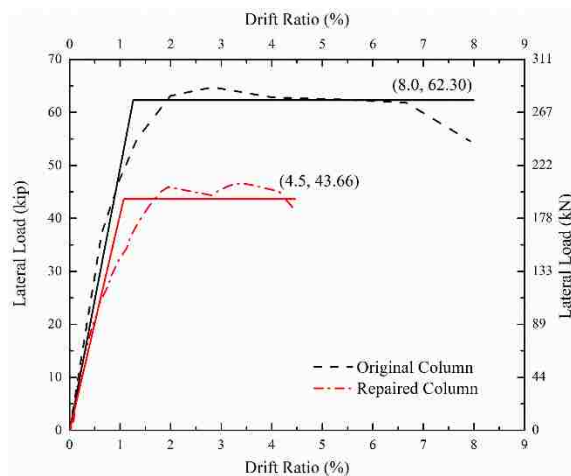


Fig. 9. Idealized load-displacement envelope for original and repaired columns

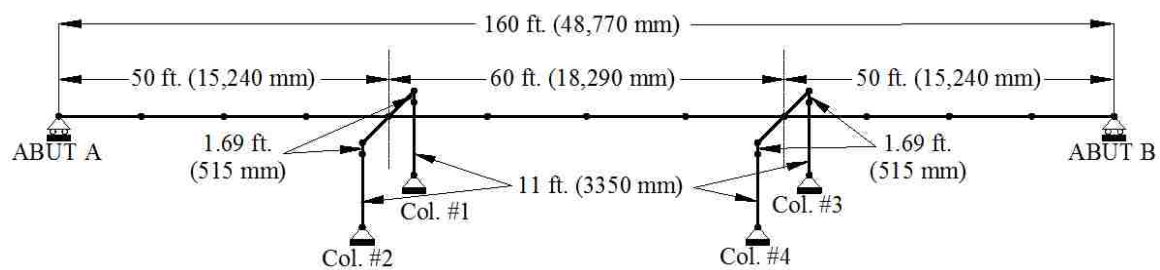


Fig. 10. Numerical model of bridge structures

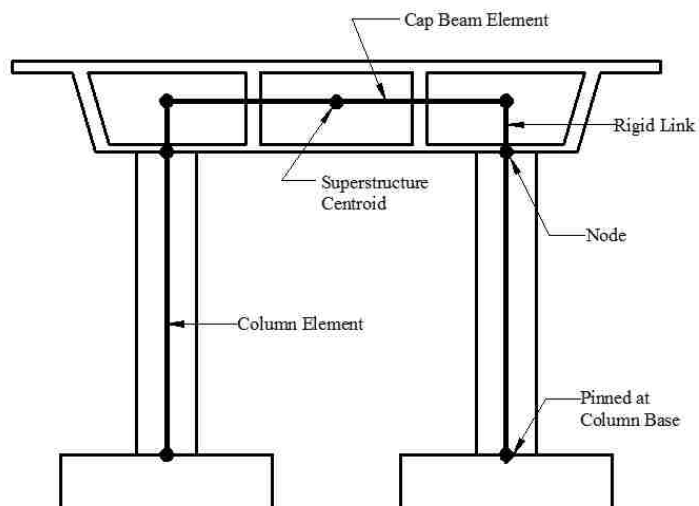


Fig. 11. Details of bent elements

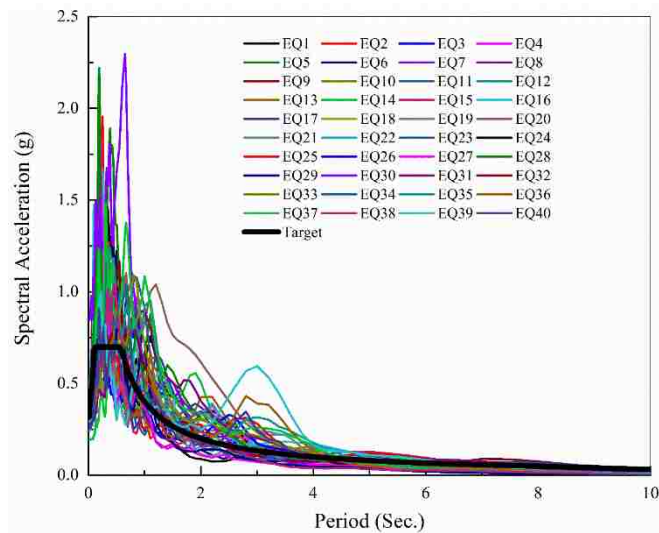


Fig. 12. Spectral acceleration for the selected GM records

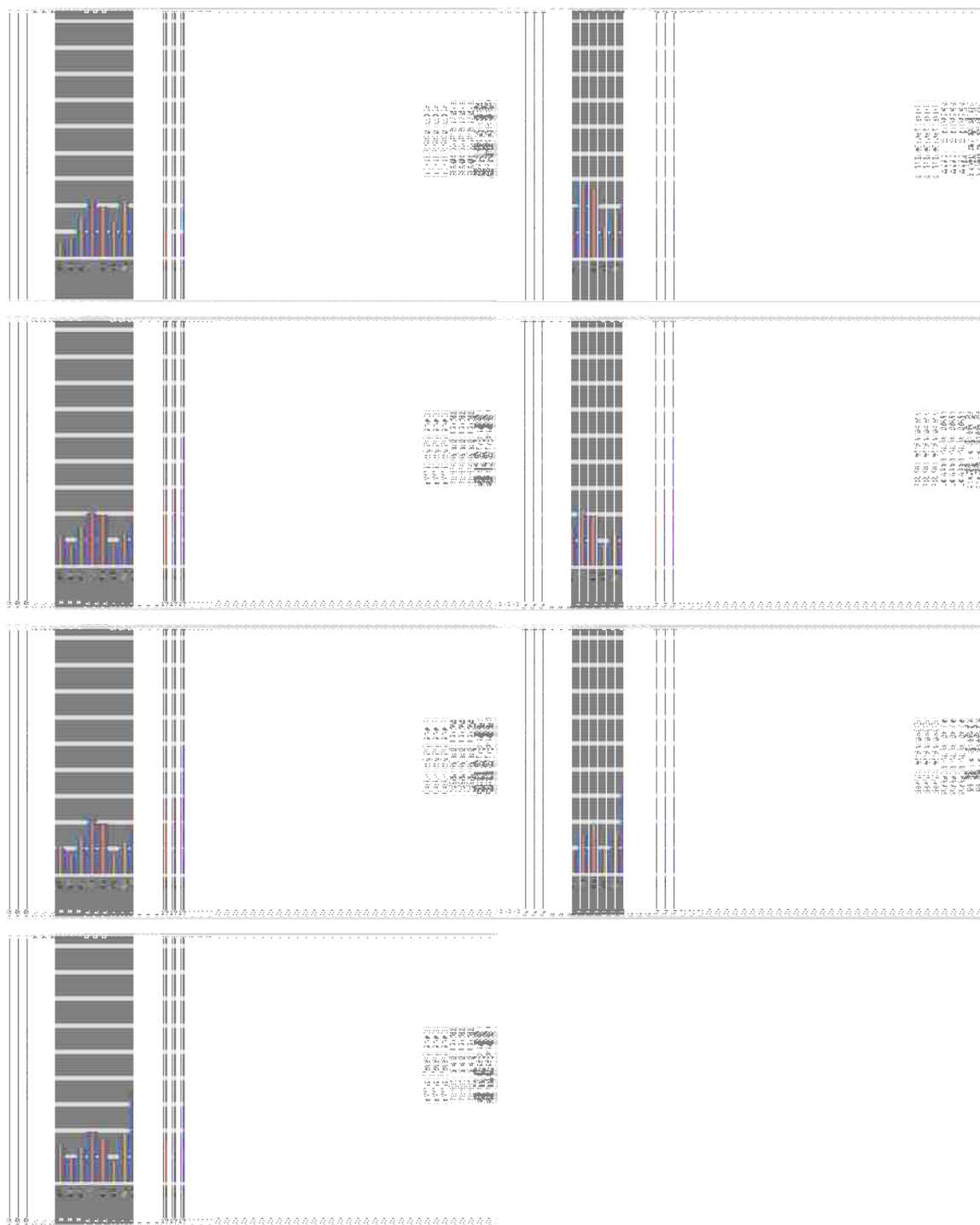


Fig. 13. Drift ratio demand of columns under selected earthquake records for each bridge model

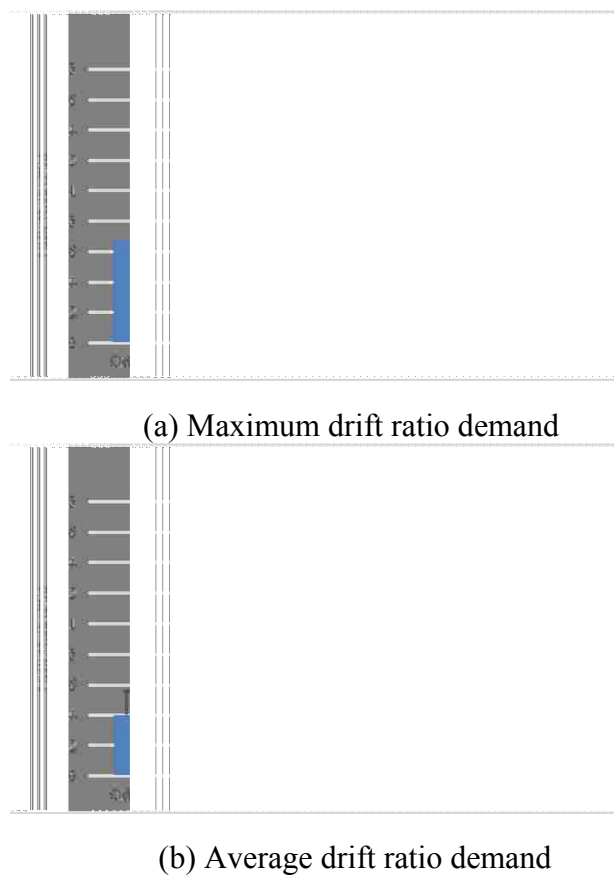
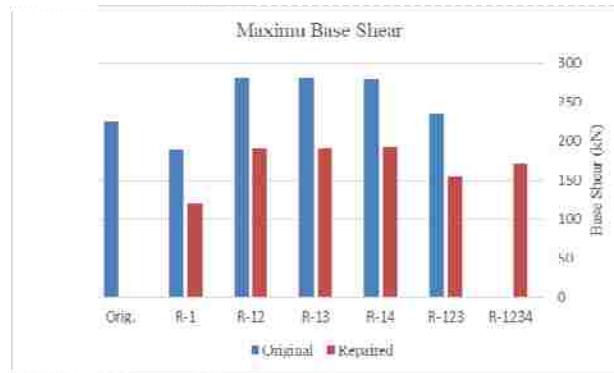
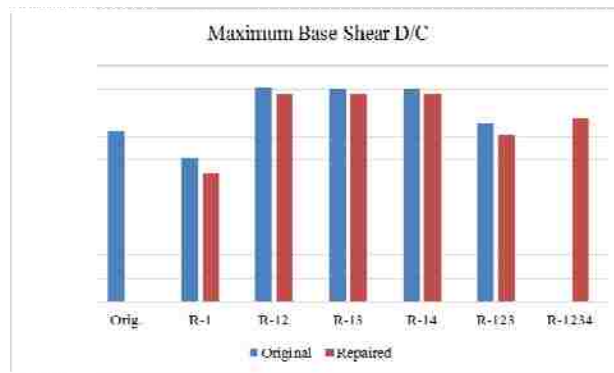


Fig. 15. Summary of drift ratio demand of columns under the selected earthquake records for each bridge model

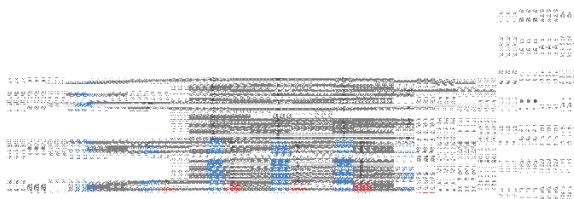


(a) Maximum base shear

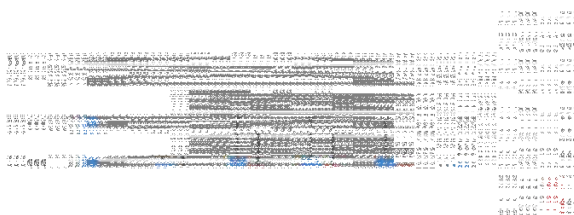


(b) Maximum base shear relative to

Fig. 16. Summary of maximum base shear demand of columns under selected earthquakes for each bridge model



(a) Average base shear demand



(b) Average base shear demand relative to capacity

Fig. 17. Average base shear demand of columns under selected earthquake records for each bridge model

SECTION

2. SUMMARY, CONCLUSIONS, AND RECOMMENDATIONS

2.1. SUMMARY OF RESEARCH WORK

The purpose of this research was to develop an effective and rapid repair technique using externally bonded CFRP composites for RC bridge columns severely damaged under combined loading effects including torsion. Both experimental and analytical studies were included in this study.

The experimental study was conducted on five half-scale square RC bridge columns that had been tested to failure under combined flexure, shear, torsion, and axial loads in previous tests (Prakash et al. 2012). The previous study evaluated the seismic performance of square RC bridge columns under combined loading effects including torsion. Because the study was focused on the interaction between bending and torque, the primary test variable was the torque-to-flexural moment ratio (T/M). All five columns were designed with the same geometric and material properties as discussed in the collected papers in this dissertation. After the original test, different damage conditions were observed to the columns due to the varied combined cyclic loading effects (T/M). Damage included cover concrete cracking and spalling, core concrete crushing, and reinforcing bar yielding, buckling, and rupturing in some of the specimens. The damage region extended farther along the column length, and the plastic hinge shifted towards the column mid-height with increasing torsional moment-to-flexural moment ratio (T/M).

Considering the short timeframe for the rapid repair, the selected repair materials were characterized by their ease of installation and compatibility and capability of achieving their required strengths within the timeframe. A quick set repair mortar and a unidirectional CFRP strengthening system were utilized in this study. The quick set mortar was used to repair the damaged concrete, while the CFRP strengthening system was used to rehabilitate the capacity decay due to material deterioration during the original tests. The repair mortar was a shrinkage-compensating micro concrete provided by BASF Company, which has characteristics including high bond strength, high early strength, and self-compacting properties. The CFRP strengthening system was comprised

of unidirectional carbon fiber sheets, MBrace primer, putty, and saturant provided by BASF Company. The properties of both the CFRP strengthening system and repair mortar provided by the manufacturer are presented in Appendix B. In addition, the compressive strength of the repair mortar was monitored by casting 2 in. (50 mm) cube specimens according to ASTM C109-11. The strength of original concrete and the repair mortar on the test day is given in Tables B.1 and B.2. Bond between the substrate and the CFRP is a concern in this application; thus, testing of the CFRP-to-concrete bond was performed in accordance with ASTM D7234, and the results are summarized in Table B.3.

The required number of layers of CFRP was designed with the objective of restoring the flexural, shear and torsional strength to that of the original condition while maintaining as much ductility and stiffness as possible. Two regions were distinguished in design, which included the region that included the plastic hinge with cover concrete spalling, and a secondary region with the same height as the plastic hinge region. The latter region was repaired using half the required thickness of CFRP sheets as the former region in order to prevent plastic hinging directly above the primary plastic hinge. The lengths of these two regions were adjusted considering the width of the CFRP sheets (20 in. [508 mm] wide). Considering that the repair was intended to be rapid and temporary, portions of the column with slight concrete cracks were left unrepaired to maximize the time efficiency. The design for each of the repaired columns was modified based on the performance of the repaired columns that previously had been tested.

Each of the columns was repaired over a three-day period. Without any treatment to ruptured and/or buckled longitudinal reinforcing bars, quickset repair mortar was cast after loose concrete and opened stirrups were removed. Longitudinal and transverse CFRP sheets were externally bonded to the prepared surfaces after the mortar was cured for at least twelve hours. The repaired columns were then tested three days after the initiation of the repair work. The details of the experimental study is discussed in Appendix A.

Measured data were analyzed to investigate the performance of the repaired columns compared to the corresponding original column responses. The repair method was proved effective in repairing damaged columns without fractured longitudinal bars,

though factors such as bending-torsion interaction and failure mode played a role in the level of restoration. However, the method was only partially successful in repairing a column with buckled and fractured longitudinal bars located near the base of the column, in which case a substantial anchorage system was required to transfer the force in the externally bonded CFRP from the column to the footing. The post-repair response of an RC bridge structure that included the partially restored column was analyzed under design earthquake loadings. First, models of the undamaged (original) and repaired columns were developed and validated with the experimental results. Then, a prototype bridge structure was analyzed with including the developed column models under 40 ground motion records selected according to the design response spectrum. Seven models of the bridge structure with varied numbers and locations of the partially restored column were analyzed and compared with each other. Based on the drift ratio demand and base shear demand on the columns of the bridge structure with repaired columns in different configurations, the repair was determined to be satisfactory.

2.2. CONCLUSIONS

This section summarizes the conclusions from both the experimental and analytical studies of the rapid repair. With regard to the experimental work, the following conclusions are presented:

- ◆ Overall, the developed repair procedure in this study was practical and achievable as a rapid emergency repair;
- ◆ The repair method was effective in restoring the bending and/or torsional strength, stiffness, and ductility for the columns without fractured longitudinal bars, though factors such as bending-torque interaction, failure mode, and repair detailing played a role in the level of strength restored;
- ◆ The method utilized in this study was found to be partially successful for columns with fractured longitudinal bars (and the critical section) located near the base due to the premature failure of the strengthening system; this is due to the fact that the fractured bars were not repaired, and as a result, large force demand is required of the anchorage system to transfer the force in the external CFRP strengthening system to the footing;

- ◆ A reduction in initial stiffness after repair was observed due to the previously tested reinforcing steel and softened concrete in the unrepaired portion of the column, however, the service stiffness was restored or enhanced after repair;
- ◆ Use of longitudinal CFRP around the entire perimeter of the column improved the performance of the repaired column by mitigating cracking and improving the flexural strength of the repaired column;
- ◆ The failure mode of the repaired column under combined axial and torsional loading (no bending) was rupture of the CFRP system, which occurred at an average stress level less than the ultimate strength of the CFRP due to stress concentration. The CFRP functioned as external reinforcement and also confined the RC column and inhibited the propagation of torsional concrete cracking. Consequently, the maximum torsional moment was increased compared to the original column;
- ◆ The rotational deformation capacity of the repaired RC column under combined axial and torsional loading was enhanced compared to that of the original column. Additionally, the rotational ductility was increased. The post-peak response was initially more gradual compared to the immediate steep post-peak response of the original column due to the confinement provided by the CFRP. This behavior is beneficial for seismic repair in terms of better energy absorption capacity;
- ◆ Comparison of the torsional stiffness attenuation of the original and torsional repaired columns indicates that the CFRP system helped provide confinement and restrain torsional crack development so that limited torsional stiffness can be maintained in the post-peak state;
- ◆ Strains measured in the CFRP on the surface of the repaired column under combined axial and torsional loading confirmed that transverse and longitudinal contributed to the resistance of the repaired column. The transverse sheets, however, were more efficient than the longitudinal sheets;
- ◆ Analysis of strains measured on CFRP surface of the repaired column under combined axial and torsional loading confirmed that the repair design assumption that the RC column can provide approximately 50% of the

original torsional capacity was reasonable. Additionally, the value of the effective strain determined by NCHRP Report 655 was reasonable in designing the transverse CFRP for this column.

Based on the analytical study, the following conclusions are presented:

- ◆ The response of the original column can be predicted by conventional modeling methods with negligible discrepancy; the new technique developed to model the repaired column can reasonably predict the response of the repaired column;
- ◆ The calculated drift ratio demand on the columns of the bridge models with repaired columns was larger than that of the bridge model with only original columns; however the increasing number of repaired columns did not strictly correlate with increasing drift ratio demand. The drift ratio demands on the columns in the seven bridge models under the ground motion records selected and scaled based on the target design spectrum were less than the drift ratio capacities of the original and repaired columns;
- ◆ The base shear demands on the columns in the seven bridge models under the ground motion records selected and scaled based on the target design spectrum were less than the lateral response capacities of the original and repaired columns;
- ◆ Though the repair method was not able to restore the base shear and drift capacities to the original condition for columns with buckled and fractured longitudinal bars near the base, the bridge models with one or more of the repaired columns were found to be capable of resisting the base shear and drift demand by the 40 ground motion records selected according to the target design spectrum.

Finally, based on the concluding remarks above, it can be concluded that the developed rapid repair method was effective as an emergency repair for the damaged column without and with fractured longitudinal bars.

2.3. RECOMMENDATIONS

Based on the objective and scope of this study, the following aspects are recommended for future research:

- ◆ Develop a rapid repair technique that can fully restore the long-term strength and deformation capacity of damaged RC columns with fractured bars;
- ◆ Assess the effectiveness of the developed repair method on damaged columns with design parameters different from those of the columns in this study, such as the shape of cross section, aspect ratio, and the ratios of reinforcement;
- ◆ Develop models that can consider the torsional effect in addition to considering the axial, bending, and shear effects as proposed in this study;
- ◆ Optimize the repair design with proposed models to decrease the required layers of CFRP in consideration of the interaction between bending, shear, and torsional effects;
- ◆ Assess the effectiveness of the developed repair method on different kinds of bridge system;
- ◆ Evaluate the capacity of the bridge system by using incremental dynamic analysis (IDA).

APPENDIX A
EXPERIMENTAL STUDY

The description of the experimental study included in the papers in this dissertation was abbreviated due to space limitations. In this appendix, the experimental study is discussed in detail, including the repair procedure, arrangement of the instrumentation, and retesting of the repaired columns.

The damaged columns were repaired and retested in the High Bay Structural Engineering Research Laboratory at Missouri S&T. Neglecting an unexpected delay that occurred during the repair of Column 1, the entire repair process involved six steps and took approximately 30 man-hours over 3 days (72 hours). The rapid repair started with removing loose concrete, followed by erecting formwork, and placing repair mortar on the first day. After the mortar set approximately 12 hours through the night, the formwork was removed, and the MBrace® CF 130 Composite Strengthening System was applied on the second day. The repaired columns were instrumented on the third day and retested on the fourth day (fifth day for Column 1). The details of each repair step are discussed in the paragraphs that follow.

Initial Straightening of the Columns - Before the three-day period repair began, the damaged column was straightened to ensure that it was capable of being repaired and retested. Trial and error method was used for the initial straightening, which took a significant amount of time for some of the columns.

There were three main types of initial deformations of the damaged columns: (1) twist about the column longitudinal axis; (2) displacement in the direction parallel and/or perpendicular to the applied load; and (3) displacement and/or twist in different directions along the column. For the displacement in the loading direction and twist about the column longitudinal axis, the two horizontal servo-controlled hydraulic actuators were used to straighten it back to the original position by pulling and/or pushing with the separate actuators. For the deformation perpendicular to the loading direction, the column was pushed or pulled back to the original position by applying a jacking force between the column cap and strong wall using a wood beam or chain as shown in Figure A.1. For the third situation, the deformed column could not be restored to the undeformed position. Columns were pulled and/or pushed in the two directions and straightened as much as

possible. The straightened condition was determined visually, and the goal was to make the column straight enough to apply the formwork for placing the repair mortar.

Removal of Loose Concrete - The repair procedure began with removing loose concrete from the column. The loose concrete was removed with a chisel and continued until light tapping with a small hammer on the chisel could not remove any more concrete. At this time, opened ties/stirrups were removed only if they were in position to interfere with the placement of formwork. Figure A.2 shows the column before and after removal of loose concrete.

After removing the loose concrete, the concrete dust was removed using an industrial vacuum and compressed air. Before placing BASF LA40 Repair Mortar, clean water was sprayed onto the concrete surface to achieve a saturated surface-dry condition as specified in the instructions for application of BASF LA40 Repair Mortar.

Placement of Repair Mortar - After removal of loose concrete and preparation of the substrate for placing the repair mortar, formwork was applied around the column section to be repaired. Depending on the extent of the damage, either custom plywood formwork or standard metal formwork (Figure A.3) was used for placement of the repair mortar.

LA40 Repair Mortar, a pre-extended micro-concrete, was mixed using a hand mixer according to the manufacturer's specifications, and then placed by hand or with the help of crane as shown in Figure A.4. For those columns of which the entire height was repaired, several holes were drilled into the custom plywood formwork, and Plexiglas was added at the hole locations to monitor the flowing of the mortar at top of the column.

In order to minimize the surface moisture content of the concrete, the surface was exposed to air as long as possible prior to CFRP installation. Therefore, the formwork was removed approximately 12 hours after the placement of the last lift of mortar.

Preparation of Concrete Surface - The concrete surface was prepared for application of the CFRP system after removing the formwork. All surfaces of the repair mortar or existing concrete on which the CFRP would be applied were prepared,

including those on the footing to which the longitudinal CFRP would be anchored. The surface was smoothed and corners were ground using a power concrete surface preparation tool as shown in Figure A.5 and a diamond cup wheel. The concrete dust was cleaned by an industrial vacuum and compressed air.

Installation of CFRP Strengthening System - After preparation of the concrete surface and before application of the MBrace® CF 130 Composite Strengthening System, MBrace® Primer and Putty were applied on the concrete surface. The MBrace® Primer was mixed according to the manufacturer's recommendations and was applied on the prepared areas using a 3/8 in. nap roller as shown in Figure A.6a. When the primed surface became tacky, the MBrace® Putty was mixed and applied by drywall taping knives as shown in Figure A.6b. The putty was applied wherever the surface was not flat or smooth enough for the application of CFRP.

Thirty minutes after applying the putty, application of the MBrace® CF 130 Composite Strengthening System began. It was demonstrated by prior experience of the technician that the wet lay-up process is more effective to impregnate the fibers and provide sound bond between CFRP and concrete, so this type of application was preferred when possible.

The longitudinal (vertical) CFRP was installed using a wet lay-up process, in which the fiber sheets were impregnated in a tank with MBrace® Saturant before placed on the concrete surface. In order to make sure that the saturant was applied both on top and beneath of the fiber sheets, the saturant was poured before and after putting the fiber sheet in the tank, and then a grooved aluminum FRP roller was used to further impregnate the fiber.

A dry lay-up process was used for application of the transverse CFRP since an initial attempt to use the wet lay-up process damaged the fibers. In the dry lay-up process, saturant was applied on the concrete surface first, and the fiber sheet was placed next while adding more saturant to the external surface of the sheet. Then the fiber sheet was impregnated in the saturant using a grooved aluminum FRP roller. The applications of the longitudinal and transverse CFRP are shown in Figure A.7.

After installation of the CFRP system, the system was allowed to cure until the start of testing. For the first two columns (Column 1 and Column 2), the temperature in the lab was relatively low; thus, an enclosure constructed using plastic sheets containing a small space heater was provided to facilitate curing as shown in Figure A.8.

For the first three columns (Column 1, Column 2, and Column 3) with small torsional moment-to-bending moment ratio, the damage location was near to the column-footing interface, and thus an anchorage system was needed to anchor the longitudinal CFRP to the footing. This task was the subject of a master's study conducted by a member of the research group, Stephen Grelle. Figure A.9 shows the novel anchorage system designed to anchor the longitudinal CFRP on two faces of the column (Grelle 2010).

Arrangement of Instrumentation - A significant amount of instrumentation was applied to evaluate the behavior of the repaired columns under cyclic loading effects. Load cells and displacement transducers in the horizontal hydraulic actuators measured the applied load and displacement. The applied axial load was measured using a load cell placed between the hydraulic jack and the top of the column. The twist and displacement of the columns at different heights were measured by ten potentiometers. Strain gauges were attached to the surface of the outmost layer of CFRP on the column to measure the longitudinal and transverse strains of the CFRP during testing. Additionally, strain gages were applied to the surface of the novel anchorage system to evaluate the bending of the steel plate. Demountable mechanical strain (DEMEC) gauges were attached to two opposite faces of the column to measure the surface strain of the CFRP system. A direct current variable displacement transducers (DC-LVDT) rosette was installed on one of the four faces. For three of the columns, tilt sensors were used to measure the tilt angles of the column. The general arrangement of the instrumentation is shown in Figure A.10.

Retesting of repaired columns - After three days of repairing the damaged column, testing began on the fourth day. A new system was designed to attach the footing to the strong floor during testing of repaired columns (comparison of the new tie-down system with the original system was shown in Figure 3 of Paper II) because the threads used to

anchor dywidag bars were damaged after the original tests. In the redesigned test setup (as shown in Figure A.11), two wide flange beams combined with two double channel beams were used to fix the test specimens to the strong floor. Similarly to the testing of original columns, hydrostone was placed in the gaps to ensure the uniform contact.

The same loading system was used to apply load to the repaired columns as for original columns. The axial load was applied using a hydraulic jack used to tension seven unbonded high-strength prestressing steel strands. The uniaxial bending-shear, torsion about the longitudinal column axis, and the combined bending-shear-torsion were generated by two horizontal servo-controlled hydraulic actuators. The uniaxial bending-shear was created by applying equal forces/displacements with the two actuators. The pure torque was imposed by applying equal but opposite force/displacement with each actuator. The combined bending-shear-torsion was generated by applying different forces/displacements with each actuator while controlling the ratio of the forces in the two actuators to maintain torsional moment-to-bending moment ratio.

For testing the repaired columns, load control mode was used first and used as far as possible since it could maintain the torsional moment-to-bending moment ratio well. The load was applied at various intervals depending on the performance of the tested column under certain loadings. Displacement control mode was used when the original peak load was reached or the column stiffness significantly decreased.



Figure A.1. Column Straightening



Figure A.2. Before and After Removal of Loose Concrete



(a) Plywood Formwork

(b) Metal Formwork

Figure A.3. Formwork for Placement of Repair Mortar



Figure A.4. Placement of Repair Mortar



(a) Smoothing Concrete Surface



(b) Smoothed Concrete Surface with Corner

Figure A.5. Concrete Surface Smoothing



(a) Application of MBrace® Primer



(b) Application of MBrace® Putty

Figure A.6. Concrete Surface Preparation



(a) Application of Longitudinal CFRP



(b) Application of Transverse CFRP

Figure A.7. Application of MBrace® CFRP System



Figure A.8. Curing of the CFRP System



(a) Temporary Placement of Anchorage Over “Wet” Saturant

(b) Injecting Epoxy Into Anchor Rod Holes



(c) Installed Novel Anchorage System

Figure A.9. Novel Anchorage System (Grelle 2010)

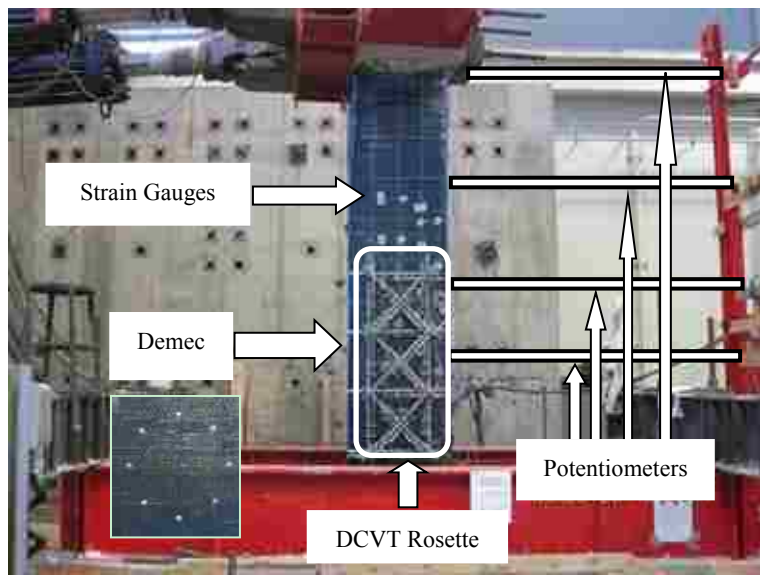


Figure A. 10. Arrangement of Instrumentation

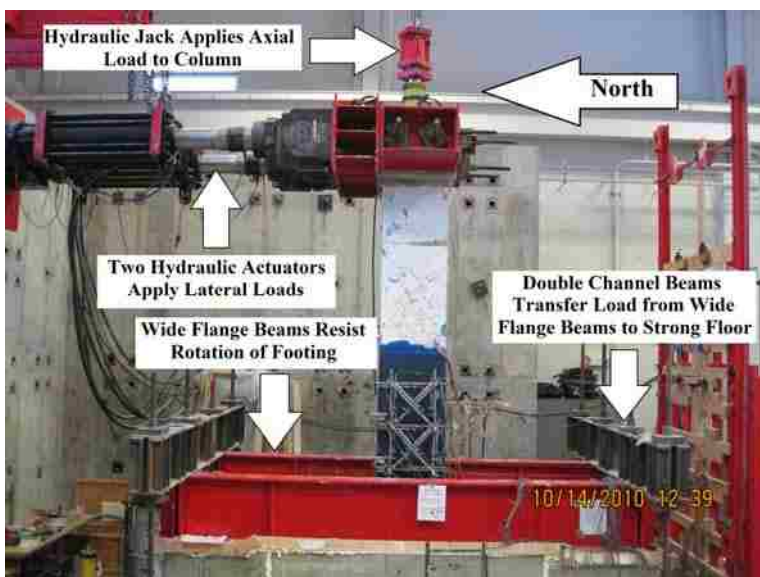


Figure A. 11. Test setup for repaired columns

APPENDIX B
REPAIR MATERIALS

This appendix includes details of the materials used for repair of the columns, which include unidirectional carbon fiber sheets, epoxies used for application of CFRP strengthening system, the repair mortar used to replace the removed loose concrete, and the materials used to fabricate and install the anchorage system that are discussed in detail in a master's thesis (Grelle, 2011).

In order to compensate for the strength decrease due to the damaged reinforcing bars, carbon fiber reinforced polymer (CFRP) was chosen to repair the columns because of its high strength- and stiffness-to-weight ratios and ease of installation compared with other jacket materials. Unidirectional high strength carbon fiber fabric for the MBrace[®] Composite Strengthening System, MBrace[®] CF 130 (as shown in Figure B.1a), was utilized in this study. It is a dry fabric constructed of high strength, aerospace grade carbon fibers. Properties of the MBrace[®] CFRP are shown in the data sheet provided by the manufacturer attached at the end of this appendix.

Three types of two-part epoxies were used to bond the carbon fiber sheets to the concrete substrate. The first was MBrace[®] Primer, which is a low-viscosity epoxy applied directly to the prepared concrete surface to enhance the bond between the CFRP and concrete surface. The second was MBrace[®] Putty, which is a high-viscosity epoxy paste used to level the concrete surface and fill in any voids or defects in the concrete. The third was MBrace[®] Saturant, which is a low-viscosity epoxy used to impregnate and encapsulate fiber sheets on the surface of the concrete member. The information for these epoxies are shown in the data sheets provided by the manufacturer attached in this appendix.

For concrete repair, a pourable and pumpable pre-extended micro concrete LA40 Repair Mortar (as shown in Figure B.1b) was used because of the following reasons: (1) the mortar can achieve a high strength in two to three days after placement; (2) the surface moisture of this mortar would be minimal a short time after placement, which is crucially important for the bond strength between the CFRP and concrete; and (3) the fluidity of the repair mortar can ensure that no voids would be present after placing the repair mortar into the form. The detailed information for this product is shown in the data sheet provided by the manufacturer in this appendix.

The compressive strength of the repair mortar was measured and compared with the original concrete strength on the test day as shown in Tables B.1 and B.2 in this appendix. The strength was determined using 2 in. cube specimens according to ASTM C109-11 (2011). The mortar cube test results for each of the repaired columns are shown in this appendix as well.

As discussed in Paper II, bond between the host concrete and externally applied CFRP is critical for flexural, shear, and torsional strengthening, so bond strength testing of the CFRP-to-concrete bond was performed in accordance with ASTM D7234 (2005) as shown in Figure B.2. The bond strength test results for each repaired column are summarized in Table B.3, and FRP pull-off test results of each repaired column are also provided in this appendix.



Figure B.1. Repair material



Figure B.2. Bond strength test

Table B.1. Summarized compressive strength of original concrete (ASTM C39)

Column	T/M	28 Day Strength (psi)	Test Day Strength (psi)
1	0	5290	5260
2	0.2	5870	5880
3	0.4	6420	5860
4	0.6	5570	5870
5	∞	4760	4730

Table B.2. Summarized compressive strength of repair mortar (ASTM C109)

Column	T/M	Test Day Strength (psi)
1	0	5410
2	0.2	5860
3	0.4	5460
4	0.6	4670
5	∞	4260

Table B.3. Summarized bond strength test results (ASTM C7234)

Column	T/M	Test Location	Average Bond Strength	Pass or fail
1	0	Original concrete, upper column	378 psi	Pass
2	0.2	Original concrete, upper column	225 psi	pass
3	0.4	Original concrete, footing	583 psi	Pass
4	0.6	No test performed	N/A	N/A
5	∞	Cube specimen constructed with repaired mortar	310 psi	Pass

Mortar Cube Test Results

For the Column 1-R:
Cast at 4:00pm 9/13/2020

SET 1: (Test at 9:15am 9/16/2010)

Mortar Cube Test Results on 3rd Day

Mortar Cube Specimens	DIMENSIONS (in.)				LOADS (lbs)	STRENGTH (psi)
	a.	b.	c.	d.		
1	2.023	1.974	1.999	2.015	23610	5886
2	2.069	2.044	2.061	2.034	22440	5329
3	2.001	2.001	2.022	2.031	22665	5589
Average Strength (psi)						5601

SET 2: (Test at 5:30pm 9/17/2010)

Mortar Cube Test Results on Test Day

Mortar Cube Specimens	DIMENSIONS (in.)				LOADS (lbs)	STRENGTH (psi)
	a.	b.	c.	d.		
1	2.053	2.033	2.001	2.003	22635	5533
2	1.997	1.996	2.036	2.036	21840	5372
3	2.041	2.037	1.997	2.001	21735	5331
Average Strength (psi)						5413

SET 3: (Test at 10:00am 10/12/2010)

Mortar Cube Test Results on 28th Day

Mortar Cube Specimens	DIMENSIONS (in.)				LOADS (lbs)	STRENGTH (psi)
	a.	b.	c.	d.		
1	2.062	2.031	2.062	2.016	37455	8976
2	2.094	2.000	2.094	2.031	30855	7308
3	2.031	2.062	2.031	2.062	40395	9645
4	2.031	2.062	2.031	2.062	32025	7646
5	2.000	2.031	2.000	2.031	19830	4881
6	2.062	2.000	2.062	2.000	32040	7767
Average Strength (psi)						7704

Mortar Cube Test Results

For the Column 2-R:

Cast at 6:00pm (around) 10/11/2010

SET 1: (Test at 2:30pm 10/14/2010)

Mortar Cube Test Results on 3rd Day

Mortar Cube Specimens	DIMENSIONS (in.)			LOADS (lbs)	STRENGTH (psi)
	L	W	H		
1	2.037	2.000	1.998	27915	6852
2	2.011	2.013	2.024	17000	4199
3	2.024	2.065	2.025	25965	6206
4	1.910	2.000	2.010	22920	6164
Average Strength (psi)					5855

SET 2: (Test at 1:30pm 10/18/2010)

Mortar Cube Test Results on 7th Day

Mortar Cube Specimens	DIMENSIONS (in.)			LOADS (lbs)	STRENGTH (psi)
	L	W	H		
1	2.011	2.043	2.031	31665	7708
2	1.921	2.008	2.005	25725	6670
3	2.001	2.017	2.002	25380	6288
Average Strength (psi)					6889

SET 3: (Test at 3:00pm 11/9/2010)

Mortar Cube Test Results on 29th Day

Mortar Cube Specimens	DIMENSIONS (in.)			LOADS (lbs)	STRENGTH (psi)
	L	W	H		
1	1.963	1.987	2.003	29490	7561
2	2.001	2.035	2.016	30945	7599
3	2.035	2.008	2.023	28515	6978
Average Strength (psi)					7379

Mortar Cube Test Results

For the Column 3-R:
Cast at 4:00pm 11/8/2020

SET 1: (Test at 9:15am 11/11/2010)

Mortar Cube Test Results on 3rd Day

Mortar Cube Specimens	DIMENSIONS (in.)			LOADS (lbs)	STRENGTH (psi)
	l	w	h		
1	2.004	1.995	2.031	23820	5958
2	2.001	2.000	1.997	20280	5067
3	1.990	1.997	2.025	21225	5341
Average Strength (psi)					5455

SET 2: (Test at 12/20/2010)

Mortar Cube Test Results on 42th Day

Mortar Cube Specimens	DIMENSIONS (in.)				LOADS (lbs)	STRENGTH (psi)
	a.	b.	c.	d.		
1	2	2	2	2	23025	5756
2	2+1/32	1+15/16	2+1/32	1+29/32	22860	5715
3	2	1+63/64	1+63/64	1+63/64	26130	6532
Average Strength (psi)					6001	

Mortar Cube Test Results

For the Column 4-R:

Cast at 2:00pm-5:00pm 12/13/2010

SET 1: (Test at 1:30pm 12/16/2010)

Mortar Cube Test Results on 3rd Day

Mortar Cube Specimens	DIMENSIONS (in.)			LOADS (lbs)	STRENGTH (psi)
	L	W	H		
1	2.015(1.988)	1.997(2.004)	1.995(1.999)	15765	3937
2	1.989(2.023)	2.019(2.008)	2.009(2.000)	19590	4850
3	2.029(2.038)	2.021(1.992)	2.012(2.015)	19425	4761
4	1.971(1.971)	2.014(2.018)	2.001(2.000)	17430	4386
Average Strength (psi)					4666

SET 2: (Test at 8:30am 12/17/2010)

Mortar Cube Test Results on 4th Day

Mortar Cube Specimens	DIMENSIONS (in.)			LOADS (lbs)	STRENGTH (psi)
	L	W	H		
1	1.997(1.995)	2.035(2.022)	2.001(2.000)	19065	4709
2	2.005(2.006)	2.040(2.036)	1.987(1.988)	18615	4554
3	1.984(1.994)	2.034(2.010)	2.013(2.017)	18615	4628
Average Strength (psi)					4630

Notes: the test was not completed on the 3rd day, so same measurements were taken on the 4th day.

SET 3: (Test at 12/21/2010)

Mortar Cube Test Results on 7th Day

Mortar Cube Specimens	DIMENSIONS (in.)				LOADS (lbs)	STRENGTH (psi)
	a.	b.	c.	d.		
1	1.9062	2.0000	1.9062	2.0000	16545	4337
2	1.9375	2.0625	1.9375	2.0625	18045	4511
3	1.8438	2.0312	1.8438	2.0312	17250	4595
Average Strength (psi)						4481

Mortar Cube Test Results

For the Column 5-R:
Cast at 2/13/2011

SET 1: (Test at 2/16/2011)

Mortar Cube Test Results on 3rd Day

Mortar Cube Specimens	DIMENSIONS				LOADS (lbs)	STRENGTH (psi)
	L (in.)	W (in.)	H (in.)	A (in. ²)		
1	2.010	2.048	2.012	4.116	23,445	5696
2	2.001	2.009	2.008	4.020	24,030	5978
3	2.010	2.019	2.012	4.058	24,855	6125
4	2.014	2.038	2.015	4.105	31,650	7710
5	2.035	2.053	2.006	4.178	26,070	6240
6	2.006	2.027	2.038	4.066	23,680	5824
Average Strength (psi)						6262

FRP Pull-off Test
(For Rapid Repair Column # 1)
9/17/2010

Data Sheet – FRP Pull-off Test

	Load (kN)	Load (lb)	Area (mm ²)	Area (in. ²)	Bond Strength (psi)
Specimen #1	5.77	1297.15	1963.5	3.04	426.21
Specimen #2	4.45	1000.4	1963.5	3.04	328.71
Specimen #3	-	-	-	-	-
Average	5.11	1148.77	1963.5	3.04	377.46

Check Bond Strength **Yes**

FRP Pull-off Test
(For Rapid Repair Column # 2)
10/14/2010

Data Sheet – FRP Pull-off Test

	Load (kN)	Load (lb)	Area (mm ²)	Area (in. ²)	Bond Strength (psi)
Specimen #1	3.39	762.10	1963.50	3.04	250.41
Specimen #2	1.94	436.13	1963.50	3.04	143.30
Specimen #3	3.81	856.52	1963.50	3.04	281.43
Average	3.05	684.92	1963.50	3.04	225.05

Check Bond Strength > 200psi **Yes**

FRP Pull-off Test
(For Rapid Repair Column #3)
11/11/2010

Data Sheet – FRP Pull-off Test

	Load (kN)	Load (lb)	Area (mm ²)	Area (in. ²)	Bond Strength (psi)
Specimen #1	5.75	1292.65	1520.53	2.3568	548.48
Specimen #2	7.35	1652.35	1520.53	2.3568	701.10
Specimen #3	5.23	1175.75	1520.53	2.3568	498.87
Average	6.11	1375.58	1520.53	2.3568	582.82

Notes:

- (1) The pull-off test was conducted on the east side of the footing (the FRP was applied on the original concrete);
- (2) Specimens #1 & 3 -----Adhesive Failure;
- (3) Specimen #2-----Concrete Failure;

Check Bond Strength>200psi **Yes**

FRP Pull-off Test
(For Rapid Repair Column #5)
2/16/2011

Data Sheet – FRP Pull-off Test

	Bond Strength (N/mm ²)	Bond Strength (psi)
Specimen #1	1.68	243.66
Specimen #2	1.68	243.66
Specimen #3	3.05	442.36
Average		309.89

Notes:

- (4) Specimen #1 with the concrete failure;
- (5) Specimen #2 with epoxy adhesive failure;
- (6) Specimen #3 with concrete & adhesive failure.

Check Bond Strength > 200psi **Yes**



The Chemical Company

PRODUCT DATA

3 03 01 00 Maintenance of Concrete

LA40 REPAIR MORTAR

Pourable and pumpable pre-extended micro concrete

Description

LA40 Repair Mortar is a one-component shrinkage-compensated micro concrete. It is designed for large volume repairs, including structural elements, typically in applications from 2" (51 mm) to full depth.

Yield

0.43 ft³ per 55 lb
(0.012 m³/25 kg) bag

0.62 ft³ per 80 lb
(0.018 m³/36 kg) bag

Packaging

55 lb (25 kg) bags

80 lb (36 kg) bags

Shelf Life

1 year when properly stored

Storage

Store in unopened containers at 40 to 90° F (4.4 to 32.2° C) in clean, dry conditions.

Features

- High bond strength
- Shrinkage compensated
- High early strength
- Low permeability
- Excellent freeze/thaw resistance
- Flowable
- One component
- Self-compacting

Benefits

- Self-bonding to SSD concrete substrates
- Dual expansion system compensates for shrinkage in plastic and hardened states
- Reduces form cycle time
- Protects against carbon dioxide and chloride intrusion
- Durable in cold, wet environments
- Placement by pumping or pouring into congested locations
- Only the site addition of clean water is required
- Minimizes honeycombing; displaces air without vibration

Where to Use

APPLICATION

- Large volume structural repairs
- Repair or replacement of spandrel beams, columns, balcony edges
- Partial or full-depth placements of structural concrete elements
- Parking garages
- Water and wastewater tanks
- Tunnels, dams, bridges
- Marine structures

LOCATION

- Interior or exterior

SUBSTRATE

- Concrete

How to Apply

Surface Preparation

CONCRETE:

1. Area being repaired must be structurally sound and fully cured.
2. Perimeter cut the edges of the repair to a depth of at least 3/8" (9 mm) to avoid featheredging and to provide a square edge.
3. Break out the concrete to the sawn edge and across the entire repair.
4. Mechanically abrade and clean the surface to remove any dust, unsound or contaminated material, oil, paint, grease, or corrosion deposits. Do not use a method of surface preparation that could damage the concrete.
5. Where breaking out is not required, roughen the surface and remove any laitance by light scabbling or



Technical Data

Composition

LA40 Repair Mortar is a proprietary blend of cement, graded aggregate, shrinkage-compensating agents, and additives.

Test Data

PROPERTY	RESULTS	TEST METHODS
Fresh wet density , lb/ft ³ (kg/m ³)	142 (2,275)	ASTM C 138
Compressive strength , psi (MPa); 2" (51 mm) cubes		ASTM C 109
1 day	2,500 (17.2)	
7 days	5,000 (34.5)	
28 days	6,000 (41.4)	
Compressive strength , psi (MPa); 3 by 6" (76 by 152 mm) cylinders, at 28 days	5,000 (34.5)	ASTM C 39
Flexural strength , psi (MPa), at 28 days	1,150 (7.9)	ASTM C 348
Slant shear bond strength , psi (MPa), at 28 days	3,000 (20.7)	ASTM C 882, (modified) ¹
Splitting tensile strength , psi (MPa), at 28 days	500 (3.4)	ASTM C 496
Drying shrinkage , μ strain, at 28 days	350	ASTM C 157, (unmodified)
Drying shrinkage , μ strain, at 21 days	611	ASTM C 157, (modified)
Freeze/thaw resistance , % RDM ²	100	ASTM C 666
Coefficient of thermal expansion , in/in/° F (cm/cm/° C)	5.5×10^{-6} (9.9×10^{-6})	CRD C 39

¹No bonding agent

²RDM = Relative Dynamic Modulus

Results were obtained with a water / powder ratio of 4 qts/80 lb (3.8 L/36 kg) bag or 2.7 qts/55 lb (2.6 L/25 kg) bag.

All application and performance values are typical for the material, but may vary with test methods, conditions, and configurations.

abrasive blasting. Remove oil and grease deposits by steam cleaning, detergent scrubbing, or degreasing.

6. Verify the effectiveness of decontamination by a pull-off test.

REINFORCING STEEL

1. Remove all oxidation and scale from the exposed reinforcing steel in accordance with ICRI Technical Guideline No. 03730 "Guide for Surface Preparation for the Repair of Deteriorated Concrete Resulting from Reinforcing Steel Corrosion."

2. For additional protection from future corrosion, coat the prepared reinforcing steel with Zincrich Rebar Primer or install Corr-Stops® CM.

Mixing

1. Ensure that LA40 Repair Mortar is thoroughly mixed; a forced-action mixer is essential. Mixing in a suitably sized container using an appropriate paddle with a slow-speed (400 – 500 rpm) heavy-duty drill is acceptable. Do not use free-fall mixers. Never mix partial bags.

2. The machine mixing capacity and the crew size must be adequate to carry out the placing operation continuously.

MIXING 80 LB (36 KG) BAGS

1. Measure 4 quarts (3.8 L) of potable water and pour 3 quarts into the mixer. With the machine in operation, add 1 full 80 lb (36 kg) bag of LA40 Repair Mortar and mix for 1 minute before adding the rest of the water. Always add powder into the water. The quantities mixed may be scaled up as required.

2. Mix for an additional 2 – 3 minutes to obtain a smooth consistency.

3. When using the drill-and-paddle mixing method, place the complete 4 quarts (3.8 L) of water in the mixing drum. With the paddle rotating, add 1 full 80 lb (36 kg) bag of LA40 Repair Mortar and mix 3 minutes until a smooth, even consistency is obtained.

4. Depending on the ambient temperatures and the desired consistency, additional water may be added. The total water content should not exceed 4.2 quarts (3.9 L) per 80 lb (36 kg) bag.

MIXING 55 LB (25 KG) BAGS

1. Measure 2.7 quarts (2.6 L) of potable water and pour 2 quarts into the mixer. With the machine in operation, add 1 full 55 lb (25 kg) bag of LA40 Repair Mortar and mix for 1 minute before adding the rest of the water. Always add powder into the water. The quantities mixed may be scaled up as required.

- Mix for a further 2 – 3 minutes to obtain a smooth consistency.
- When using the drill-and-paddle mixing method, place the complete 2.7 quarts (2.6 L) of water in the mixing drum. With the paddle rotating, add 1 full 55 lb (25 kg) bag of LA40 Repair Mortar and mix 3 minutes to reach a smooth, even consistency.
- Depending on the ambient temperatures and the desired consistency, additional water may be added. The total water content should not exceed 2.9 quarts (2.7 L) per 55 lb (25 kg) bag.

HOT- AND COLD-WEATHER CONDITIONS

- For cold-weather applications, refer to ACI 306R Cold Weather Concreting; for hot-weather applications, refer to ACI 305R, Hot Weather Concreting.

Application

- Keep the unrestrained surface area of the repair to a minimum. The formwork should be rigid and tight to prevent loss of material. Properly seal the faces of forms to ensure they absorb no water from the repair material.
- The formwork should include drainage outlets for presoaking and, if beneath a soffit, provision for air venting. Provide suitable access points to pour or pump the mixed concrete into place.
- Form design should allow for a minimum of 1-1/2" (38 mm) cover around all steel.
- Use a suitable form-release agent to facilitate the removal of forms from the cast material.
- Refer to ACI 347R, Recommended Practice for Concrete Formwork.
- Several hours before placing LA40 Repair Mortar, saturate the prepared concrete substrates by filling the prepared formwork with clean water.
- Immediately before the placement of LA40 Repair Mortar, completely drain this water and seal the drainage outlets, leaving the substrate saturated surface-dry (SSD) with no ponded water remaining.
- In jobsite circumstances where the formwork cannot be filled with water, spray the substrate with clean water to achieve a saturated surface-dry (SSD) condition immediately before placing LA40 Repair Mortar.
- When using a combination surface-applied bonding agent and corrosion-resistant rebar primer, use Epoxy Adhesive 24LPL or Rebar Primer and Bonding Agent 3. Refer to the appropriate product data sheets for further details (Form Nos. 1018987 and 1018966).

10. Immediately after mixing, pump or pour the LA40 Repair Mortar into the formed area. The material does not require vibrating.

Curing

- Leave the formwork in place until the compressive strength of the LA40 Repair Mortar reaches 2,500 psi (17.2 MPa) or a strength specified by the engineer.
- LA40 Repair Mortar must be cured immediately after the formwork is stripped in accordance with good concrete practices. Refer to ACI 308 Standard Practice for Curing Concrete.
- If the repair area will receive a coating, wet curing is recommended.
- In cold conditions, protect the finished repair from freezing.

Clean Up

Remove LA40 Repair Mortar from tools, equipment, and mixers with clean water immediately after use. Cured material can only be removed mechanically. Clean hands and skin immediately with soap and water or industrial hand cleaner; do not use solvents.

For Best Performance

- Minimum ambient, surface, and material temperatures should be 40° F (4° C) and rising at the time of application.
- Do not mix partial bags.
- Do not use to make overlay repairs where the surface of fresh, wet LA40 Repair Mortar will remain unrestrained during cure.
- Do not expose to rain or moving water during application.
- Do not vibrate LA40 Repair Mortar while in the fluid consistency.
- Do not use additives with LA40 Repair Mortar.
- When the minimum placement depth is less than 2", use LA Repair Mortar (see Form No. 1018996).
- Make certain the most current versions of product data sheet and MSDS are being used; call Customer Service (1-800-433-9517) to verify the most current version.
- Proper application is the responsibility of the user. Field visits by BASF personnel are for the purpose of making technical recommendations only and not for supervising or providing quality control on the jobsite.

Health and Safety

LA40 REPAIR MORTAR

Caution

Risks

Product is alkaline on contact with water and may cause injury to skin or eyes. Ingestion or inhalation of dust may cause irritation. Contains a small amount of free respirable quartz, which has been listed as a suspected human carcinogen by NTP and IARC. Repeated or prolonged overexposure to free respirable quartz may cause silicosis or other serious and delayed lung injury.

Precautions

KEEP OUT OF THE REACH OF CHILDREN. Avoid contact with skin, eyes and clothing. Prevent inhalation of dust. Wash thoroughly after handling. Keep container closed when not in use. DO NOT take internally. Use only with adequate ventilation. Use impervious gloves, eye protection and if the TLV is exceeded or used in a poorly ventilated area, use NIOSH/MSHA approved respiratory protection in accordance with applicable federal, state and local regulations.

First Aid

In case of eye contact, flush thoroughly with water for at least 15 minutes. In case of skin contact, wash affected areas with soap and water. If irritation persists, SEEK MEDICAL ATTENTION. Remove and wash contaminated clothing. If inhalation causes physical discomfort, remove to fresh air. If discomfort persists or any breathing difficulty occurs or if swallowed, SEEK IMMEDIATE MEDICAL ATTENTION. Refer to Material Safety Data Sheet (MSDS) for further information.

Proposition 65

This product contains material listed by the state of California as known to cause cancer, birth defects, or other reproductive harm.

VOC Content

0 lbs/gal or 0 g/L, less water and exempt solvents

**For medical emergencies only,
call ChemTrec (1-800-424-9300).**

PRODUCT DATA

3 03 01 00 Maintenance of Concrete

MBRACE® CF 130

Unidirectional high strength carbon fiber fabric for the MBrace® Composite Strengthening System

Description

MBrace® CF 130 is a dry fabric constructed of very high strength, aerospace grade carbon fibers. These fabrics are applied onto the surface of existing structural members in buildings, bridges, and other structures using the MBrace® family of performance polymers. The result is an externally bonded FRP (fiber reinforced polymer) reinforcement system that is engineered to increase the strength and structural performance of these members. Once installed, the MBrace® System delivers externally bonded reinforcement with outstanding long-term physical and mechanical properties.

Yield

269 ft² (25 m²) per roll

Packaging

Available in rolls 20 in (500 mm) wide, 162 ft (50 m) long

ROLL	WIDTH	LENGTH
269 ft ² (25 m ²)	20 in (508 mm)	162 ft (50 m)

Color

Black

Features

- High strength to weight ratio
- Excellent resistance to creep and fatigue
- Extremely durable
- Easy installation
- Low aesthetic impact

Benefits

- Can add significant strength to a structure without adding significant dead load
- Withstands sustained and cyclic load conditions
- Extremely resistant to a wide range of environmental conditions
- Can be installed quickly, even in areas of limited access
- Easy to conceal, will not significantly change existing member dimensions, will form around complex surfaces

Shelf Life

3 years in unopened containers

Storage

Store in a cool, dry place (50 to 90 °F [10 to 32 °C]) away from direct sunlight, flame, or other hazards.

Where to Use

APPLICATION

- Increase load bearing capacity of concrete beams, slabs, walls and columns
- Improve the seismic ductility of concrete columns
- Improve the seismic response of concrete beam-column connections, shear walls and collector elements
- Improve the seismic performance of masonry shear walls and in-fill walls
- Restore structural capacity to damaged or deteriorated concrete structures
- Increase the strength of concrete pipes, silos, tanks, chimneys and tunnels

- Substitute reinforcing steel mistakenly omitted in the construction of concrete and masonry structures
- Improve the blast resistance of concrete and masonry structures
- Strengthening of some steel and timber structures

LOCATION

- Vertical
- Horizontal
- Exterior
- Interior

SUBSTRATE

- Concrete
- Masonry
- Timber
- Steel



Technical Data**Composition**

MBrace® CF 130 is composed of a dense network of high strength carbon fibers held in a unidirectional alignment with a light thermoplastic glass fiber cross weave yarn

Physical Properties

PROPERTY	REQUIREMENT
Fiber Material	High Strength Carbon
Fiber Tensile Strength	720 ksi (4950 MPa)
Areal Weight	0.062 lb/ft ² [300 g/m ²]
Fabric Width	20 inch [500 mm]
Nominal Thickness, t_f⁽¹⁾	0.0065 in/ply [0.165 mm/ply]

Functional Properties

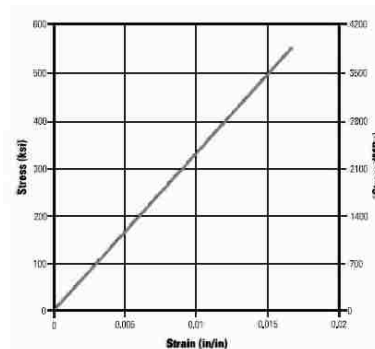
PROPERTY	REQUIREMENT
CTE	-0.21·10 ⁻⁴ /F (-0.38·10 ⁻⁴ /C)
Thermal Conductivity	65.1-Btu-in/hr-ft ² -F (9.38-W/m-K)
Electrical Resistivity	1.6·10 ⁻³ Ω-cm

0° Tensile Properties^(2,3)

PROPERTY	REQUIREMENT
Ultimate Tensile Strength, f_{fu}	550 ksi [3800 MPa]
Tensile Modulus, E_f	33000 ksi [227 GPa]
Ultimate Tensile Strength per Unit Width, $f_{fu}^* t_f$	3.57 kips/in/ply [0.625 kN/mm/ply]
Tensile Modulus per Unit Width, $E_f t_f$	215 kips/in/ply [38 kN/mm/ply]
Ultimate Rupture Strain, ϵ_{fu}^*	1.67%

90° Tensile Properties^(2,4)

PROPERTY	REQUIREMENT
Ultimate Tensile Strength	0
Tensile Modulus	0
Ultimate Rupture Strain	n/a

**NOTES:**

- (1) The nominal fabric thickness is based on the total area of fibers (only) in a unit width. From experience, the actual cured thickness of a single ply laminate (fibers plus saturating resins) is 0.020 to 0.040 in (0.6 to 1.0 mm).
- (2) The tensile properties given are those to be used for design. These values are derived by testing cured laminates (per ASTM D3039) and dividing the resulting strength and modulus per unit width by the nominal fabric thickness.
- (3) The 0° direction denotes the direction along the length of the fabric.
- (4) The 90° direction denotes the direction along the width of the fabric.



The Chemical Company

PRODUCT DATA

3 03 01 00 Maintenance of Concrete

MBRACE® PRIMER

Low viscosity epoxy primer for the MBrace® Composite Strengthening System

Description

MBrace® Primer is a low viscosity, 100% solids, polyamine cured epoxy. As the first applied component of the MBrace® System, it is used to penetrate the pore structure of cementitious substrates and to provide a high bond base coat for the MBrace® System. MBrace® Primer is based on a unique adduct curing technology that results in tolerance for surface moisture and for temperatures down to 35 °F (2 °C).

Yield

Steel:

250 to 325 ft²/gal (6.1 to 8.0 m²/L)

Concrete:

200 to 250 ft²/gal (4.9 to 6.1 m²/L)

Masonry (Concrete):

150 to 200 ft²/gal (3.8 to 4.9 m²/L)

Masonry (Clay):

200 to 250 ft²/gal (4.9 to 6.1 m²/L)

(Coverage rate on concrete and masonry may vary depending on density and porosity of the substrate)

Packaging

Available in 1 gal (3.8 L) units. Each unit is packaged as follows:

	VOLUME	PACKAGING	WEIGHT
Part A	3 qts	2 gal pail	7 lbs
Part B	1 qt	1 qt can	2 lbs

Features

- Moisture tolerant
- Low viscosity
- 100% solids epoxy
- Suitable for low-temperature application

Benefits

- Can be applied on some damp substrates
- Easily penetrates pore structure of concrete
- Low odor, low VOC's
- Can be applied if temperature is 35 degrees F and rising; extends application window in cooler conditions

Color

Part A: Amber

Part B: Clear

Mixed: Amber

Shelf Life

18 months properly stored in unopened containers (Part A and B)

Storage

Store in a cool, dry place (50 to 90° F [10 to 32° C]) away from direct sunlight, flame, or other hazards.

Where to Use

APPLICATION

MBrace® Primer is the first component of the MBrace® System that is applied to concrete, steel, and masonry substrates. MBrace® Primer is used to provide excellent adhesion of the MBrace® System to the substrate.

- MBrace® Primer is the first component any MBrace® installation

LOCATION

- Vertical
- Horizontal
- Exterior
- Interior

SUBSTRATE

- Concrete
- Masonry
- Steel



Technical Data

Composition

MBrace® Primer is a two component polyamine cured epoxy

Handling Properties

PROPERTY	VALUE
Mixed Weight	9.2 lb/gal (1103 g/L)
VOC Content	0.71 lb/gal (84.1 g/L)
Flash Point	Part A: 204 °F (95 °C) Part B: > 200 °F (93 °C) (Pensky-Martens Closed Cup)
Mixed Viscosity	
at 50 °F (10 °C)	1200 cps
at 77 °F (25 °C)	400 cps
at 90 °F (32 °C)	200 cps

Physical Properties

PROPERTY	VALUE
Installed Thickness(approx)	3 mils (0.075 mm)
Density	68.8 pcf (1102 kg/m ³)

Tensile Properties (1)

PROPERTY	VALUE
Yield Strength	2100 psi (14.5 MPa)
Strain at Yield	2.0%
Elastic Modulus	105 ksi (717 MPa)
Ultimate Strength	2500 psi (17.2 MPa)
Rupture Strain	40%
Poisson's Ratio	0.48

Compressive Properties (2)

PROPERTY	VALUE
Yield Strength	3800 psi (26.2 MPa)
Strain at Yield	4.0%
Elastic Modulus	97 ksi (670 MPa)
Ultimate Strength	4100 psi (28.3 MPa)
Rupture Strain	10%

Flexural Properties (3)

PROPERTY	VALUE
Yield Strength	3500 psi (24.1 MPa)
Strain at Yield	4.0%
Elastic Modulus	86.3 ksi (595 MPa)
Ultimate Strength	3500 psi (24.1 MPa)
Rupture Strain	Large deformation with no rupture

Functional Properties (4)

PROPERTY	VALUE
CTE	20-10 ⁻⁶ /F (35-10 ⁻⁶ /C)
Thermal Conductivity	1.39 Btu-in/hr-ft ² F (0.20 W/m·K)
Glass Transition Temp, T_g	171 °F (77 °C)

NOTES:

1. Based on testing of cured samples per ASTM D 638 at 72°F (20°C) and 40% relative humidity.
2. Based on testing of cured samples per ASTM D 695 at 72°F (20°C) and 40% relative humidity.
3. Based on testing of cured samples per ASTM D 790 at 72°F (20°C) and 40% relative humidity.

How to Apply**Surface Preparation**

1. Substrate should be fully cured, clean, sound, and dry. Any damaged areas, spalled areas, delaminated areas, or areas with corrosion damage must be repaired prior to applying the MBrace system.

2. For concrete and masonry substrates, mechanically prepare the substrate to remove coatings, laitance, and all miscellaneous surface contaminants and to provide a proper surface profile. Surface profile should be a minimum of ICRI CSP 3 (similar to 80 grit sandpaper).

3. For steel substrates, abrasive blast to "white metal" in accordance with Society for Protective Coatings (SSPC) Specification SP-5-89 or NACE No. 1, using clean, dry abrasive to obtain a minimum 3 mil profile.

Mixing

1. The mix ratio is 3:1 (Part A to Part B) by volume or 100:30 (Part A to Part B) by weight. Mix only the amount of material that can be used within the working time of the material. Approximate working times for a 1 Gal (3.8 L) unit are:

75 min	at 50° F (10° C)
20 min	at 77° F (25° C)
10 min	at 90° F (32° C)

2. Carefully measure (ratio) each component and then add Part B (hardener) to Part A (resin).

3. Mix Parts A and B using a low-speed drill (600 rpm) and mixing paddle (e.g., a Jiffy mixer). Carefully scrape the sides and bottom of the container while mixing. Keep the paddle below the surface of the material to avoid entrapping air. Proper mixing will take at least 3 – 5 minutes. Well-mixed material will be free of streaks or lumps.

Application

1. Apply the material in areas to receive the MBrace system using a 3/8" nap roller or short bristle brush to a wet film thickness of approximately 3-mils.

2. Spray application is not recommended.

Clean Up

Use T-471, methyl ethyl ketone or acetone. Observe fire and health precautions with solvents.

Maintenance

Periodically inspect the applied material and repair localized areas as needed. Consult a BASF representative for additional information. Visit us on the web for the most current product information and news: www.BASFBUILDINGSYSTEMS.COM.

For Best Performance

- Only apply MBrace® Primer when the ambient temperature is between 35° and 120°F (2° and 50°C).
- Subsequent components of the MBrace® System should be applied within 48 hours of applying MBrace® Primer to the substrate to assure proper adhesion.
- Make certain the most current versions of product data sheet and MSDS are being used; call Customer Service (1-800-433-9517) to verify the most current version.
- Proper application is the responsibility of the user. Field visits by BASF personnel are for the purpose of making technical recommendations only and are not for supervising or providing quality control on the jobsite.

Health and Safety

MBrace® PRIMER

Warning

Vapor may be harmful. Contains epoxy resins and curing agent. May cause skin sensitivity or other allergic responses. Keep away from heat, sparks or open flame. In enclosed areas or where ventilation is poor use an approved air mask and utilize adequate safety precautions to prevent fire or explosion. In case of skin contact, wash with soap and water. For eyes, flush immediately (seconds count) with water for 15 minutes and CALL A PHYSICIAN. If swallowed, CALL A PHYSICIAN IMMEDIATELY.

Product Material Safety Data Sheets (MSDS) are available and should be consulted and on hand whenever handling these products.

These products are for professional and industrial use only and are only installed by trained and qualified applicators. Trained applicators must follow installation instructions.



The Chemical Company

PRODUCT DATA

3 03 01 00 Maintenance of Concrete

MBRACE® PUTTY

High viscosity epoxy paste for the MBrace® Composite Strengthening System

Description

MBrace® Putty is a 100% solids non sag epoxy paste for use with the MBrace® Composite Strengthening System. It is used level small surface defects and to provide a smooth surface to which the MBrace® System will be applied.

Yield

100 to 250 ft²/gal (4.9 to 6.1 m²/L)
(Depending on surface roughness)

Packaging

Available in 1 gal (3.8 L) units. Each unit is packaged as follows:

	VOLUME	PACKAGING	WEIGHT
Part A	3 qts	2 gal pail	8 lbs
Part B	1 qt	1 qt can	2.5 lbs

Color

Part A: Light Gray

Part B: Charcoal

Mixed: Gray

Features

- 100% solids epoxy
- Suitable for low-temperature application
- High viscosity

Benefits

- Low odor, low VOC's
- Can be applied if temperature is 35 degrees F and rising; extends application window in cooler conditions
- Can be used in vertical and overhead applications

Shelf Life

18 months if properly stored in unopened containers (Part A and B)

Storage

Store in a cool, dry place (50 to 90°F [10 to 32°C]) away from direct sunlight, flame, or other hazards.

Where to Use

APPLICATION

- Fill small voids or smooth small offsets on cementitious substrates.
- Sealing of cracks prior to epoxy-injection.

LOCATION

- Vertical
- Horizontal
- Exterior
- Interior

SUBSTRATE

- Concrete
- Masonry
- Steel

How to Apply

Surface Preparation

1. MBrace® Putty should be applied to a substrate primed with MBrace® Primer. The putty can be applied before or after the primer coat has achieved full cure. Surfaces with a tack-free primer coat must be lightly sanded and cleaned of any dust, oils, or other surface contaminants.



MBT® PROTECTION AND REPAIR PRODUCT DATA
MBRACE® PUTTY

Technical Data

Composition

Two part, 100% solids, non-sag epoxy paste

Handling Properties

PROPERTY	VALUE
Mixed Weight	10.5 lb/gal (1259 g/L)
VOC Content	0.74 lb/gal (89 g/L) (EPA Method 24)
Flash Point	Part A: 210 °F (99 °C) Part B: >200 °F (93 °C) (Pensky-Martens Closed Cup)

Mixed Viscosity

at 50 °F (10 °C) 74,000 cps
 at 77 °F (25 °C) 45,000 cps
 at 90 °F (32 °C) 33,000 cps

Physical Properties

PROPERTY	REQUIREMENT
Density	75.8 pcf (1258 kg/m ³)

Tensile Properties (1)

PROPERTY	REQUIREMENT
Yield Strength	1800 psi (12 MPa)
Strain at Yield	1.5%
Elastic Modulus	260 ksi (1800 MPa)
Ultimate Strength	2200 psi (15.2 MPa)
Rupture Strain	7%
Poisson's Ratio	0.48

Compressive Properties (2)

PROPERTY	REQUIREMENT
Yield Strength	3300 psi (22.8 MPa)
Strain at Yield	4.0%
Elastic Modulus	155 ksi (1076 MPa)
Ultimate Strength	3300 psi (22.8 MPa)
Rupture Strain	10%

Flexural Properties (3)

PROPERTY	REQUIREMENT
Yield Strength	3800 psi (26.2 MPa)
Strain at Yield	4.0%
Elastic Modulus	130 ksi (895 MPa)
Ultimate Strength	4000 psi (27.6 MPa)
Rupture Strain	7%

Functional Properties (4)

PROPERTY	REQUIREMENT
CTE	20-10 ⁻⁵ /F (35-10 ⁻⁵ /C)
Thermal Conductivity	1.32 Btu-in/hr-ft ² -F (0.19 W/m·K)
Glass Transition Temp, T_g	168 °F (75 °C)

NOTES:

1. Based on testing of cured samples per ASTM D 638 at 72 °F (20 °C) and 40% relative humidity.
2. Based on testing of cured samples per ASTM D 695 at 72 °F (20 °C) and 40% relative humidity.
3. Based on testing of cured samples per ASTM D 790 at 72 °F (20 °C) and 40% relative humidity.
4. Based on testing of cured samples at 72 °F (20 °C) and 40% relative humidity.

Mixing

- The mix ratio is 3:1 (Part A to Part B) by volume or 100:30 (Part A to Part B) by weight. Mix only the amount of material that can be used within the working time of the material. Approximate working times for a 1 gal (3.8 L) unit are:

95 min	at 50°F (10°C)
40 min	at 77°F (25°C)
15 min	at 90°F (32°C)
- Part A (resin) must be pre-mixed using a low speed drill (600 rpm) and mixing paddle (e.g., a Jiffy Mixer). Keep the paddle below the surface of the material to avoid entrapping air. Pre-mix for a minimum of 3 minutes.
- Carefully measure (ratio) each component and then add Part B (hardener) to Part A (resin).
- Mix Parts A and B using a low-speed drill (600 rpm) and mixing paddle (e.g., a Jiffy mixer). Carefully scrape the sides and bottom of the container while mixing. Keep the paddle below the surface of the material to avoid entrapping air. Proper mixing will take at least 3 – 5 minutes. Well-mixed material will be free of streaks or lumps.
- If a thicker consistency is desired, silica flour (S-11 Powder) may be mixed into the material using a low-speed drill and mixing paddle. Add as much silica flour as is needed to achieve the desired consistency.

Application

- Apply the Mbrace® Putty to the primed substrate using a spring-steel trowel.
- The material should be applied by pulling a "tight" trowel. That is the Mbrace® Putty should only fill small voids and smooth small offsets in the substrate. High build or thick applications of the Mbrace® Putty are not recommended.

Clean Up

Use T-471, methyl ethyl ketone or acetone. Observe fire and health precautions with solvents.

Maintenance

- Periodically inspect the applied material and repair localized areas as needed. Consult a BASF representative for additional information.
- Visit us on the web for the most current product information and news:
www.BASFBuildingSystems.com.

For Best Performance

- Only apply Mbrace® Putty when the ambient temperature is between 35° and 120°F (2° and 50°C).
- Subsequent components of the Mbrace® System should be applied within 48 hours of applying Mbrace® Putty to the substrate to assure proper adhesion.
- Make certain the most current versions of product data sheet and MSDS are being used; call Customer Service (1-800-433-9517) to verify the most current versions.
- Proper application is the responsibility of the user. Field visits by personnel are for the purpose of making technical recommendations only and not for supervising or providing quality control on the jobsite.

Observe Working Time Limitations

- Catalyze no more material than can be applied within the work time period.
- Available work time, temperature and complexity of the application area will determine how much material should be catalyzed at one time.
- Keep material cool and shaded from direct sunlight in warm weather. During hot weather, work time can be extended by keeping material cool before and after mixing or by immersing pot in ice water.

Health and Safety**Mbrace® PUTTY****Warning**

Vapor may be harmful. Contains epoxy resins and curing agent. May cause skin sensitivity or other allergic responses. Keep away from heat, sparks or open flame. In enclosed areas or where ventilation is poor use an approved air mask and utilize adequate safety precautions to prevent fire or explosion. In case of skin contact, wash with soap and water. For eyes, flush immediately (seconds count) with water for 15 minutes and CALL A PHYSICIAN. If swallowed, CALL A PHYSICIAN IMMEDIATELY. Product Material Safety Data Sheets (MSDS) are available and should be consulted and on hand whenever handling these products. These products are for professional and industrial use only and are only installed by trained and qualified applicators. Trained applicators must follow installation instructions.



The Chemical Company

PRODUCT DATA

3 03 01 00 Maintenance of Concrete

MBRACE® SATURANT

Epoxy encapsulation resin for the MBrace® Composite Strengthening System

Description

MBrace® Saturant is a 100% solids, low viscosity epoxy material that is used to encapsulate MBrace® carbon and glass fiber fabrics. When reinforced with MBrace® fiber fabrics, the MBrace® Saturant cures to provide a high performance FRP laminate. The resulting FRP laminate can provide additional strength to concrete, masonry, steel, and wood structural elements.

Yield

COVERAGE

CF 130 Fabric 55 ft²/gal (1.35 m²/L)

CF 160 Fabric 45 ft²/gal (1.1 m²/L)

EG 900 Fabric 35 ft²/gal (0.85 m²/L)

Coverage rates are based on square footage (meters) of fabric. Contact a BASF representative for coverage rates for other fabric types.

Packaging

Available in 1 gal (3.8 L) and 4 gal (15.2 L) units

Color

Part A: Blue

Part B: Clear

Mixed: Blue

Shelf Life

18 months properly stored in unopened containers (Part A and B)

Storage

Store in a cool, dry area (50 to 90° F [10 to 32° C]) away from direct sunlight, flame, or other hazards.

Features

- Moderate viscosity
- 100% solids epoxy

Benefits

Can be applied in vertical and overhead applications, but still adequately saturates MBrace® fabrics

Low odor, low VOC's

Where to Use

APPLICATION

- Used to encapsulate any MBrace® fabric

LOCATION

- Vertical
- Horizontal
- Exterior
- Interior

SUBSTRATE

- Concrete
- Masonry
- Steel

How to Apply

Surface Preparation

1. MBrace® Saturant should be applied to a substrate prepared with MBrace® Primer and MBrace® Putty. The Saturant can be applied before or after the Primer and Putty have achieved full cure.
2. Surfaces with a tack-free primer/putty coat must be lightly sanded and cleaned of any dust, oils, or other surface contaminants.

Mixing

1. The mix ratio is 3:1 (Part A to Part B) by volume or 100:30 (Part A to Part B) by weight. Mix only the amount of material that can be used within the working time of the material. Approximate working times for a 1 gal (3.8 L) unit are:

200 min at 50° F (10° C)

45 min at 77° F (25° C)

15 min at 90° F (32° C)

2. Part A (resin) must be pre-mixed using a low speed drill (600 rpm) and mixing paddle (e.g., a Jiffy Mixer). Keep the paddle below the surface of the material to avoid entrapping air. Pre-mix for a minimum of 3 minutes.
3. Carefully measure (ratio) each component and then add Part B (hardener) to Part A (resin).
4. Mix Parts A and B using a low-speed drill (600 rpm) and mixing paddle (e.g., a Jiffy mixer). Carefully scrape the sides and bottom of the container while mixing. Keep the paddle below the surface of the material to avoid entrapping air. Proper mixing will take at least 3 – 5 minutes. Well-mixed material will be free of streaks or lumps.



Technical Data**Composition**

Two part, 100% solids, sag resistant epoxy

Handling Properties

PROPERTY	VALUE
Mixed Weight	8.2 lb/gal (984 g/L)
VOC Content	0.21 lb/gal (25 g/L) (EPA Method 24)
Flash Point	Part A: 230 °F (110 °C) Part B: > 200 °F (93 °C) (Pensky-Martens Closed Cup)
Mixed Viscosity	
at 50 °F (10 °C)	2500 cps
at 77 °F (25 °C)	1350 cps
at 90 °F (32 °C)	900 cps

Physical Properties

PROPERTY	REQUIREMENT
Density	61.3 pcf (983-kg/m ³)

Tensile Properties (1)

PROPERTY	REQUIREMENT
Yield Strength	7900 psi (54 MPa)
Strain at Yield	2.5%
Elastic Modulus	440 ksi (3034 MPa)
Ultimate Strength	8000 psi (55.2 MPa)
Rupture Strain	3.5%
Poisson's Ratio	0.40

Compressive Properties (2)

PROPERTY	REQUIREMENT
Yield Strength	12500 psi (86.2 MPa)
Strain at Yield	5.0%
Elastic Modulus	380 ksi (2620 MPa)
Ultimate Strength	12500 psi (86.2 MPa)
Rupture Strain	5%

Flexural Properties (3)

PROPERTY	REQUIREMENT
Yield Strength	20000 psi (138 MPa)
Strain at Yield	3.8%
Elastic Modulus	540 ksi (3724 MPa)
Ultimate Strength	20000 psi (138 MPa)
Rupture Strain	5%

Functional Properties (4)

PROPERTY	REQUIREMENT
CTE	20-10 ⁻⁶ /°F (35-10 ⁻⁶ /°C)
Thermal Conductivity	1.45 Btu-in/hr-ft ² -°F (0.21 W/m-°K)
Glass Transition Temp, T_g	163 °F (71 °C)

NOTES:

- Based on testing of cured samples per ASTM D 638 at 72 °F (20 °C) and 40% relative humidity.
- Based on testing of cured samples per ASTM D 695 at 72 °F (20 °C) and 40% relative humidity.
- Based on testing of cured samples per ASTM D 790 at 72 °F (20 °C) and 40% relative humidity.
- Based on testing of cured samples at 72 °F (20 °C) and 40% relative humidity.

Application

1. Apply the Mbrace® Saturant using a 3/8" nap roller or short bristle brush to a wet film thickness of 18 to 22 mils.
2. Apply the desired Mbrace® fabric into the saturant before the saturant becomes tacky. (Note some fabrics may require additional Mbrace® Saturant be applied directly onto the fabric prior to placing the fabric.)
3. Apply a second layer of Mbrace® Saturant over the Mbrace® fabric using a 3/8" nap roller or short bristle brush to a wet film thickness of 18 to 22 mils.
4. If additional layers of Mbrace® fabric are required, repeat steps 1 through 3.

Clean Up

Use T-471, methyl ethyl ketone or acetone. Observe fire and health precautions with solvents.

Maintenance

Periodically inspect the applied material and repair localized areas as needed. Consult a BASF representative for additional information. Visit us on the web for the most current product information and news: www.buildingsystems.basf.com

For Best Performance

- Only apply Mbrace® Saturant when the ambient temperature is between 50 and 120° F (10 and 50° C).
- Surfaces should be protected with Mbrace® Topcoat, Topcoat ATX, or Topcoat FRL within two days.
- Surfaces should be coated - consult your local sales representative for available options. Coatings applied over Mbrace® Saturant should be applied within 48 hours.
- Catalyze no more material than can be applied within the work time period.
- Available work time, temperature and complexity of the application area will determine how much material should be catalyzed at one time.
- Keep material cool and shaded from direct sunlight in warm weather.
- During hot weather, work time can be extended by keeping material cool before and after mixing or by immersing pot in ice water.
- Make certain the most current versions of product data sheet and MSDS are being used; call Customer Service (1-800-433-9517) to verify the most current versions.
- Proper application is the responsibility of the user. Field visits by personnel are for the purpose of making technical recommendations only and not for supervising or providing quality control on the jobsite.

Health and Safety

Mbrace® SATURANT PART A

Warning

Contains epoxy resin, alkyl(C11-C14) glycidyl ether, aliphatic diglycidyl ether, ethyl benzene.

Risks

May cause skin, eye and respiratory irritation. May cause dermatitis and allergic responses. Potential skin and/or respiratory sensitizer. Ingestion may cause irritation. Suspect cancer hazard. Contains material which may cause cancer. Risk of cancer depends on duration and level of exposure.

Precautions

Use only with adequate ventilation. Avoid contact with skin, eyes and clothing. Keep container closed when not in use. Wash thoroughly after handling. DO NOT take internally. Use impervious gloves, eye protection and if the TLV is exceeded or used in a poorly ventilated area, use NIOSH/MSHA approved respiratory protection in accordance with applicable Federal, state and local regulations.

First Aid

In case of eye contact, flush thoroughly with water for at least 15 minutes. In case of skin contact, wash affected areas with soap and water. If irritation persists, SEEK MEDICAL ATTENTION. Remove and wash contaminated clothing. If inhalation causes physical discomfort, remove to fresh air. If discomfort persists or any breathing difficulty occurs or if swallowed, SEEK IMMEDIATE MEDICAL ATTENTION.

Proposition 65

This product contains materials listed by the State of California as known to cause cancer, birth defects or other reproductive harm.

VOC Content

96 g/L or 0.80 lbs/gal less water and exempt solvents.

MBT® PROTECTION AND REPAIR PRODUCT DATA
MBRACE® SATURANT

MBRACE® SATURANT PART B

DANGER – CORROSIVE

Contains: Polyoxypropylenediamine; Isophorone diamine; Epoxy resin; Benzyl alcohol; 2,2,4-trimethyl-1,6-hexanediamine; 2,4,4-trimethyl-1,6-hexanediamine; Imidazole.

Risks

Contact with skin or eyes may cause burns. Ingestion may cause irritation and burns of mouth, throat and stomach. Inhalation of vapors may cause irritation. May cause dermatitis and allergic responses. Potential skin and/or respiratory sensitizer. Repeated or prolonged contact with skin may cause sensitization. Reports associate repeated or prolonged occupational overexposure to solvents with permanent brain, nervous system, liver and kidney damage. **INTENTIONAL MISUSE BY DELIBERATELY INHALING THE CONTENTS MAY BE HARMFUL OR FATAL.**

Precautions

DO NOT get in eyes, on skin or clothing. Wash thoroughly after handling. Keep container closed. DO NOT take internally. Use only with adequate ventilation. DO NOT breathe vapors. Use impervious gloves, eye protection and if the TLV is exceeded or used in a poorly ventilated area, use NIOSH/MSHA approved respiratory protection in accordance with applicable Federal, state and local regulations.

First Aid

In case of eye contact, flush thoroughly with water for at least 15 minutes. In case of skin contact, wash affected areas with soap and water. If irritation persists, SEEK MEDICAL ATTENTION. Remove and wash contaminated clothing. If inhalation causes physical discomfort, remove to fresh air. If discomfort persists or any breathing difficulty occurs or if swallowed, SEEK IMMEDIATE MEDICAL ATTENTION.

Proposition 65

This product does not knowingly contain materials listed by the State of California as known to cause cancer, birth defects or other reproductive harm.

VOC Content

0 g/L or 0 lbs/gal less water and exempt solvents.

Product Material Safety Data Sheets (MSDS) are available and should be consulted and on hand whenever handling these products. These products are for professional and industrial use only and are only installed by trained and qualified applicators. Trained applicators must follow installation instructions.

BASF Corporation Building Systems

889 Valley Park Drive
 Shakopee, MN, 55379

www.BuildingSystems.BASF.com

Customer Service 800-433-9517
Technical Service 800-243-6739



LIMITED WARRANTY NOTICE: Every reasonable effort is made to apply BASF exacting standards both in the manufacture of our products and in the information which we issue concerning these products and their use. We warrant our products to be of good quality and will replace or, at our election, refund the purchase price of any products proved defective. Satisfactory results depend not only upon quality products, but also upon many factors beyond our control. Therefore, except for such replacement or refund, BASF MAKES NO WARRANTY OR GUARANTEE, EXPRESS OR IMPLIED, INCLUDING WARRANTIES OF FITNESS FOR A PARTICULAR PURPOSE OR MERCHANTABILITY, RESPECTING ITS PRODUCTS, and BASF shall have no other liability with respect thereto. Any claim regarding product defect must be received in writing within one (1) year from the date of shipment. No claim will be considered without such written notice or after the specified time interval. User shall determine the suitability of the products for the intended use and assume all risks and liability in connection therewith. Any authorized change in the printed recommendations concerning the use of our products must bear the signature of the BASF Technical Manager.

This information and all further technical advice are based on BASF's present knowledge and experience. However, BASF assumes no liability for providing such information and advice including the extent to which such information and advice may relate to existing third party intellectual property rights, especially patent rights. In particular, BASF disclaims all CONDITIONS AND WARRANTIES, WHETHER EXPRESS OR IMPLIED, INCLUDING THE IMPLIED WARRANTIES OF FITNESS FOR A PARTICULAR PURPOSE OR MERCHANTABILITY. BASF SHALL NOT BE RESPONSIBLE FOR CONSEQUENTIAL, INDIRECT OR INCIDENTAL DAMAGES (INCLUDING LOSS OF PROFITS) OF ANY KIND. BASF reserves the right to make any changes according to technological progress or further developments. It is the customer's responsibility and obligation to carefully inspect and test any incoming goods. Performance of the product(s) described herein should be verified by testing and carried out only by qualified experts. It is the sole responsibility of the customer to carry out and arrange for any such testing. Reference to trade names used by other companies is neither a recommendation, nor an endorsement of any product and does not imply that similar products could not be used.

For professional use only. Not for sale to or use by the general public.

Form No. 1031105-11/13
 Printed on recycled paper including 10% post-consumer fiber.

© 2013 BASF
 Printed in U.S.A.

APPENDIX C
REPAIR DESIGN METHODOLOGY

This appendix provides the repair design methodology used in this study. Three different repair design methods were developed in this study for severely damaged RC columns under different loading conditions (see Table C.1).

To maximize the time efficiency, only the region of the column near the plastic hinge with cover concrete spalling (primary region) and the region adjacent to it (secondary region) were repaired. Portions of the column with slight concrete cracks were left unrepaired, considering that the repair is rapid and temporary, and the repaired column is not intended to experience an additional earthquake load. The CFRP strengthening systems were designed for the primary region. A secondary region with the same length as the primary region was repaired using half the designed thickness of CFRP used in the primary region to prevent shifting of the plastic hinge directly above the existing plastic hinge (as shown in Figure C.1). The lengths of these two regions were adjusted considering the width of the CFRP sheets (20 in. [508 mm] wide).

The design was conducted based on the material properties provided in Appendix B, repair objectives, and assumptions as follows:

Repair Objectives – The objective of the rapid repair in this research was to restore the strength to the original condition in flexure, shear, and torsional moment while maintaining as much ductility and stiffness as possible.

Assumptions – The buckled reinforcing bars were assumed to provide only tensile strength (no compressive strength); and the strength of the mortar used to repair the column was assumed to be 4000 psi on the test day.

Repair Design

Design 1 – All the terminology in this design can be found in Paper III collected in this dissertation. In Design 1, the longitudinal CFRP was preliminarily designed to compensate for the flexural strength loss due to the ruptured longitudinal reinforcing bars by providing the same tensile strength as the yield force of the ruptured bars, which is calculated by Equation C.1.

$$A_s f_y = n t_f w_f f_f \quad \text{Equation C.1}$$

Transverse CFRP was preliminarily designed to restore the shear strength (Caltrans 2006) and confinement according to the provisions used for RC column retrofit (Caltrans 2007) using Equations C.2 and C.3.

$$t_j = \frac{f_l D}{2\alpha_j E_j \varepsilon_j} \quad \text{Equation C.2}$$

$$t_j = \frac{V_0 / \phi - (V_c + V_s)}{2 \times 0.004 \times E_j \times D} \quad \text{Equation C.3}$$

A sectional analysis was used to finalize the design. Moment-curvature analysis was conducted using a layer-by-layer approach in which the cross section was discretized into layers containing concrete confined by CFRP and/or steel ties, longitudinal reinforcing steel, and CFRP. The stresses in the concrete, reinforcing steel, and CFRP in each layer were determined from the average strain in the layer and the stress-strain relationships and used to satisfy the equilibrium equations of force and moment. Equations C.4 and C.5 were used to conduct this sectional analysis.

$$P = \sum_{i=1}^n f_{ci} A_{ci} + \sum_{i=1}^n f_{si} A_{si} + \sum_{i=1}^n f_{Fi} A_{Fi} \quad \text{Equation C.4}$$

$$M = \sum_{i=1}^n f_{ci} A_{ci} d_{ci} + \sum_{i=1}^n f_{si} A_{si} d_{si} + \sum_{i=1}^n f_{Fi} A_{Fi} d_{Fi} - P \cdot \frac{h}{2} \quad \text{Equation C.5}$$

Design 2 – All the terminology used in this design can be found in Paper IV collected in this dissertation. In Design 2, the ultimate torsional strength of an RC member strengthened with externally bonded CFRP was estimated by adding the individual torsional strength contributions of the RC member and the externally bonded CFRP strengthening system as shown in Equation C.6. The contribution of the CFRP was calculated by Equations C.7-C.9.

$$T = T_{RC} + T_f \quad \text{Equation C.6}$$

$$T_f = \frac{2A_0 A_f f_{fe}}{s_f} \quad \text{Equation C.7}$$

$$N_f^e = (t_f \times 1) E_f \left(0.004 + \frac{1}{2} \left(\frac{1}{2} \varepsilon_{fu} - 0.004 \right) \right) \quad \text{Equation C.8}$$

$$\alpha_t = 0.66 + 0.33(y_1/x_1) \leq 1.5 \quad \text{Equation C.9}$$

Design 3 – Design 3 was conducted based on ACI 318 (2011). The CFRP wrap was designed to restore the shear strength from both lateral load and torque, which considered the interaction between these two effects. The longitudinal CFRP was designed to restore the flexural and torsional strength. Then, the adequacy of the repaired column was checked by considering the interaction of bending and torsion. Each of the equations listed in this section were based on ACI 318 (2011), and the terms used here are defined in the nomenclature later in this appendix.

Design of transverse CFRP

(1) Determine the shear and torsional force demand from the original test results;

Shear: V_u

Torsion: T_u

(2) Determine the shear stress from the shear and torsional force demand;

$$\text{Shear: } v_u = \frac{V_u}{bd} \quad \text{Equation C.10}$$

$$\text{Torsion: } v_{tu} = \frac{T_u}{\frac{1}{3}b^3} \quad \text{Equation C.11}$$

To ensure that under combined torsion and shear a diagonal concrete compression failure is preceded by yielding of the web reinforcement, it is essential to set an upper limit to the combined load. Therefore, maximum allowable nominal combined stresses were checked using the Equation C.12.

$$v_{u,\max} \leq \frac{10\sqrt{f'_c}}{\sqrt{[1 + (v_{tu} / 1.2v_u)^2]}} \quad \text{Equation C.12}$$

The permissible nominal ultimate shear stress that can be carried by the concrete alone in the presence of torsion was calculated by Equation C.13.

$$v_c = \frac{2.0\sqrt{f'_c}}{\sqrt{[1 + (v_{tu} / 1.2v_u)^2]}} \quad \text{Equation C.13}$$

The permissible nominal ultimate torsional stress that can be carried by the concrete alone v_{tc} is related to the calculated v_c by Equation C.14.

$$\frac{v_{tu}}{v_u} = \frac{v_{tc}}{v_c} \quad \text{Equation C.14}$$

(3) Calculate the web reinforcement for shear and torsion;

Transverse reinforcement required for shear resistance was calculated by Equations C.15 and C.16.

$$v_u = v_c + v_s \quad \text{Equation C.15}$$

$$A_v = \frac{sb}{f_f} v_s \quad \text{Equation C.16}$$

Transverse reinforcement required to resist torsion was calculated by Equations C.17, C.18, and C.19.

$$A_t = \frac{T_f s}{\alpha_t f_f d^2} \quad \text{Equation C.17}$$

$$\alpha_t = 0.66 + 0.33 \quad \text{Equation C.18}$$

$$T_f = (v_{tu} - v_{tc}) \frac{b^3}{3} \quad \text{Equation C.19}$$

(4) The total transverse reinforcement needed is the sum of the amounts needed for shear and torsion, which can be calculated using Equation C.20.

$$A_{t,total} = \frac{1}{2} A_v + A_t \quad \text{Equation C.20}$$

This design, considering the combination of torsion and shear, could have been obtained with the aid of an interaction chart such as the one shown in Figure C.2, which was constructed to demonstrate the interaction of the ACI code more clearly. The chart indicates the combination of ultimate shear and torsion that could be carried by a section for various reinforcement contents.

Design of longitudinal CFRP

- (1) Estimate the longitudinal CFRP needed to resist flexural moment A_{lb} ;

A sectional analysis was used to determine the longitudinal CFRP required to resist the flexural moment, in which the damaged reinforcement and the confinement effect from the designed transverse CFRP were considered.

- (2) Calculate the longitudinal CFRP needed for torsion;

The ACI 318 design equation for stirrups to resist torsion is based on the condition that at least an equal amount of longitudinal bars will be provided, therefore, Equation C.21 was used to calculate the longitudinal CFRP needed to resist torsion.

$$A_{lt} = 2A_t \frac{2d}{s} \quad \text{Equation C.21}$$

- (3) The total longitudinal CFRP needed was taken as the sum of the CFRP needed to resist flexural moment and torsional moment as shown in Equation C.22;

$$A_{l,total} = A_{lb} + A_{lt} \quad \text{Equation C.22}$$

- (4) Check the adequacy of the repaired column by considering the interaction of bending and torsion.

Based on the designed transverse and longitudinal CFRP, the flexural and torsional capacity of the repaired columns was obtained. Then, an interpolated parabolic interaction relationship for pure torsion and pure flexure was used to check the adequacy using Equation C.23..

$$\left(\frac{T_u}{T_{uo}} \right)^2 = 1 - \frac{M_u}{M_{uo}} \quad \text{Equation C.23}$$

NOMENCLATURE

- A_{lb} Longitudinal CFRP required to resist bending moment
 A_{lt} Longitudinal CFRP required to resist torsional moment
 $A_{l,total}$ Total longitudinal CFRP required to resist bending and torsional moments
 A_t Area of transverse CFRP required to resist torsion

A_v	Area of CFRP as shear reinforcement
b	Cross-sectional width of the column
d	Distance from the column face to the centroid of longitudinal tension reinforcement
f'_c	Specified compressive strength of concrete, psi
f_f	Tensile strength of the CFRP
M_u	Maximum bending moment resisted by the original column
M_{uo}	Calculated flexural moment capacity of the repaired column
V_u	Maximum shear force resisted by the original column
s	Center spacing of the CFRP sheets
T_f	Nominal torsional strength provided by CFRP
T_u	Maximum torsional moment resisted by the original column
T_{uo}	Calculated torsional capacity of the repaired column
v_c	Shear strength provided by concrete
v_s	Shear strength provided by shear reinforcement
v_{tc}	Torsional strength provided by concrete
v_{tu}	Normal shear stress calculated from T_u
v_u	Normal shear stress calculated from V_u
$v_{u,max}$	Maximum allowable nominal shear strength under combined torsion and shear
α_t	Factor considering the dimension of the cross section

Table C.1. Repair design methodology categories

	Design Action			
	Axial	Shear	Bending	Torsion
Design 1(Column 1)	×	×	×	
Design 2 (Column 5)	×			×
Design 3 (Columns 2, 3, & 4)	×	×	×	×

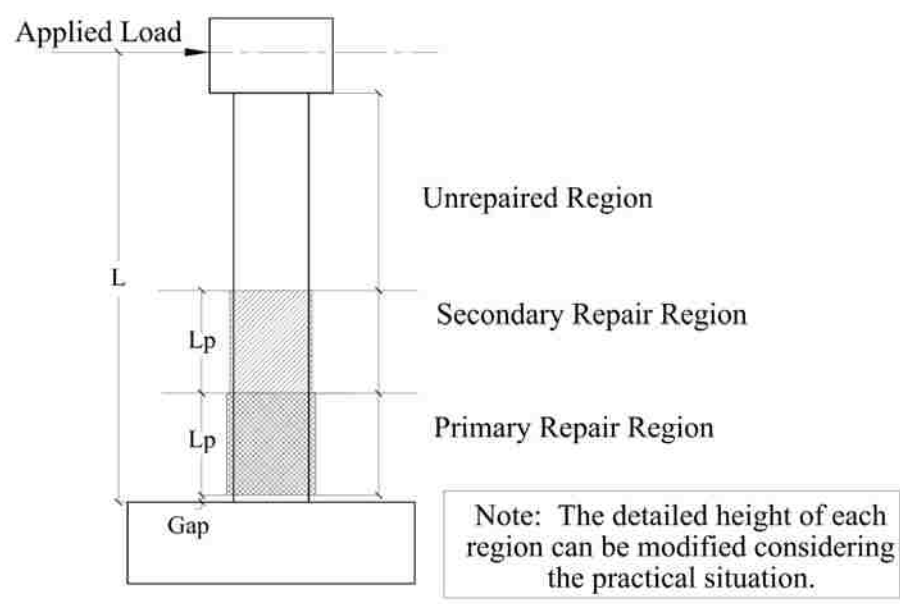


Figure C.1. General concept for repair design

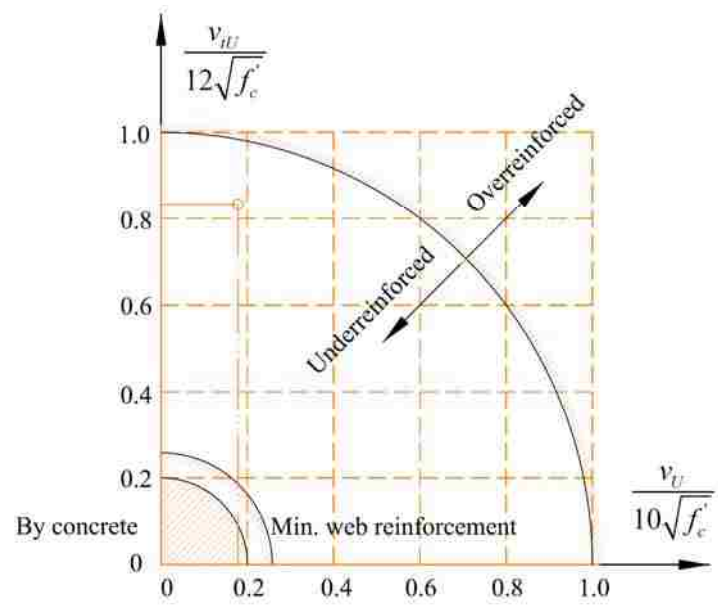


Figure C.2. An interaction diagram for shear and torsion

APPENDIX D
CFRP SURFACE STRAIN ANALYSIS

This appendix provides the CFRP surface strain analysis for the five repaired columns. Locations of the strain gauges applied on each column are shown in Figures D.1-D.5, and the time history of the strain during the cyclic loading in both transverse and longitudinal directions is shown in Figures D.6-D.56.

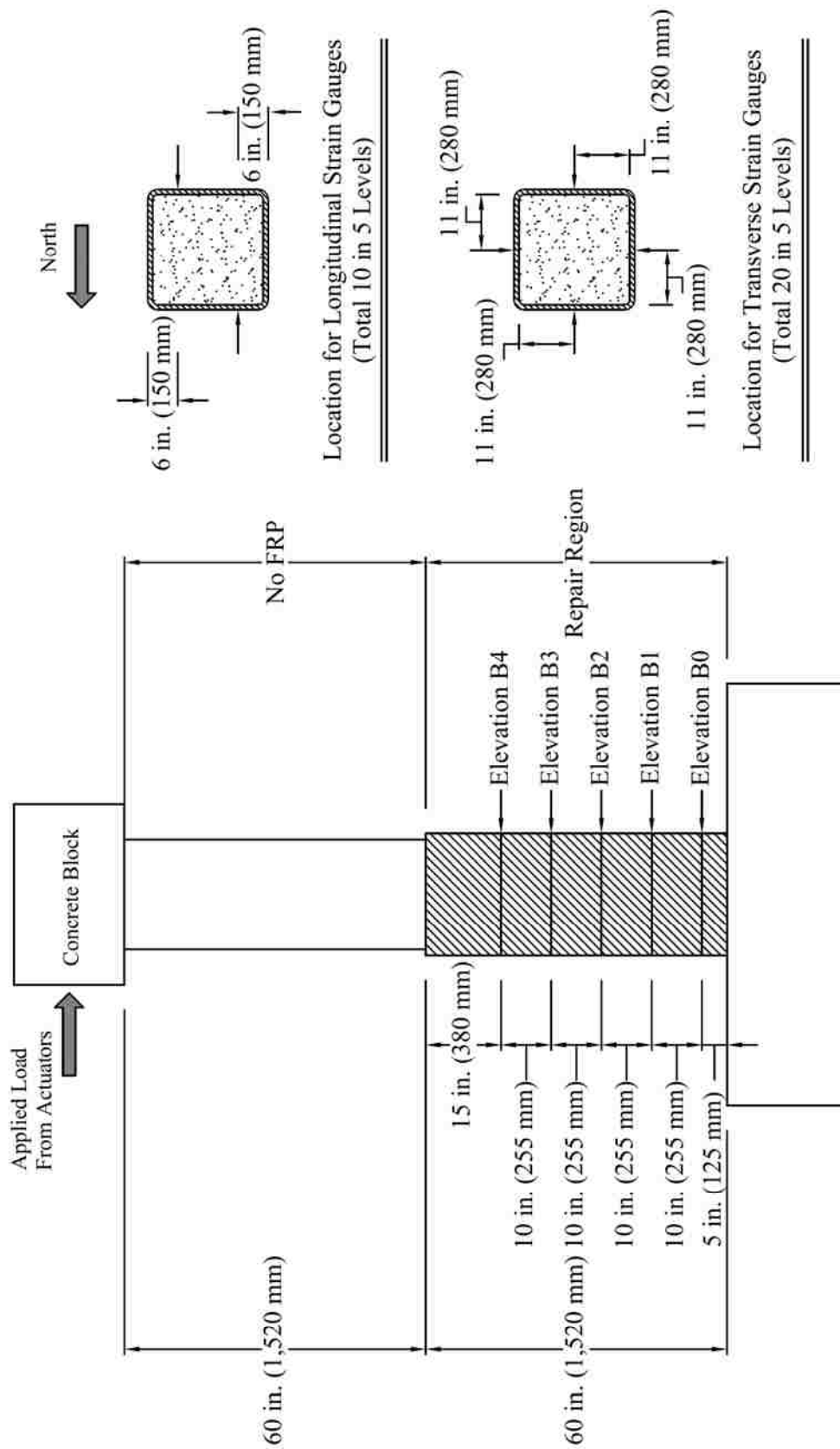


Figure D.1. Location of the strain gauges on CFRP on Column I-R (T/M=0)

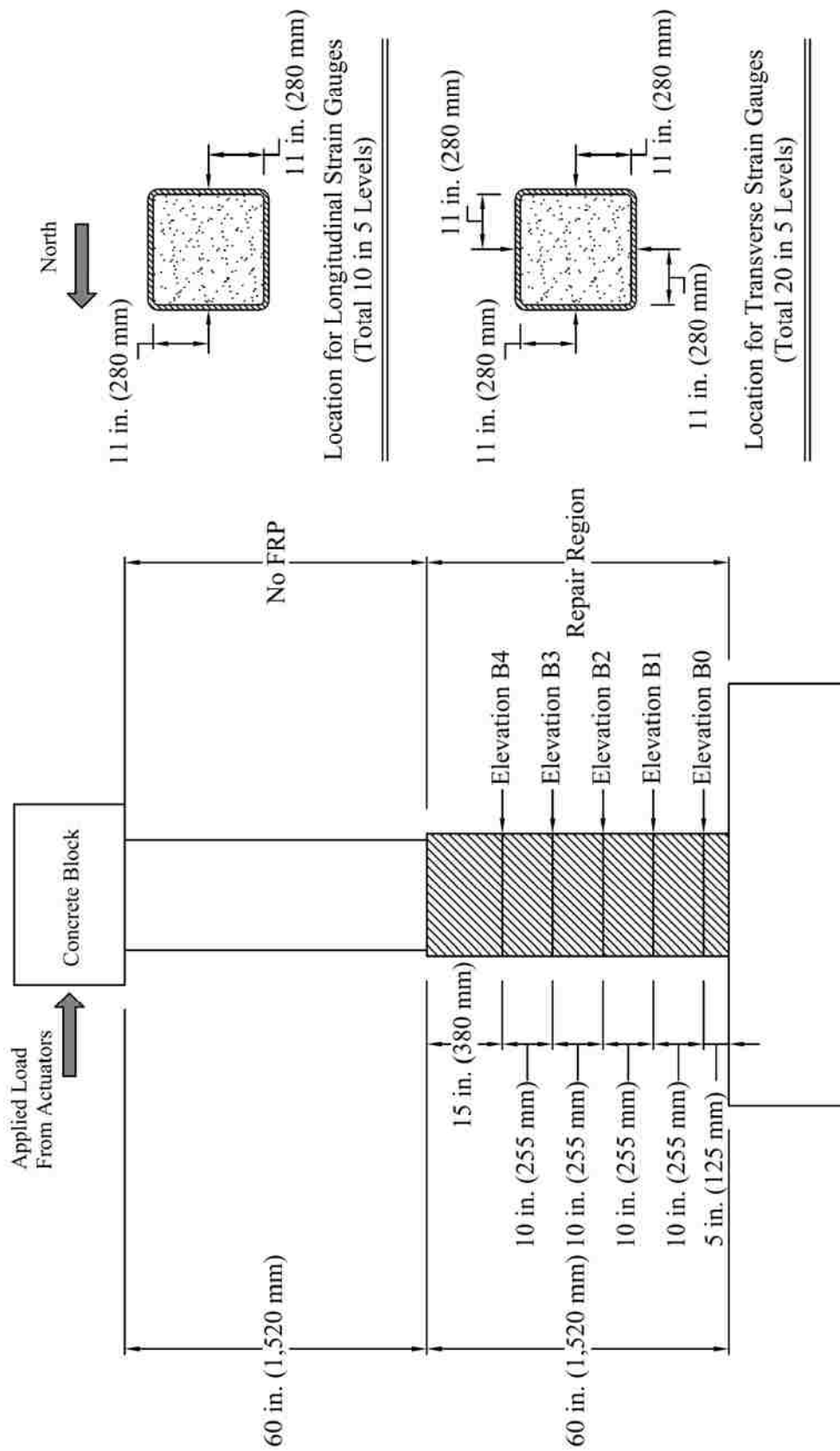


Figure D.2. Location of the strain gauges on CFRP on Column 2-R (T/M=0.2)

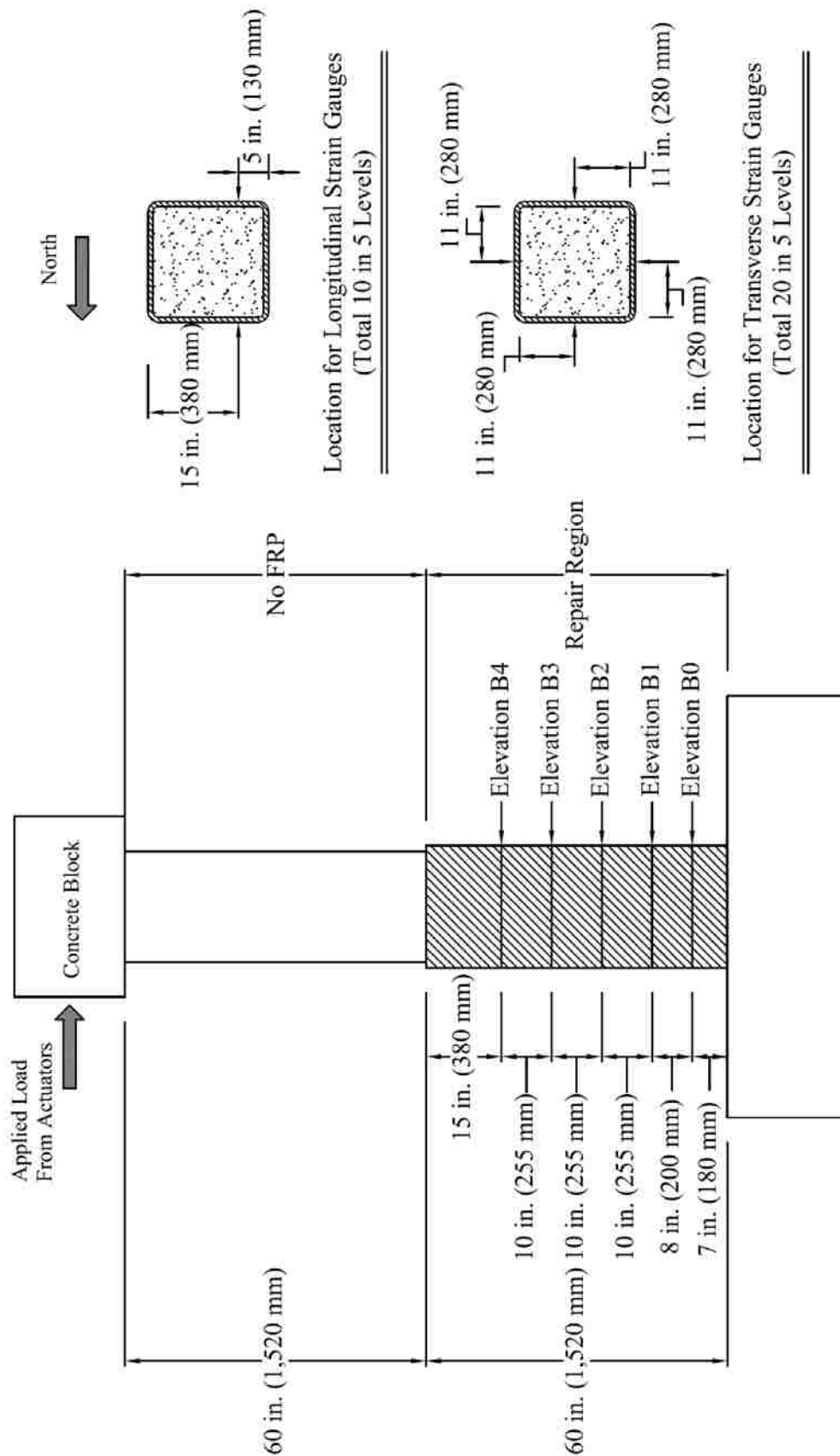
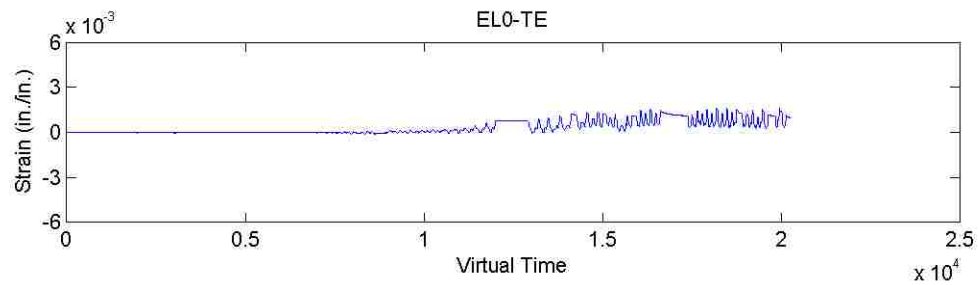
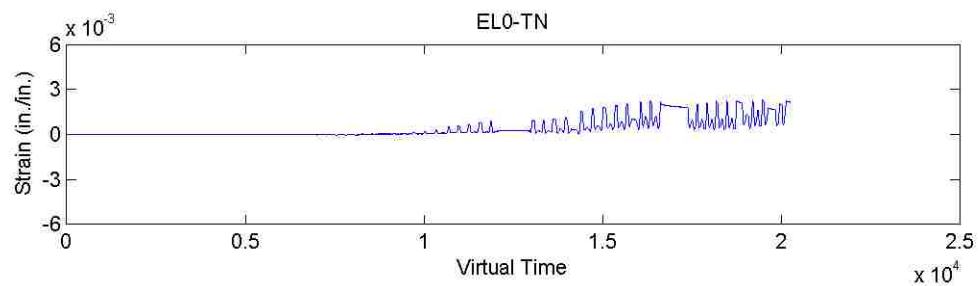


Figure D.3. Location of the strain gauges on CFRP on Column 3-R (T/M=0.4)

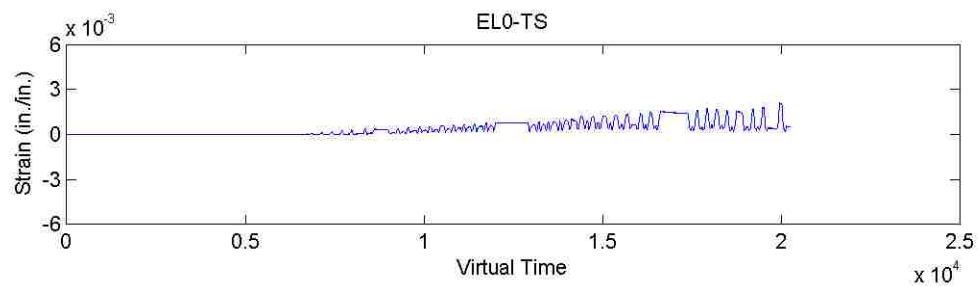
Strain Data for Column 1-R (T/M=0)



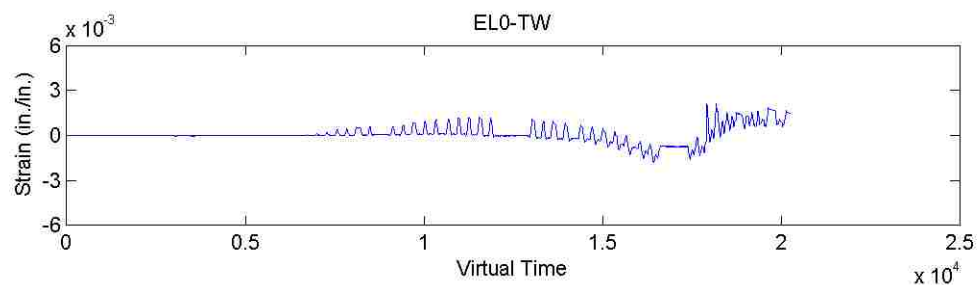
(a) East side of the column



(b) North side of the column

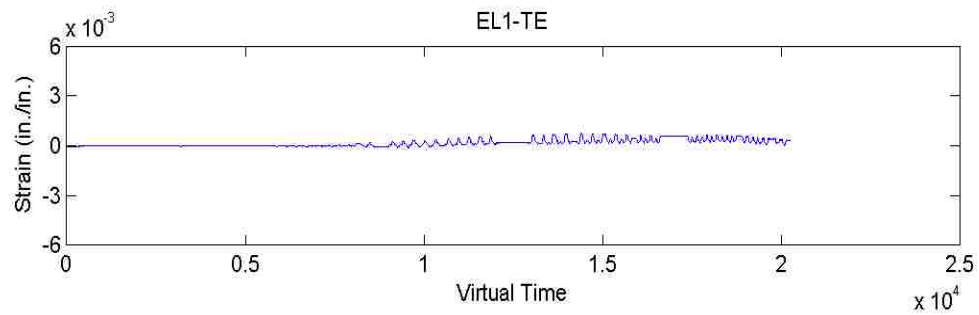


(c) South side of the column

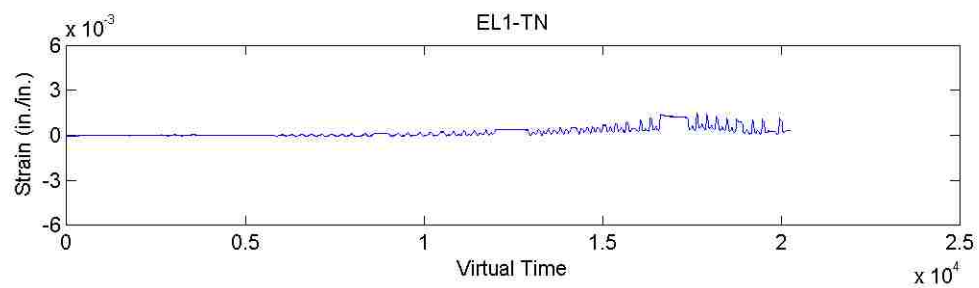


(d) West side of the column

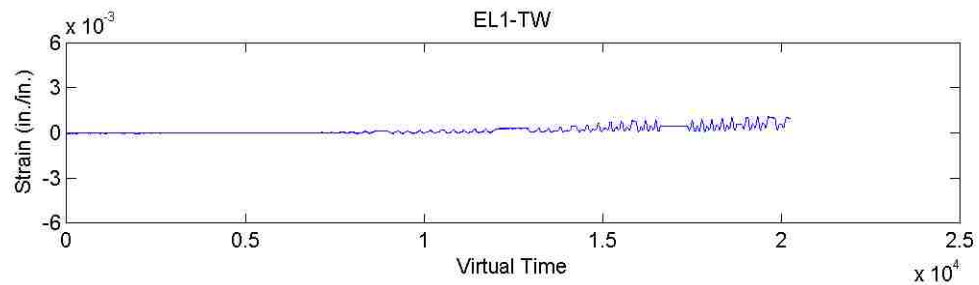
Figure D.6. Transverse strain in CFRP at 1st level of Column 1-R (T/M=0)



(a) East side of the column

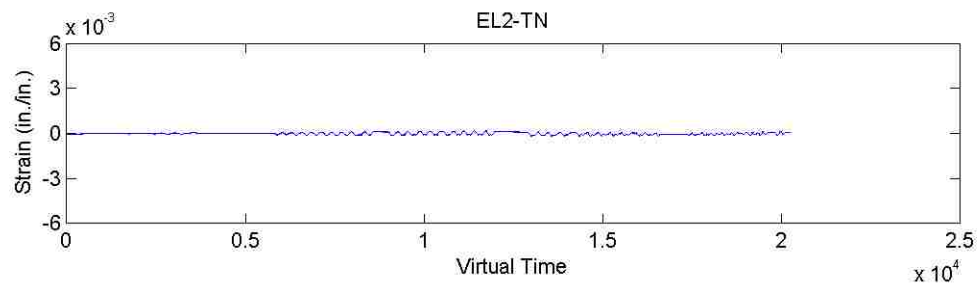


(b) North side of the column

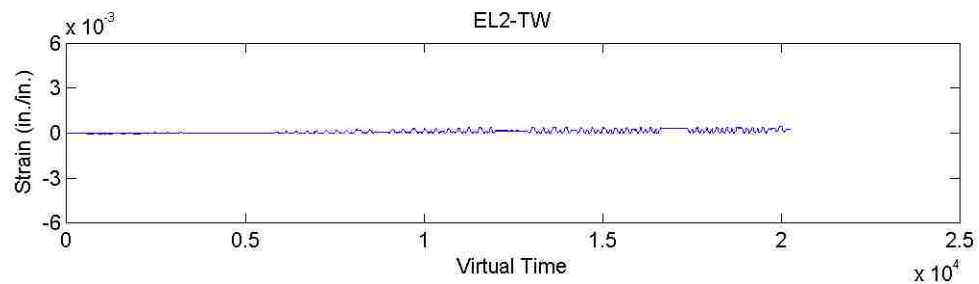


(c) West side of the column

Figure D.7. Transverse strain in CFRP at 2nd level of Column 1-R (T/M=0)

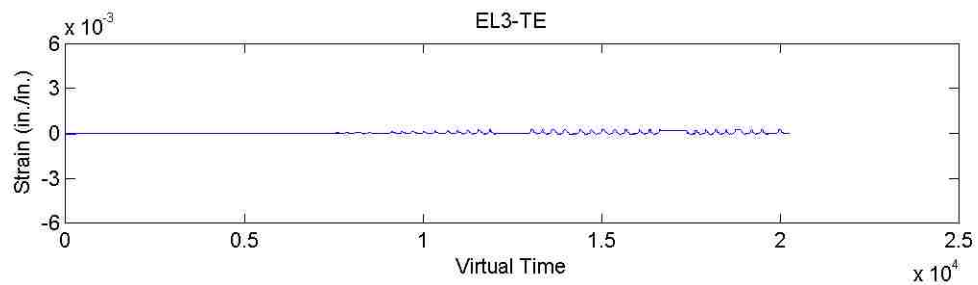


(a) North side of the column

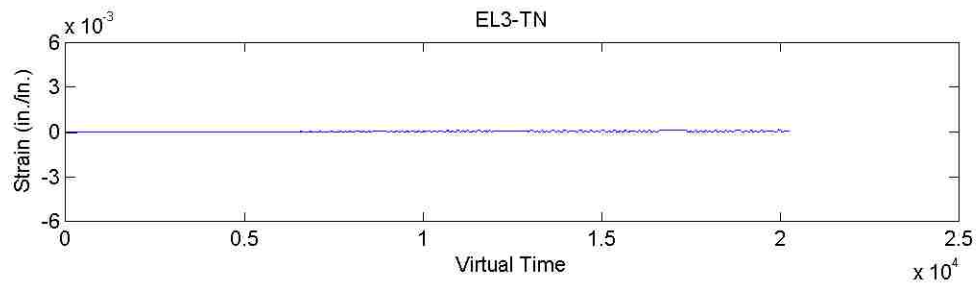


(b) West side of the column

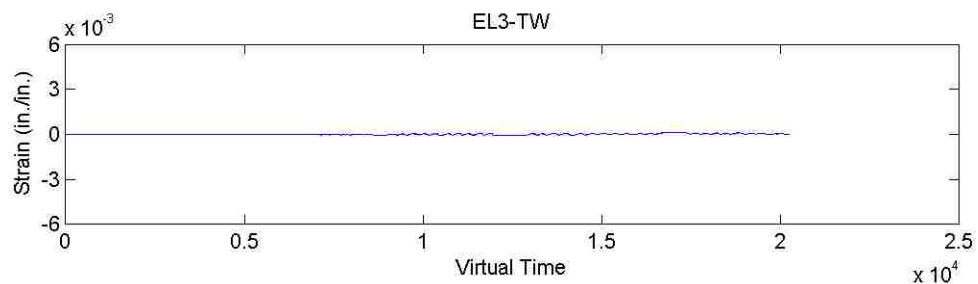
Figure D.8. Transverse strain in CFRP at 3rd level of Column 1-R (T/M=0)



(a) East side of the column

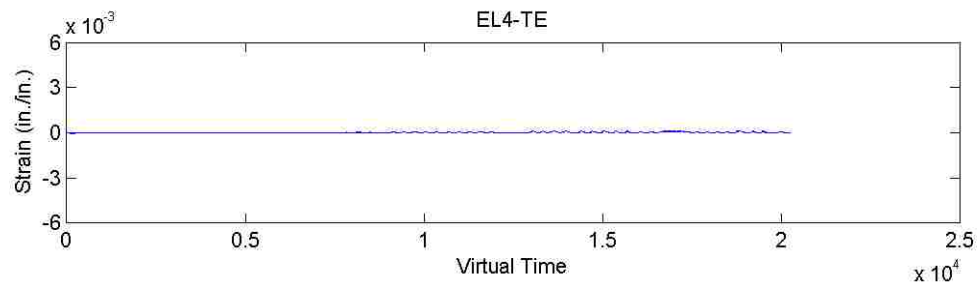


(b) North side of the column

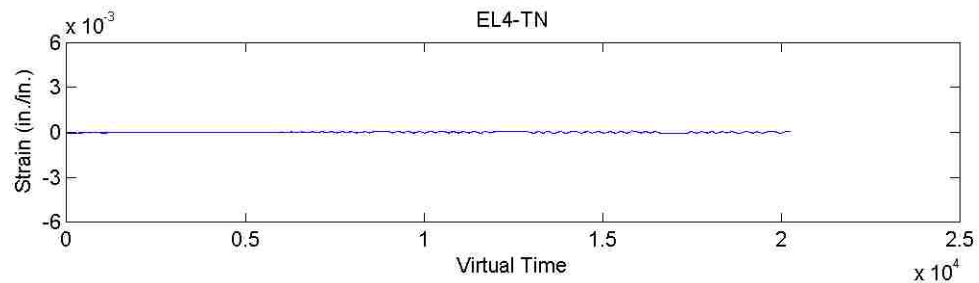


(c) West side of the column

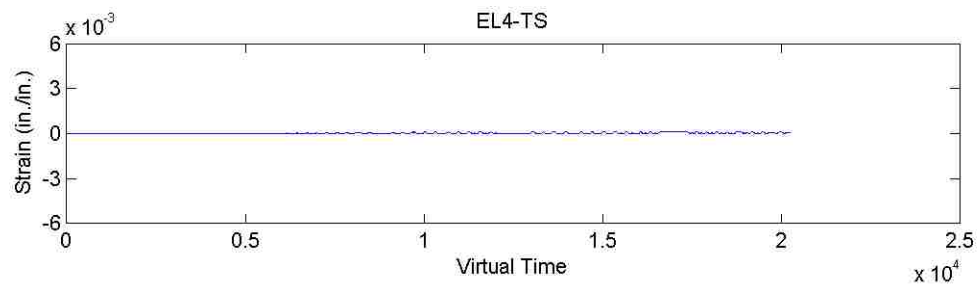
Figure D.9. Transverse strain in CFRP at 4th level of Column 1-R (T/M=0)



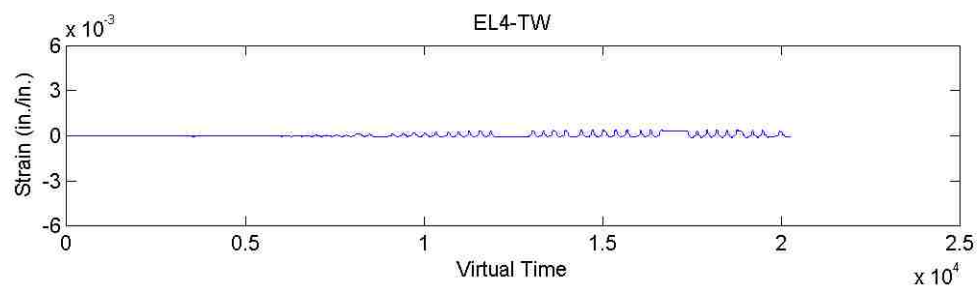
(a) East side of the column



(b) North side of the column

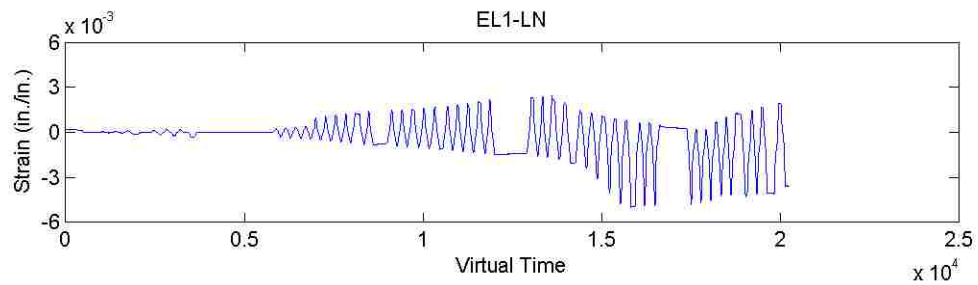


(c) South side of the column

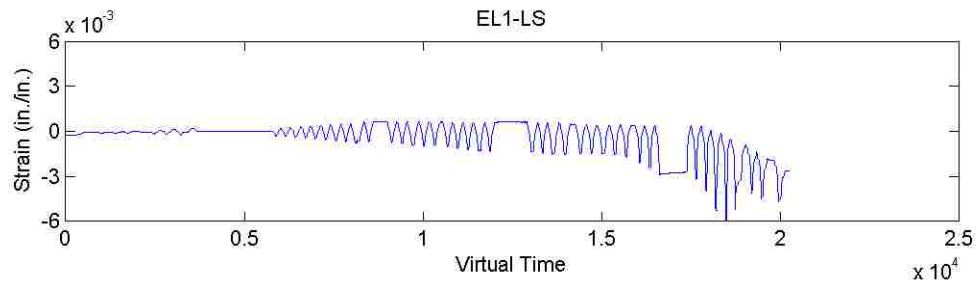


(d) West side of the column

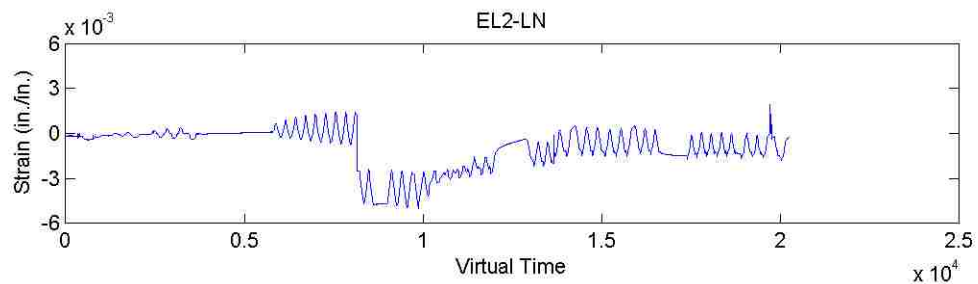
Figure D.10. Transverse strain in CFRP at 5th level of Column 1-R (T/M=0)



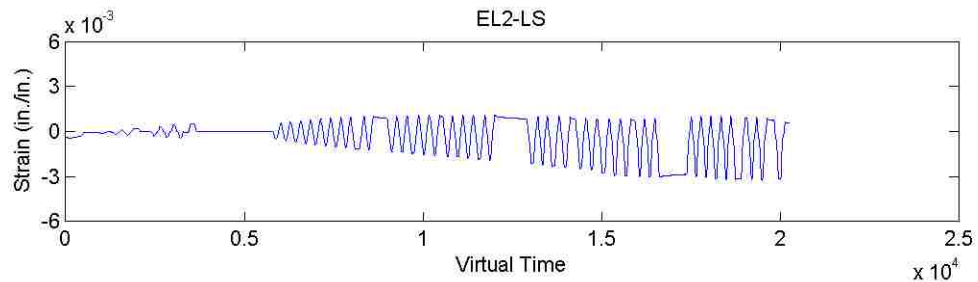
(a) North side of the column



(b) South side of the column

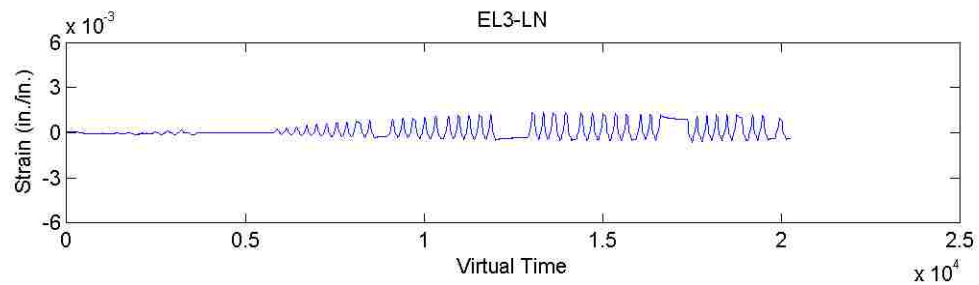
Figure D.11. Longitudinal strain in CFRP at 2nd level of Column 1-R (T/M=0)

(a) North side of the column

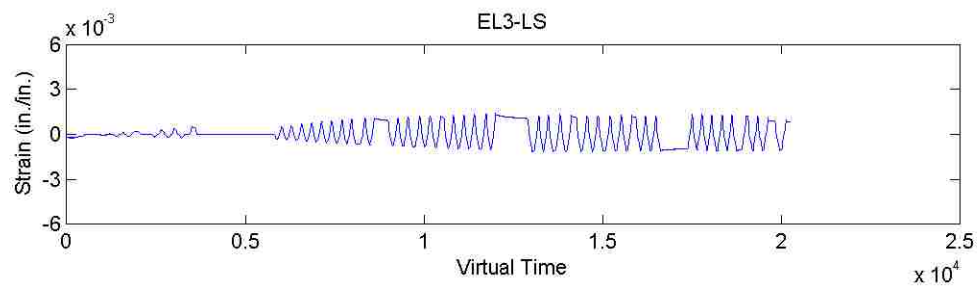


(b) South side of the column

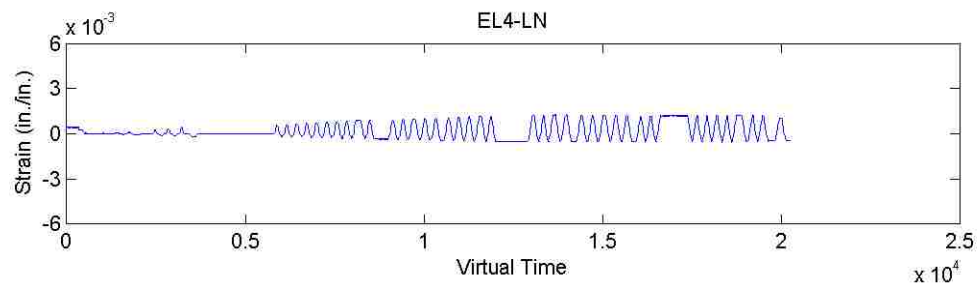
Figure D.12. Longitudinal strain in CFRP at 3rd level of Column 1-R (T/M=0)



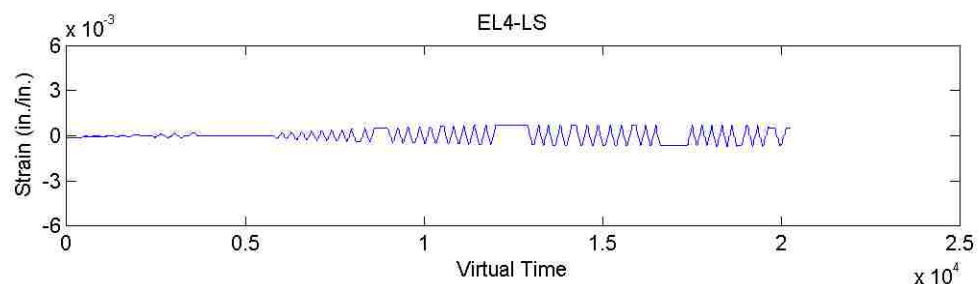
(a) North side of the column



(b) South side of the column

Figure D.13. Longitudinal strain in CFRP at 4th level of Column 1-R (T/M=0)

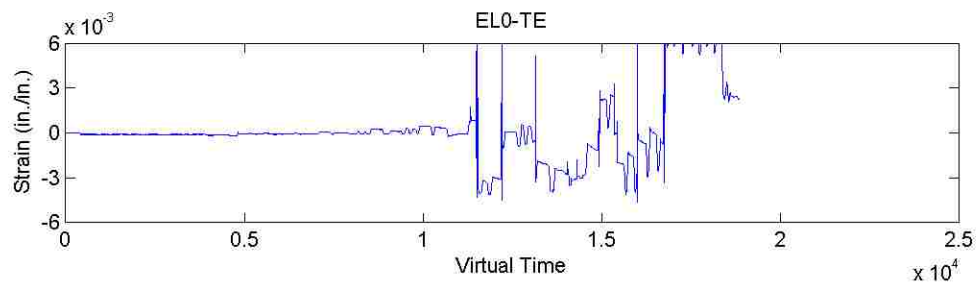
(a) North side of the column



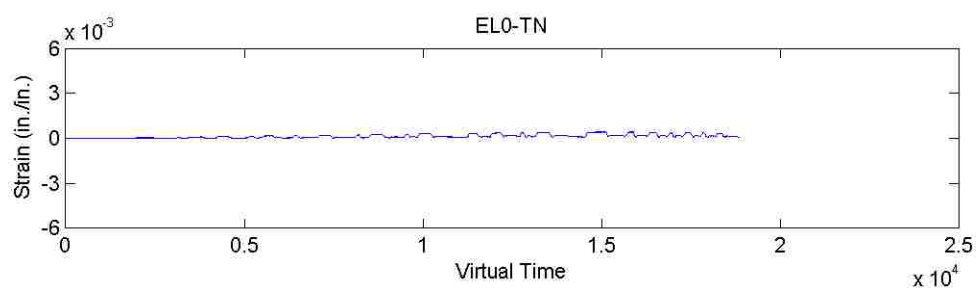
(b) South side of the column

Figure D.14. Longitudinal strain in CFRP at 5th level of Column 1-R (T/M=0)

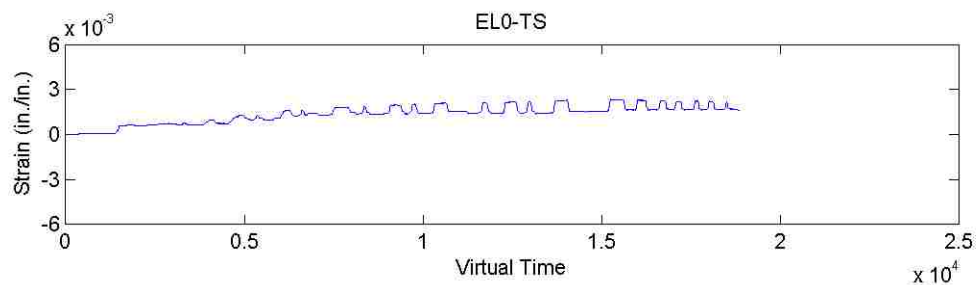
Strain Data for Column 2-R (T/M=0.2)



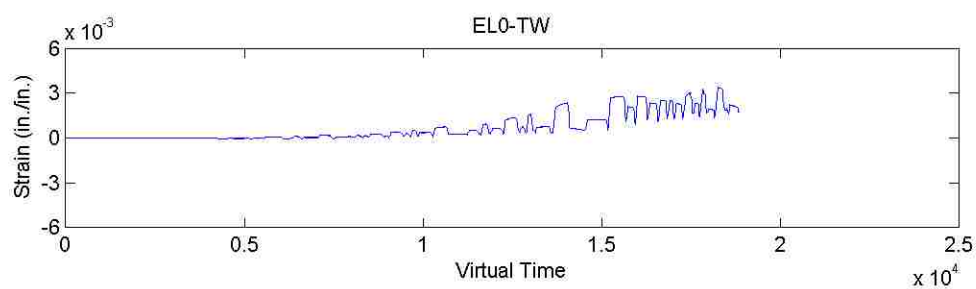
(a) East side of the column



(b) North side of the column

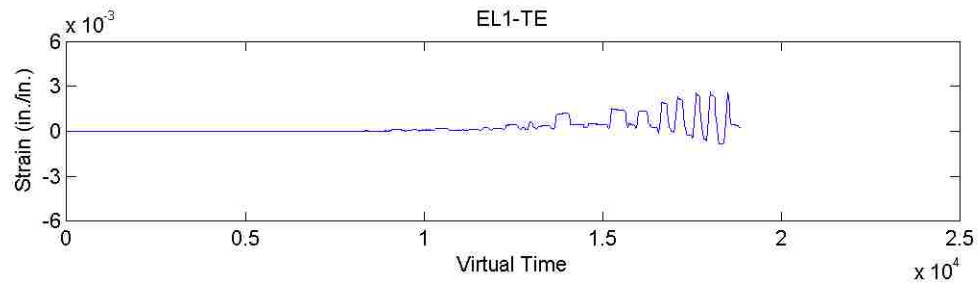


(c) South side of the column

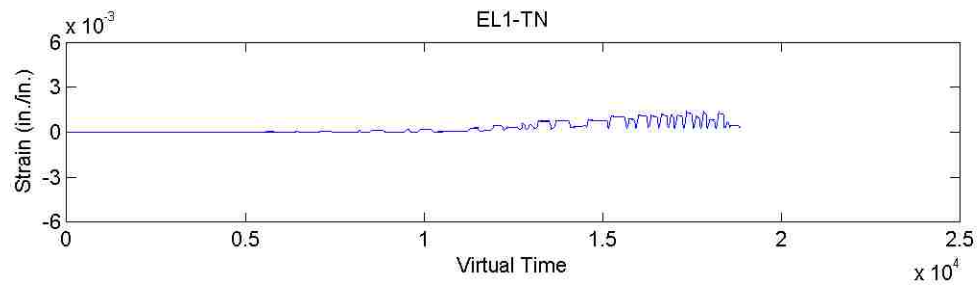


(d) West side of the column

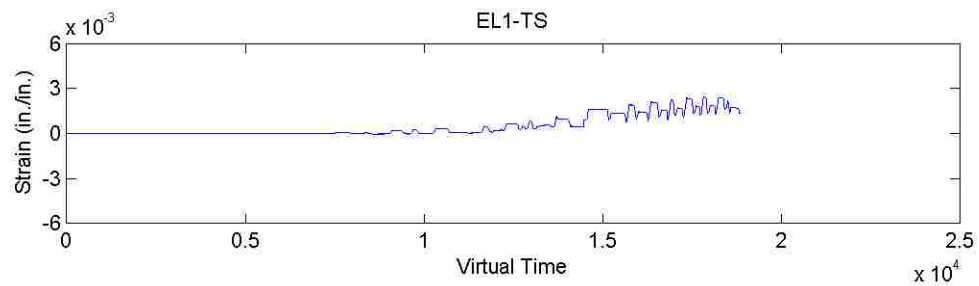
Figure D.15. Transverse strain in CFRP at 1st level of Column 2-R (T/M=0.2)



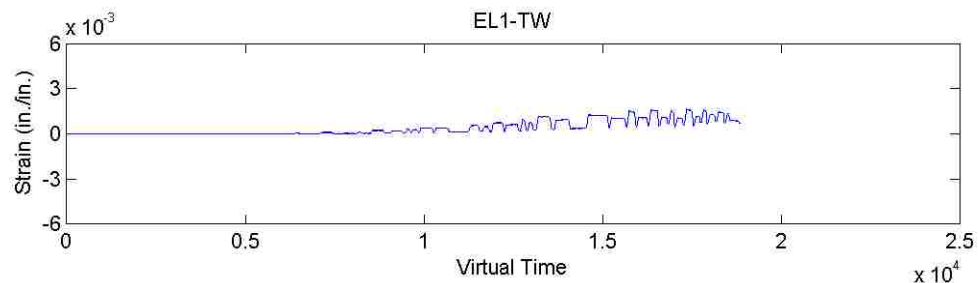
(a) East side of the column



(b) North side of the column

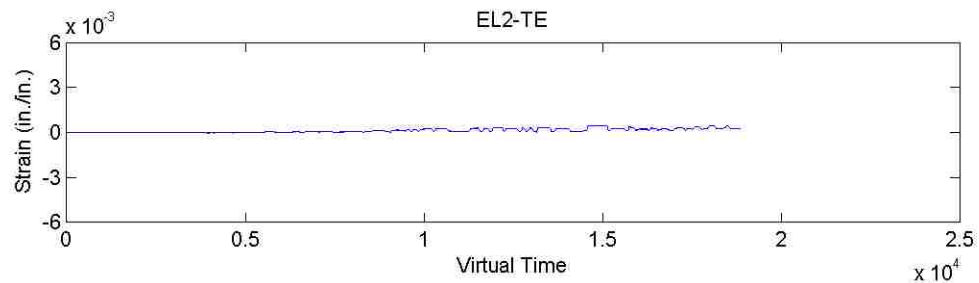


(c) South side of the column

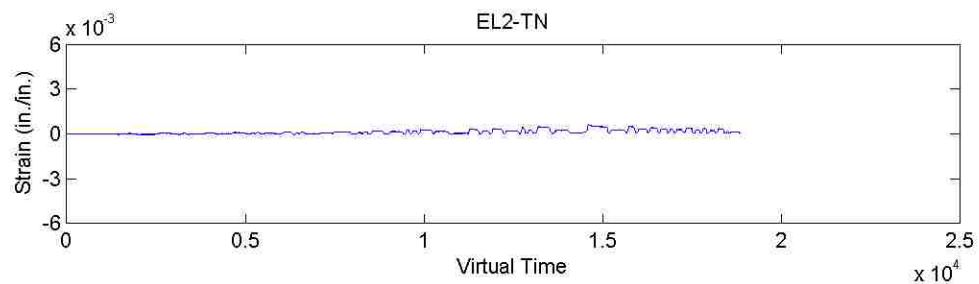


(d) West side of the column

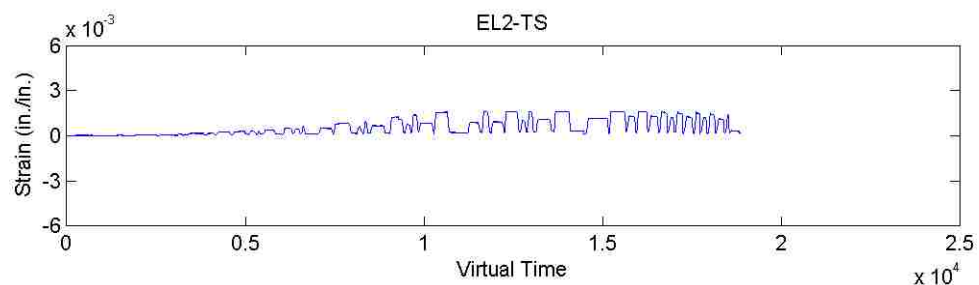
Figure D.16. Transverse strain in CFRP at 2nd level of Column 2-R (T/M=0.2)



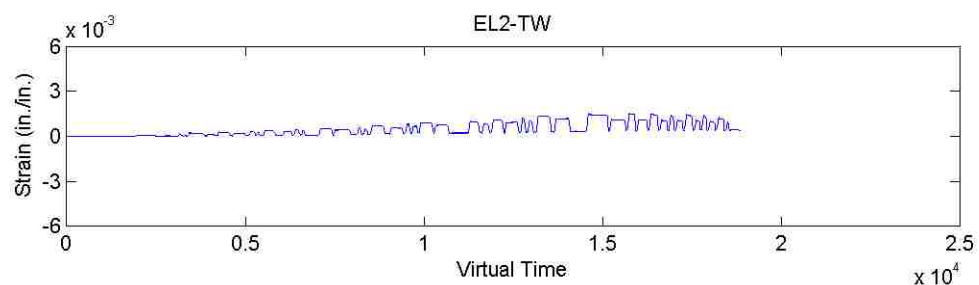
(a) East side of the column



(b) North side of the column

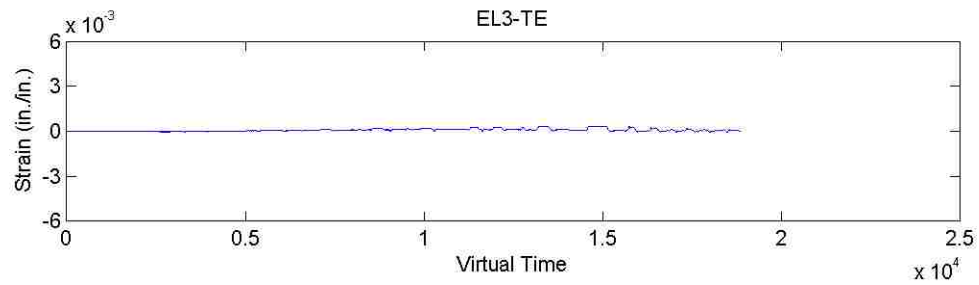


(c) South side of the column

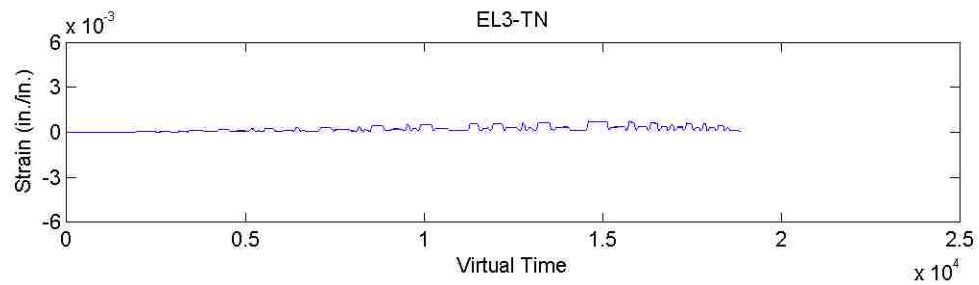


(d) West side of the column

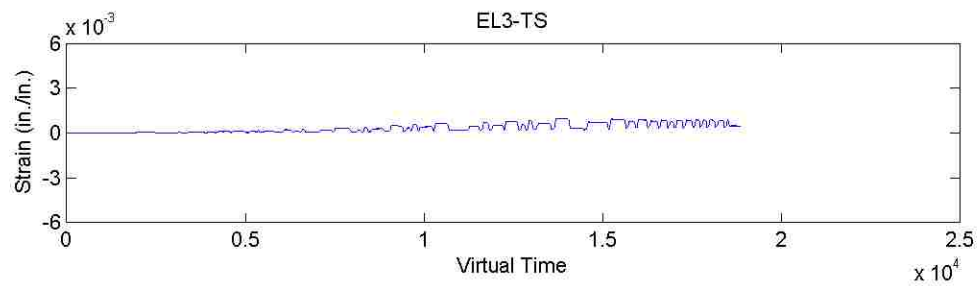
Figure D.17. Transverse strain in CFRP at 3rd level of Column 2-R (T/M=0.2)



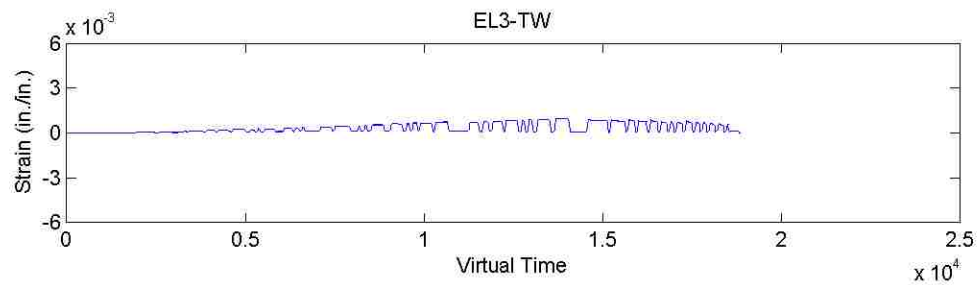
(a) East side of the column



(b) North side of the column

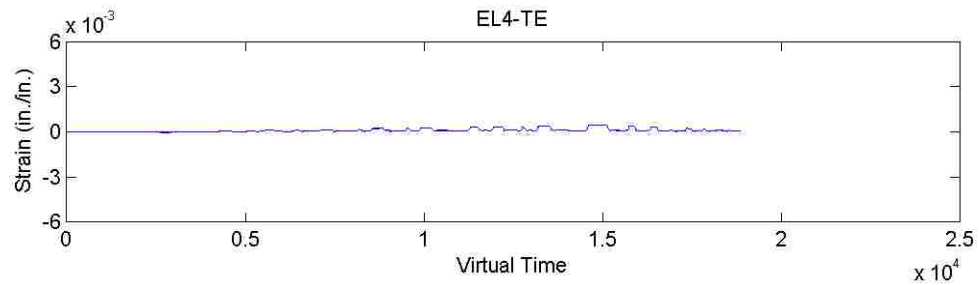


(c) South side of the column

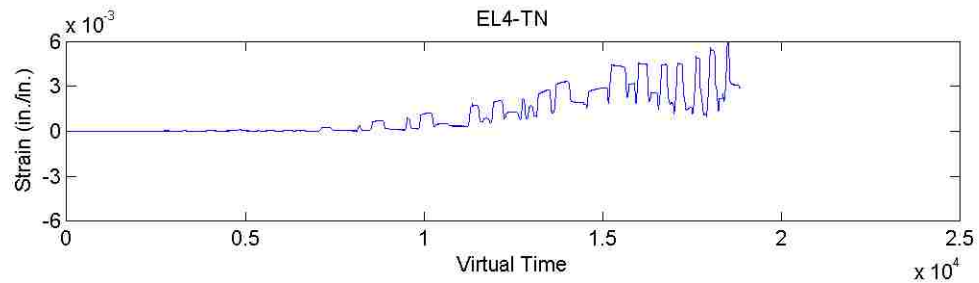


(d) West side of the column

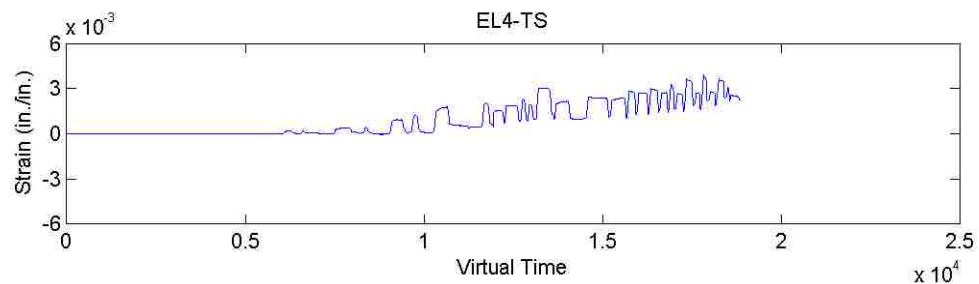
Figure D.18. Transverse strain in CFRP at 4th level of Column 2-R (T/M=0.2)



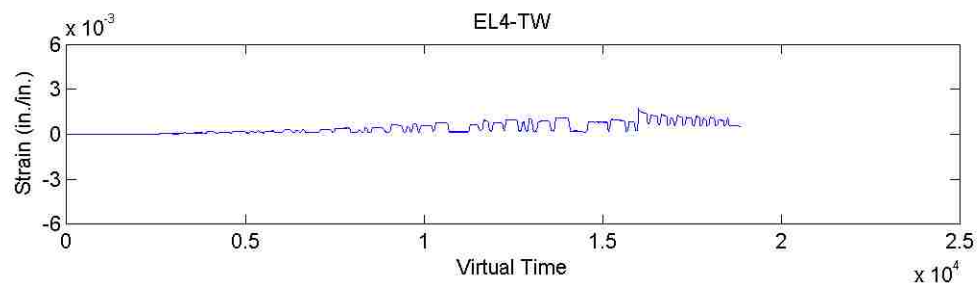
(a) East side of the column



(b) North side of the column

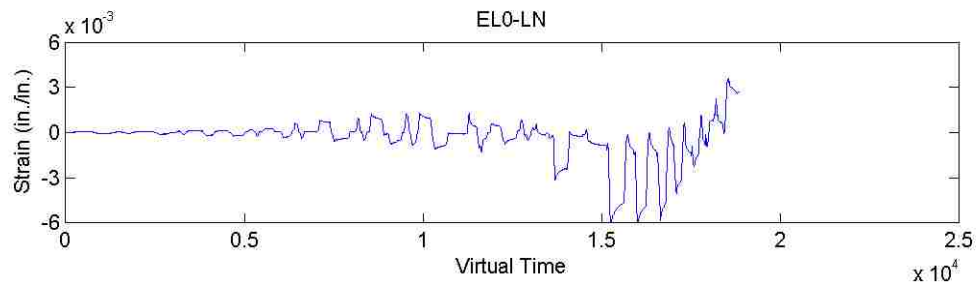


(c) South side of the column

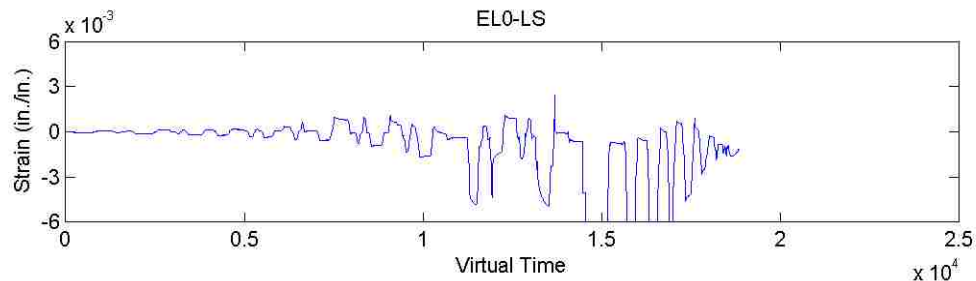


(d) West side of the column

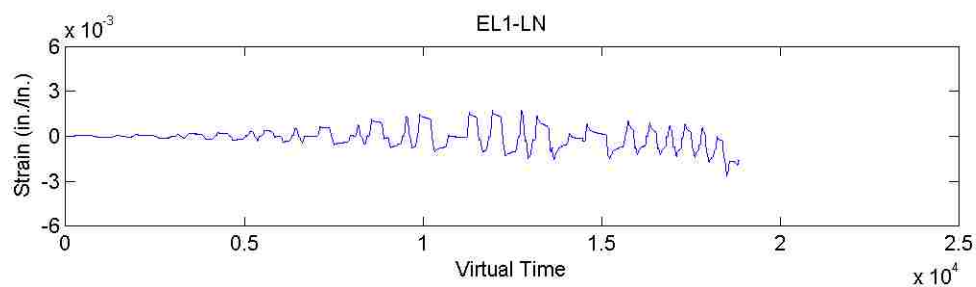
Figure D.19. Transverse strain in CFRP at 5th level of Column 2-R (T/M=0.2)



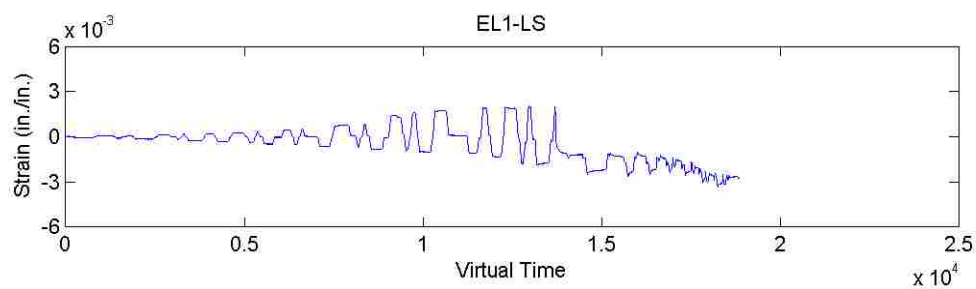
(a) North side of the column



(b) South side of the column

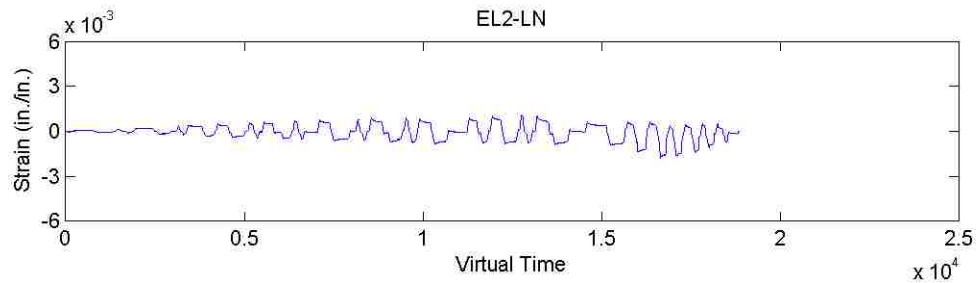
Figure D.20. Longitudinal strain in CFRP at 1st level of Column 2-R (T/M=0.2)

(a) North side of the column

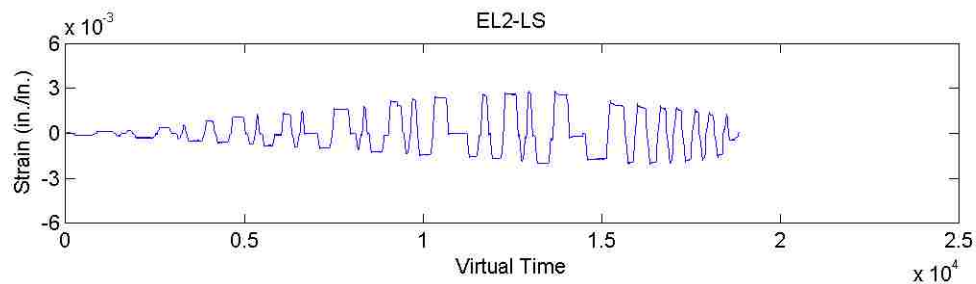


(b) South side of the column

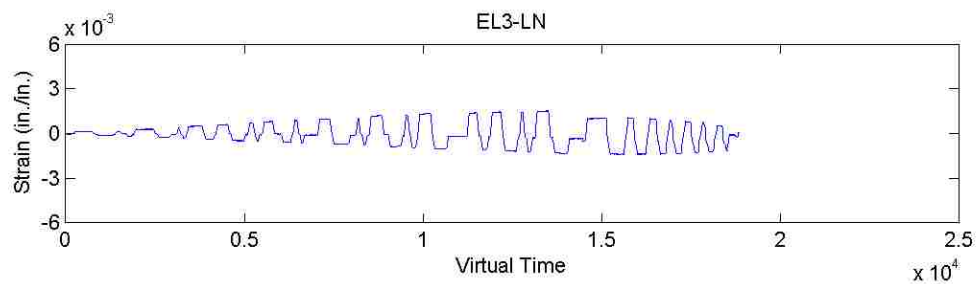
Figure D.21. Longitudinal strain in CFRP at 2nd level of Column 2-R (T/M=0.2)



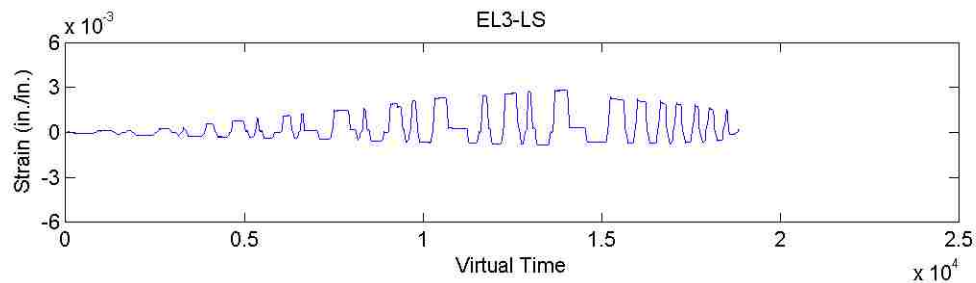
(a) North side of the column



(b) South side of the column

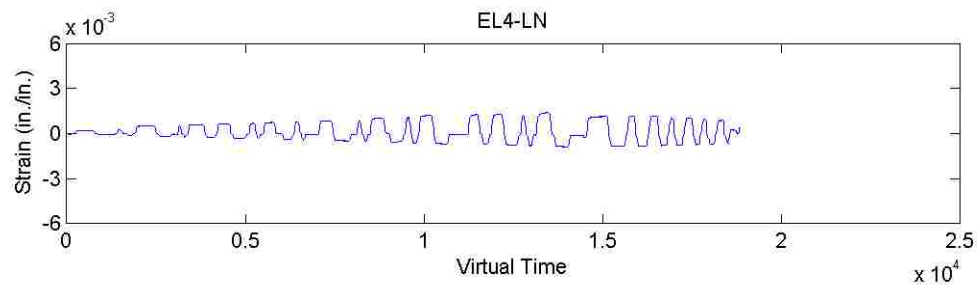
Figure D.22. Longitudinal strain in CFRP at 3rd level of Column 2-R (T/M=0.2)

(a) North side of the column

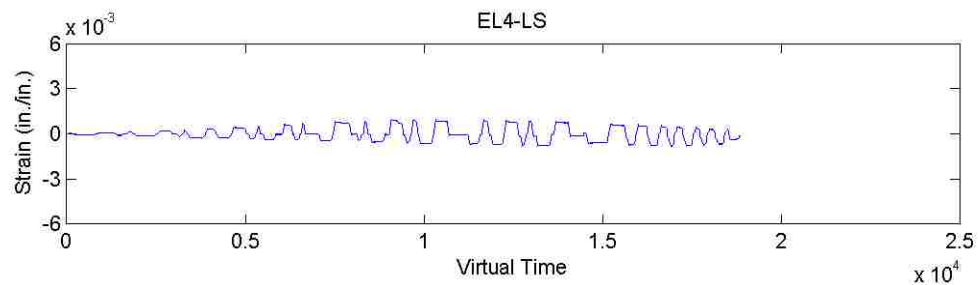


(b) South side of the column

Figure D.23. Longitudinal strain in CFRP at 4th level of Column 2-R (T/M=0.2)



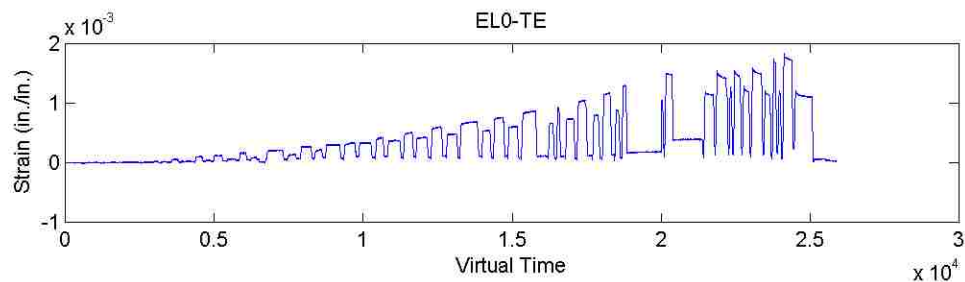
(a) North side of the column



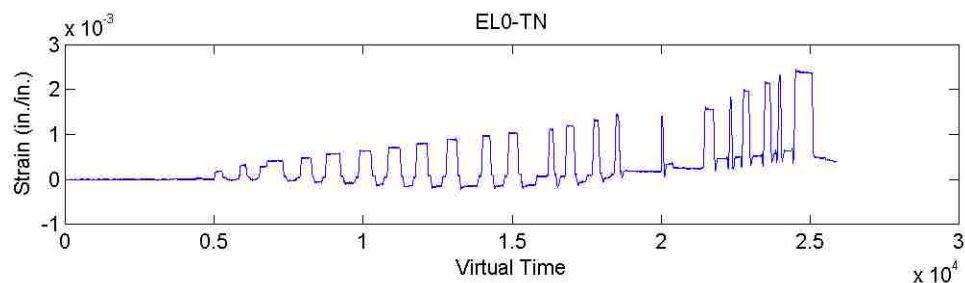
(b) South side of the column

Figure D.24. Longitudinal strain in CFRP at 5th level of Column 2-R (T/M=0.2)

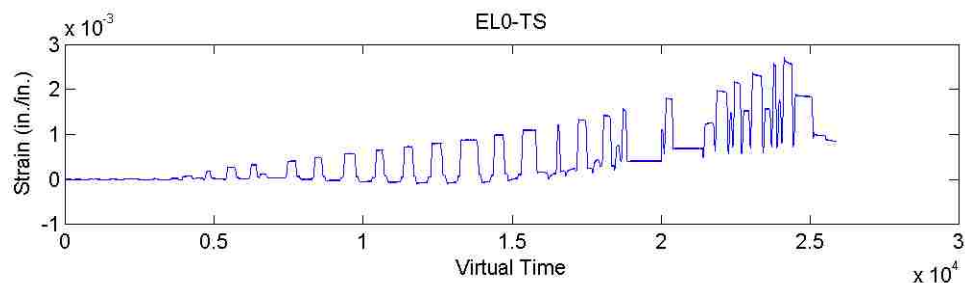
Strain Data for Column 3-R (T/M=0.4)



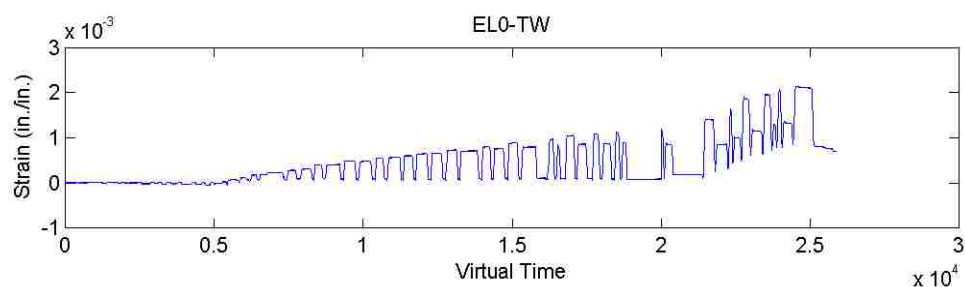
(a) East side of the column



(b) West side of the column



(c) South side of the column



(d) West side of the column

Figure D.25. Transverse strain in CFRP at 1st level of Column 3-R (T/M=0.4)

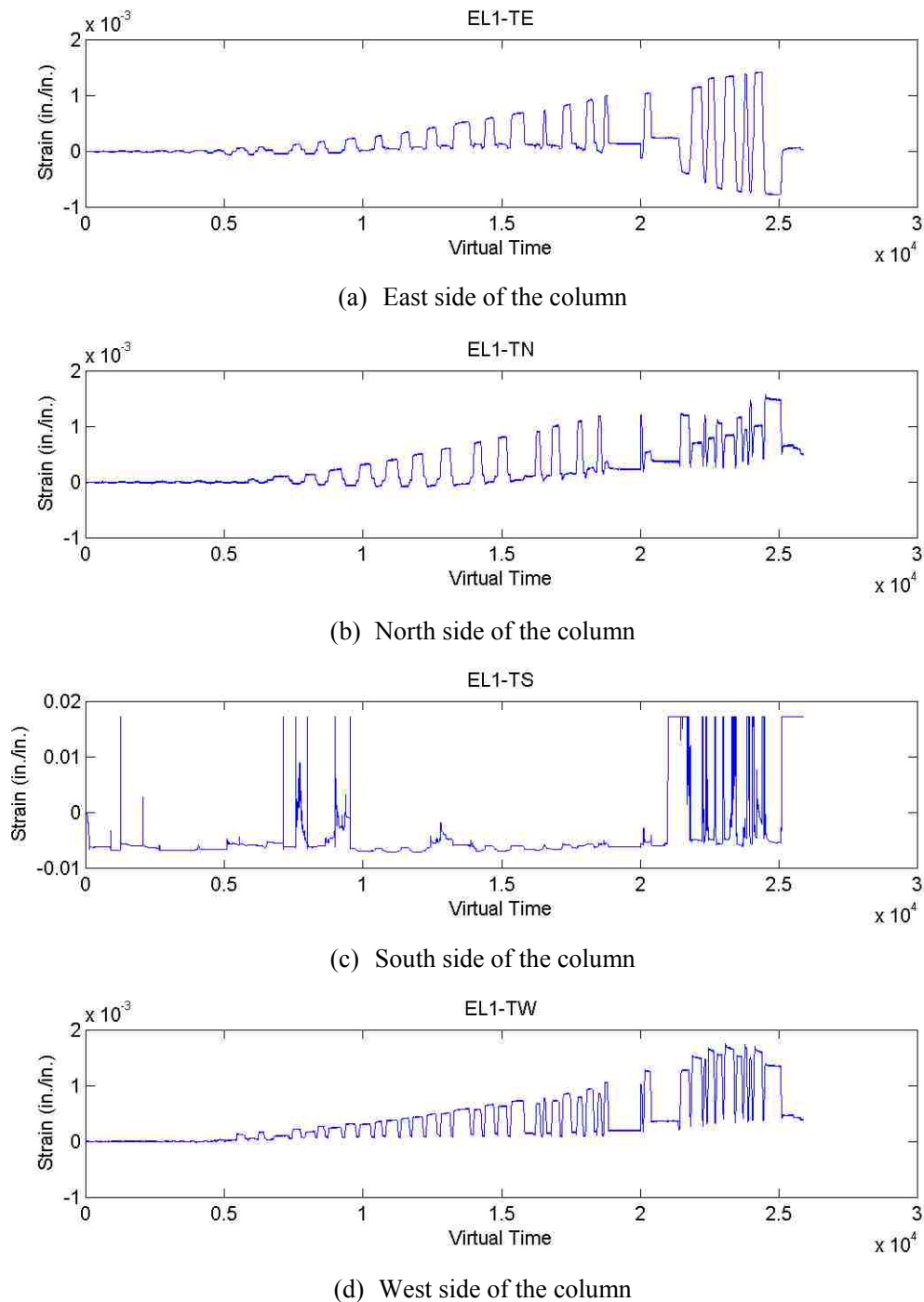


Figure D.26. Transverse strain in CFRP at 2nd level of Column 3-R (T/M=0.4)

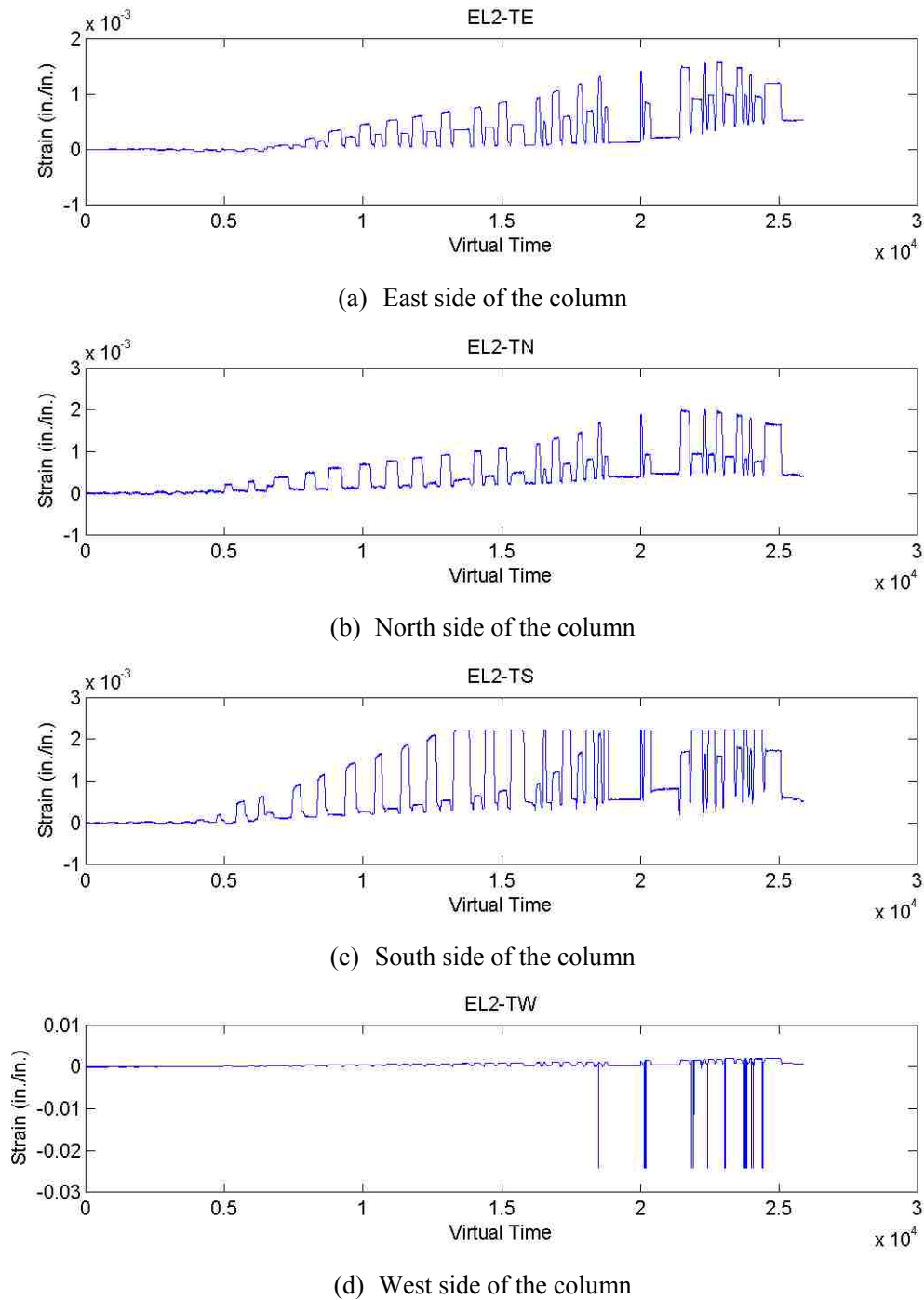
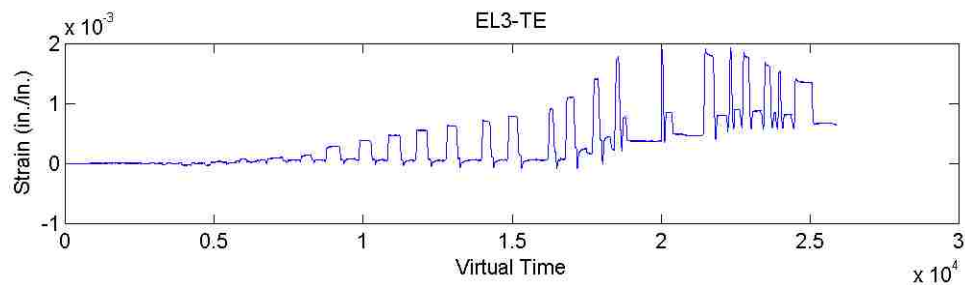
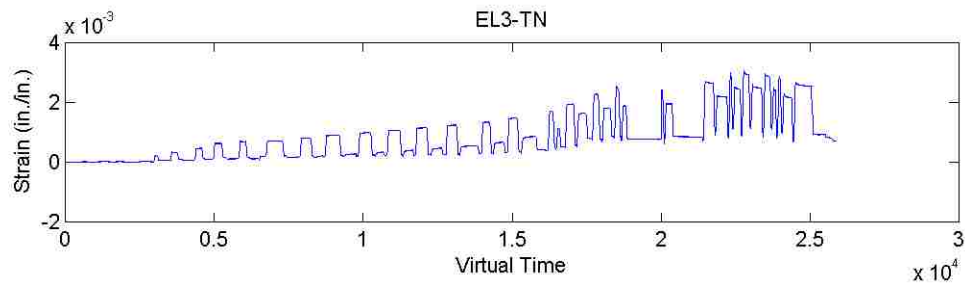


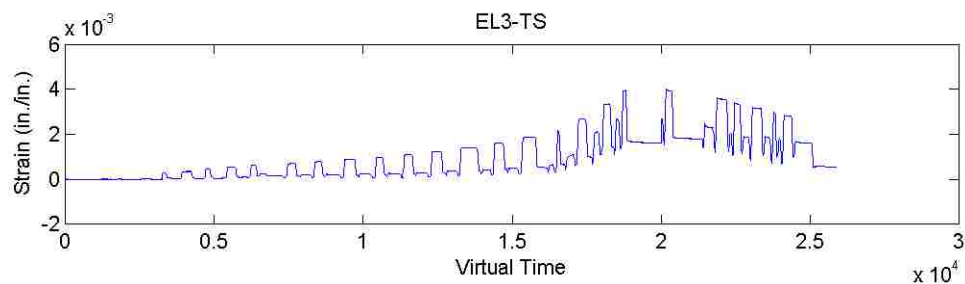
Figure D.27. Transverse strain in CFRP at 3rd level of Column 3-R (T/M=0.4)



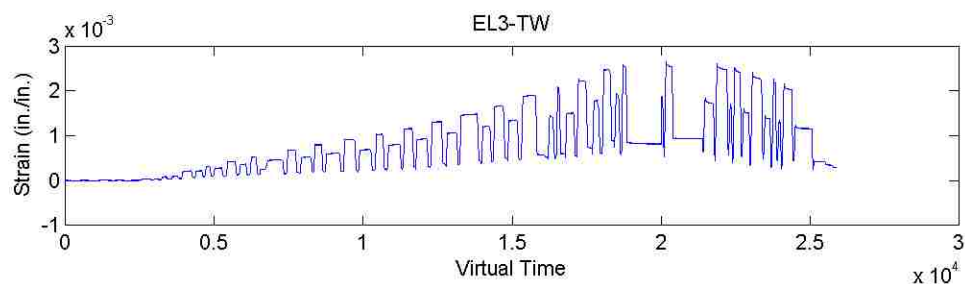
(a) East side of the column



(b) North side of the column



(c) South side of the column



(d) West side of the column

Figure D.28. Transverse strain in CFRP at 4th level of Column 3-R (T/M=0.4)

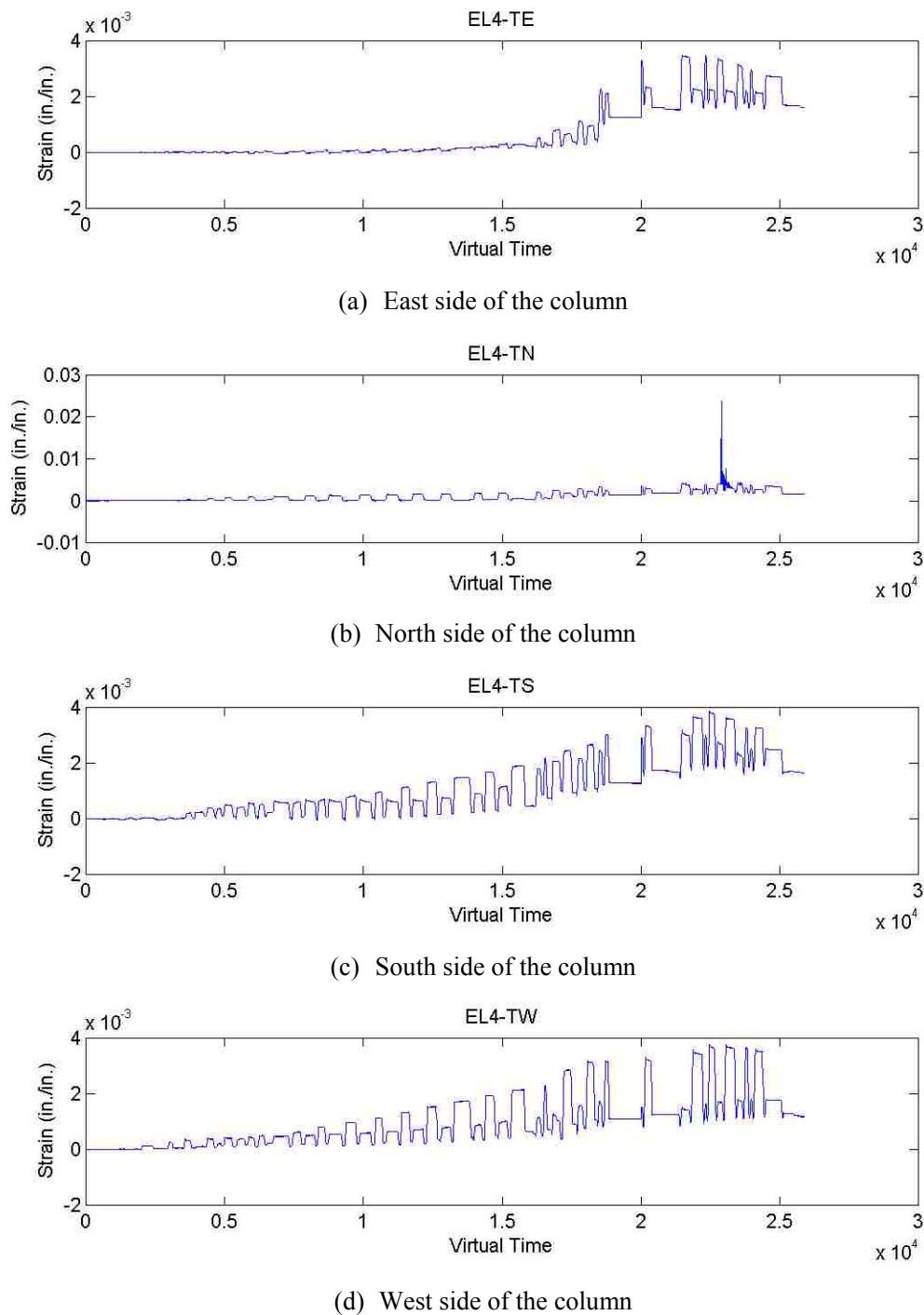
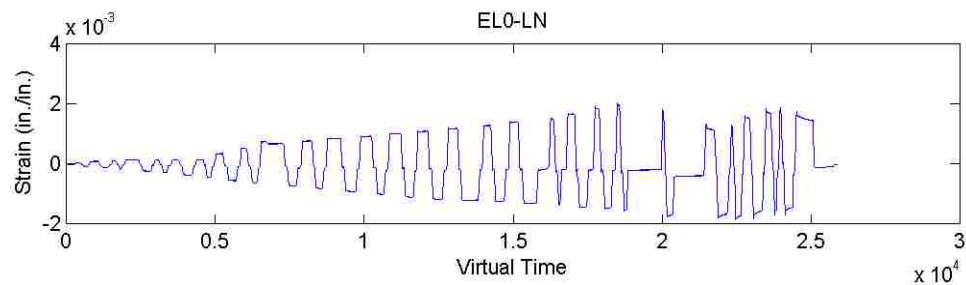
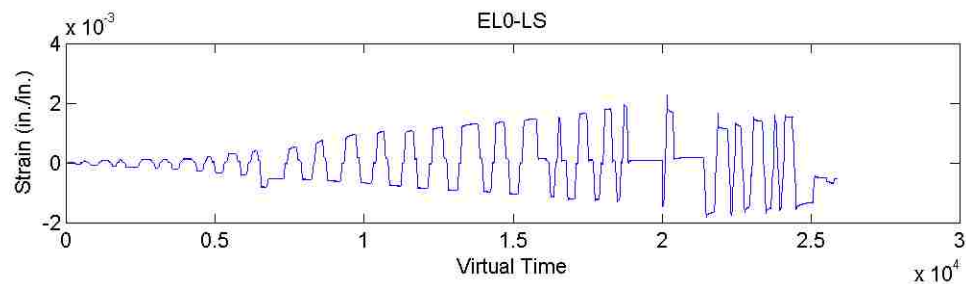


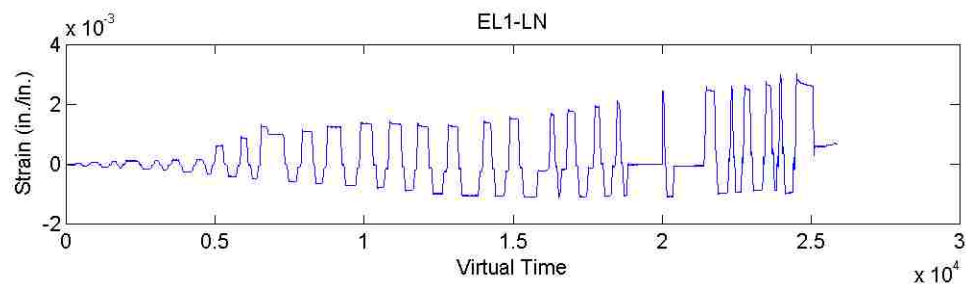
Figure D.29. Transverse strain in CFRP at 5th level of Column 3-R (T/M=0.4)



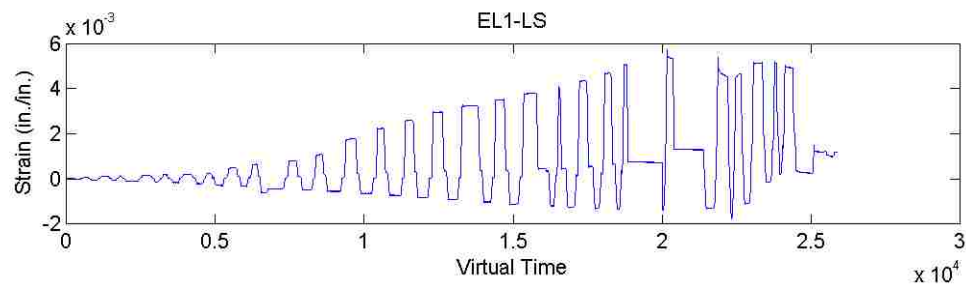
(a) North side of the column



(b) South side of the column

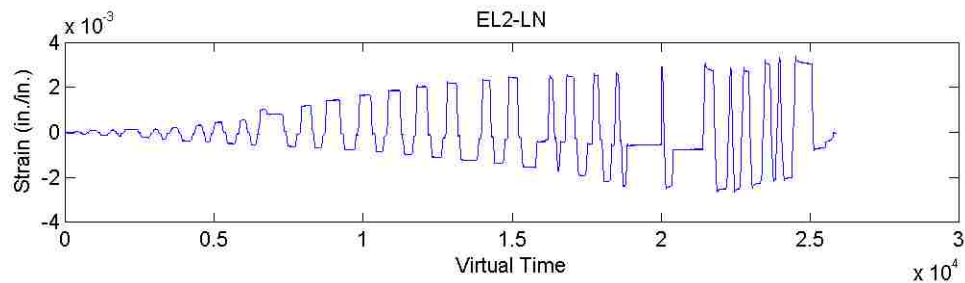
Figure D.30. Longitudinal strain in CFRP at 1st level of Column 3-R (T/M=0.4)

(a) North side of the column

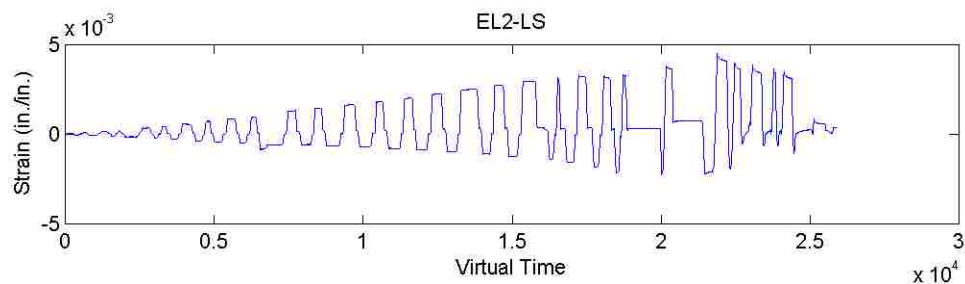


(b) South side of the column

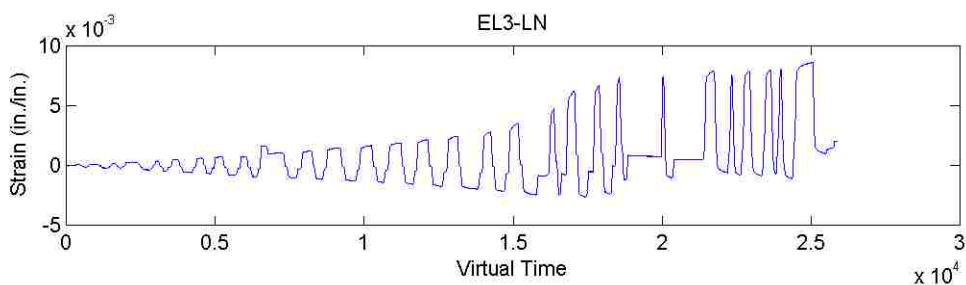
Figure D.31. Longitudinal strain in CFRP at 2nd level of Column 3-R (T/M=0.4)



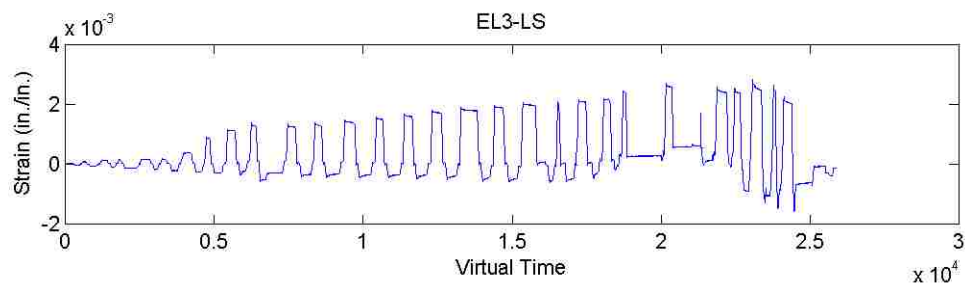
(a) North side of the column



(b) South side of the column

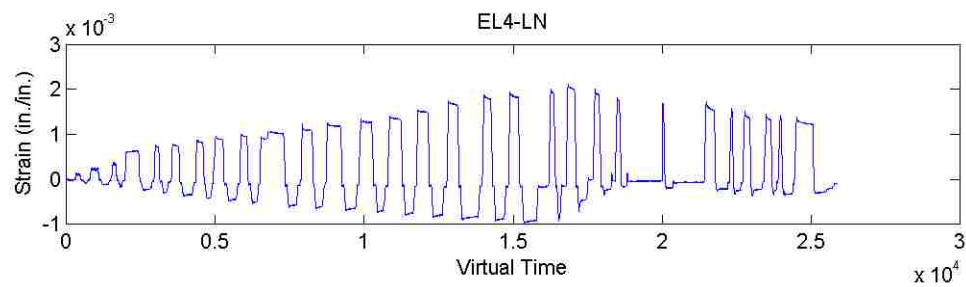
Figure D.32. Longitudinal strain in CFRP at 3rd level of Column 3-R (T/M=0.4)

(a) North side of the column

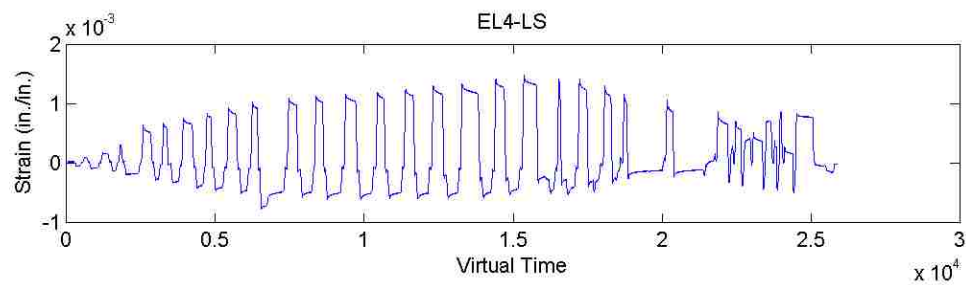


(b) South side of the column

Figure D.33. Longitudinal strain in CFRP at 4th level of Column 3-R (T/M=0.4)



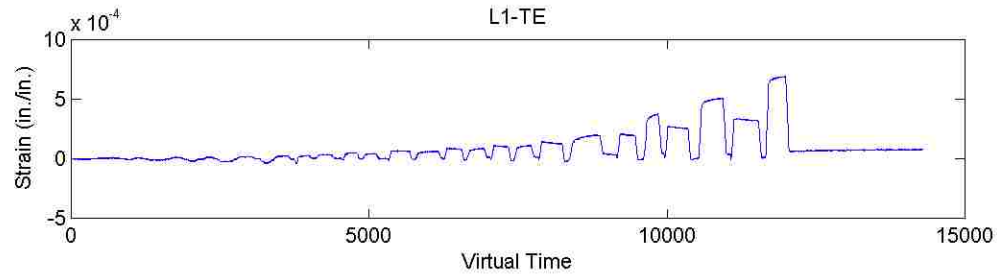
(a) North side of the column



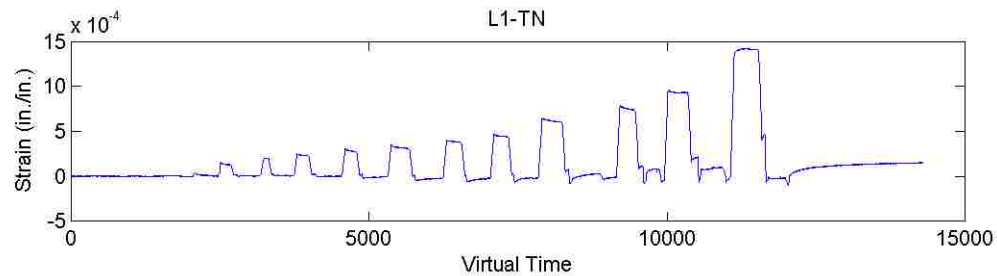
(b) South side of the column

Figure D.34. Longitudinal strain in CFRP at 5th level of Column 3-R (T/M=0.4)

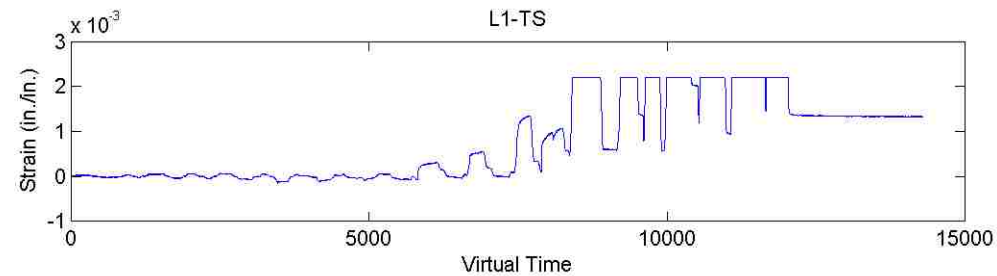
Strain Data for Column 4-R (T/M=0.6)



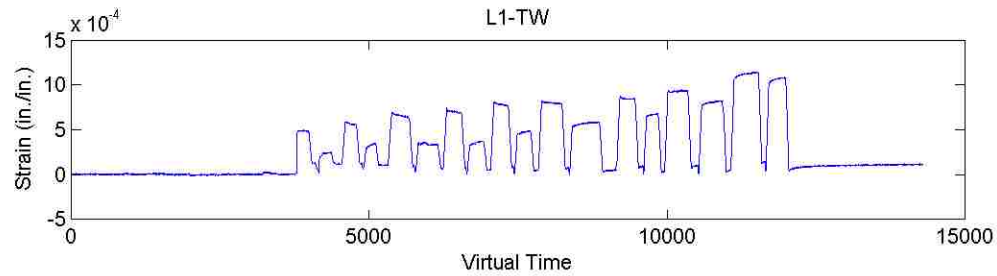
(a) East side of the column



(b) North side of the column

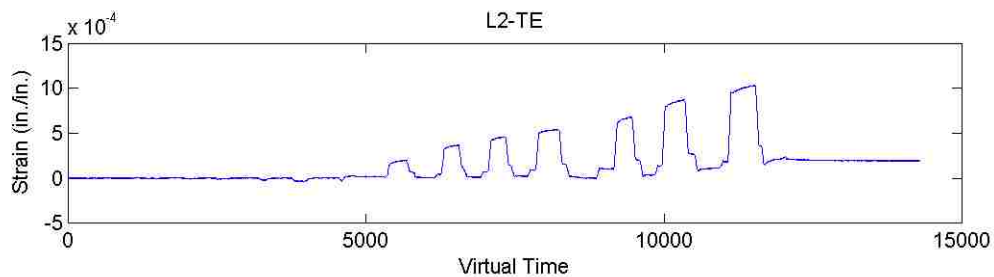


(c) South side of the column

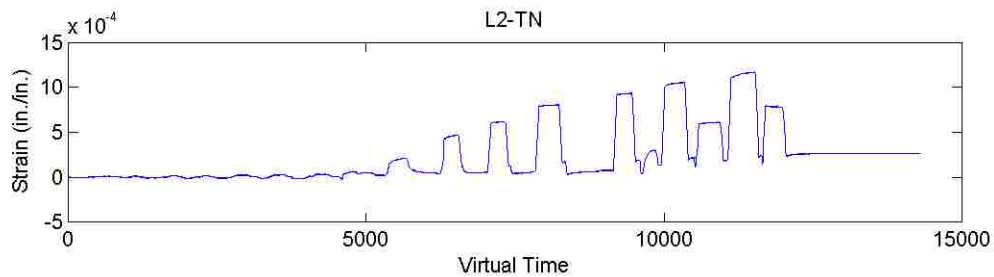


(d) West side of the column

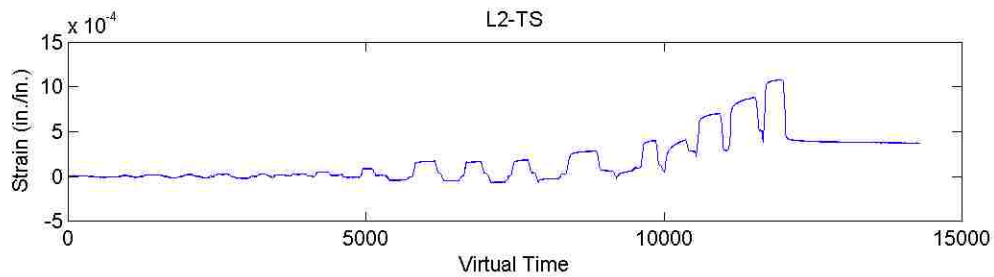
Figure D.35. Transverse strain in CFRP at 1st level of Column 4-R (T/M=0.6)



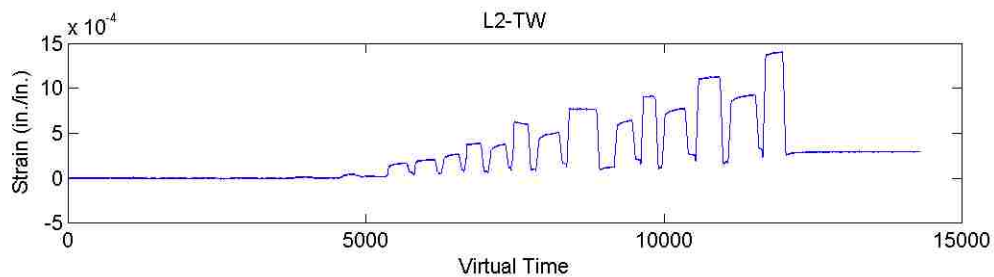
(a) East side of the column



(b) North side of the column

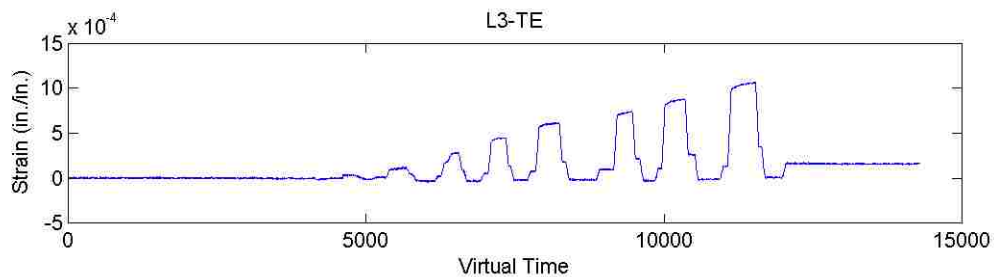


(c) South side of the column

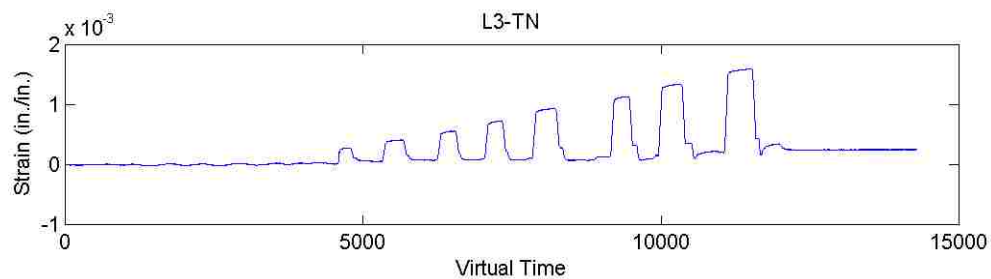


(d) West side of the column

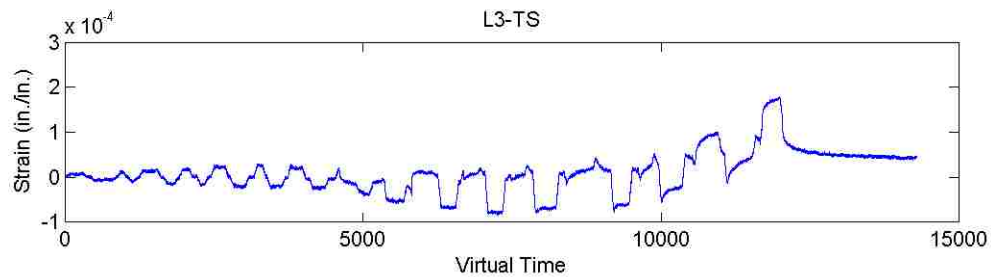
Figure D.36. Transverse strain in CFRP at 2nd level of Column 4-R (T/M=0.6)



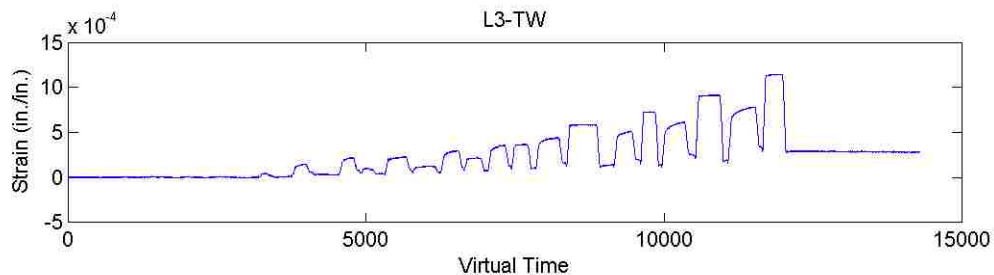
(a) East side of the column



(b) North side of the column

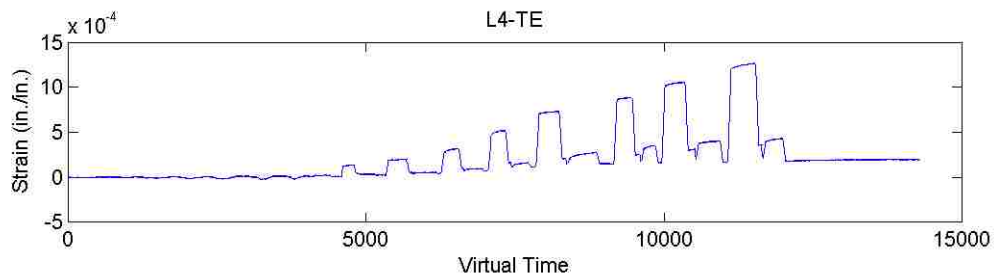


(c) South side of the column

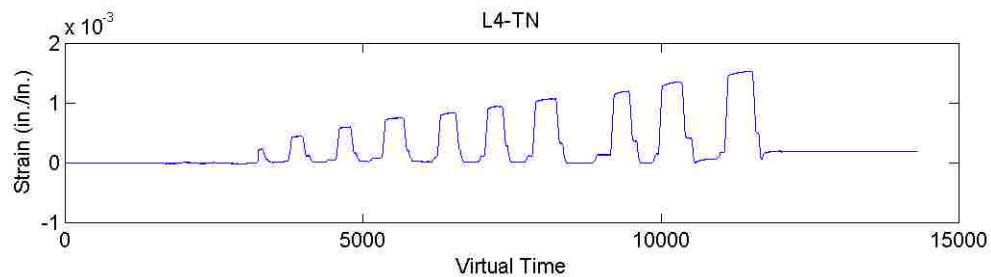


(d) West side of the column

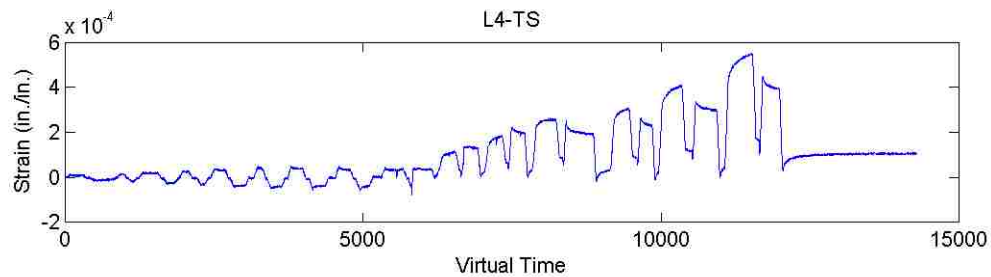
Figure D.37. Transverse strain in CFRP at 3rd level of Column 4-R (T/M=0.6)



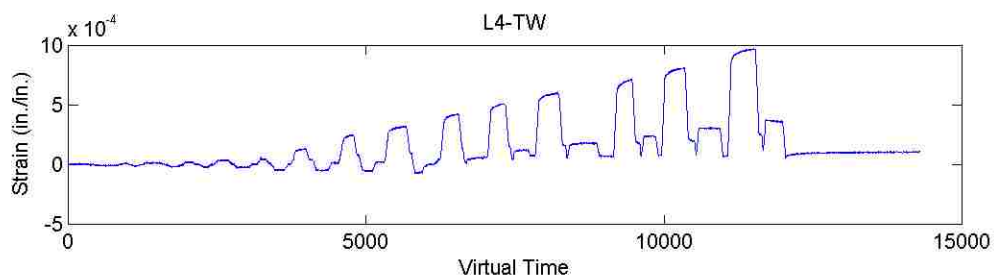
(a) East side of the column



(b) North side of the column

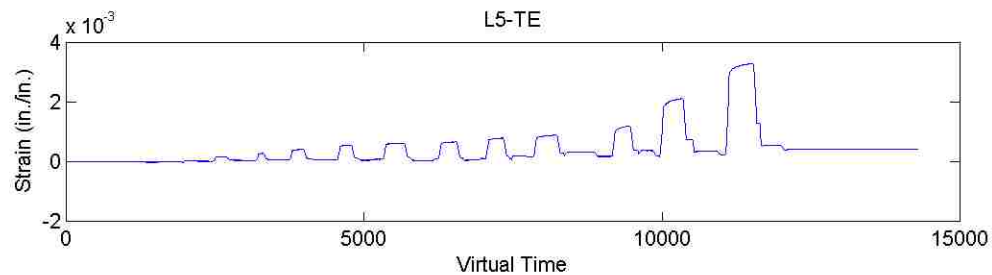


(c) South side of the column

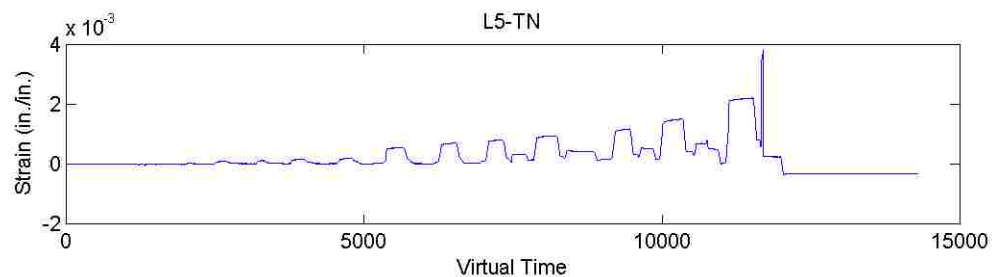


(d) West side of the column

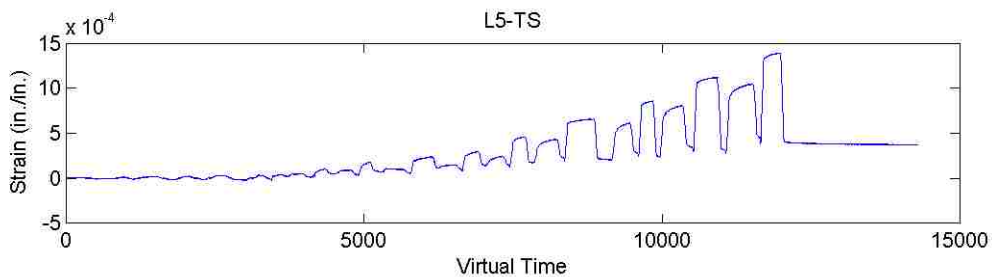
Figure D.38. Transverse strain in CFRP at 4th level of Column 4-R (T/M=0.6)



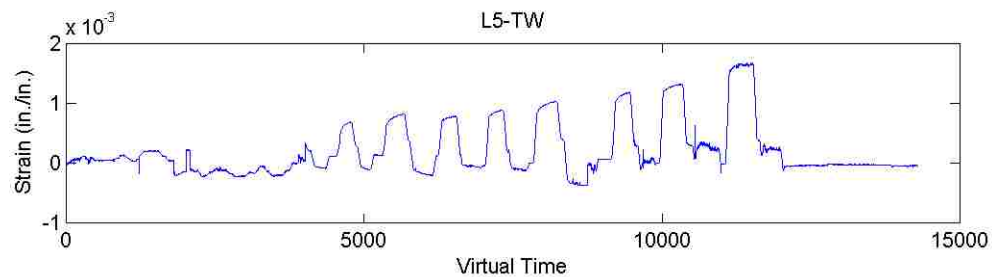
(a) East side of the column



(b) North side of the column

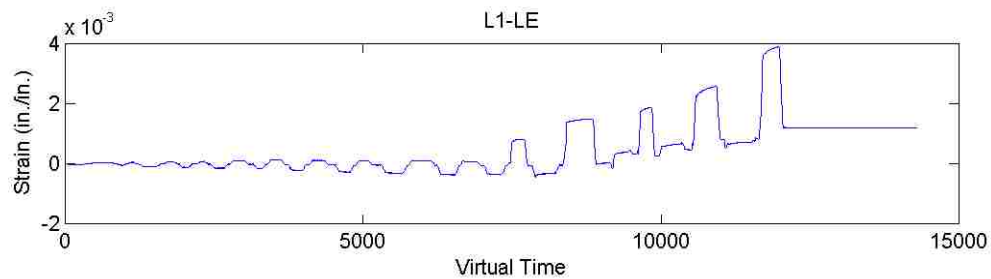


(c) South side of the column

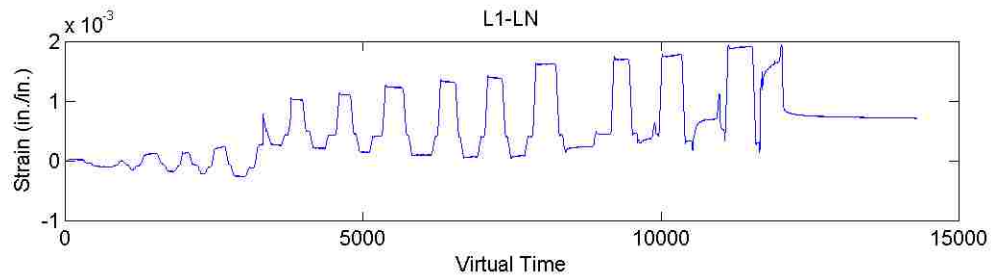


(d) West side of the column

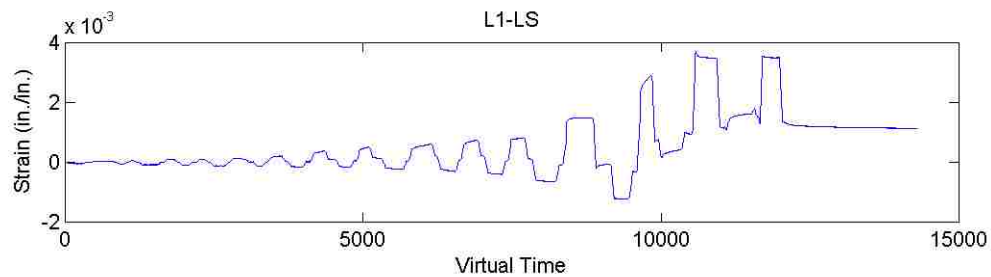
Figure D.39. Transverse strain in CFRP at 5th level of Column 4-R (T/M=0.6)



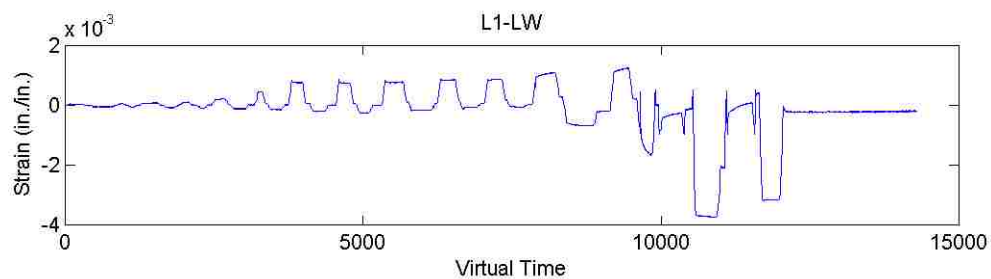
(a) East side of the column



(b) North side of the column

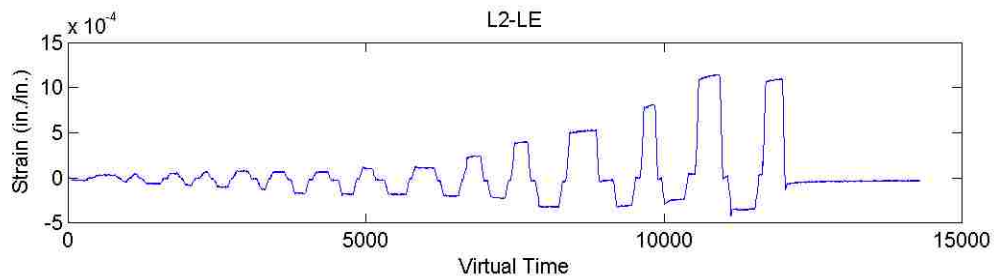


(c) South side of the column

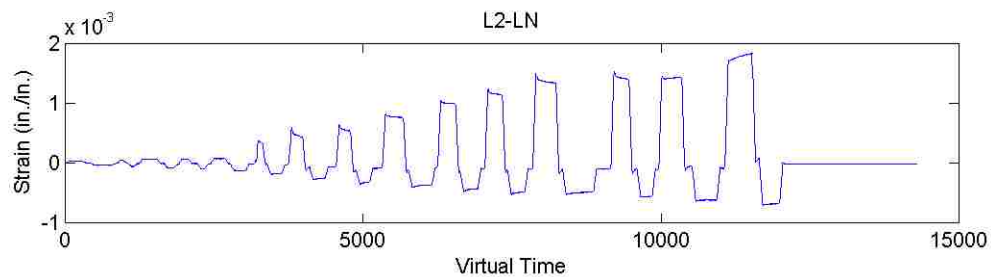


(d) West side of the column

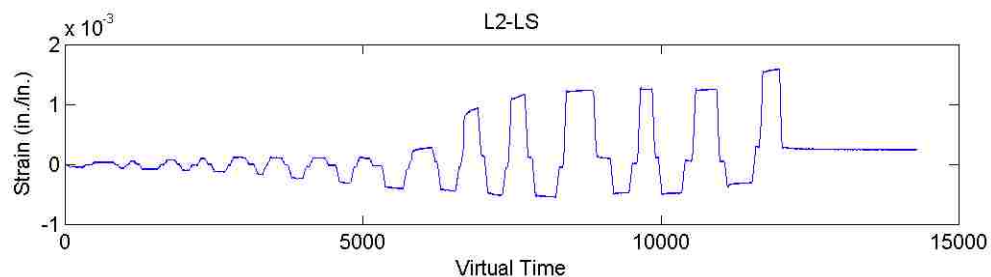
Figure D.40. Longitudinal strain in CFRP at 1st level of Column 4-R (T/M=0.6)



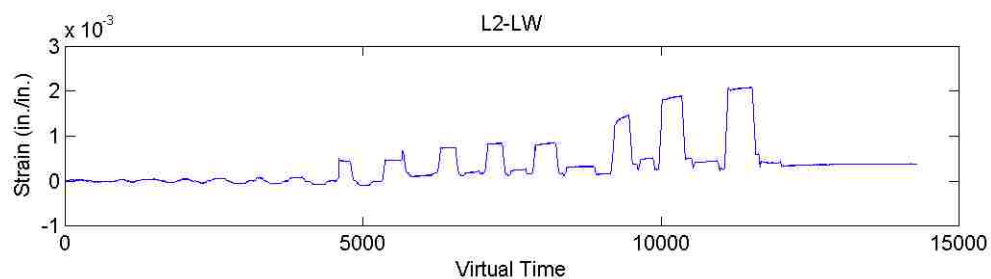
(a) East side of the column



(b) North side of the column

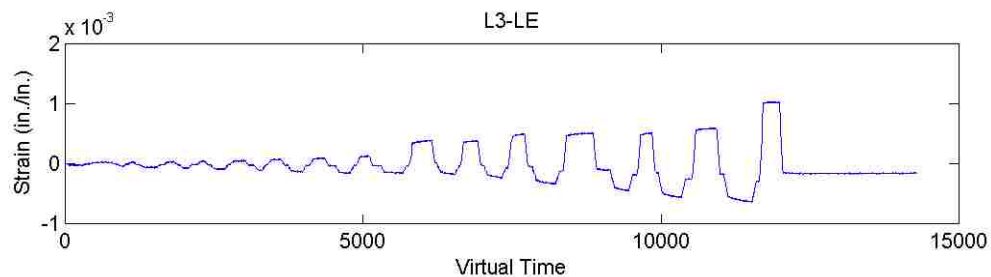


(c) South side of the column

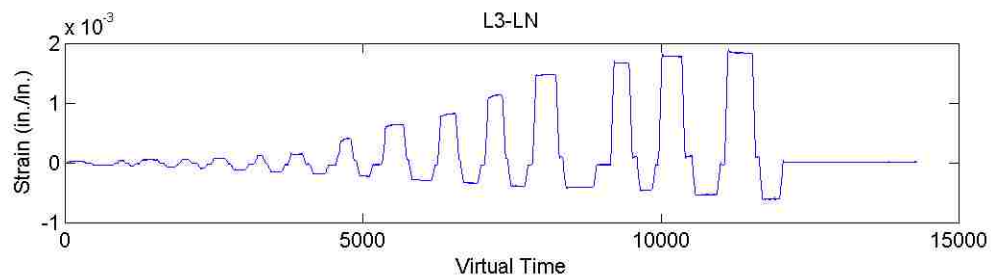


(d) West side of the column

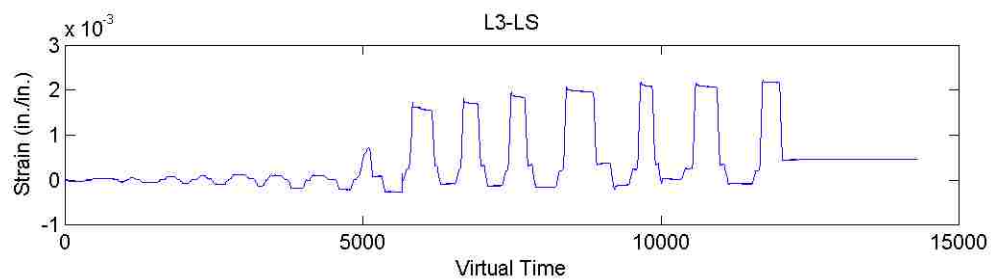
Figure D.41. Longitudinal strain in CFRP at 2nd level of Column 4-R (T/M=0.6)



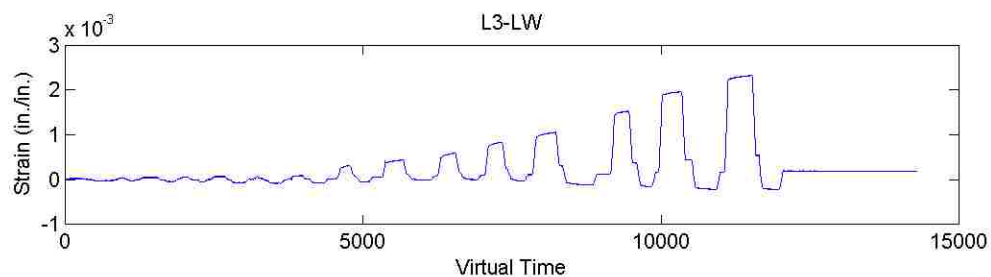
(a) East side of the column



(b) North side of the column

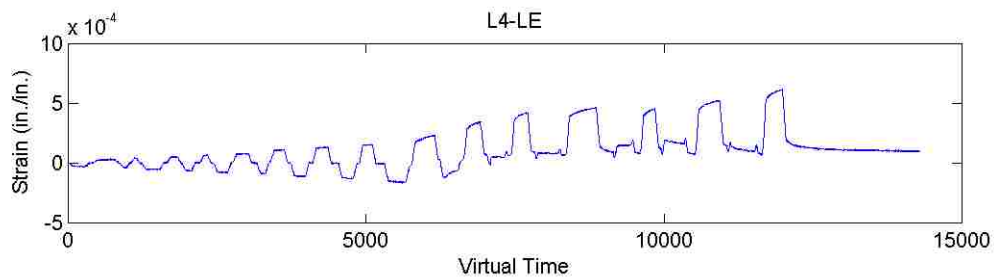


(c) South side of the column

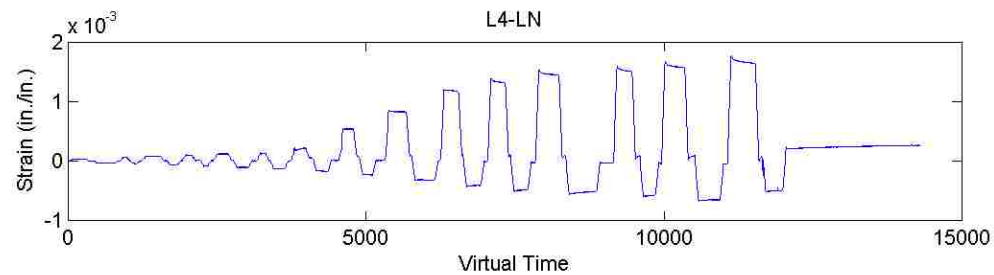


(d) West side of the column

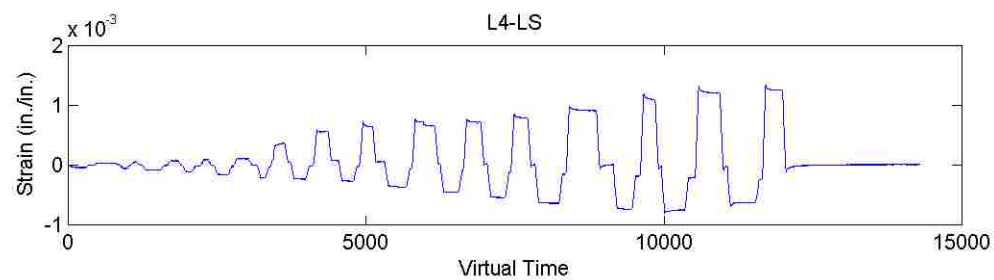
Figure D.42. Longitudinal strain in CFRP at 3rd level of Column 4-R (T/M=0.6)



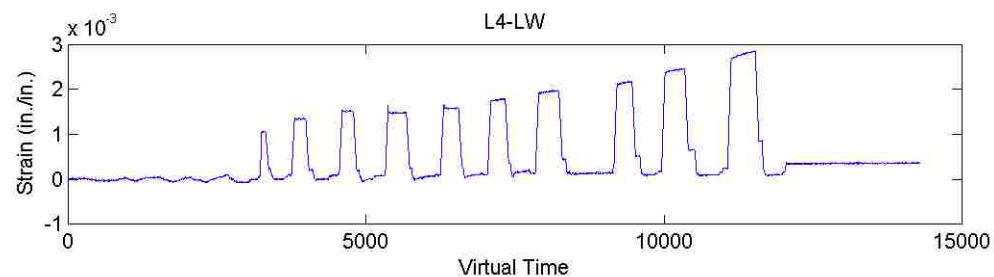
(a) East side of the column



(b) North side of the column

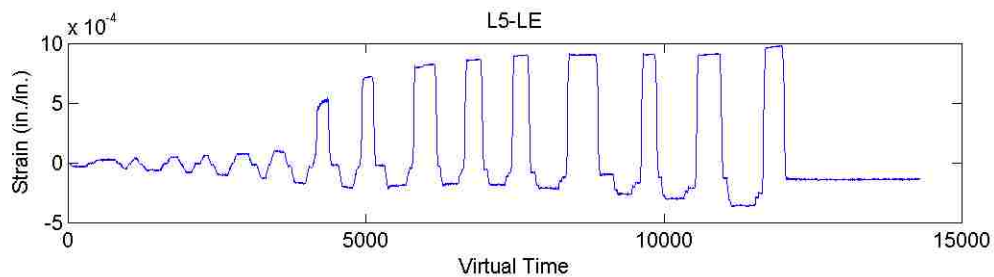


(c) South side of the column

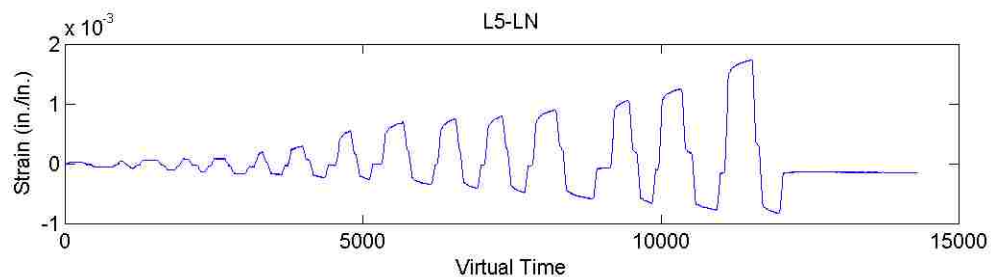


(d) West side of the column

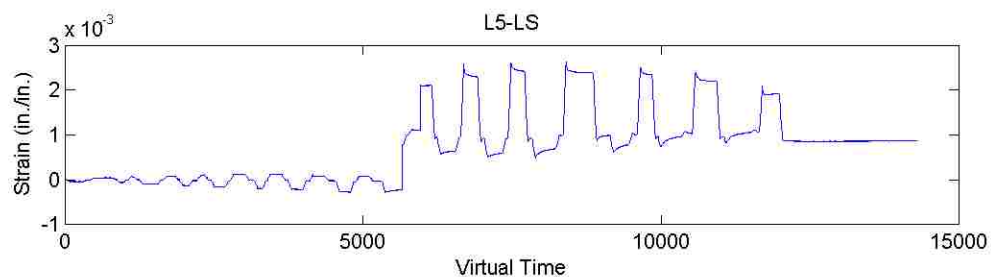
Figure D.43. Longitudinal strain in CFRP at 4th level of Column 4-R (T/M=0.6)



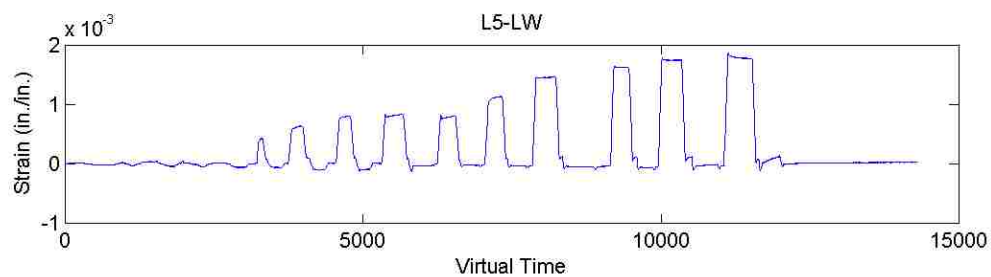
(a) East side of the column



(b) North side of the column



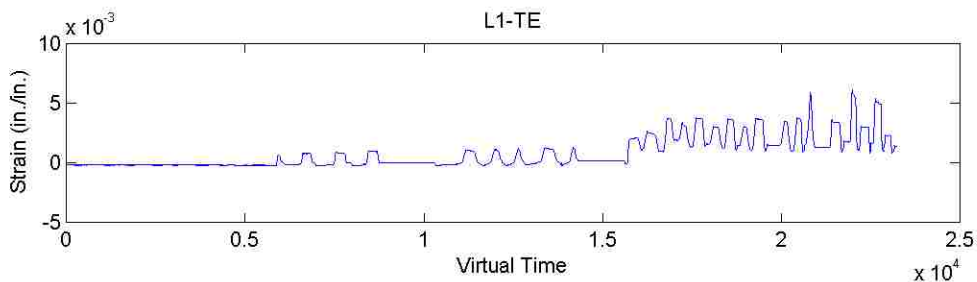
(c) South side of the column



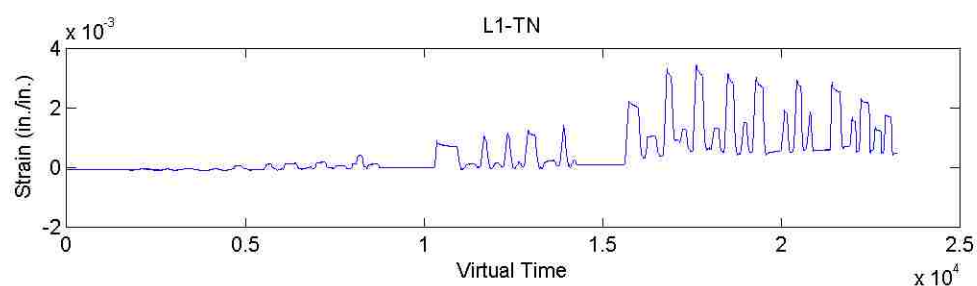
(d) West side of the column

Figure D.44. Longitudinal strain in CFRP at 5th level of Column 4-R (T/M=0.6)

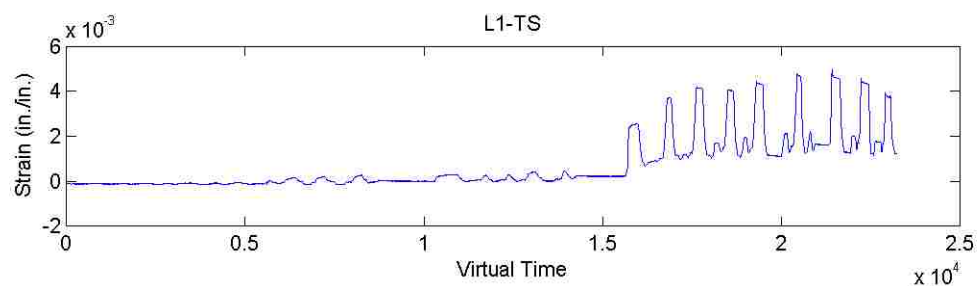
Strain Data for Column 5-R ($T/M=\infty$)



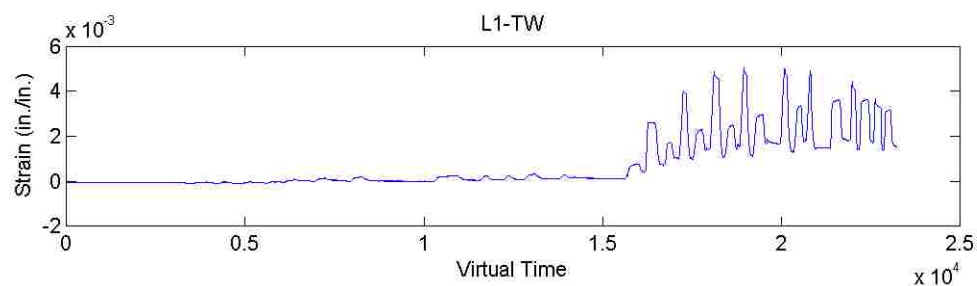
(a) East side of the column



(b) North side of the column

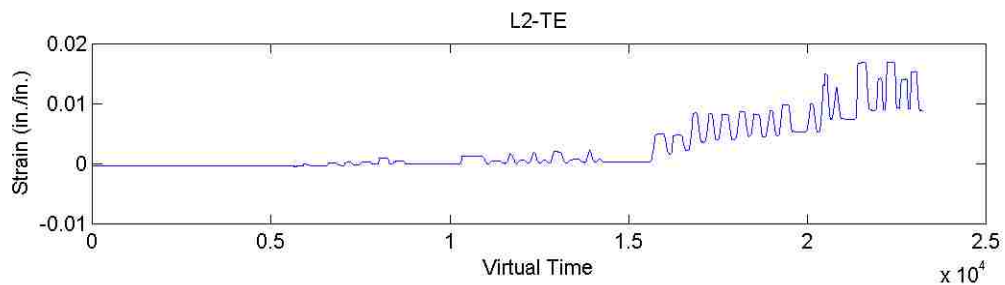


(c) South side of the column

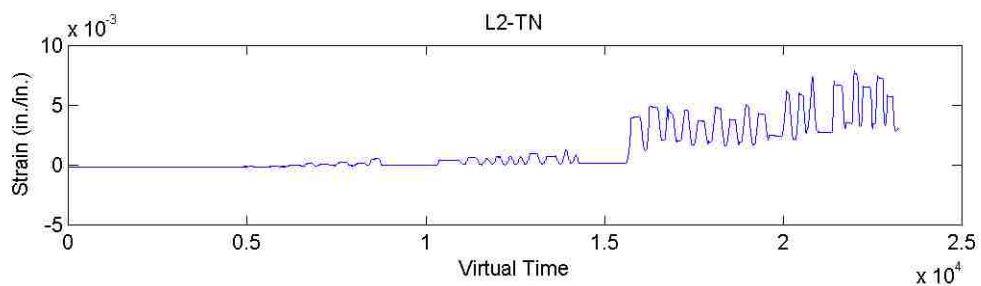


(d) West side of the column

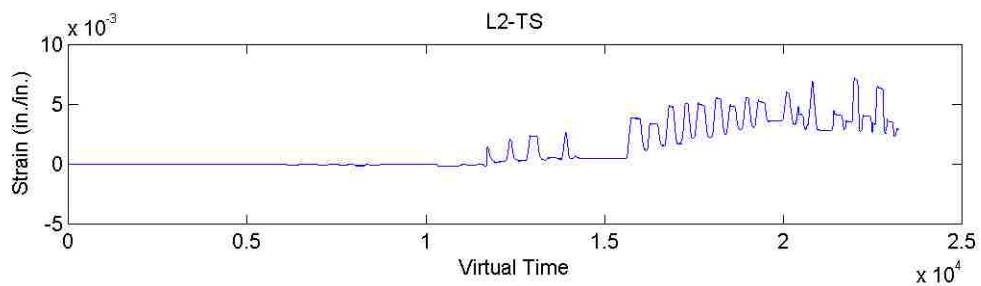
Figure D.45. Transverse strain in CFRP at 1st level of Column 5-R ($T/M=\infty$)



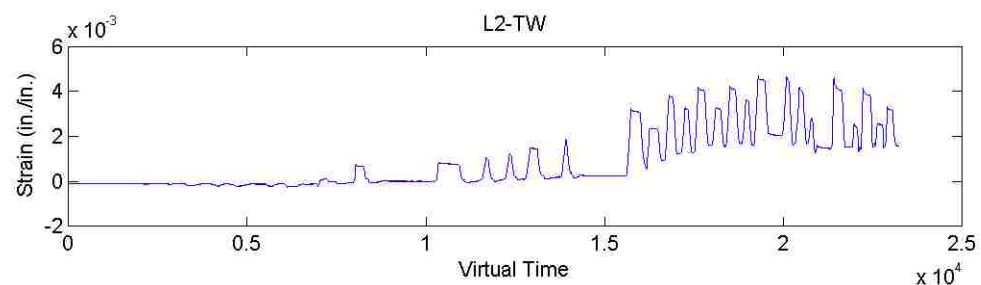
(a) East side of the column



(b) North side of the column

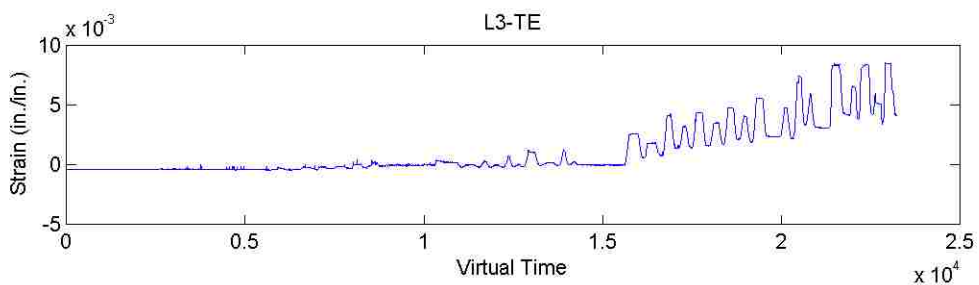


(c) South side of the column

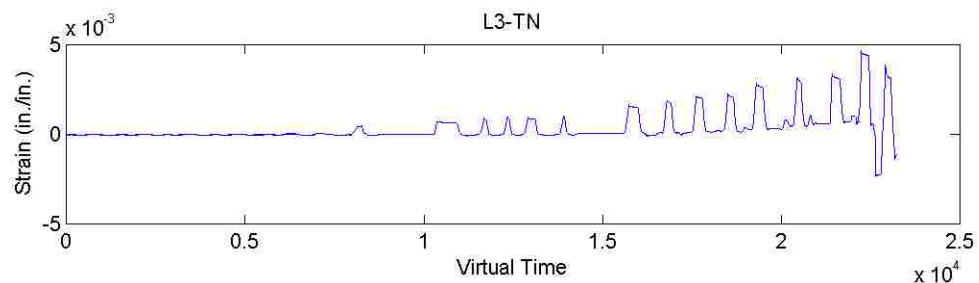


(d) West side of the column

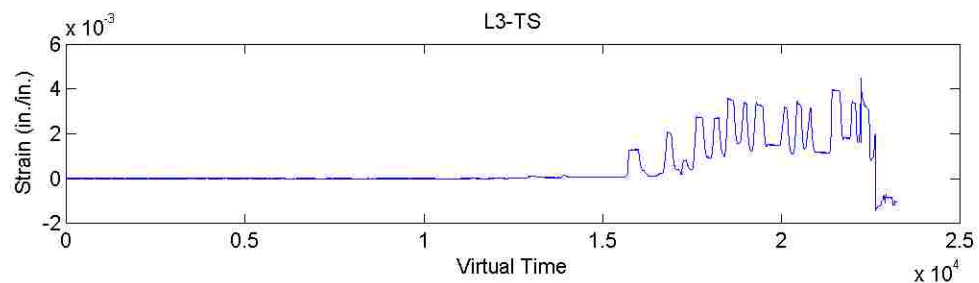
Figure D.46. Transverse strain in CFRP at 2nd level of Column 5-R (T/M= ∞)



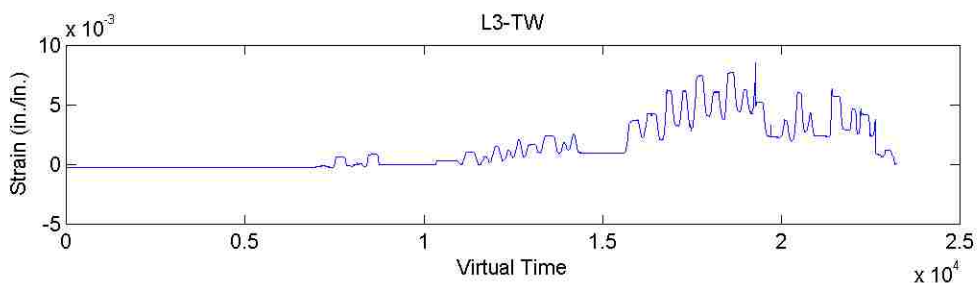
(a) East side of the column



(b) North side of the column

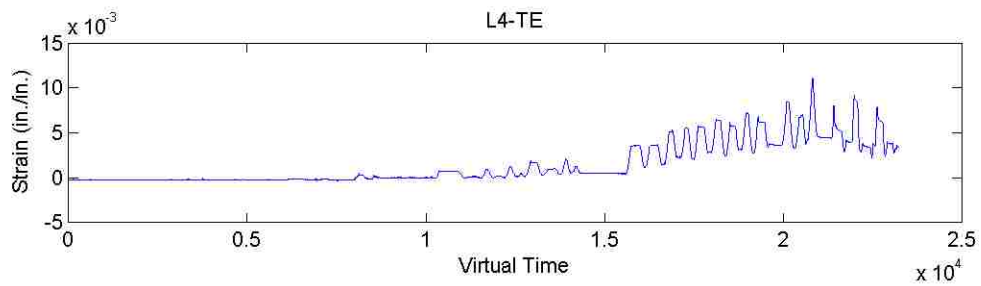


(c) South side of the column

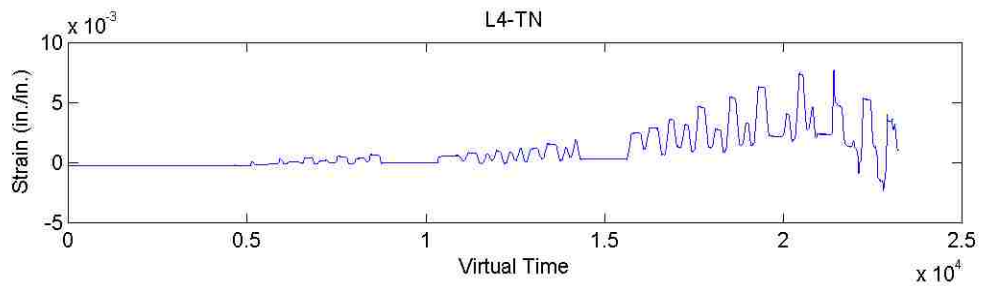


(d) West side of the column

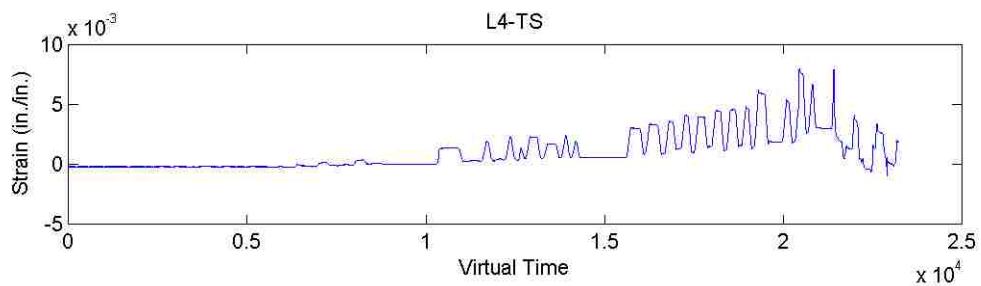
Figure D.47. Transverse strain in CFRP at 3rd level of Column 5-R ($T/M=\infty$)



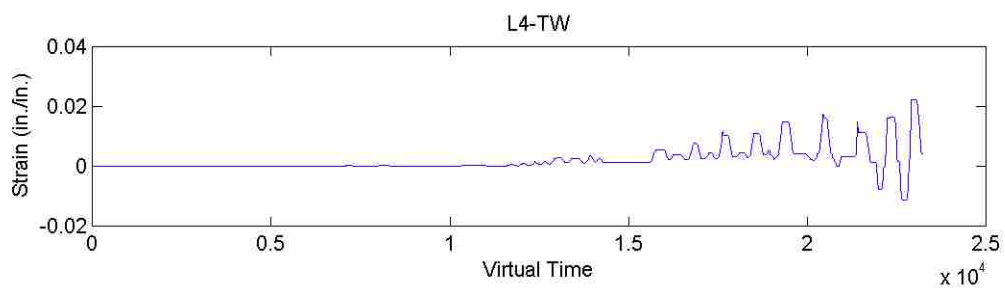
(a) East side of the column



(b) North side of the column

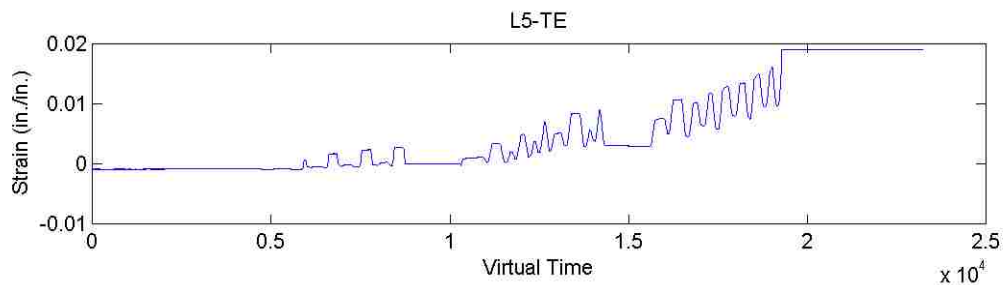


(c) South side of the column

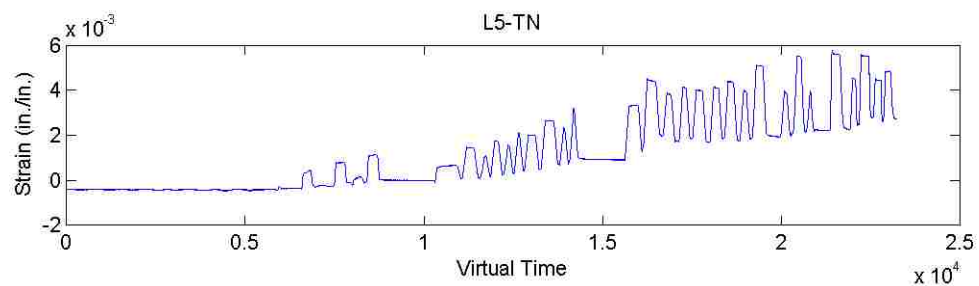


(d) West side of the column

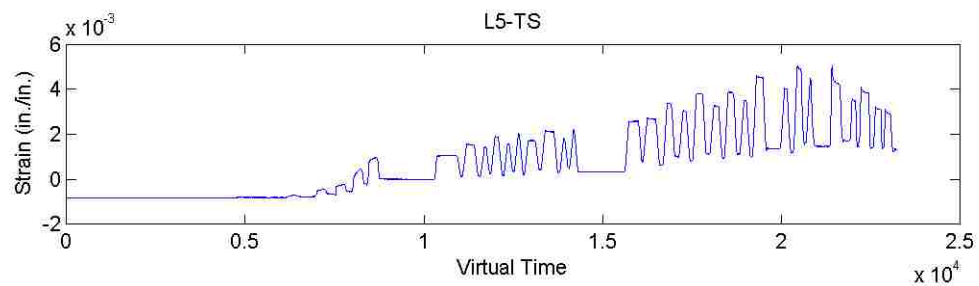
Figure D.48. Transverse strain in CFRP at 4th level of Column 5-R (T/M=∞)



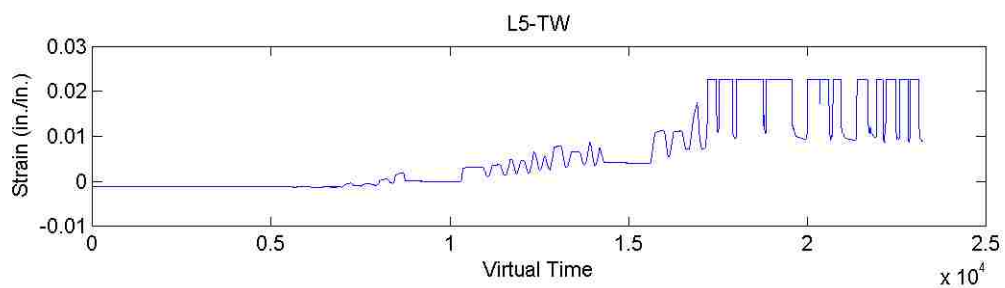
(a) East side of the column



(b) North side of the column

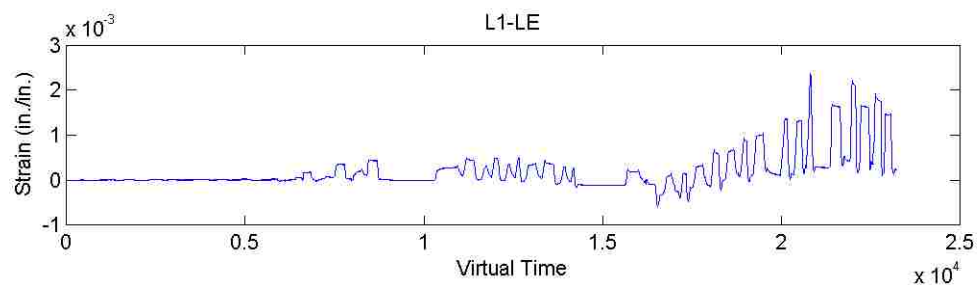


(c) South side of the column

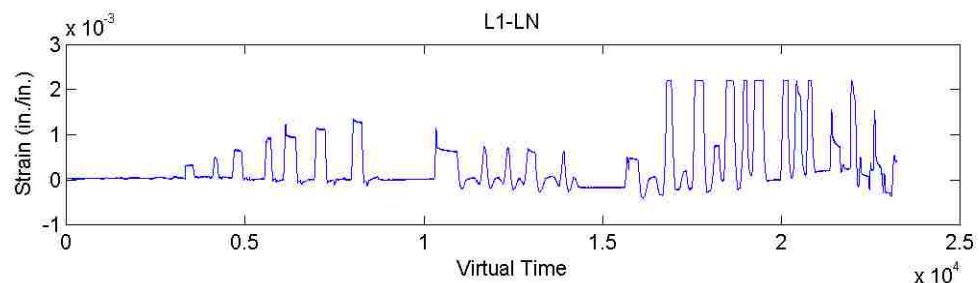


(d) West side of the column

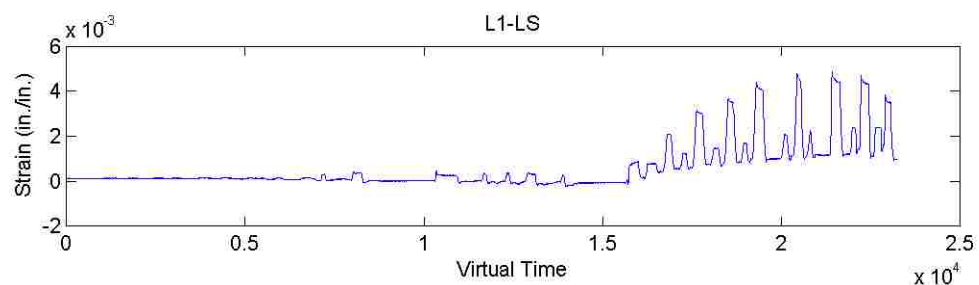
Figure D.49. Transverse strain in CFRP at 5th level of Column 5-R ($T/M=\infty$)



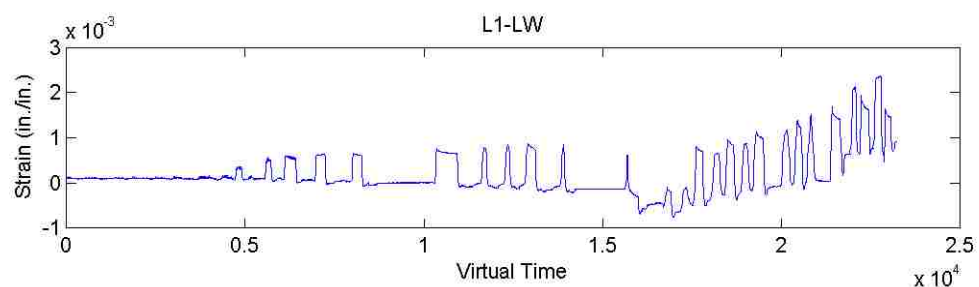
(a) East side of the column



(b) North side of the column

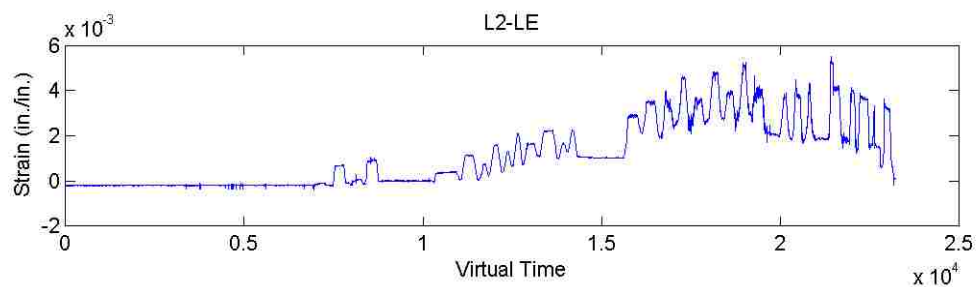


(c) South side of the column

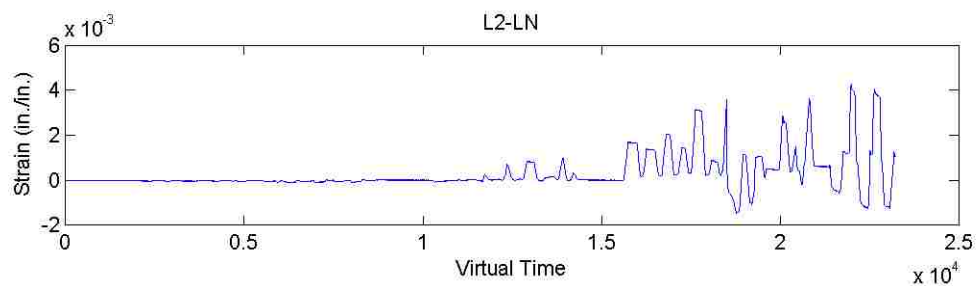


(d) West side of the column

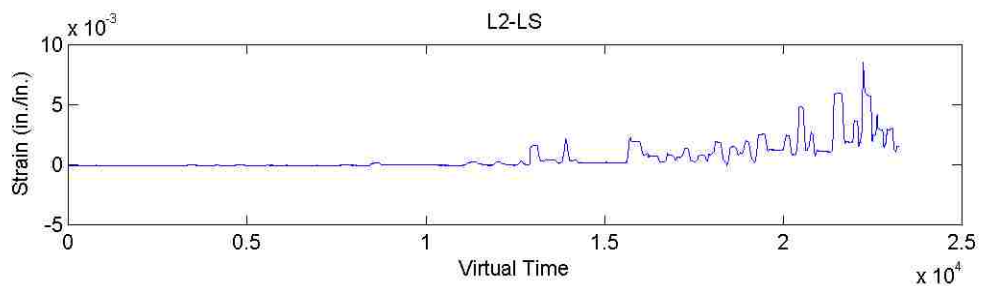
Figure D.50. Longitudinal strain in CFRP at 1st level of Column 5-R (T/M=∞)



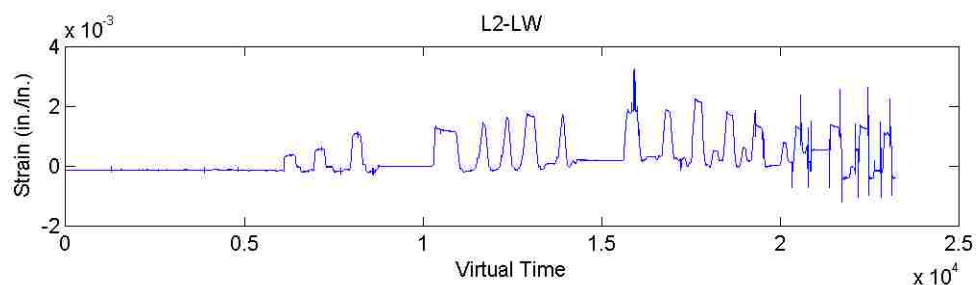
(a) East side of the column



(b) North side of the column



(c) South side of the column



(d) West side of the column

Figure D.51. Longitudinal strain in CFRP at 2nd level of Column 5-R (T/M=∞)

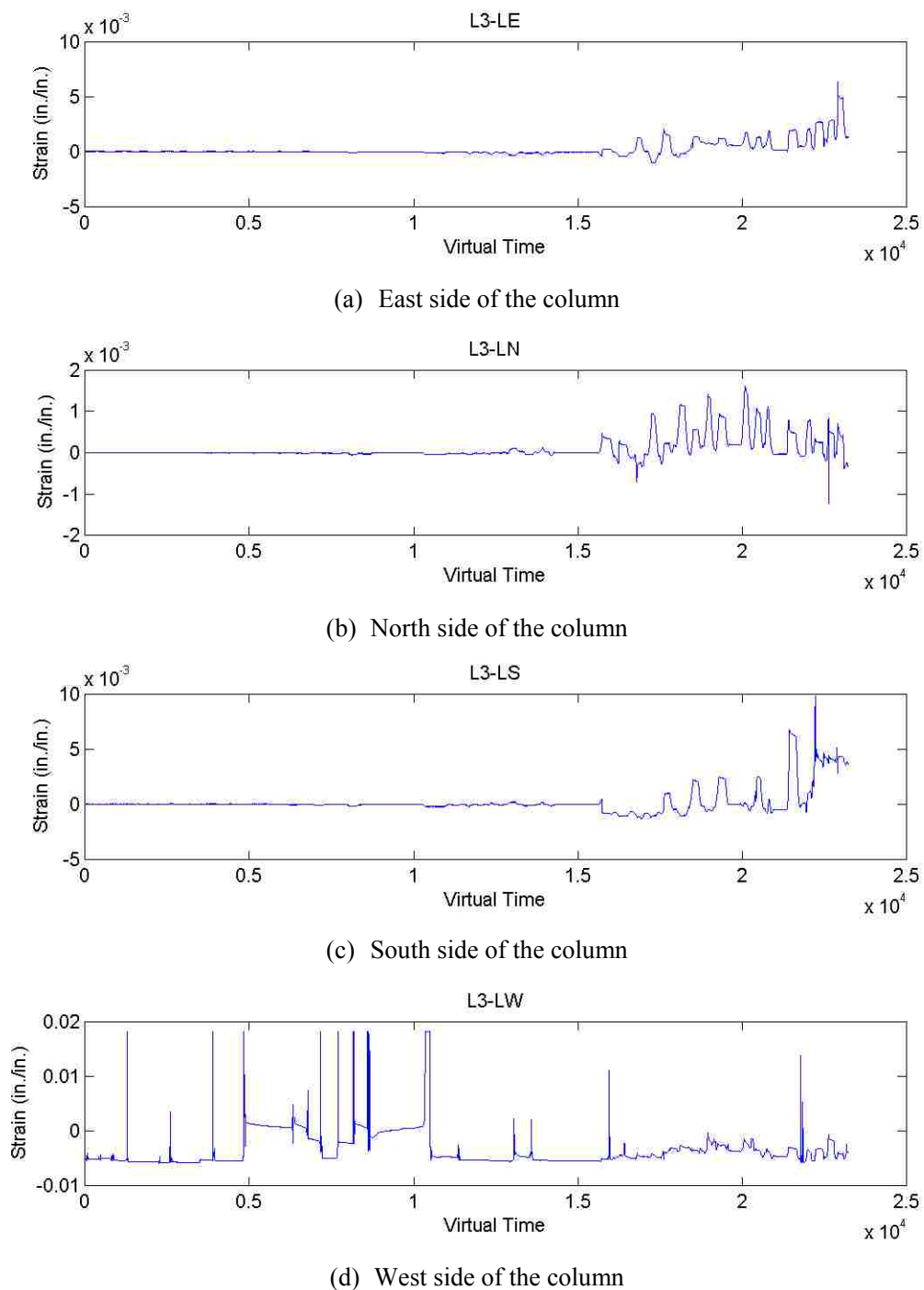
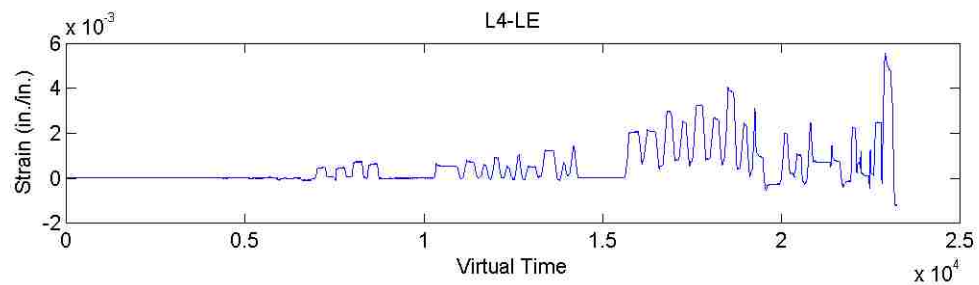
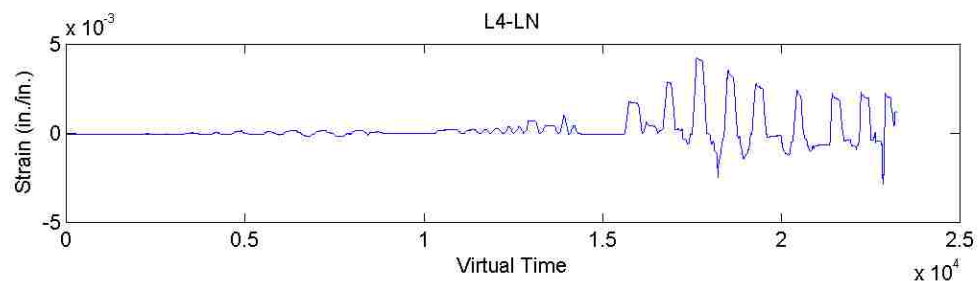


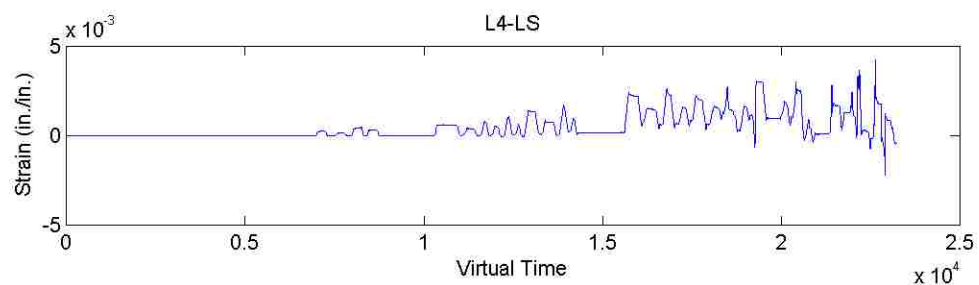
Figure D.52. Longitudinal strain in CFRP at 3rd level of Column 5-R ($T/M=\infty$)



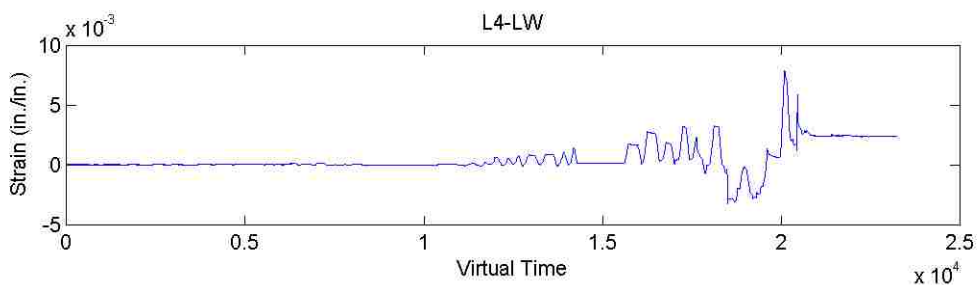
(a) East side of the column



(b) North side of the column

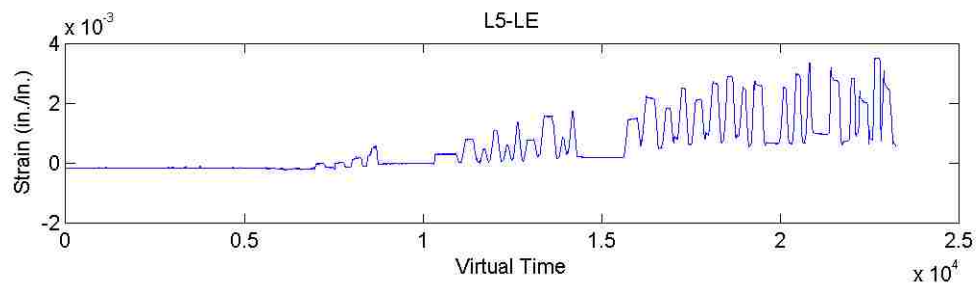


(c) South side of the column

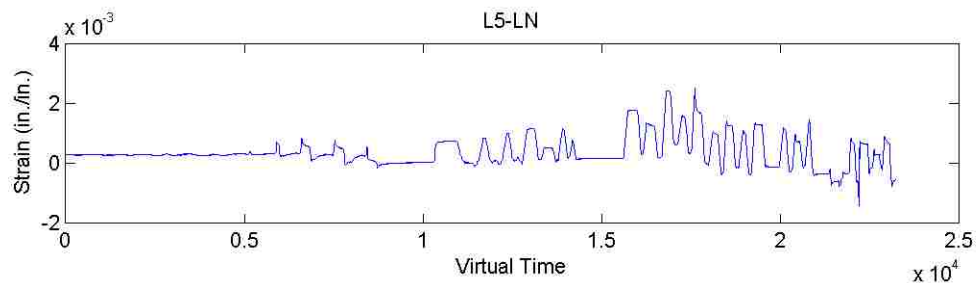


(d) West side of the column

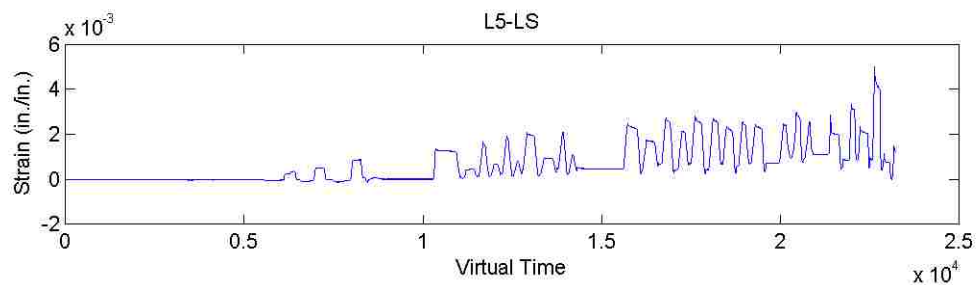
Figure D.53. Longitudinal strain in CFRP at 4th level of Column 5-R (T/M=∞)



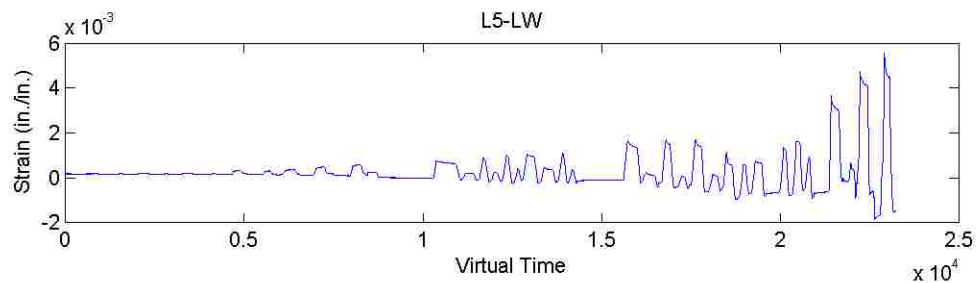
(a) East side of the column



(b) North side of the column

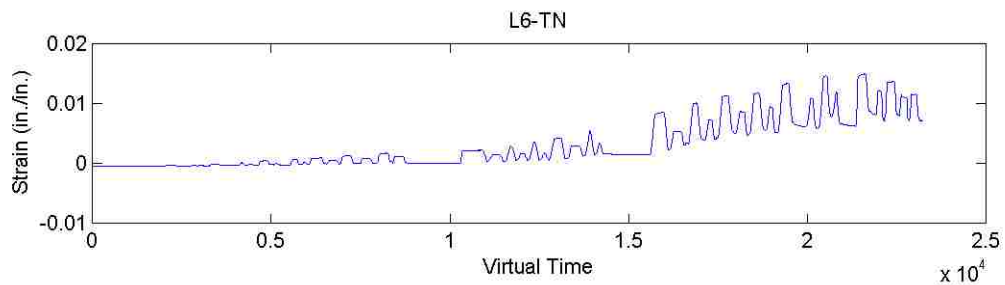


(c) South side of the column

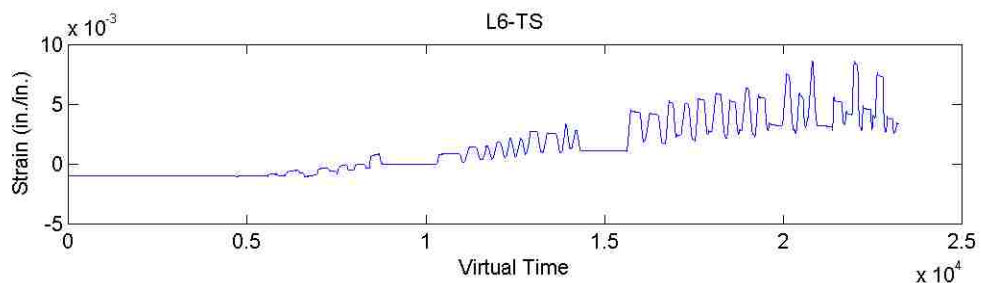


(d) West side of the column

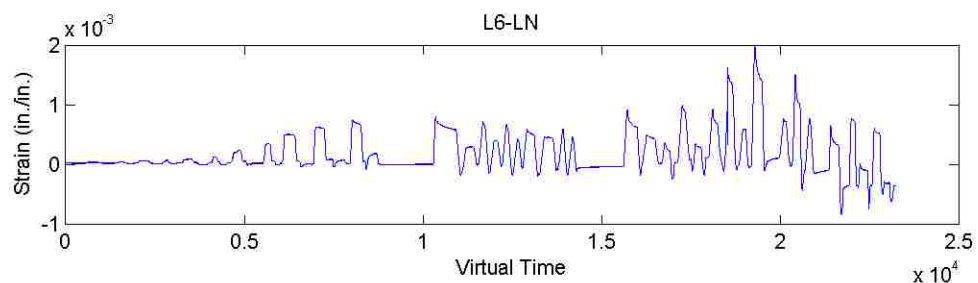
Figure D.54. Longitudinal strain in CFRP at 5th level of Column 5-R (T/M=∞)



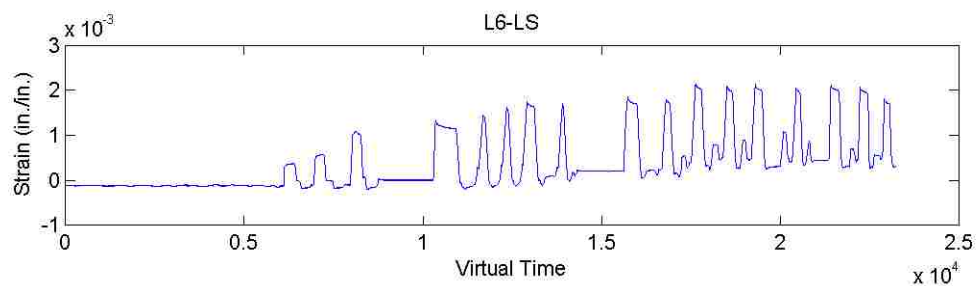
(a) North side of the column



(b) South side of the column

Figure D.55. Transverse strain in CFRP at 6th level of Column 5-R ($T/M=\infty$)

(a) North side of the column



(b) South side of the column

Figure D.56. Longitudinal strain in CFRP at 6th level of Column 5-R ($T/M=\infty$)

APPENDIX E
SELECTED GROUND MOTION RECORDS

This index provides the 40 ground motion records employed in the analytical study discussed in Paper V. The record number in each of the figure title is corresponding to the number listed in Table 2 in Paper V. The acceleration shown in the following figures is after scale as discussed in Paper V.

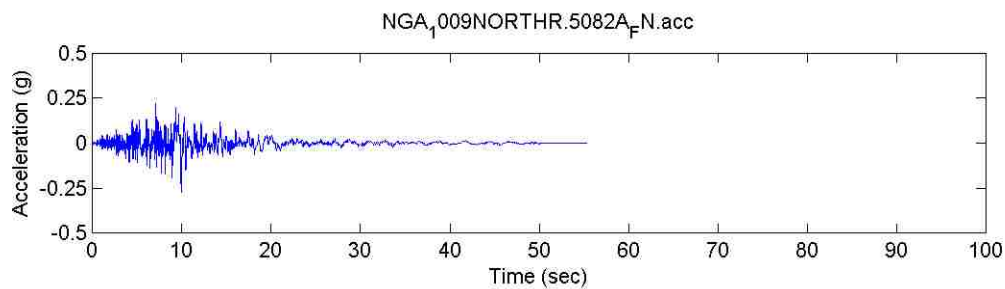


Figure E.1. GM record No. 1

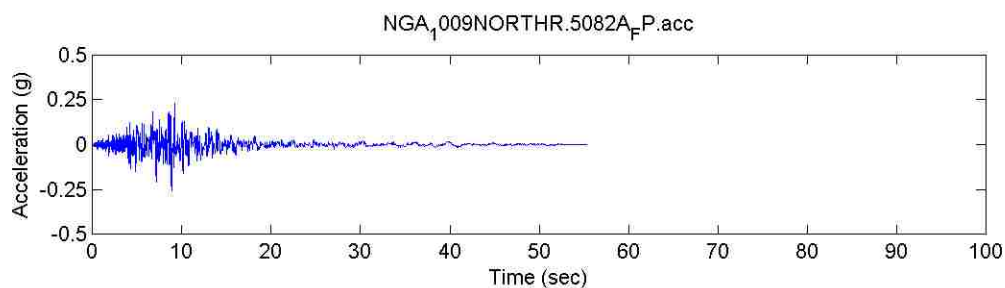


Figure E.2. GM record No. 2

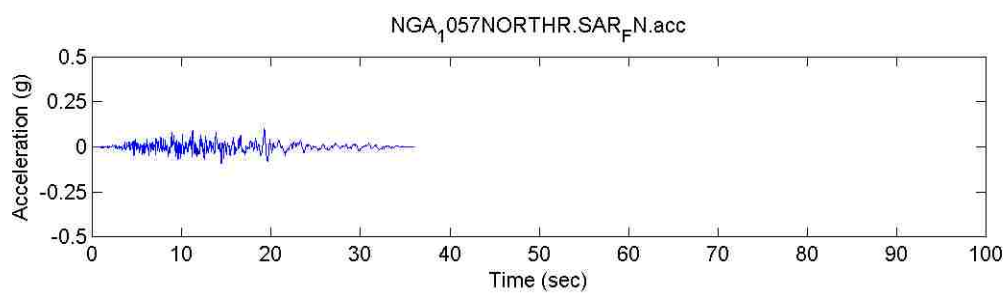


Figure E.3. GM record No. 3

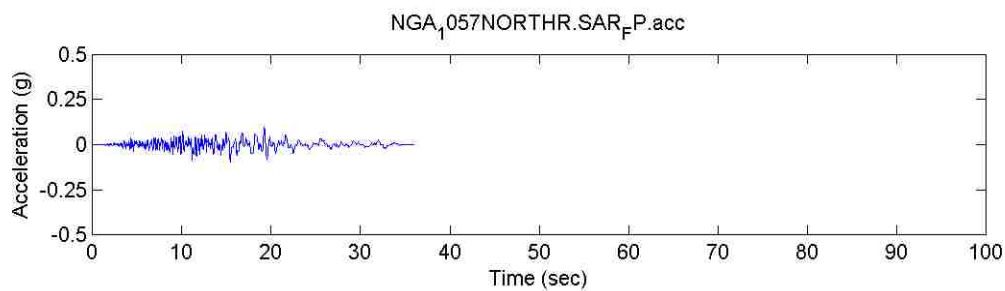


Figure E.4. GM record No. 4

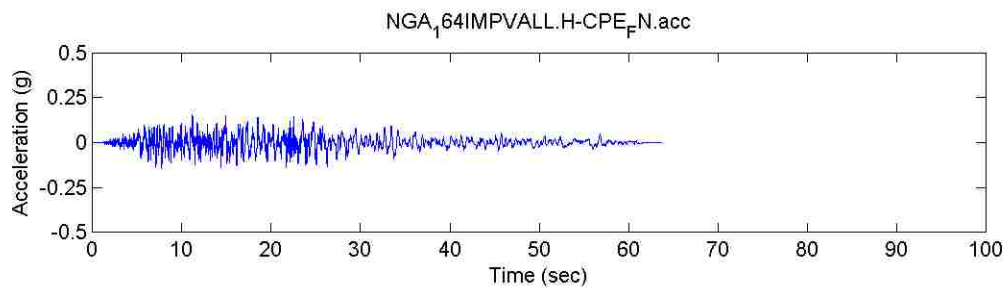


Figure E.5. GM record No. 5

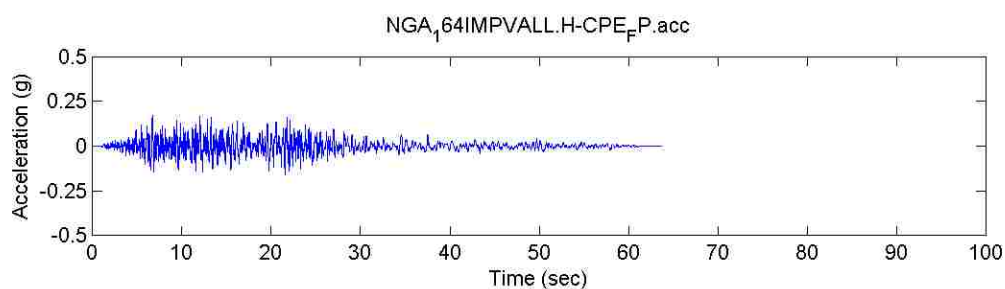


Figure E.6. GM record No. 6

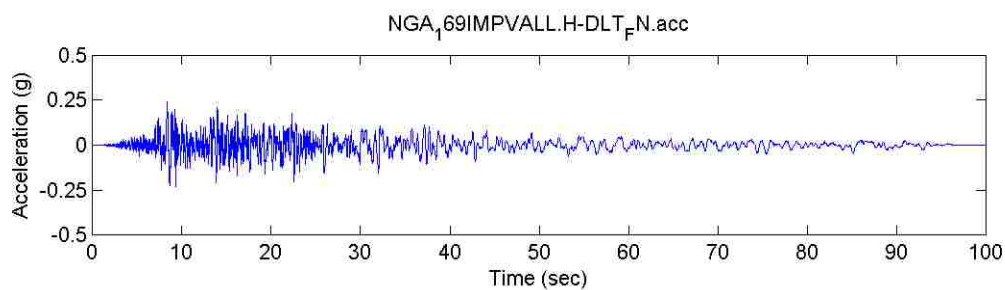


Figure E.7. GM record No. 7

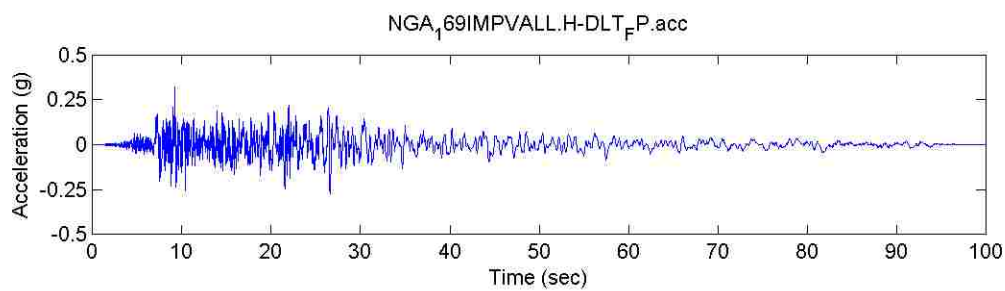


Figure E.8. GM record No. 8

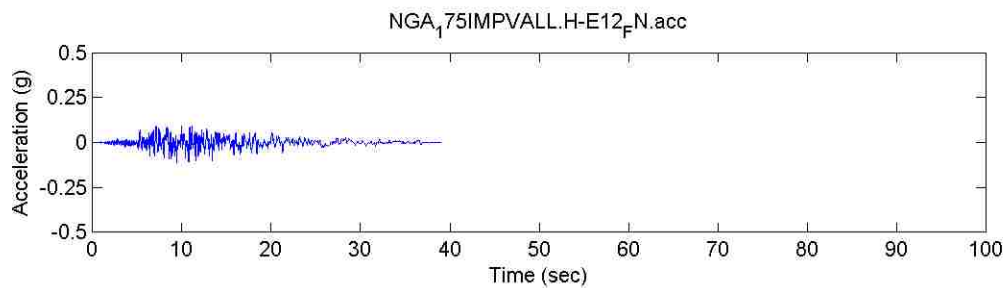


Figure E.9. GM record No. 9

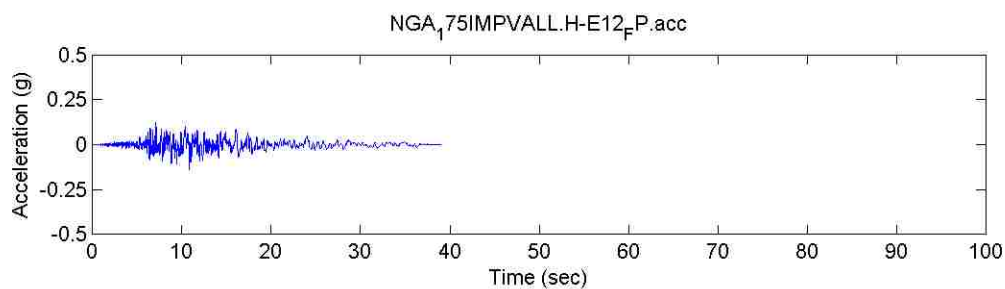


Figure E.10. GM record No. 11

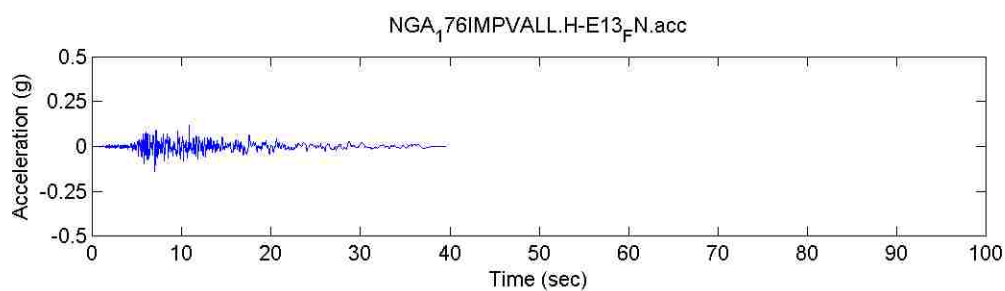


Figure E.11. GM record No. 11

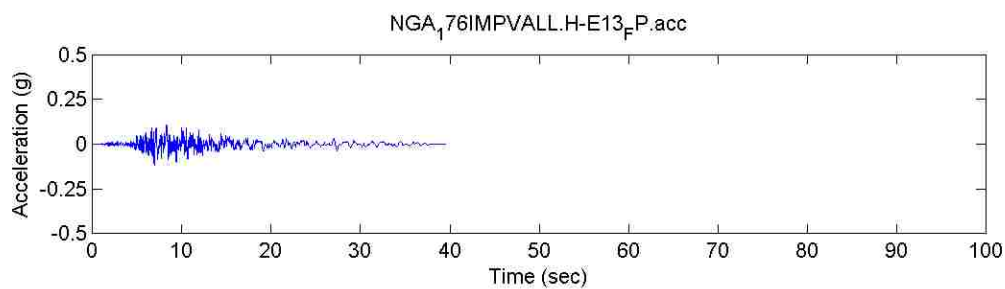


Figure E.12. GM record No. 12

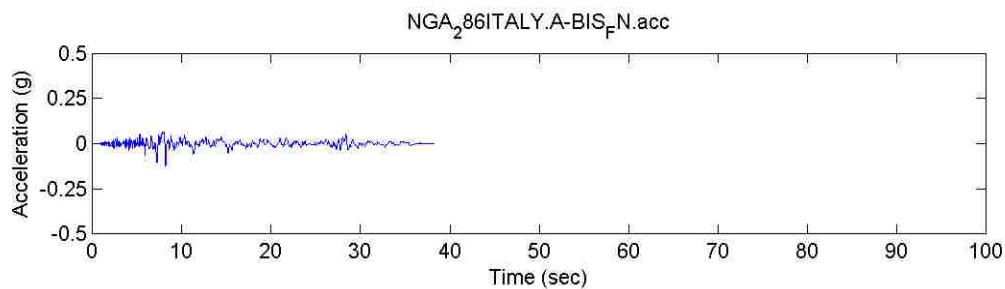


Figure E.13. GM record No. 13

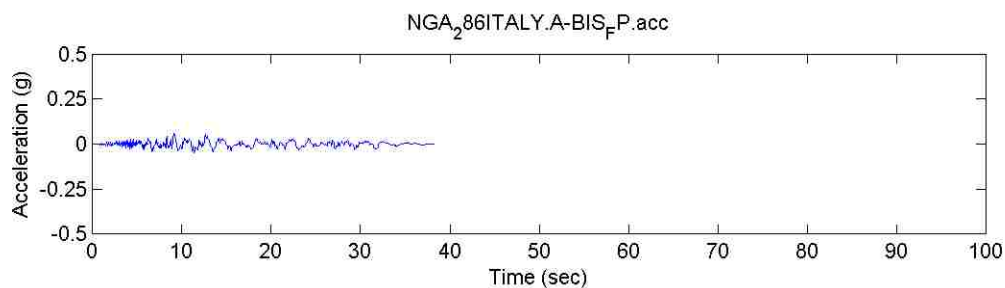


Figure E.14. GM record No. 14

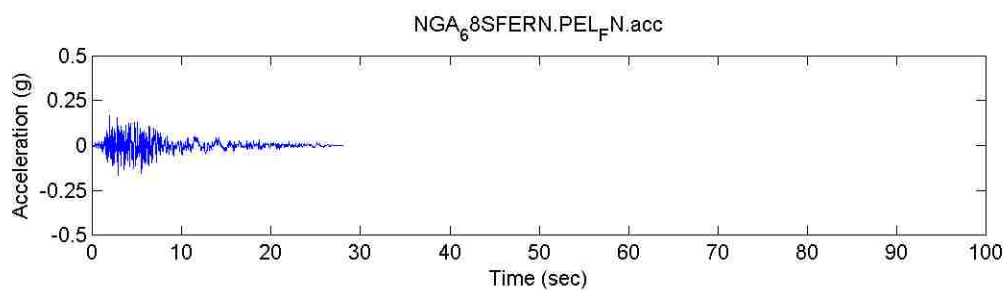


Figure E.15. GM record No. 15

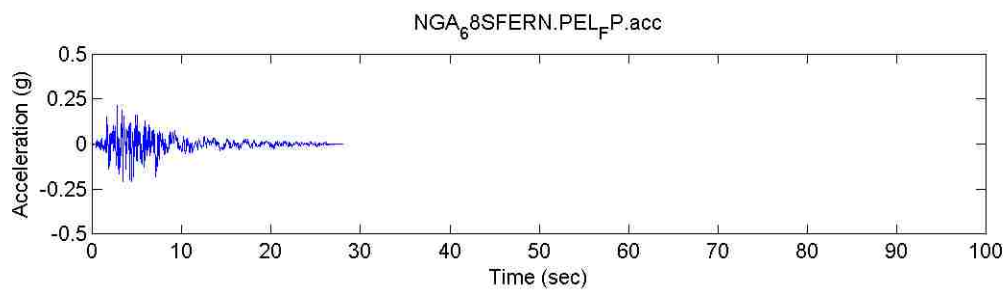


Figure E.16. GM record No. 16

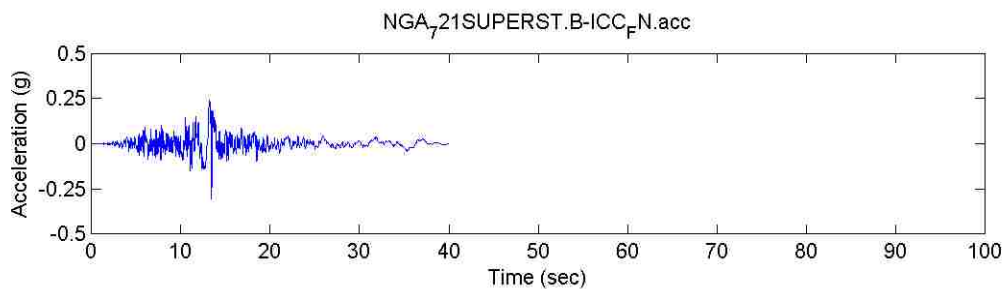


Figure E.17. GM record No. 17

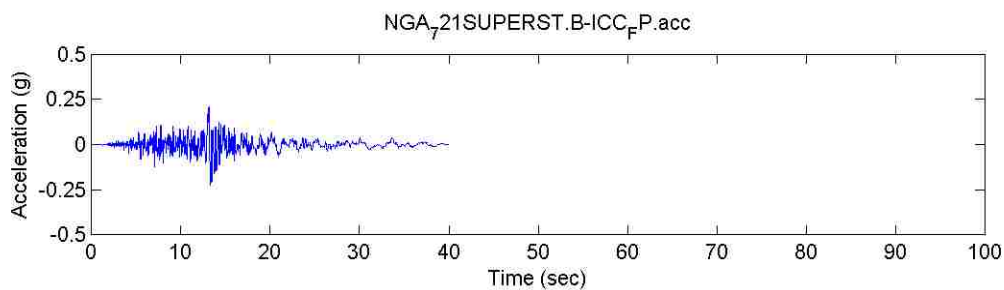


Figure E.18. GM record No. 18

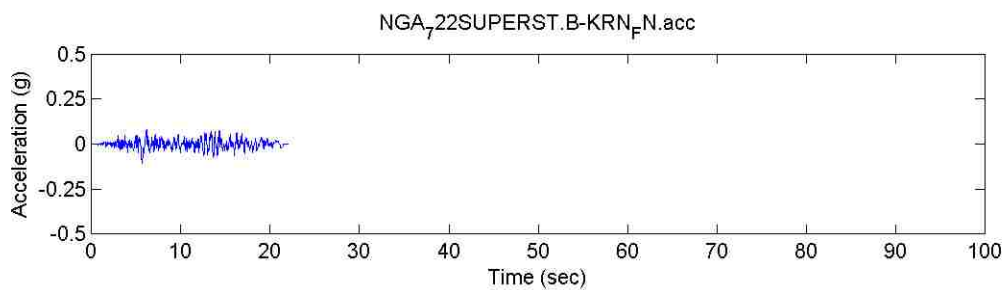


Figure E.19. GM record No. 19

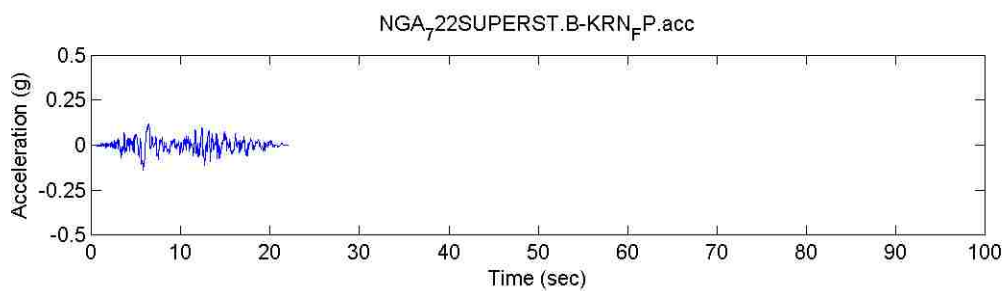


Figure E.20. GM record No. 20

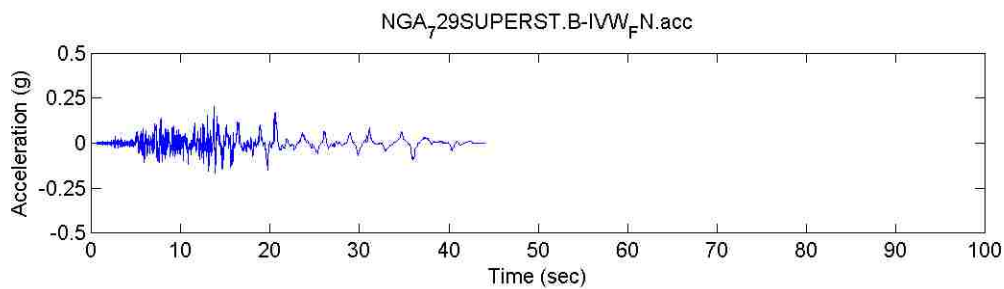


Figure E.21. GM record No. 21

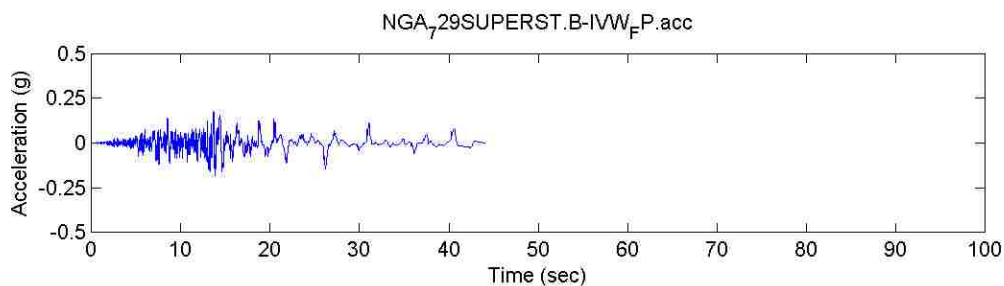


Figure E.22. GM record No. 22

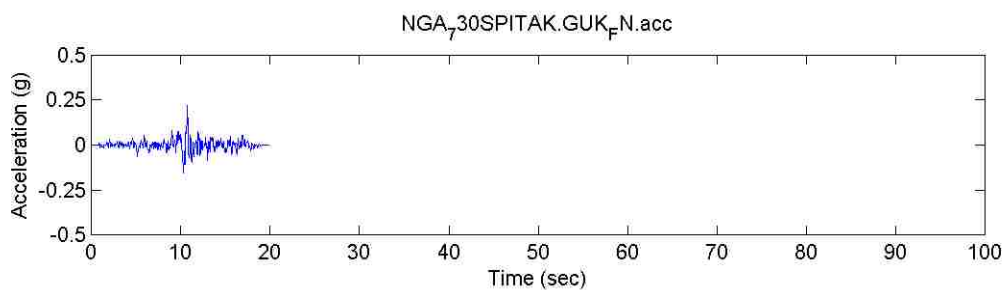


Figure E.23. GM record No. 23

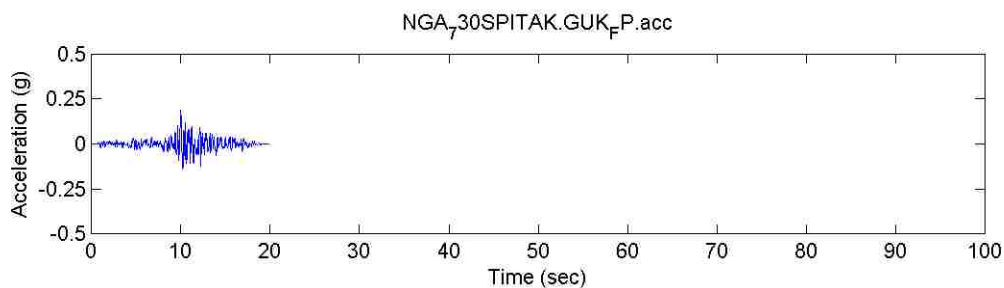


Figure E.24. GM record No. 24

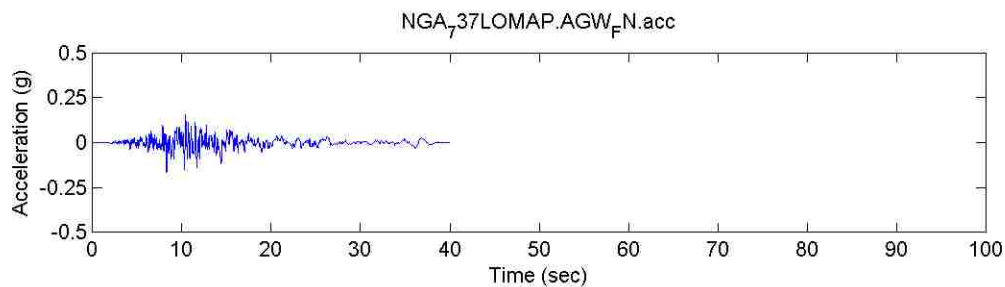


Figure E.25. GM record No. 25

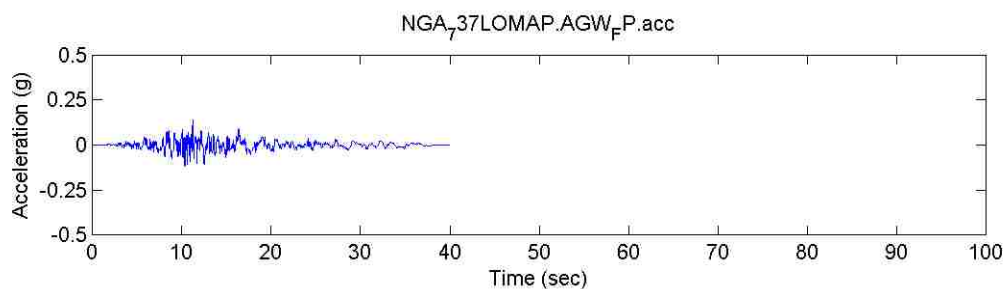


Figure E.26. GM record No. 26

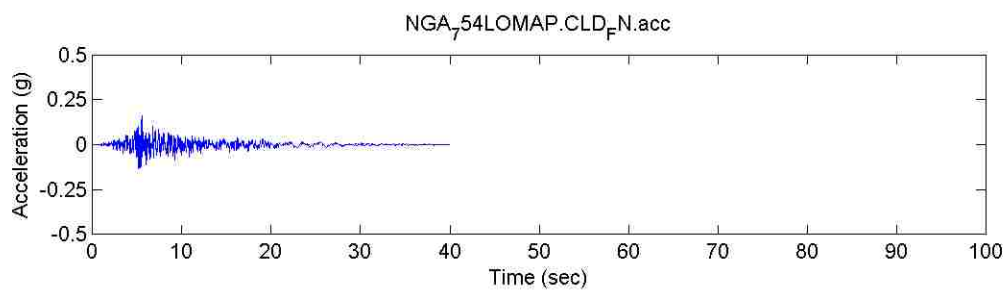


Figure E.27. GM record No. 27

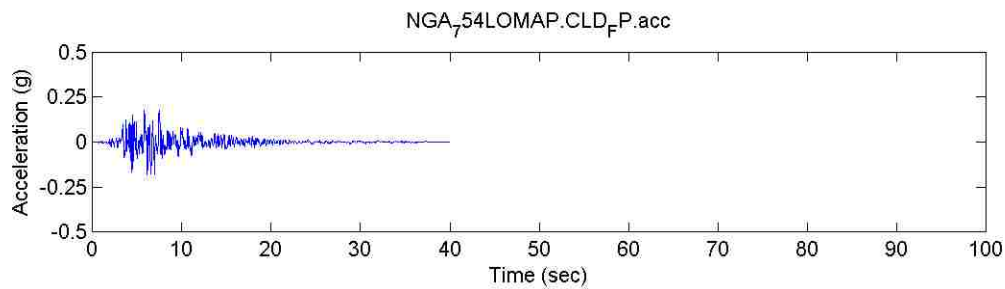


Figure E.28. GM record No. 28

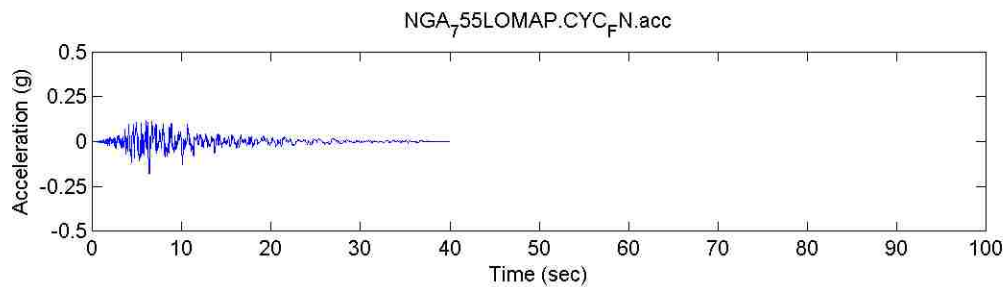


Figure E.29. GM record No. 29

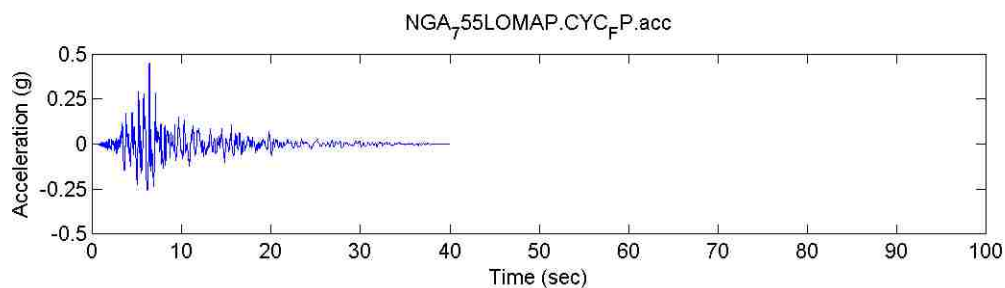


Figure E.30. GM record No. 30

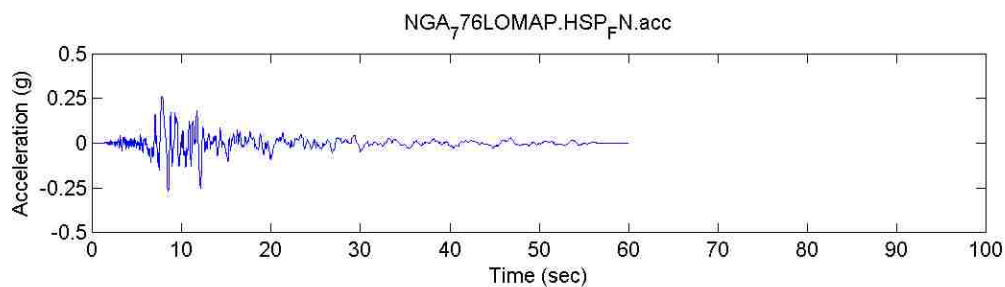


Figure E.31. GM record No. 31

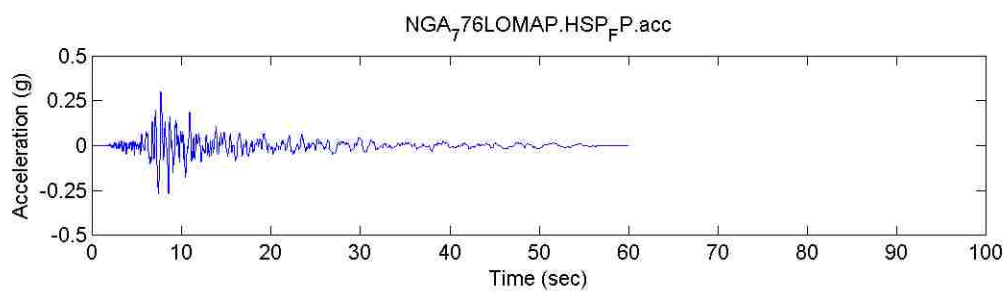


Figure E.32. GM record No.32

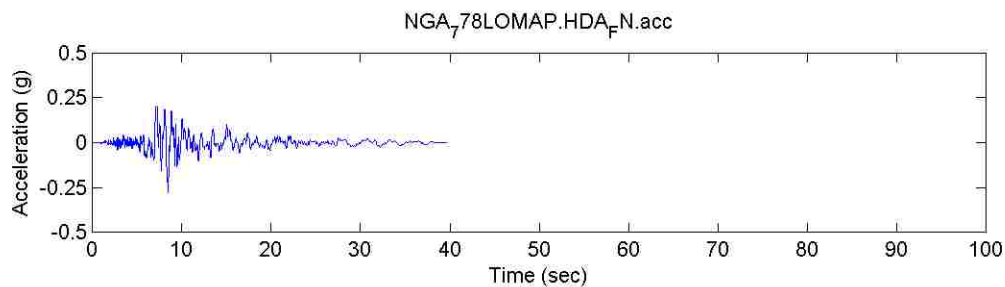


Figure E.33. GM record No.33

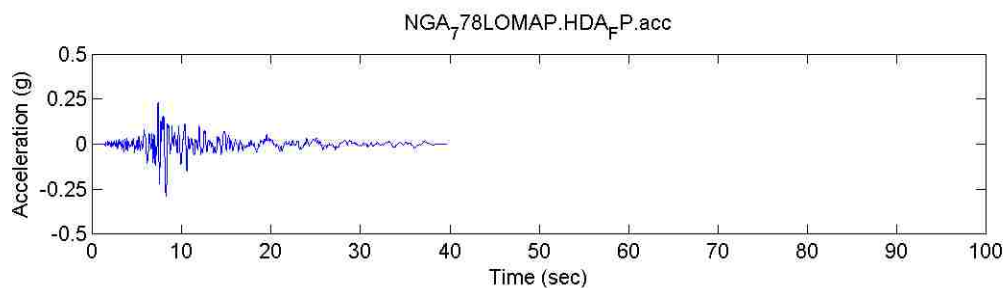


Figure E.34. GM record No.34

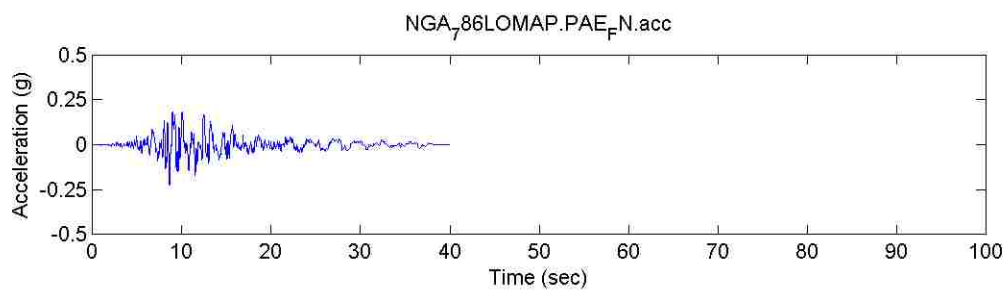


Figure E.35. GM record No.35

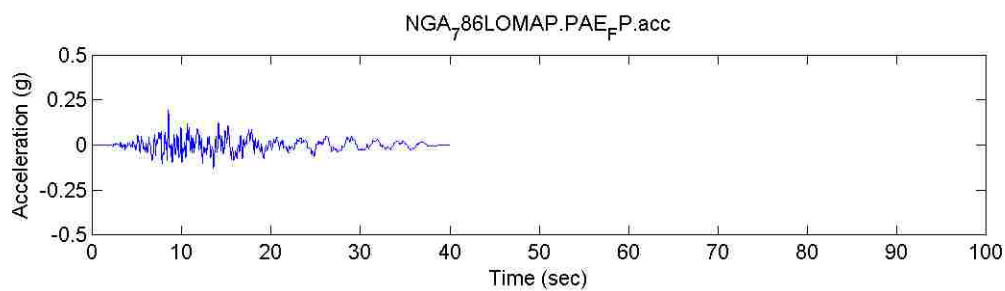


Figure E.36. GM record No.36

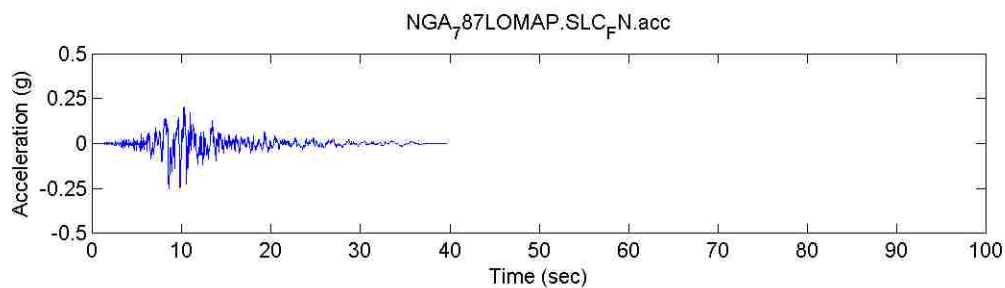


Figure E.37. GM record No.37

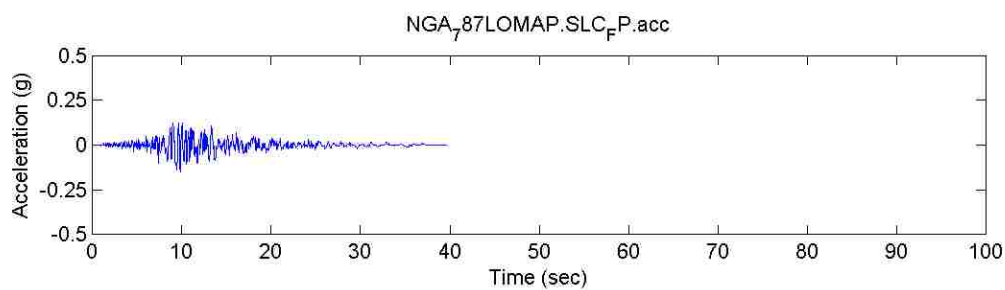


Figure E.38. GM record No.38

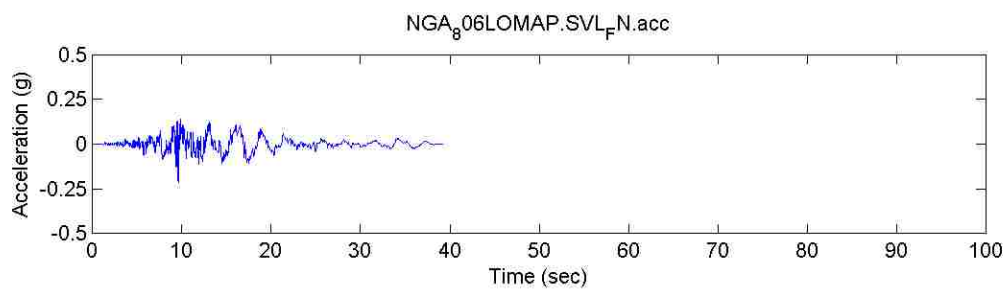


Figure E.39. GM record No.39

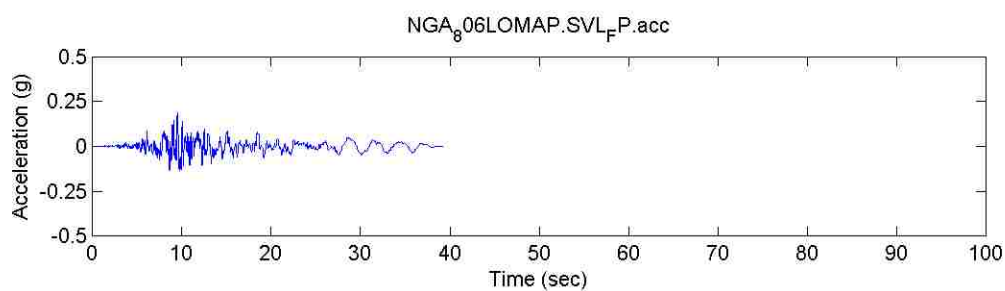


Figure E.40. GM record No.40

BIBLIOGRAPHY

- American Concrete Institute (ACI) Committee 318. (2011). "Building Code Requirements for Structural Concrete and Commentary," ACI 318-11, Farmington Hills, Mich.
- Applied Technology Council (ATC) (1997). "Seismic Design Criteria for Bridges and Other Highway Structures: Current and Future," ATC-18, Redwood City, Calif.
- ASTM C109-11/C109M-11 (2011). "Standard Test Method for Compressive Strength of Hydraulic Cement Mortars (Using 2 in. or 50 mm Cube Specimens)," ASTM International; p. 9.
- ASTM D 7234-05 (2005). "Standard Test Method for Pull-off Adhesion Strength of Coatings on Concrete Using Portable Pull-off Adhesion Testers," ASTM International; P. 8.
- Belarbi, A. (DJ), Silva, P. F., Bae, S. W. (2008). "Retrofit of RC Bridge Columns Under Combined Axial, Shear, Flexure, and Torsion Using CFRP Composites," Challenges for Civil Engineering (CCC), Porto.
- California Department of Transportation (Caltrans). (2006). "Seismic Design Criteria Version 1.4," California, USA: Engineering Service Center, Earthquake Engineering Branch.
- California Department of Transportation (Caltrans). (2007). "Memo to Designers 20-4 attachment B," California, USA: Engineering Service Center, Earthquake Engineering Branch.
- Ceresa, P., Petrini, L., Pinho, R. (2007). "Flexure-shear Fiber Beam-Column Elements for Modeling Frame Structures Under Seismic Loading-State of the Art," *Journal of Earthquake Engineering*, No. 11, pp: 46-88.

- Chai, Y. H., Priestley, M. J. N., and Seible, F. (1991). "Seismic Retrofit of Circular Bridge Columns for Enhanced Flexural Performance," *ACI Structural Journal*, V. 88, No. 5, September-October, pp. 572-584.
- Chalioris, C. E. (2008). "Torsional Strengthening of Rectangular and Flanged Beams Using Carbon Fiber-Reinforced-Polymers – Experimental Study," *Construction and Building Materials*, Vol. 22.
- Cheng, C. T., Yang, J. C., Yeh, Y. K., and Chen S. E. (2003). "Seismic Performance of Repaired Hollow-Bridge Piers," *Construction and Building Materials*, V. 17, pp. 339-351.
- Elwood, K.J. (2004). "Modeling Failures in Existing Reinforced Concrete Columns," *Canadian Journal of Civil Engineering*, No. 31, pp: 846-859.
- Ghobarah, A., Ghorbel, M. N., Chidiac, S. E. (2002). "Upgrading Torsional Resistance of Reinforced Concrete Beams Using Fiber-Reinforced Polymer," *Journal of Composites for Construction*, ASCE, Vol. 6, No. 4, November 1.
- Grelle, S. V. (2011). "Categorization and Experimental Evaluation of Anchorage Systems for FRP Laminates Bonded to Reinforced Concrete Structures," Master's Thesis, Missouri University of Science and Technology, Rolla, MO.; p.159.
- Hii, A. and Al-Mahaidi, R. (2007). "Torsional capacity of CFRP strengthened reinforced concrete beams." *Journal of Composites for Construction*, 11(1), 71-80.
- Laplace, P. N., Sanders, D., Saiidi, M., Douglas, B., and El-Azazy, S. (2005). "Retrofitted Concrete Bridge Columns under Shaktable Excitation," *ACI Structural Journal*, V. 102, No. 4, July-August, pp. 662-628.
- Lehman, D. E., Gookin, S., Nacamuli, A. M., and Moehle, J. P. (2001). "Repair of Earthquake-Damaged Bridge Columns," *ACI Structural Journal*, V. 98, No. 2, March-April, pp. 233-242.

- Li, Y. F. and Sung Y. (2003). "Seismic Repair and Rehabilitation of a Shear-Failure Damaged Circular Bridge Column Using Carbon Fiber Reinforced Plastic Jacketing," *Canadian Journal of Civil Eng.*, V. 30, pp. 819-829.
- Massone, L. M. (2006). "RC Wall Shear – Flexure Interaction: Analytical and Experimental Responses," Ph.D. Dissertation, University of California, Los Angeles, 398 pp.
- Matthys, S., Triantafillou, T. (2001). "Shear and Torsion Strengthening with Externally Bonded FRP Reinforcement," *ASCE Conf. Specialty Workshop of Composites in Construction Proceedings of the International Workshop*.
- Mohammadizadeh, M. R, Fadaee, M. J., Ronagh, H. R., and Ahmadinezhad, A. (2008). "Behavior of high-strength concrete beams strengthened with CFRP sheets in torsion." 4th international conference on FRP composites in Civil Engineering, CICE 2008, Zurich, Switzerland
- Panchacharam, S., Belarbi, A. (2002). "Torsional Behavior of Reinforced Concrete Beams Strengthened with FRP Composites," Torsional Behavior of Reinforced Concrete Beams Strengthened with FRP Composites, First FIB Congress, Osaka, Japan, October, 13-19.
- Park, R. and Paulay, T. (1975). "Reinforced Concrete Structure." John Wiley & Sons, Inc. p. 769.
- Prakash, S. S., and Belarbi, A. (2010). "Towards Damage-Based Design Approach for RC Bridge Columns under Combined Loadings Using Damage Index Models," *Journal of Earthquake Engineering*, Vol. 14, pp. 363-389.
- Prakash, S.S., Li, Q., and Belarbi, A. (2012). "Behavior of Circular and Square Reinforced Concrete Bridge Columns Under Combined Loading Including Torsion," *ACI Structural Journal*. 109(3), pp. 317-327.

- Priestley, M. J. N. and Seible, F. (1993). "Repair of Shear Column Using Fiberglass/Epoxy Jacket and Epoxy Injection," Report No. 93-04, Job No. 90-08, Seqad Consulting Engineer, July.
- Priestley, M. J. N., Seible, F., Xiao, Y., and Verma, R. (1994a). "Steel Jacket Retrofitting of Reinforced Concrete Bridge Columns for Enhanced Shear Strength-Part 1: Theoretical Considerations and Test Design," ACI Structural Journal, V. 91, No. 4, July-August, pp. 394-405.
- Priestley, M. J. N., Seible, F., Xiao, Y., and Verma, R. (1994b). "Steel Jacket Retrofitting of Reinforced Concrete Bridge Columns for Enhanced Shear Strength-Part 1: Test Results and Comparison with Theory," ACI Structural Journal, V. 91, No. 5, September-October, pp. 537-551.
- Priestley, M. J. N., Seible, F., and Calvi, G. M. (1996). "Seismic Design and Retrofit of Bridges," John Wiley and Sons, New York, USA.
- Saadatmanesh, H., Ehsani, M. and Jin, L. (1996). "Seismic Strengthening of Circular Bridge Pier Models with Fiber Composites," ACI Structural Journal, Vol. 93, No. 6, November-December, pp. 639-647.
- Saadatmanesh, H., Ehsani, M. and Jin, L. (1997). "Repair of Earthquake-Damaged RC Columns with FRP Wraps," ACI Structural Journal, Vol. 94, No. 2, March-April, pp. 206-215.
- Saiidi, M. and Cheng, Z. (2004). "Effectiveness of Composites in Earthquake Damage Repair of RC Flared Columns," Journal of Composites for Construction, ASCE, V. 8, No. 4, pp. 306-314.
- Saiidi, M., Wehbe, N., Sanders, D., and Caywood, C. (2001). "Shear Retrofit of Flared RC Bridge Columns Subjected to Earthquake," Journal of Bridge Engineering, ASCE, V. 6, No. 3, May-June, pp. 189-197.

- Salom, P. R., Gergely, J., and Young, D. T. (2004). "Torsional Strength of Spandrel Beams with Fiber-Reinforced Polymer Laminates," *Journal of Composites for Construction*, ASCE, Vol. 8, No. 2, April 1, 2004.
- Seible, F., Priestley, M. J. N., Hegemier, G., and Innamorate, D. (1997). "Seismic Retrofit of RC Columns with Continuous Carbon Fiber Jackets," *Journal of Composites for Construction*, ASCE, V. 1, No. 2, May, pp. 52-62.
- Shanmugam, S. P. (2009). "Seismic Behavior of Circular Reinforced Concrete Bridge Columns under Combined Loading Including Torsion," A Dissertation for Doctor of Philosophy, Missouri University of Science and Technology, Rolla, Mo.
- Shin, M., and Andrawes, B. (2011). "Emergency Repair of Severely Damaged Reinforced Concrete Columns Using Active Confinement with Shape Memory Alloys," *Smart Materials and Structures*, V. 20, 9pp.
- Stoppenhagen, D. R., Jirsa, J. Q., and Wyllie, Jr., L.A. (1995). "Seismic repair and strengthening of a severely damaged concrete frame," *ACI Structural Journal*, V.92, No. 2, pp. 177-187.
- Vosooghi, A, Saiidi, M. S., and Gutierrez, J. (2008). "Rapid Repair of RC Bridge Columns Subjected to Earthquakes," *Proceedings of 2nd International Conference on Concrete Repair, Rehabilitation, and Retrofitting (ICCRRR)*, Cape Town, South Africa, 24-26 November, pp. 1113-1119.
- Vosooghi, A., and Saiidi, M. S. (2009). "Rapid Repair of High-Shear Earthquake-Damaged RC Bridge Columns," *Proceedings of the 25th US-Japan Bridge Engineering Workshop*, Tsukuba, Japan, Session 7, October.
- Vossoghi, A., and Saiidi, M. S. (2010). "Post-Earthquake Evaluation and Emergency Repair of Damaged RC Bridge Columns Using CFRP Materials," Report Number CCEER-10-05, September.

Zureick, A. H., Ellingwood, B. R., Nowak, A. S., Mertz, D. R., and Triantafillou, T. C. (2010). "Recommended Guide Specification for the Design of Externally Bonded FRP Systems for Repair and Strengthening of Concrete Bridge Elements," NCHRP Report 655. 28-43, Washington, D. C.

VITA

Ruili He was born in Shenmu, Shaanxi, China. She obtained her Bachelor's Degree in Civil Engineering with distinction in July 2006 from Tongji University, Shanghai, China. She was one of the recipients of best outgoing students for her overall academic performance. She began her graduate studies in September 2006 at the School of Aerospace Engineering and Applied Mechanics, Tongji University, Shanghai, China. Her research was focused on composites analysis and solid mechanics. During her master's study, she also had the unique opportunity to work at the Shanghai Linyoo Information & Technology Ltd. Her research work during her masters involved finite element simulation of mechanical properties of fiber reinforced composites. She received her Master of Science in Solid Mechanics in June 2009.

Ruili He came to Missouri University of Science and Technology (formerly University of Missouri Rolla) in August 2009 to pursue her Ph.D. in Civil Engineering. Her research has been focused on rapid repair of reinforced concrete columns severely damaged by combined loading effects using externally-bonded carbon fiber reinforced polymer (CFRP), which was sponsored by University of Missouri Research Board and the Center for Transportation Infrastructure and Safety (CTIS). She has published and presented the results and findings in several journal papers and American Concrete Institute (ACI) conventions. As a doctoral candidate, she acted as an active member of ACI, and she was awarded the International Concrete Repair Institute Scholarship from ICRI Great Plains Chapter in 2011. She earned her Ph.D. in Civil Engineering from the Missouri University of Science and Technology in August 2014.